UNIVERSITY OF OKLAHOMA

GRADUATE COLLEGE

FRAC HIT ANALYSIS IN SHALES: WOODFORD, MERAMEC AND WOLFCAMP FORMATIONS

A DISSERTATION

SUBMITTED TO THE GRADUATE FACULTY

in partial fulfillment of the requirements for the

Degree of

DOCTOR OF PHILOSOPHY

By

ISHANK GUPTA
Norman, Oklahoma
2020

FRAC HIT ANALYSIS IN SHALES: WOODFORD, MERAMEC, WOLFCAMP AND MARCELLUS FORMATIONS

A DISSERTATION APPROVED FOR THE
MEWBOURNE SCHOOL OF PETROLEUM AND GEOLOGICAL ENGINEERING

BY THE COMMITTEE CONSISTING OF

Dr. Chandra Rai, Chair

Dr. Carl Sondergeld

Dr. Deepak Devegowda

Dr. Matthew Pranter

Dr. Moghanloo Rouzbeh

Dedicated to

“My Professors, Family and Friends”

Acknowledgements

I would like to thank IC^3 consortium members and Marathon for providing the financial support, data and vital feedback during the meetings.

I would like to thank Dr. Chandra Rai for accepting me as his PhD student. He reminds me of the Latin quote by Descartes – 'Cogito Ergo Sum'. It means 'I think, therefore I am'. He has inspired me and nurtured me throughout my time at OU. He has held my hand like a newborn yet pushed me out of the nest when I needed to learn to fly. Life is nothing but a sum of choices you make, and I am honored that he chose me.

Dr. Carl Sondergeld is my other pillar. He reminds me of another Latin quote – 'Vivamus, Moriendum Est.' which means 'Let us live, since we must die'. He has taught me that the most valuable gift you can give someone, is the gift of time and thus, every second you are not doing something, you are depriving yourself and people you love of that precious gift.

I would also like to thank my other committee members Dr. Deepak Devegowda, Dr. Matthew Pranter and Dr. Moghanloo Rouzbeh for their guidance, support and most importantly the smile on their faces because in Oklahoma, you may see four seasons in one day but their smile and willingness to help stays constant throughout the year.

I would also like to thank my parents and my sister, Swati, family and friends for they are the reason I exist. When I was born, my father told everybody that his son would be a doctor. I fell in love with engineering and this was the only way to keep his word. Him and my mother have made countless sacrifices so that I can stand here today and claim my doctorate. They only asked that I do the same one day for my children and I promise, I will. My sister is younger yet stronger than I am both willfully and physically. She is the reason I don't stop and because when I left, she said – 'I am always watching you'. I think she meant through Facebook, WhatsApp,

and Instagram. Lastly, five years is a long time, but my friends made it fly by and here I am writing this dissertation, and I stop and pause for a minute because wait – 'Now I need to leave OU'. To all my friends from the bottom of my heart as Cicero said 'Amicitiae nostrae memoriam spero sempiternam fore'.

Finally, I also have a few words for my girlfriend Ngoc. She has stood beside me in this journey and her salads have kept me healthy to keep going. She is my travel buddy and we have the same motto in life – 'Work hard, but party harder'. I am glad I found her.

Table of Contents

List of Figures

List of Tables

Abstract

Frac hit was initially coined to refer to the phenomenon when an infill well fracture interacts with the adjacent well during the hydraulic fracturing process. But, over the years, its use has been extended to any type of well-interference or interaction in unconventional reservoirs. Frac hit impact is dictated by a complex interplay of petrophysical properties (high-perm streaks, mineralogy, matrix permeability and natural fractures), geomechanical properties (near-field and far-field stresses, tensile strength, Young's modulus and Poisson's ratio), completion parameters (stage length, cluster spacing, pumping rate, fluid and proppant amount) and development decisions (well spacing, completion design and well scheduling).

It is difficult to predict the impact of frac hits because they impact both parent and child wells. The impact on the child wells is predominantly negative but the impact on parent wells can be either positive or negative. Overall, frac hits tend to negatively impact the production. The different strategies proposed to minimize negative impact of frac hits are codevelopment thus avoiding parent-child wells (Tank, Cube development methods), repressuring or refracturing parent wells, using far-field diverters and high permeability plugging agents in child wells frac fluid, optimizing stage and cluster spacing through modeling studies and field tests to reduce stress shadow effects and promote uniform fracture growth.

First, to understand the impact of frac hits and maximize utilization of public databases, an automated machine-learning workflow was developed. The workflow helped analyze over 6000 wells from Meramec, Woodford and Wolfcamp. We systematically evaluated field production and completions data to understand the impact of frac hits on the parent and the child wells production. The parent wells in all three formations had both positive and negative impact of the frac hits. Around 60-67 % wells were negatively impacted while 33-40 % wells were positively

impacted. For the child wells, 71-85 % wells were negatively impacted and 15-29 % of the wells were positively impacted. Overall, i.e., combining the impact on parent and child wells, the impact is dominated by the child wells as 69 to 82% of the parent-child pairs were negatively impacted and only 18-31 % of the pairs were positively impacted. Considering percent loss in the cumulative oil volumes in the next 5-years, in the Meramec, parent wells on average show a 16% reduction while child wells show a 39% reduction due to frac hits. The corresponding numbers for the Woodford formation are 19% and 37% and for the Wolfcamp formation are 20% and 22%, respectively. This translates to a parent well losing on average 40-50 kbbls over the next five years and a child well losing on average 80-150 kbbls over the same period. Together a parent-child pair can lose on average between 125 to 225 kbbls in the 5-year period. The results show that the key factors governing the extent of the impact are the extent of depletion and producing oil rates of the parent well before frac hit, completion design parameters (fluid and proppant amount) and well spacing. Machine learning based regression models were also developed to predict the impact of frac hits. These regression models were then coupled with economic analysis to determine optimum spacing for any given completion design or optimum completion design for any given spacing.

Next, an independent analysis was done in small regions (< 10 wells) where extensive data like core, logs, microseismic and fiber optics were available to tie the impact of frac hits to the petrophysical and geomechanical properties of the rocks. One such study was done in Meramec formation. The logs were used to calculate pore pressure and closure stress profiles, mechanical properties such as Young's modulus and Poisson's ratio. Fracture modeling and microseismic data helped to understand fracture growth, i.e. fracture dimensions, complex versus planar fracture networks, inter-stage interactions and stress shadow effect. This additional information

provided critical insights into frac hits and how they can be managed. The field data was complemented by extensive numerical modeling in GOPHER which was used to carry out sensitivity studies with different completion design parameters. The key findings were while fracture fluid is likely the most important factor governing fracture geometry, amount of proppant directly correlates to fracture width and fracture conductivity. Additionally, large number of clusters per stage can cause disproportionate fracture growth and increase the risk of frac hits. Latin hypercube sampling was used to optimize number of simulations required to generate response surfaces for fracture height and length that can be used to select the best design to maximize production and minimize frac hits.

Another study was done in Marcellus where the analysis shows that the pre-existing natural fracture network controls both the hydraulic fracture geometry as wells as the production from the reservoir. Natural fractures promote complex fracture networks with shorter half-lengths which increase production from the reservoir while minimizing frac hits and neighboring well interactions. The natural fracture network is itself controlled by the geomechanical properties of the rock. A machine-learning workflow was developed to predict the geomechanical facies along the horizontal laterals using the surface drilling data. The facies originally derived using the core- and well-log data can be reliably predicted using drilling data and supervised classification techniques. This machine learning workflow provides a powerful tool for real-time optimization of the wellbore trajectory and completions and minimize frac hits.

Finally, the dissertation concludes with a recommended approach to manage frac hits. There is no silver bullet and problem of frac hits in each shale play is as unique as the shale play itself. But, using all the data available and harnessing the published knowledge, to understand how the

fractures propagate downhole, measures can be taken to minimize or even completely avoid frac hits.

Chapter 1: Introduction

George Mitchell considered as the father of shale revolution spent 20 years perfecting the formula for hydraulic fracturing in shales with his colleagues Nicholas Steinsberger and Kent Bowker (Zuckerman 2013). They developed something called slick-water design which is now being applied to almost every well being drilled in the shale reservoirs. The design fluid mainly comprised of water with some friction reducers and polymers. It was designed to reduce surface friction and increase lubricity. The idea was that due to ultra-low matrix permeability in shales, the ability of the matrix to transport hydrocarbons over long distances to one big planar fracture is next to impossible. Thus, to drain these reservoirs, a complex fracture network is required. Therefore, the lower viscosity of the slickwater would facilitate leak-off into the weak bedding interfaces and natural fractures creating complex hydraulic fracture network in the process. Unconventional shale development has been made possible by multi-stage hydraulically fractured horizontal wells which can create millions of square feet of contact area within the ultra-low permeability shale reservoirs.

The term frac hit (well bashing) was originally coined to refer to the interwell communication when the parent well was affected by the hydraulic fracturing treatment in a child well. This connection can be easily noticed in the parent well due to pressure spike and high and abrupt increase in the water cut. Various studies (Lawal et al. 2013, King and Valencia 2016) attributed this behavior to the connection (or overlapping) of the hydraulic fracture networks of the parent and the child wells (Figure 1(a)). With time, however, the hydraulic fractures closed and the communication between the parent and the child wells decreased or even completely disappeared (King 2014). Rucker et al. (2016) showed that in the Niobrara, the conductive fracture length dropped from initial 660’ to 200’ within six months of production. Warpinski et al. (2008) also

reported that fluid can reactivate natural fractures, bedding planes, high perm streaks, faults, and other formation discontinuities during hydraulic fracturing due to high pressure. These may cause frac hit in near-by parent wells, but these openings may close as soon as pumping stops and there may be no communication with the parent wells during the production phase. Thus, the term frac hit did not include long-term inter-well communication when it was coined.

While referring to frac hits as well-interference phenomenon is not technically incorrect, as the term 'well-interference' has been traditionally reserved for the overlap of drainage areas (during production) of adjacent wells in conventional reservoirs. In unconventional formations, this might mean that the fracture networks of the child and parent wells do not intersect but are close enough to cause communication through the matrix (Figure 1(b)). Awada et al. (2015) made this distinction in their study on identifying and analyzing communication through hydraulic fractures. Yu et al. (2016) suggested another common form of well interaction prominent in unconventional shales where the parent and child well fracture networks are connected through the pre-existing natural fracture network in the shale formations (Figure 1(c)). This extended connection through natural fractures can cause both frac hits and long-term inter-well communication. Together, the different forms of parent-child interactions is collectively referred to as well-to-well fracture-driven interactions or simply FDI (Daneshy and King 2019, Rassenfoss 2017). But, the use of term frac hit to refer to parent-child interactions is still widespread in unconventional reservoirs. It is also difficult to separate the impact of different forms of well-interactions within FDI. In this dissertation, the term frac hits and FDI are used interchangeably and frac hits refer to all forms of inter-well interactions in unconventional formations.

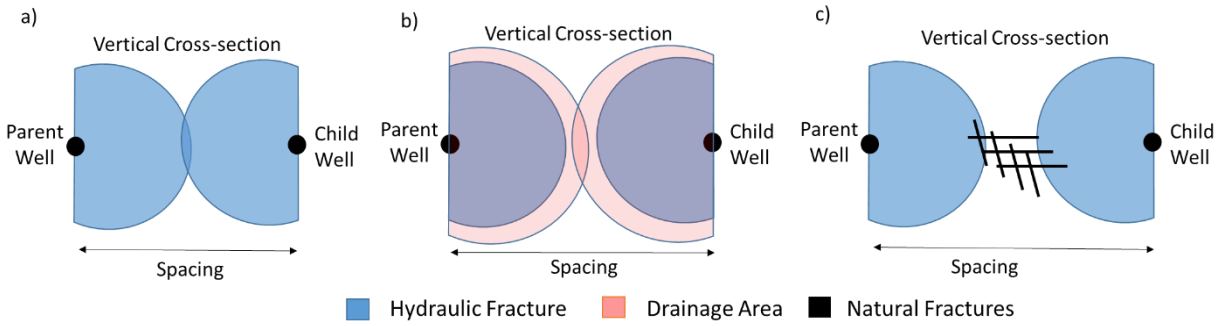

Figure 1: Various forms of inter-well communication between the parent and child wells in unconventional shale formations. (a) Communication is through overlapping fracture networks of the parent and child wells. This form of communication is also commonly referred to as frac hit. (b) Well-interference when fracture networks of the parent and child wells are close enough to communicate through the matrix. (c) Well-interaction when the fracture networks are connected by the pre-existing natural fracture system.

The reason frac hits have become one of the biggest concerns for shale operators is shown in Figure 2. The figure (Figure 2a) shows the percentage of parent and child wells drilled in the Midland basin as a function of time (Xu et al. 2018). It is evident that the percentage of child wells has increased significantly over time i.e. much larger number of infill wells are drilled today compared to 2012. This essentially implies the well spacing has decreased. Currently, operators are drilling at a well spacing varying between 250 to 800 ft (roughly 30 to 100 acre) spacing (**Table 1**). Figure 2b shows a corresponding increase in the lateral length, total proppant and frac fluid per well to boost hydrocarbon productivity. Combined with tighter well spacing, this is causing a significant increase in the occurrence of frac hits.

Even though well spacing and bigger completion sizes are big catalysts for frac hits, several authors (King 2014; King et al. 2017; Schaeffer et al. 2017; Vargas-Silva et al. 2018) have proposed possibility of natural fractures and other formation heterogeneities (high perm streaks and faults) to form conductive conduits between the fracture networks of adjacent wells. Presence of natural fractures is more common in low-permeability unconventional reservoirs

(Gale and Holder 2010) compared to conventional reservoirs because these fractures are created when cooked hydrocarbon creates over pressure which results in micro-cracks in shales. The natural fractures may create high permeability streaks and increase the risk of frac hits. This implies that an understanding of the geological depositional processes, petrophysical properties like maturity and geomechanical properties and stress states in the formation during deposition and hydrocarbon generation are paramount to predicting the occurrence and impact of frac hits.

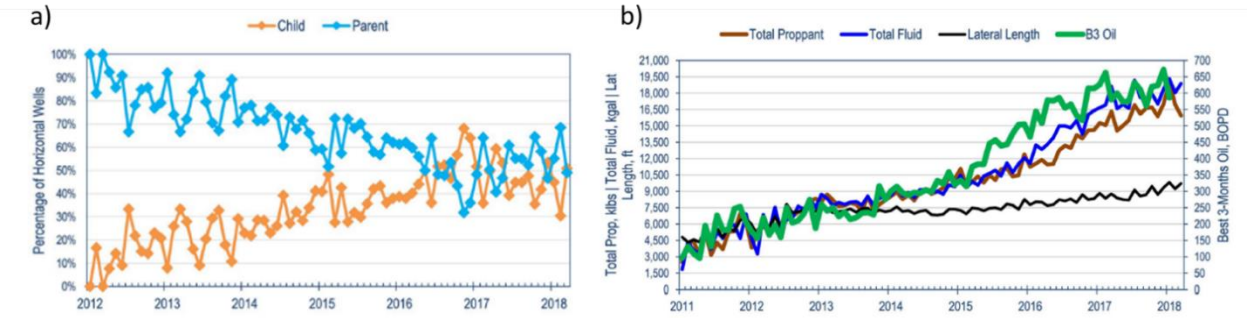

Figure 2: (a) The percentage of parent and child wells drilled in the Midland basin as a function of time. It is evident that the percentage of child wells have increased significantly over time. (b) The trend of increase in lateral length, total proppant and frac fluid used per well evident in the Midland basin (Xu et al. 2018). The increase in completion size has resulted in a corresponding increase in fracture dimensions. Combined with tighter well spacing, it explains why there is a multi-fold rise in the occurrence of frac hits.

Table 1: Well spacing between two lateral wells and corresponding wells per section (WPS). This table considers lateral length to be 1 mile or 5280 ft.

WPS	1	2	3	4	5	6	7	8	9	10	15	20
Well Spacing (ft)	5280	2640	1760	1320	1056	880	754	660	587	528	352	264
Well Spacing (acre)	640	320	213	160	128	106	91	80	71	64	42	32

1.1 Factors Affecting Fracture Propagation and Frac Hits

The key factors which impact fracture propagation and in turn frac hits can be divided into two groups (Figure 3). Factors that are controllable, i.e. can be optimized by the operators and factors that are beyond the control of the operators. The former category includes variables like well

spacing, completion design and depletion control measures like well scheduling and water injection in parent wells. Well spacing here refers to both vertical and lateral spacing of the child wells with respect to the parent wells. The latter category includes variables like in-situ stresses, petrophysical and geomechanical properties of the reservoirs. **Table 2** gives a comprehensive review of the literature where different authors have identified the important factors governing frac hits (or FDI) which come under the two categories listed above. Below is a brief description of the different variables and factors that affect the fracture propagation and frac hits.

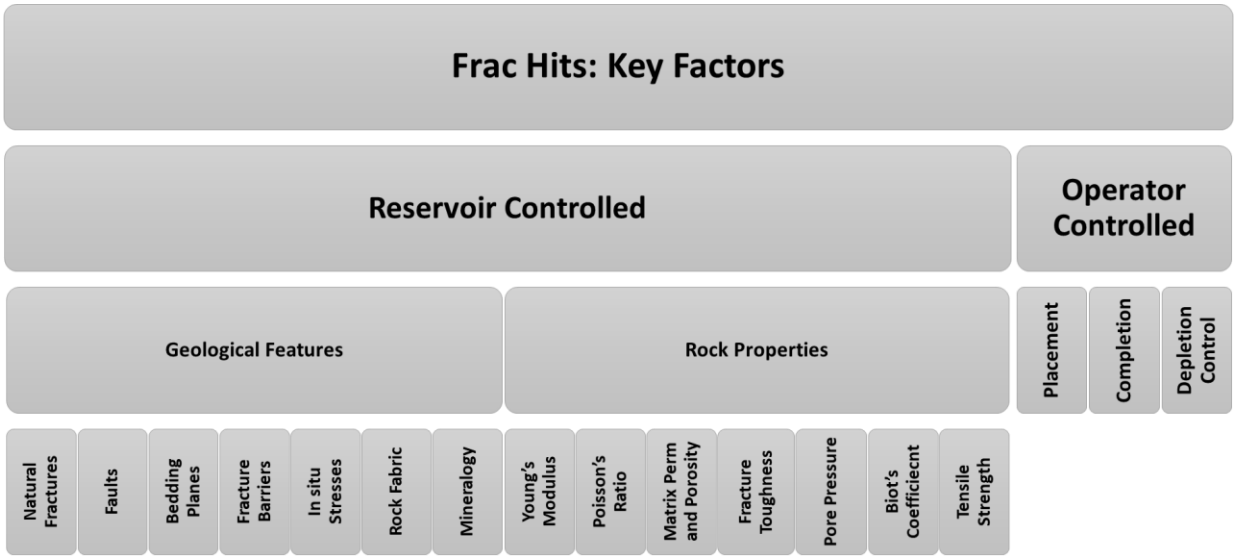

Figure 3: Key factors that influence frac hits can be divided into two categories – reservoir controlled, and operator controlled. The former category includes properties like natural fractures, faults, Young's modulus and Poisson's ratio. The latter category includes factors decided by the operators like parent-child spacing, well completions and depletion control. Depletion control includes child well timing with respect to parent well, parent well shut-in and injection.

1.1.1 Well (Parent-Child) Spacing

The contribution of matrix (unstimulated rock volume) is much smaller than the stimulated rock volume which makes infill drilling a valuable proposition for shale reservoirs. Ample data from numerical modeling (Bharali et al. 2014) and field studies (Ajani and Kelkar 2012) have shown

that decreasing the well spacing decreases the EUR per well due to interwell communication but increases the recovery from a particular area (or section).

Table 2: Summary of studies analyzing the key factors controlling frac hits (FDI) in unconventional reservoirs.

Study	Play	Key Factors Controlling Frac hits
Ajani and Kelkar (2012)	Woodford	Parent well depletion, parent-child spacing, stress-anisotropy
Okouma et al. (2012)	Montney	Parent-child spacing
Lawal et al. (2014)	Not Reported	Matrix permeability
King (2014)	Not Reported	Natural fractures, fracturing fluid viscosity and proppant size, parent-child spacing, presence of faults or high perm streaks
Sani et al. (2015)	Haynesville	Parent well depletion, parent-child spacing
Kurtoglu and Salman (2015)	Meramec	Parent well depletion, parent-child spacing, natural fractures, depth
Anderson et al. (2016)	Eagle Ford	Parent-child spacing
Patel et al. (2016)	Eagle Ford	Stress shadowing, natural fractures
Rucker et al. (2016)	Niobrara	Parent-child spacing, stress anisotropy
Schaeffer et al. (2017)	Wolfcamp	High perm streaks, parent well depletion
Yu et al. (2017)	Eagle Ford	Parent-child spacing
Rezaei et al. (2017)	Haynesville	Parent well depletion, stress anisotropy
King et al. (2017)	Woodford, Eagle Ford	Parent-child spacing, dog leg severity of parent wells, natural fractures, parent-well depletion, faults.
Shin & Popovich (2017)	Wolfcamp	Parent-child spacing
Esquivel and Blasingame (2017)	Haynesville	Parent well depletion. parent-child spacing, completion size
Ajisafe et al. (2017)	Avalon	Parent well depletion
Rafiee and Grover (2017)	Eagle Ford	Parent-child spacing, completion size, stress barriers
Vargas-Silva et al. (2018)	Wolfcamp	Natural fractures, permeability anisotropy, pressure depletion, heterogeneity of mechanical properties
Haustveit & Greenwood (2018)	Meramec	Low porosity and high process zone stress barriers
Rainbolt & Esco (2018)	Wolfcamp	Parent-child spacing and completion size
Lindsay et al. (2018)	Multiple	Reservoir depletion, matrix permeability
Ayers et al. (2018)	Marcellus	Parent-child spacing, completion size and Azimuth
Guo et al. (2018)	Eagle Ford	Parent well depletion, parent-child spacing, Perforation cluster location
Cipolla et al. (2018)	Bakken	Parent well depletion
Manchanda et al. (2018)	Wolfcamp	Parent well depletion
Thomson et al. (2018)	Wolfcamp	Parent well depletion, parent-child spacing
Scherz et al. (2019)	Wolfcamp	Stress anisotropy, fracture and stress shadow, parent well depletion
Zheng et al. (2019)	Wolfcamp	Parent well depletion, parent-child spacing, completion design
McDowell et al. (2019)	Wolfcamp	Parent-child spacing, presence of “buffer” well, azimuth
Lougheed et al. (2019)	Montney	Parent well depletion, parent-child spacing

Majority of the studies in **Table 2** unanimously agree that smaller spacing leads to stronger negative impact from frac hits on both parent and child wells. For instance, Ajani and Kelkar (2012) in their analysis of Woodford found that about 40% of the wells within 1500 ft of the child well are likely to get negatively impacted by frac hits. The probability goes down to 0 at large distances greater than 5000 ft. Bommer et al. (2017) observed frac hits and sanding out of parent wells due to child fracs with parent wells spaced up to 1400 ft away from the child wells. Okouma et al. (2012) studied 74 wells in Montney siltstone and found infill wells drilled closer than 1300 ft of the parent wells establish strong communication with the parent wells causing a negative impact on both parent and child wells.

Jacobs (2017a) report operators have seen frac hits in wells over a mile away. These were small pressure surges (>10 psi) but it shows how interconnected fractures could be – both induced and natural. The upper limit for well spacing at which no frac hit occurs is variable and depends on several factors (see **Table 2**). Since these factors vary widely even within a single shale play or formation, optimum spacing will vary widely within a shale play as well as between different shale plays. Bharali et al. (2014) found the optimum spacing for his Eagle Ford shale study area that generates highest NPV to be 1000 ft based on numerical modeling. Lalehrokh and Bouma (2014) did numerical modeling in Eagle Ford as well and concluded optimum spacing was 330 ft. Thomson et al. (2018) on the other hand found optimum spacing in his Wolfcamp study area to be 660 ft based on field tests and optimization efforts.

1.1.2 Completion Design

The completion design is a broad term which not only includes the amounts of proppant and frac fluid but many other variables like cluster spacing, stage length, frac fluid pumping rate and frac fluid type. All of them play a significant role in fracture propagation. The role of total proppant

and fluid is clear as higher fluid amount generates larger and far reaching fractures around the wellbore and a large amount of proppant is required to keep these fractures from closing. Together large amounts of proppant and fluid are directly proportional to a larger fracture network which can overlap with the fracture network of adjacent parent/child well and can cause increased interference.

Several studies (**Table 2**) suggest that increase in the completion size is directly proportional to the intensity of frac hits. Larger completion size has been correlated with negative frac hits. Krishnamurthy et al. (2019) suggested that positive frac hits could be due to the parent wells being initially under stimulated and gaining access to new reservoir through the child fracs. Other studies point out that completion variables like frac fluid type, injection rate, number of clusters and cluster spacing are also important. Anderson et al. (2016) analyzed Eagle Ford shale wells and found that uneven proppant/fluid intake by clusters in traditional plug and perf completions caused disproportionate fracture growth causing interactions with adjacent wells (frac hits). They proposed pin-point completions, i.e. using one entry point per stage to reduce frac hits. Pin-point completions will cause uniform distribution of treatment volumes, reducing uneven fracture growth and inter-well communication. Yi et al. (2019) and Zheng et al. (2019) also pointed out that fewer perforations-per-cluster were found to promote uniform fluid and proppant placement. Somanchi et al. (2017) identified that maintaining high bottomhole treating pressures (BHTP) and high differential perforation friction pressures (> 1200 psi) across the clusters is key to effective stimulation. They used fiber-optics and concluded extreme limited entry completions led to 40% more uniform fluid distribution across different clusters. Extreme limited entry uses a combination of reduced perforations and increased treatment rates. Generally, fracturing initiates in the cluster with the lowest breakdown pressure. Increasing

injection rate and bottomhole tubing pressures (BHTP), subsequent zones in other clusters break down and start taking fluids, thus improving the cluster efficiency.

Okouma et al. (2012) used production-logging results to show that reducing the cluster spacing from 100 m to 50 m can increase the non-productive clusters from 15 to 30% but may also reduce frac hits by creating more numerous but smaller fractures. Almasoodi (2019) identified the optimum cluster spacing of Meramec to be 50 ft based on numerical modeling and assuming matrix permeability to be 1000 nD. Bazan et al. (2010) carried out sensitivity analysis on cluster spacing in gas producing Eagle Ford region and concluded optimum cluster spacing to be 25 ft. The matrix permeability for his models varied between 100 to 370 nD. Fowler et al. (2019) based on modeling studies observed that cluster spacing must be optimized based on matrix permeability. Higher matrix permeability does not need tighter cluster spacing. In their studies, as matrix permeability increased from 25 nD to 850 nD, cluster spacing can be increased from 25 to 75 ft. to attain the same level of reservoir drainage. Thus, optimization of completion parameters is inherently tied to the knowledge of petrophysical and geomechanical properties of the reservoir.

King et al. (2017) also suggested that the frac fluid injection rates could be modified to more step-wise ramp-up as opposed to achieving full fracture design rate in a few seconds to facilitate complex fracture growth. Patel et al. (2016) concluded that cyclic injection process also leads to increased microseismicity and complex fracture growth. Both slower injection and cyclic injection affect strain behavior and is believed to open more naturally occurring fractures that are generally closed in-situ. The frac fluid itself strongly controls if the fracture growth would be planar or complex (Warpinski et al. 2008; Warpinski 2009; King et al. 2008; King et al. 2017). The gel-based fluids focus on leak-off control and long fracture extension. Thus, they lead to

more planar but longer fractures while slick-water fluids promote shorter more complex fractures. Longer planar fractures have a higher tendency to intersect with an existing fracture network of adjoining parent/child fracture networks and cause frac hits. Rafiee and Grover (2017) successfully found reducing the frac fluid injection rate from 75 bbl/min to 35 bbl/min helped minimize frac hits and overlap of conductive fractures during production.

Amount and type of proppant and fracturing fluid also controls the proppant transport inside the primary and secondary fracture networks and controls the propped fracture area. Raterman et al. (2018) conducted mine back studies in Eagle Ford formation. They observed in fractures extending up to 1000 ft laterally, only 75 ft of the fracture length was abundantly propped. Anschutz et al. (2019) observed that carrying capacity of fluids drop 10-20-fold as fluids enter the fracture from tubing. They found that higher mesh proppant (smaller size) can travel farther into the shale fracture network possibly extending the propped length in unconventional hydraulic fractures. Warpinski (1991) also recommended to use 100-mesh proppant throughout the hydraulic fracture treatment to preserve the permeability of the opened natural and secondary fracture network. Elliot and Gale (2018) found evidence in mine back studies in Wolfcamp formation that majority of the proppant recovered from opened natural fractures was similar to 100-mesh injected proppant. Considering that unpropped fractures tend to close with time, the choice of proppant size can significantly affect the well interference over time. Improving proppant transport in hydraulic fracturing can reduce the need for large completion sizes thereby reducing the occurrence of frac hits.

Proppant transport into primary and secondary fracture networks is not enough to ensure high productivity from shale rocks. The strong decline in production in shales is attributed to strong decline in fracture conductivity due to proppant embedment, crushing, fines migration and

diagenesis (Mittal et al. 2018; Gupta et al. 2019). Warpinski et al. (2008) published the decrease in conductivity for commonly used proppants with stress using split core experiments and slick water fluid (Figure 4). This plot suggests that secondary fractures which do not have any shear offset or proppant (aligned fracture case) will likely close as the pumping stops, and stress increases beyond 3000 psi. The primary and secondary fractures which have proppant will show varying levels of loss of conductivity depending on the type of proppant, the formation and changing stresses with time, among other factors. Thus, inter-well communication will strongly depend on proppant transport and proppant conductivity losses during fracture treatment and later during producing life of the well. This might have a strong impact on temporary or permanent nature of inter-well communication between the parent and the child wells.

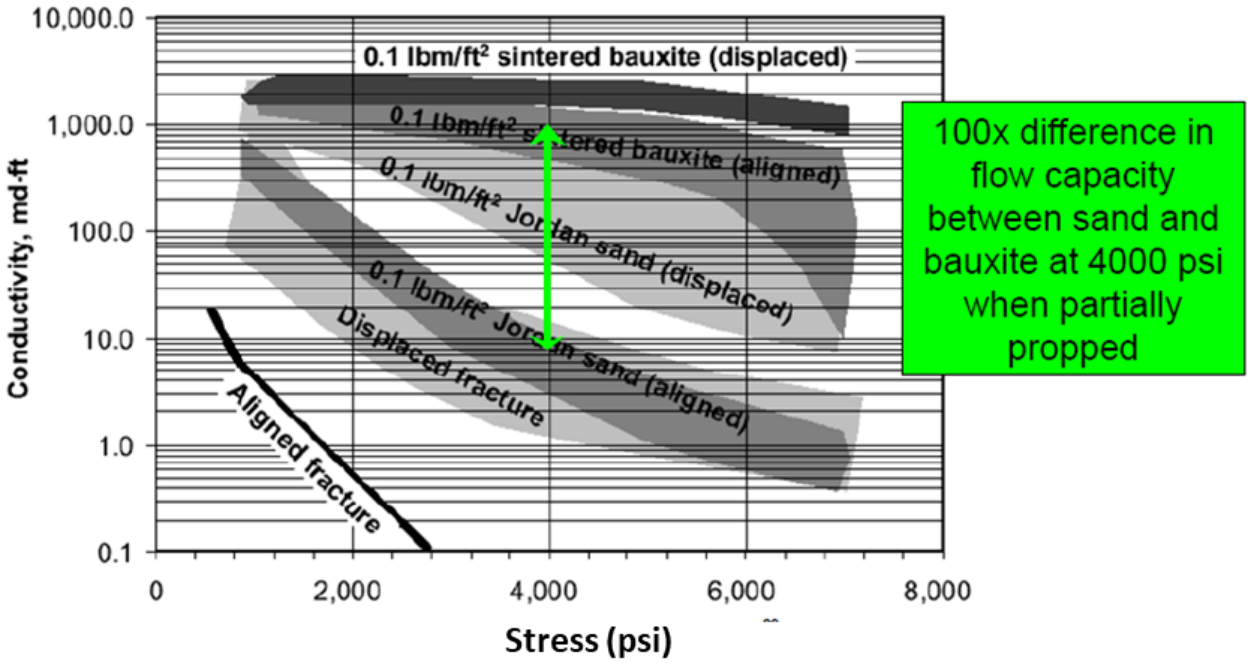

Figure 4: Propped conductivity of split cores from cotton valley sandstones with different proppants (Warpinski et al. 2008). The aligned fracture is the base case with no proppant. Above 3000 psi stress, aligned fracture conductivity almost reduces to zero. Adding white Jordan sand (20/40 mesh) increases the fracture conductivity 10-100 folds. Adding stronger proppants like bauxite (20/40 mesh) further increases the conductivity by up to 100 folds compared to white sand.

Kassis and Sondergeld (2010) conducted similar experiments for Barnett shale. The authors found that in Barnett shale, displaced or offset fractures had similar permeabilities as propped fractures, but both increased permeabilities over 1000-fold compared to the initial aligned fracture values. The pressure dependence of permeabilities in propped fractures were stronger than offset fractures. The permeabilities followed Walsh (1981) law over a limited range of pressures. Ceramic proppant offered no significant advantage over the Ottawa sand, even at high effective stresses up to 6000 psi. This is likely because of the softer and ductile nature of Barnett shale which caused strong embedment in both ceramic proppant and Ottawa sand.

1.1.3 Depletion Control

Depletion control includes well scheduling which determines when the infill/child wells are drilled which dictates the timing of the child wells with respect to the parent well. This dictates the depletion around the parent well at the time of infill/child well drilling. Depletion control also includes other decisions taken by the operators like shut-in of the parent well or fluid injection in the parent well to increase pressure and reduce depletion. Almost all the studies done (**Table 2**) suggest that depletion in the parent well causes asymmetric growth of the child well fracture in the depleted zone thereby negatively impacting the production of the child well. Figure 5 shows evidence from both numerical modeling and field microseismic measurements which clearly show asymmetric fracture growth of the child wells into depleted parent wells. The impact on parent wells when child well fractures grow into the depleted parent well zones is not well understood. Both negative and positive hits have been seen on the parent wells. Krishnamurthy et al. (2019) suggested that positive frac hits in parent wells could be because they were initially under stimulated and they got access to new reservoir through child fracs. Jacobs (2017a) suggested that negative impact on parent wells could be due to gas trapping by the injected water

of the child wells. Since, depleted parent wells are likely below bubble point, there is a large free gas saturation which can get trapped and later hinder oil production in the parent wells.

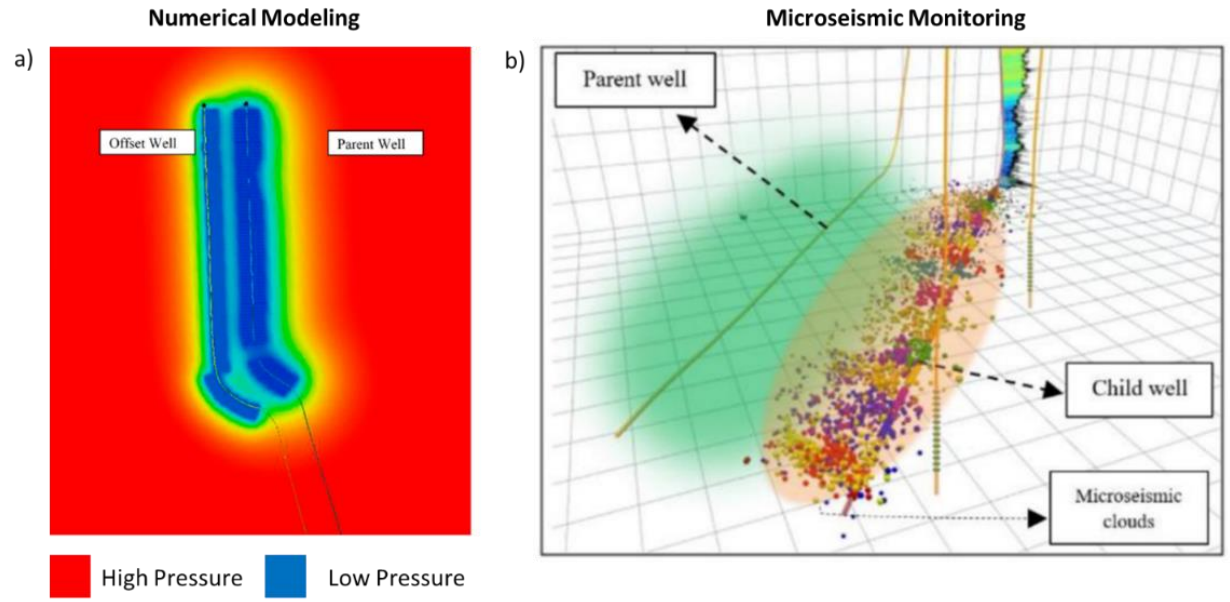

Figure 5: (a) Numerical modeling results (Krishnamurthy et al. 2019) show the asymmetric growth of the offset child well towards the parent well (b) Microseismic data from Li et al. (2019) also show the asymmetric growth of the child well towards the depleted parent well.

Sani et al. (2015) observed that depleted parent wells also promote planar fracture growth in the child wells increasing the probability of intersecting the parent fractures. On the other hand, virgin rock promotes complex fractures due to increased shear failure (Warpinski 2009). Matrix permeability anisotropy (Kx and Ky) and the hydraulic fracture itself (opening in maximum stress direction) promotes non-uniform pressure depletion. Thus, with increase in the production time, the horizontal stress component parallel to the initial fracture (generally σ_H) reduces more than the horizontal stress component orthogonal to the fracture (generally σ_h). This causes anisotropic variation in the in-situ stresses. First, this decrease in stress around the fracture tip attracts the child well fractures which tend to follow the path of least resistance. Second, if the induced stress changes are large enough to overcome the effect of the initial horizontal stress

contrast (σ_H - σ_h), it may cause complete stress reversal around the fracture tip. Stress reversal can lead to several scenarios - child well fractures deflected from the parent well fractures to the parent wellbore itself causing more serious frac hits, they may be deflected towards adjacent stages still causing frac hits or they may steer away from the parent fractures, reducing impact of frac hits (Guo et al. 2018).

1.1.4 Petrophysical Properties

Warpinski and Teufel (1987), King (2014), Kurtoglu and Salman (2015), and Patel et al. (2016) also stressed on the importance of reservoir properties like presence of natural fractures, faults, bedding planes and high-perm streaks in determining the fracture propagation and hence, the extent of frac hits. Presence of natural fractures (Figure 6**b**, Figure 6**c**) and faults (Figure 6**a**) can improve the well connectivity much beyond the primary fracture network and can increase the risk of frac hits. Rivera (2018) studied cores from mineback in Eagle Ford and observed propped horizontal fractures. Elliot and Gale (2018) also analyzed the cores from mineback at Permian HFTS project and found large number of natural fractures connected to hydraulic fractures and filled with proppant (Figure 6**c**). Majority of the recovered proppant was similar to 100-mesh sand injected. They concluded that natural fractures can become a part of propped connected fracture network and increase communication. On the contrary, Litchfield and Lehman (2013) reported that wells that develop planar fractures are more susceptible to long-term inter-well communication post frac hits while wells that develop smaller complex fracture network generally do not suffer long-term consequences of the frac hits. This was attributed to the relative ease of closure of the low-conductivity, smaller-width complex-fractures compared to the high-conductivity, larger-width, propped planar fractures. King (2014) also suggested that in Barnett shale, since fracture network growth is often complex, this might explain the absence of long-

term inter-well communication. Thus, in literature, natural fractures have been reported to both cause and prevent frac hits.

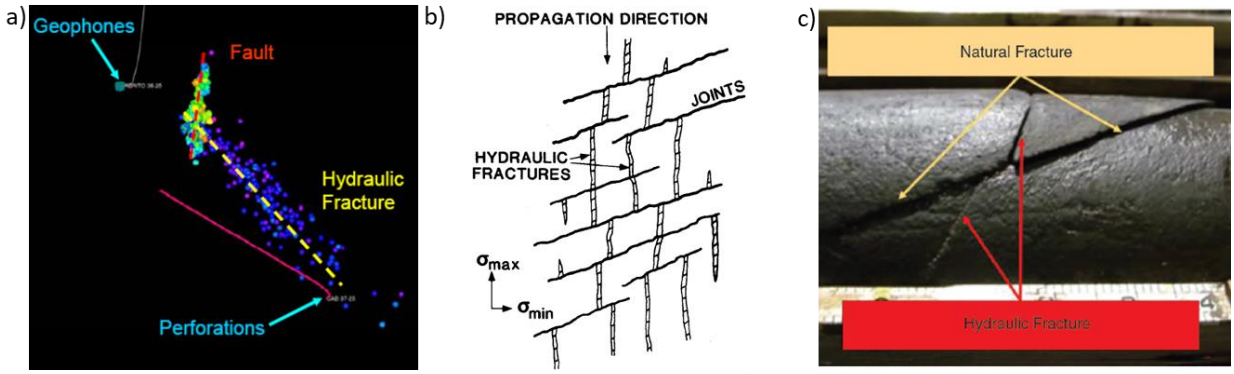

Figure 6: (a) The microseismic data shows fault reactivation during a hydraulic fracture treatment (Warpinski 2009). As the figure shows, wells much farther away from fracked well (beyond the fracture half length) can be affected and experience frac hits due to reactivated fault. (b) Recreation of fracture network around natural fractures based on several mineback experiments (Warpinski and Teufel 1987). Natural fractures can increase connectivity and create a large complex fracture network. (c)) Intersection of hydraulic fracture with natural fractures was found a common occurrence in the cores during mineback studies on the hydraulic fracturing test site 1 in the Permian basin (HFTS 1) (Rassenfoss 2018).

Warpinski et al. (1990) suggested that the orientation of natural fractures with respect to hydraulic fracture is important as hydraulic fractures created parallel to natural fractures may not have significant connectivity. When hydraulic fractures intersect natural fractures, three types of interactions were observed in the mineback experiments. The hydraulic fractures either (1) crossed the natural fracture, (2) were arrested by opening and dilating the natural fracture as indicated by fluid flow along the natural fracture, or (3) were arrested by shear slippage of the natural fracture with no dilation and no fluid flow along the natural fracture. Warpinski and Teufel (1987) showed that the interaction is a function of differential horizontal stress (σ_H - σ_h) and the angle at which the hydraulic fracture approaches the natural fractures. Based on several tests, the authors concluded that hydraulic fractures crossed the natural fractures if differential

stress was high (> 1000 psi) and angle of approach was high (>60º). At high differential stress but low angle of approach (<60 º), authors observed that hydraulic fractures were arrested by shear slippage of the natural fractures. At low differential stress (<1000 psi) and approach angles (<60 º), the fluid pressure in hydraulic fractures was sufficient to open and divert the fluid along natural fractures.

Shear slippage of the natural fractures generally offsets the hydraulic fracture while dilation of the natural fractures generally opens up multiple weakness points along the natural fracture causing multiple fractures. Since, a lot of fluid energy is spent in filling and dilating the natural fractures, they can reduce the primary fracture lengths and heights but on the other hand, they increase complexity and can improve well connectivity beyond the primary fracture. Warpinski (1991) suggested there is a threshold stress (**Equation 1**) above which the natural fractures rapidly open and conductivities increase by an order of magnitude. The natural fractures will dilate if the net treatment pressure exceeds p_f. (υ represents the Poisson's ratio of the rock medium).

$$p_f = \frac{\sigma_H - \sigma_h}{1-2v} \text{.....1}$$

Mineback studies by Warpinski et al. (1993) showed that presence of several bedding planes actually provide an excellent vertical containment for fracture height. Rho et al. (2018) suggested that in layered formations, layers having different mechanical properties lead to weak interfaces which can slip and exhibit shear failure while hydraulic fracturing. The stronger the contrast between mechanical properties, the weaker the interface between them. The slippage and shear failure across the different layers prevents vertical fracture growth and provides excellent confinement. Thus, layered formations appear to be tougher compared to homogenous formations. Rivera (2018) reported that layered rock can be up to 40% tougher than homogenous

rock. This suggests that heterogeneous and layered reservoirs like Wolfcamp may not have large fracture heights and vertically staggering the adjacent wells can reduce the impact of frac hits. A big question is when formation has both weakly bonded bedding planes and natural fractures, which ones get preferentially opened. Warpinski and Teufel (1987) showed the occurrence of shear slippage is governed by a simple linear friction law shown in **Equation 2** where τ is shear stress, τ_0 is the inherent shear strength of the interface between two layers or of a natural fracture, K_f is the coefficient of friction and σ_n is the normal stress. At higher depths in deeper shale reservoirs normal (overburden) stress is much higher compared to horizontal stresses. Thus, shear opening of horizontal bedding planes against overburden is much more difficult compared to shear opening of the natural fractures in which case the normal stress is either σ_H or σ_h.

$$\tau = \tau_0 + K_f \sigma_n \quad \text{.....2}$$

The other important properties of interest are matrix permeability (Lawal et al. 2014, Jacobs 2017a), fracture barriers and pore pressure (King 2014, Kurtoglu and Salman 2015, Patel et al. 2016). The impact of frac hits generally reduces with increasing matrix permeability, increasing vertical to horizontal permeability anisotropy and presence of fracture barriers. Higher pore pressure not only act as a stress barrier diverting the child frac away from the parent well but also provides energy to clean/lift the parent well of the excess water pumped by the child well thus, minimizing the long-term damage caused by a frac hit.

1.1.5 Geomechanical Properties and in-situ Stresses

Eaton's (1975) stress equation (**Equation 3**) gives a simplistic idea of what factors control fracture propagation (Shoemaker et al. 2019). In the equation, S_h is the minimum horizontal stress which the pump pressure must overcome to prevent fracture closure, E_s is the Young's

modulus, ν_s is the Poisson's ratio, S_v is the overburden gradient, α is the Biot constant, P_p is the pore pressure, subscripts h is for horizontal and v for vertical.

$$S_h = \left(\frac{E_{sh}}{E_{sv}}\right)\frac{\nu_{sv}}{1-\nu_{sh}}\left(S_v - \alpha_v P_p\right) + \alpha_h P_p \ldots\ldots\ldots\ldots\ldots\ldots\ldots\ldots\ldots 3$$

Equation 3 reduces to **Equation 4** assuming isotropy, uniaxial strain and neglecting pore pressure. In this case, minimum stress is strongly influenced by Poisson's ratio. Shales and carbonates generally have a higher Poisson's ratio compared to sandstones. Thus, it results in much higher stresses in shales and carbonates which makes them an effective fracture barrier.

$$S_h = \frac{\nu}{1-\nu}(S_v) \ldots\ldots\ldots\ldots\ldots\ldots\ldots\ldots\ldots\ldots 4$$

In **Equation 3**, if formation is considered isotropic, Poisson's ratio is assumed to be 0.25 and α = 1, the **Equation 3** reduces to **Equation 5**. It shows that minimum horizontal stress is directly proportional to pore pressure. Thus, reduction in pore pressure causes reduction in stresses which explains why child well fractures are attracted to parent wells.

$$S_h = \frac{1}{3}(S_v) + \frac{2}{3}(P_p) \ldots\ldots\ldots\ldots\ldots\ldots\ldots\ldots\ldots\ldots 5$$

Theoretically, hydraulic fractures should propagate along maximum horizontal stress direction and the fractures open up against the minimum stress direction. Sharma et al. (2013) carried out experiments on Lyons sandstone and showed unless there is high contrast between minimum and maximum horizontal stresses, hydraulic fracturing is dominated by rock texture (Figure 7).

In shales, stress changes are a cumulative effect of pore pressure depletion and mechanical deformation of the rock. Stress shadow refers to cumulative stress build up within the active well with each subsequent fracture. Stress shadow has a strong effect on fracture geometry especially fracture width as it increases the minimum horizontal stress. Fisher et al. (2004) suggested that fractures (i.e. clusters assuming each cluster gives rise to a fracture) should be placed 1.5 times the fracture height, distance away from each other to avoid stress shadow effects. However, this

may lead to inefficient recovery. Thus, operators resort to smaller cluster spacing which significantly increases the stress shadow effects and reduces the cluster efficiency (Zheng et al. 2019) and fracture widths. Smaller fracture volume and low leak off would contribute to fast propagation of the child well fractures and lead to slender longer fractures (Rainbolt and Esco 2018). Wu et al. (2012) showed the evidence of stress shadow in the microseismic data (Figure 8). They showed the stages in which clusters were tightly spaced, their microseismic cloud had a smaller width, longer length and was more planar. The above discussion clearly shows that stress shadow can cause disproportionate fracture growth in different stages/within stages of the parent and child wells. Few of these stages/clusters having longer fracture lengths in a child well can connect with the parent fracture network and cause frac hits. Thus, higher stress shadow effect can increase the risk of frac hits.

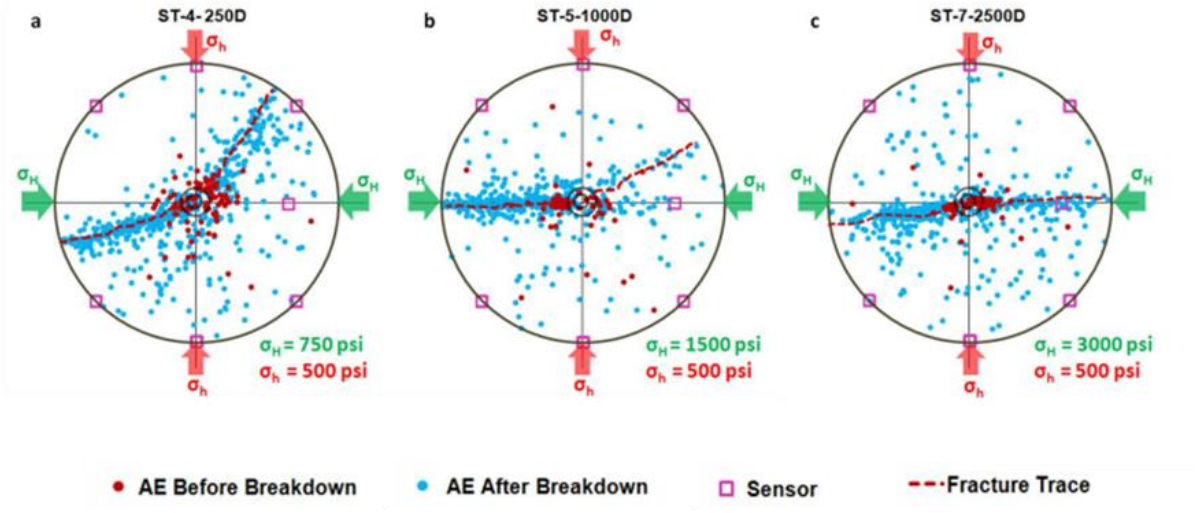

Figure 7: Top view of the acoustic events measured in Lyons sandstone fractured at various horizontal stress differentials. The difference between the minimum and maximum horizontal stress increase from left to right. It is evident that fracture propagates along maximum horizontal stress direction only when the stress differential is large (Sharma et al. 2013). When stress differential is not large, fracture growth is dominated by rock texture.

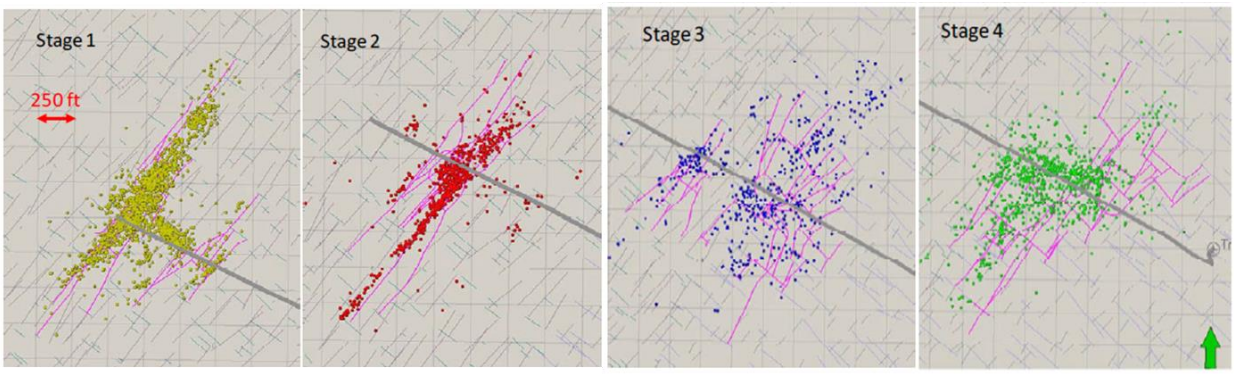

Figure 8: Evidence of stress shadow effects in microseismic data (Wu et al. 2012).The clusters were tightly spaced in stages 1 and 2 compared to stages 3 and 4. The microseismic cloud in stages 1 and 2 has a smaller width, longer length and is more planar compared to stages 3 and 4.

1.2 Impact of Frac Hits

Ajani and Kelkar (2012) are among the pioneers who started investigating the impact of frac hits in unconventional formations. They analyzed daily gas data from 179 horizontal wells in the Woodford formation. They used the 60-day IP (Initial Production) normalized to lateral length as the metric to identify impact of frac hits and found both parent and child wells to be negatively impacted (**Table 3**). Lawal et al. (2014) used rate transient analysis (RTA) to calculate stimulated fracture area and use that to quantify the impact of frac hits. They observed up to 60% reduction in stimulated fracture area of the parent well after a frac hit and a corresponding 16% reduction in cumulative oil production in 20-year period.

Kurtoglu and Salman (2015) did a study on Meramec and Bakken formations and found both instances where the parent wells were positively and negatively impacted by the child fractures (**Table 3**). They concluded that parent wells receiving positive frac hits were characterized by high initial GOR and high current pore pressure. On the other hand, parent wells getting negative frac hits were characterized by low initial GOR and high depletion. Esquivel and Blasingame (2017) analyzed 65 frac hits in Haynesville formation and found that parent wells predominantly get positively impacted by the frac hits though there were some cases in which production

decreased after frac hits (~15% wells). Haynesville has higher pore pressure compared to some of the other US shale plays and this may explain why parent wells seem to recover from frac hits and are even positively impacted. The findings in Haynesville further support the arguments made by Kurtoglu and Salman (2015).

Table 3: Summary of studies analyzing the impact of frac hits on the parent and child wells in unconventional formations. The parent and child impact columns generally show the percent impact on hydrocarbon (oil/gas) production or cumulative oil. For Lindsay et al. (2018) the columns represent the percentage of wells that were negatively impacted by frac hits.

Study	Play	Parent Well Impact	Child Well Impact
Ajani and Kelkar (2012)	Woodford	Negatively Impacted	-43 % (60 Day IP)
Lawal et al. (2014)	Haynesville, Marcellus	-16% (20 Years Cum Oil)	Not Reported
Kurtoglu and Salman (2015)	Meramec	+11% to -26% (EUR)	Not Reported
Kurtoglu and Salman (2015)	Bakken	+9% to -10% (EUR)	Not Reported
Esquivel and Blasingame (2017)	Haynesville	Positively Impacted	Negatively Impacted
Ajisafe et al. (2017)	Avalon	Not Reported	-28% (6-month Oil)
Haustveit & Greenwood (2018)	Meramec	Not Reported	-20% (9-Month Oil)
Lindsay et al. (2018)	Bakken	Not Reported	Negative Impact (74% Wells)
Lindsay et al. (2018)	Barnett	Not Reported	Negative Impact (65% Wells)
Lindsay et al. (2018)	Bone Springs	Not Reported	Negative Impact (61% Wells)
Lindsay et al. (2018)	Eagle Ford	Not Reported	Negative Impact (76% Wells)
Lindsay et al. (2018)	Fayetteville	Not Reported	Negative Impact (73% Wells)
Lindsay et al. (2018)	Haynesville	Not Reported	Negative Impact (79% Wells)
Lindsay et al. (2018)	Marcellus	Not Reported	Negative Impact (66% Wells)
Lindsay et al. (2018)	Niobrara	Not Reported	Negative Impact (66% Wells)
Lindsay et al. (2018)	Wolfcamp	Not Reported	Negative Impact (79% Wells)
Lindsay et al. (2018)	Woodford	Not Reported	Negative Impact (76% Wells)
Cipolla et al. (2018)	Bakken	Positively Impacted	Negatively Impacted
Thomson et al. (2018)	Wolfcamp	-30 to -100 % (~6 Months)	-50 % (EUR)

Lindsay et al. (2018) did study (**Table 3**) in several shale plays and found that majority of the child wells were negatively impacted, only a small percentage of the child wells were positively impacted by frac hits. These wells are likely drilled in a better reservoir quality area compared to the parent wells. Summarizing the different case studies in **Table 3**, it is evident that the child

wells almost always have a negative impact when drilled close to a depleted parent well. The impact of frac hits on the parent wells can be negative or positive. It appears that better cleanup of parent wells post child frac due to higher pore pressure and when parent wells get access to new reservoir through a child fracture network it results in a positive outcome. Negative frac hits in parent wells are more common as they generally have low pore pressure due to depletion and child fracture network can also damage the parent fracture network as shown by Lawal et al. (2014).

The data in **Table 3** suggest a weak play dependence on frac hits in parent wells with Bakken, Haynesville and Meramec having higher proportion of positive frac hits compared to Wolfcamp and Woodford. It seems that the key factors that control positive frac hits in parent wells are higher pore pressure at the time of child well drilling and smaller completion size in parent wells. Since, these factors can be found in other plays as well, positive frac hits can occur in all shale plays.

1.3 Frac Hit Diagnostics

Frac hit diagnostics represent a collection of techniques to evaluate the occurrence and impact of frac hits. These techniques include field diagnostics using surface and downhole pressure gauges, electromagnetic/radioactive proppant, chemical fluid tracers, microseismic acquisition, diagnostic fracture injection tests (DFIT) and stable isotope analysis.

Monitoring well head and bottomhole pressure data in fracked and offset wells is one of the oldest and standard techniques to understand the extent of fracture growth and impact of frac hits on near-by wells (Sardinha et al., 2014; Awada et al.; 2015, Kumar et al. 2018b). The pressure at the offset wells (downhole at ESP intake, or at the well head) is monitored to see if and how much are the offset wells affected by the frac hits. When the fractures of the child well start

communicating with the parent well, the pressures in the parent wells spike up and higher the interaction, larger the spike will be. Operators in recent years have put the pressure data to much more use than its conventional use to detect frac hits. McDowell et al. (2019) based on his observations in Midland basin concluded that slow pressure build-up in an offset well indicates complex fracture network. Cipolla (1996) and King et al. (2008) identified that net pressure continuously rising through the pumping treatment may be an indication of developing complex fractures as well. Sullivan et al. (2019) presented an interesting case study where Chevron used the wellhead pressure data of the fracked child well to estimate the performance of each fractured stage. The authors did the study in Duvernay shale. They plotted the pressure data on pressure versus logarithm of time. The curve ultimately stabilizes when the fracture extension stops and fluid starts leaking-off into the matrix. The slope of this line is called decay exponent and it is indicative of connectivity and fracture complexity. The idea is that the more complex the fracture , the higher the connectivity and faster the leak-off.

Kumar et al. (2018b) analyzed chemical tracer data for 11 wells in the HFTS 1 project. They found that communication existed between all the wells thousands of feet apart (Figure 9). The authors also analyzed the radioactive proppant data (Figure 10) and concluded that proppant generally does not travel as far as fluid, and the frac barrier between middle and upper Wolfcamp was ineffective to prevent frac hits. However, long-term (1-year) pressure interference analysis showed that while pathways within the same zone remain open and wells show communication but inter-zone communication between middle and upper Wolfcamp stopped suggesting closure of vertical connections. Travers et al. (2019) on the other hand used stable isotope analysis to differentiate fracturing water from formation water in Niobrara/Codell formations. They utilized

the natural tracers in the water (oxygen isotope ratio, hydrogen isotope ratio) to identify occurrence of frac hits, extent of their impact, track magnitude and duration of well clean up.

RTA can also be used to identify impact of frac hits (Yadav and Motealleh 2017). Plotting 1/PI versus √t where PI represents well productivity index and t represents production time, results in a straight line with a slope which is a measure of contributing fracture area to flow. The slopes before and after the frac hit could be compared to calculate the increase or decrease in connected fracture area. The advantage of the RTA method over Decline Curve Analysis (DCA) is that it includes pressure which is not accounted by the DCA method. RTA's limitations are; it is only applicable to linear transient flow regime which could be a few years due to ultra-low matrix permeability in shales, an independent measurement of initial reservoir pressure is needed, and high frequency and good quality pressure and flowrate data is required for accurate analysis.

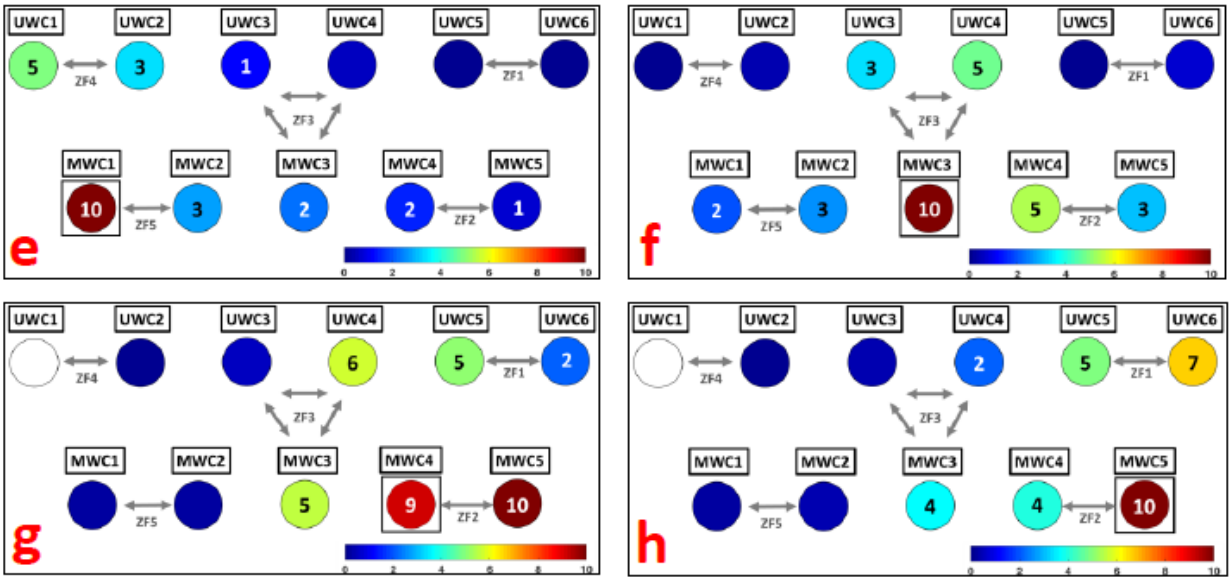

Figure 9: Water soluble chemical tracer analysis. Each graph represents a case study where the well with a black square box around is the well where chemical tracer was injected, and in rest of the wells tracer was monitored during three months of flowback/production. The numbers 1 to 10 represent the degree of connectivity between the two wells, with connectivity increasing from 1 to 10. The well marked in white is the well where no tracer was observed. The authors concluded that the fracture network of 11 wells is connected till at least three months of production (Kumar et al. 2018b).

Several studies (King et al. 2008; Litchfield and Lehman 2013; Sani et al. 2015; King et al. 2017) have pointed out that developing complex fractures reduces the frac hit intensity as the fracture lengths are smaller thus avoiding the fracture network of the adjacent wells. Thus, it is important if during the frac job, there is a way to determine if fracture development is planar or complex. Warpinski (2009) and Cipola et al. (2008) presented detailed studies on using microseismic data beyond its traditional use of determining fracture height, length and SRV. They presented several ways to calculate complexity of the fractures in each stage and for the total well itself.

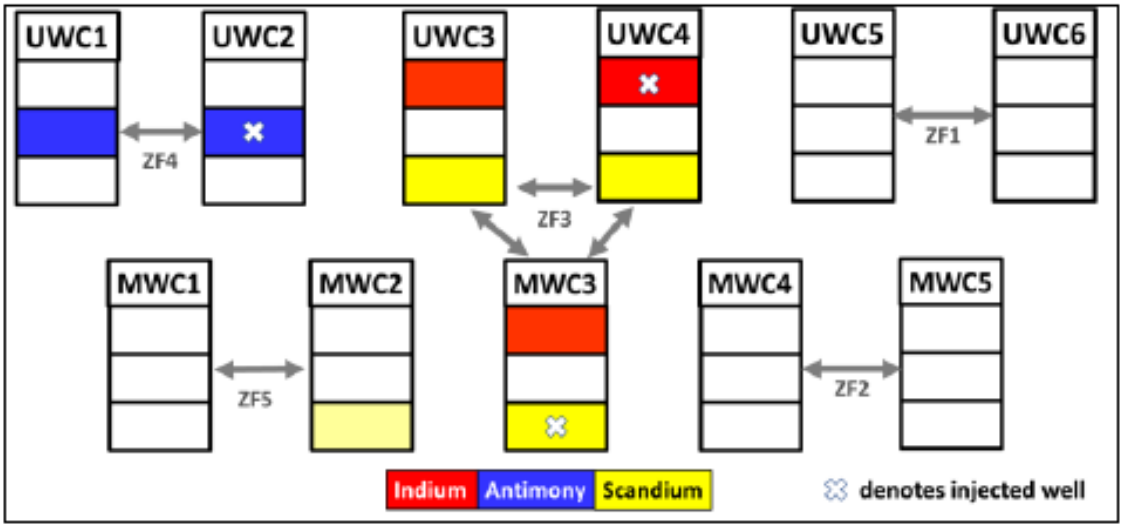

Figure 10: Radioactive proppant data for the case when MWC3 well was injected with radioactive proppant. The corresponding case in Figure 9 is case f. This plot clearly shows that propped fracture pathways were established between upper and middle Wolfcamp shown by Scandium (yellow) tracer tagged to the proppant of middle Wolfcamp well MWC3 being found in the upper Wolfcamp wells UWC3 and UWC4. The frac barrier between middle and upper Wolfcamp was ineffective. The comparison also shows that proppant generally does not travel as far as fluid as wells far away from MWC3 do not see Scandium tracer. (Kumar et al. 2018b).

DFITs are regularly used to estimate pore pressures, initial shut-in pressures (ISIP), breakdown pressure, closure stress, matrix permeability and pressure dependent leak-off in shale reservoirs. These tests are critical for providing data to design completions and for calibration of numerical

and geomechanical models. DFIT can also be used to identify stress barriers. Zones with low porosity and high Process Zone Stress (PZS) which is the difference between the Initial Shut-in Pressure (ISIP) and closure pressure, indicate fracture barriers. Warpinski (1991) showed that pressure dependent leak-off identified in DFITs can be an indication of natural fractures. This is because fluid in the natural fractures can open and dilate them at certain pressure? threshold, after which the leak-off increases tremendously which is identified on a DFIT as pressure dependent leak-off.

Another interesting methodology proposed to determine effective fracture height, child wells responsible for frac hits and production profiling to estimate stage efficiency, is called DNA Diagnostics technology (Lascelles et al. 2017). The idea is that every depth in the reservoir has a unique set of microbes characteristic of that depth due to unique combination of temperature, pressure, water salinity and oil composition at that depth. These microbes can be used to define markers or fingerprints for the entire pay zone. These fingerprints can have multiple applications. For instance, markers developed on a vertical pilot hole can be used to analyze lateral section oil production to determine effective fracture height growth.

1.4 Strategies to Mitigate Frac Hits

One of the simplest strategies to avoid frac hits is to stagger the well placement like a wine rack (Figure 11) to use the inherent permeability anisotropy in shales to an advantage (Jacobs 2017b). Lascelles et al. (2017) found the strategy successful in multi-layered formations like in Permian basin as it avoided frac hits or at least minimized their impact.

The extensive literature survey of the various techniques proposed in the literature to avoid frac hits are summarized in **Table 4.** Completion strategies proposed to reduce fracture growth of child wells into the depleted parent wells is by using far-field diverters in the child wells which

can plug the high permeability pathways/low stress regions and promote complex fracture growth (Gakhar et al. 2017; Jacobs 2018b; Bommer et al. 2017).

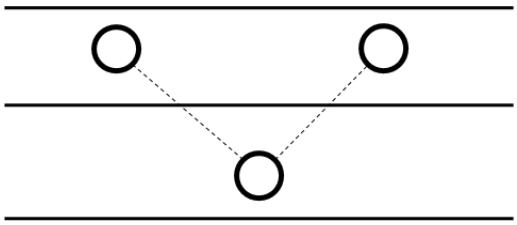

Figure 11: Staggered well placement (wine rack) in multi-layered formation (Jacobs 2017b)

Zipper fracking involves completing multiple wells (generally 2 to 4) at the same time to reduce the stress anisotropy due to parent well depletion. Warpinski (2009) concluded that zipper fracturing approaches increase the amount of microseismicity and promote more complex fractures. This has led to many operators to go for co-development where a large area is developed at once eliminating the parent-child concept. Tank development proposed by Thomson et al. (2018) is a form of co-development (Figure 12**a**). It uses the pressure build up from drilled and completed wells (not producing) to shield the consecutive wells from adjacent producing child wells. Tank development also supercharges the reservoir which promotes increased shear failure leading to more complex fracture systems and larger simulated reservoir area (SRA). Cube development is another form of co-development championed by Encana and later optimized by other operators like Occidental Petroleum (Jacobs 2018a). Figure 12**b** shows a typical schematic of cube development. The technique uses the geomechanical understanding of fracture propagation to create vertical and lateral isolation for the wells drilled thereby allowing symmetric fracture growth and improved productivity. It involves completing over half a dozen or more horizontal wells at the same time. Encana observed 70% rise in well productivity due to cube development. The shortcomings with co-development are that it is capital intensive and if

the area is not as productive as it was thought to be, all this investment can be lost. Moreover, due to long lead times, production is delayed.

Table 4: Summary of studies giving recommendations on preventing and mitigating the occurrence and impact of Frac hits.

Study	Play	Recommendations to Minimize Frac Hits
Ajani and Kelkar (2012)	Woodford	Simultaneous well/pad development
Okouma et al. (2012)	Montney	Smaller cluster spacing
Sani et al. (2015)	Haynesville	Stress barrier in parent wells (reloading with water)
Kurtoglu and Salman (2015)	Meramec	Refracturing or gas loading old parent wells, Simultaneous well development, adjust well spacing or completion design
Anderson et al. (2016)	Eagle Ford	Pinpoint (Single entry point per stage) completions
Patel et al. (2016)	Eagle Ford	Staggered zipper fracking
Schaeffer et al. (2017)	Wolfcamp	Track drilling gas (proxy for reservoir permeability)
Gakhar et al. (2017)	Eagle Ford	Refracturing/Recharging parent well, fiber-based diverters
Barree et al. (2017)	Bakken	Refracturing parent well
Bommer et al. (2017)	Bakken	Recharging parent wells, diverters in parent wells
King et al. (2017)	Woodford, Eagle Ford	Step-wise ramp-up of fluid injection rate, Shut-in of young wells and recharging/refracturing old wells, diverters and blocking agents, offsetting perforations in parent-child wells, reduce completion size, sand slugs.
Esquivel and Blasingame (2017)	Haynesville	Refracturing parent wells
Ajisafe et al. (2017)	Avalon	Vertically offset child wells
Rafiee and Grover (2017)	Eagle Ford	Stacked/Staggered development
Bommer and Bayne (2018)	Bakken	Recharging parent wells
Lindsay et al. (2018)	Multiple	Simultaneous development, completion optimization, diverters, refracturing parent wells, enhanced oil recovery (EOR)
Whitfield et al. (2018)	Eagle Ford	Recharging parent wells
Cipolla et al. (2018)	Bakken	Microseismic depletion delineation (MDD), spacing and completion design optimization
Manchanda et al. (2018)	Wolfcamp	Refracture parent well, optimize completion design
Swanson et al. (2018)	Woodford	Surfactants/Chemical remediation
Thomson et al. (2018)	Wolfcamp	Tank development (different from simultaneous or sequential development)
Vidma et al. (2019)	Bakken	Far-field diverters
Zheng et al. (2019)	Wolfcamp	Gas loading in parent wells
Wutherich et al. (2019)	Utica	MSE to identify depleted zones in child wells
Xu et al. (2019)	Wolfcamp	Surfactants/Chemical remediation
Li et al. (2019)	Eagle Ford	Parent well water injection

Since, one of the biggest causes of frac hits is parent well depletion, numerous authors (**Table 4**) have recommended repressurization of the parent wells to build a stress barrier which protects the parent wells as well as promote symmetric fracture growth in child wells. But many case studies also show that clay swelling and increased capillary pressure in such cases lead to lower productivity in the parent wells after flow back (Zheng et al. 2019). This effect is especially more pronounced in gas reservoirs. Zheng et al. (2019) recommended loading wells with gas instead of water to avoid clay swelling and water blockage. Based on their modeling results, they observed that soaking (shutting the parent well) after repressurization results in diffusion of the injected fluid deeper into the formation. Thus, its efficiency as a protective barrier is reduced. Some authors (Barree et al. 2017 and Manchanda et al. 2018) believe water pressurization is not enough as it is difficult to compensate for years of production and difficult to inject far away from the current fracture network due to low permeability in shales. They recommend refracturing the wells as it can build a stronger stress barrier around the parent wells and simultaneously increase the SRA in the parent wells as well. Vincent (2010) provided an excellent collection of 100 case studies of refracturing, summarizing the key learnings. He pointed out that highly depleted wells may have difficulty in recovering the fracture fluids during flow back which can create water blockage. Also, it is important to check the mechanical integrity of the casing to make sure it can sustain a refracturing operation. Barree et al. (2017) pointed out that refracturing may be beneficial in cases where initial completion design was poor, tracer studies show unstimulated areas, and well has not reached boundary dominated flow as after that it becomes tougher to increase reservoir contact area through refracturing. Hou et al. (2017) recommended refracturing using gases like CO_2 and N_2 to avoid clay swelling and pore blockage. Their results also showed that lower gas injection rates while hydraulic fracturing as

opposed to high injection rates lead to lower breakdown pressures and more complex fractures. They attributed this to the gas invasion into the pore space when injection rates are lower. The gas invasion increases the pore pressure and destabilizes the rock around the injection point creating multiple microcracks causing breakdown at a lower pressure. Hubbert and Willis (1957) proposed the equation for formation breakdown pressure, **Equation 6**. The breakdown pressure (p_{bd}) is a function minimum horizontal stress (S_h), maximum horizontal stress (S_H), tensile strength (T_o) and pore pressure (P_p). The equation can be used to quantify the reduction in breakdown pressure by increasing the pore pressure.

$$p_{bd} = 3S_h - S_H + T_o - P_p \quad \text{.....6}$$

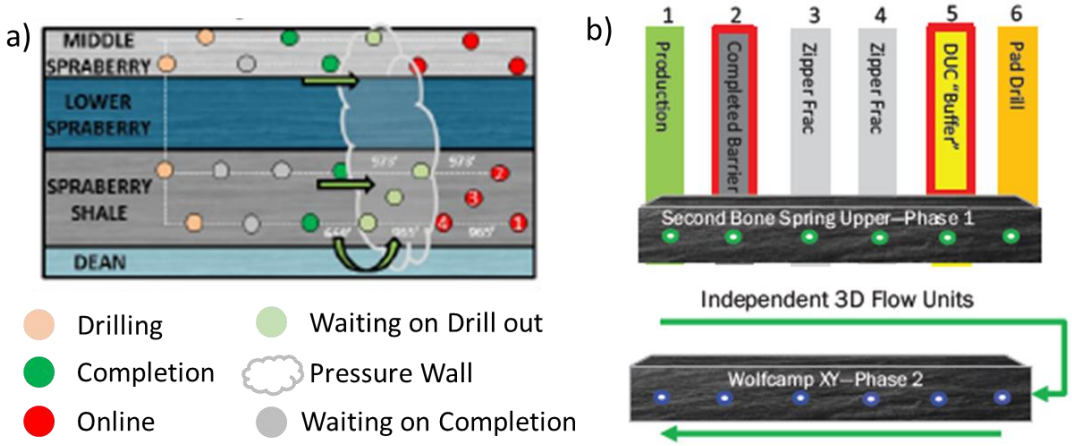

Figure 12: (a) Tank development proposed by Thomson et al. (2018). The development goes from right to left. The first set of wells (red bubbles) are zipper fracked. They are completed but not brought online until the light green wells are drilled and fracked. Subsequently, the red wells are brought online. Next, the dark green wells are drilled and fracked. The light green wells are not yet producing. They not only create a stress barrier but also supercharge the formation which leads to higher complexity symmetric fractures in the dark green wells. This process is repeated from right to left. (b) Cube Development (Jacobs 2018a): Wells 1 and 2 are drilled using Zipper frac method. While well 1 is brought on production, well 2 is kept shut. This second well acts as a barrier or pressure wall and its purpose is to protect the next set of wells from frac hits. Subsequently, wells 3 and 4 are Zipper fracked. Zipper fracking generates more complex fracture networks but also saves costs by using the completion crews more efficiently. Well 5 is drilled but not completed (DUC) to prevent interference between the wells that are Zipper fracked and other wells being completed on the other side of DUC. Development generally follows from shallower to deeper zones.

1.5 Organization of Chapters

The second chapter discusses about the different decline curve analysis (DCA) methods commonly used to model production in unconventional reservoirs. The accurate prediction of impact of frac hits requires accurate production modeling. An ideal DCA method should be capable of simultaneously modeling the flow regime prevalent around the well and the changes in reservoir properties with time, to be able to successfully represent the production performance of the well and predict in future. To complement the work on frac hits in this study, a new simplified decline curve equation is proposed by modifying the existing Arps exponential decline equation, where the constant decline rate is replaced by a power-law function variable decline rate. This method is very robust and can account for different flow regimes and changes in fracture conductivity with time.

The third chapter talks about utilization of information commonly available in public databases like the production and completion data. An automated machine-learning workflow was developed which helped analyze over 6000 wells from Meramec, Woodford and Wolfcamp to understand the impact of frac hits on parent and child wells production. Regression models were also developed to predict the impact of frac hits based on parameters like parent-child spacing, completion size and parent well production characteristics before the frac hit. which are available in the public databases. These regression models are then coupled with economic analysis to determine optimum spacing for any given completion design or optimum completion design for any given spacing.

In order to understand impact of frac hits and develop mitigation strategies, the connection between frac hits and petrophysical or geomechanical properties of rock must be understood. Thus, an independent analysis was done in small regions where extensive data like core, logs,

microseismic and fiber optics were available to tie the impact of frac hits to the petrophysical and geomechanical properties of the rocks. The fourth chapter talks about one such study done in Meramec formation. The logs were used to calculate pore pressure and closure stress profiles, mechanical properties like Young's modulus and Poisson's ratio. Fracture modeling and microseismic data helped understand fracture growth i.e. fracture dimensions, complex versus planar fracture networks, stage interactions and stress shadow effect. This additional information provided critical insights into frac hits and how they can be managed.

In chapter five, extensive numerical modeling in GOPHER was done for the same area as analyzed in chapter four, to carry out sensitivity studies with different completion design parameters. Field tests for various combinations of different completion design parameters are rarely available. Numerical modeling offers a reliable and cheap alternative to evaluate various designs and study their impact on well productivity and ability to minimize frac hit risk.

Chapter six discusses another study which was done in Marcellus where a variety of surface and downhole information like triple combo and sonic logs, drilling data, fiber optics data, image logs and microseismic were available. All the data were available in vertical as well as lateral sections. Particularly interesting was the role of natural fractures which had a strong impact on both well productivity and fracture geometry. The analysis show that determining natural fractures across the lateral length can play a key role in minimizing the frac hits in this area. Further, a machine-learning workflow was developed to use the drilling data to determine three different facies with different natural fracture density characteristics.

Finally, chapter seven of the dissertation concludes with a recommended approach to manage frac hits. The approach combines reservoir characterization, frac hit diagnostics, numerical and empirical modeling, available production and completion data analysis to make key decisions

regarding parent-child spacing, completion design and child well scheduling with respect to parent wells to minimize frac hits and maximize economic returns.

Chapter 2: Variable Exponential Decline - Modified Arps

Different Decline Curve Analysis (DCA) methods have been proposed to predict production performance of both conventional and unconventional shale reservoirs. These methods range from empirical to semi-empirical and theoretical. The different methods were developed on specific datasets, have their own assumptions and limitations and thus, are not applicable universally. An ideal DCA method should be capable of simultaneously modeling the flow regime prevalent around the well, changes in reservoir properties with time, represent the production performance of the well and predict future production. In shales, flow regimes can be linear, bilinear, multi-fracture linear, post-linear, stimulated reservoir volume (SRV) dominated boundary flow and compound linear The change in fracture conductivity due to fines migration, embedment, crushing, diagenesis and changing stresses due to production, is another important phenomenon that a DCA method must account for. On close examination, it was found that both the linear flow regimes and changes in fracture conductivity with time follow a power-law function. A new simplified decline curve equation is proposed by modifying the Arps exponential decline equation, where the constant decline rate is replaced by a power-law function variable decline rate. The application of this method is shown using production data from both gas shales like Haynesville and liquid rich-shales like Eagle Ford. The average error in cumulative production prediction for 20 wells was found to be only 3% in Haynesville wells and 2% in Eagle Ford wells. This method is very robust and can be applied to both gas and liquid-rich shales.

2.1 Existing DCA Methods – Advantages and Disadvantages

Production performance prediction in shale reservoirs is affected by many factors like geological complexities, presence of natural fractures, in-situ stress states, completion and fracture

characteristics and multi-phase flow characteristics. (Kabir et al. 2011). Complex fracture geometries and nano-Darcy permeabilities of the matrix make it impractical to run numerical models to simulate the well production performance. Moreover, due to the cost, effort, and time required in numerical simulation, many operators resort to semi-analytical and empirical models. These methods require much less data than numerical models and are much faster.

The most common DCA methods that have been historically applied to shale reservoirs are Arps (1944), Fetkovich (1973), Hsieh (2001), Blasingame and Rushing (2005), Ilk et al. (2008), Valko and Lee (2010), Duong (2010), Fulford and Blasingame (2013) among others. The first four methods originally developed for conventional reservoirs find use in unconventional reservoirs, though with certain limitations. On the other hand, the latter methods were specifically developed for unconventional shale reservoirs.

Arps (1944) published three empirical equations to predict production performance of wells. These were exponential, hyperbolic, and harmonic. These equations were valid for reservoirs producing at constant bottomhole pressure (BHP). The reservoir and fluid properties were assumed constant throughout the life of the well. Also, the Arps solution was valid only if the well did not encounter any workover/well intervention in the future. **Table 5** shows the different Arps equations. Arps hyperbolic and harmonic equations are more suitable for solution-gas drive and water drive reservoirs while exponential equation is suitable for finite reservoirs with no pressure support.

Table 5: Equations for exponential, hyperbolic and harmonic published by Arps (1944)

Exponential Decline	Hyperbolic Decline	Harmonic Decline
$q = q_i e^{-D_i t}$	$q = q_i[1 + bD_i t]^{-1/b}$	$q = q_i[1 + D_i t]^{-1}$
$D = D_i$	$D = aq^b, D_i = aq_i^b$	$D = aq, D_i = aq_i$
$D = D_i$	$D = \frac{1}{1/D_i + bt}$	$D = \frac{1}{1/D_i + t}$

In the equations, q refers to the gas production rate, q_i is the initial production rate, t refers to the time in days, D is the instantaneous decline rate, D_i is the initial decline rate, and b is the decline exponent. Fetkovich (1973) showed the theoretical basis behind the Arps empirical equations by combining the constant pressure solutions of Moore, Schilthuis, Hurst and Van Everdingen with material balance equations (Craft and Hawkins 1959). He developed type curves which combined the transient solution for early time flow with Arps empirical equations for late time flow. He also observed that b values greater than 1 are required to match the early time transient data if Arps hyperbolic equation were to be used.

The drawbacks of Arps and Fetkovich equations were that reservoir and fluid properties were assumed constant throughout the life of the reservoir. However, it is well known that these properties change as a function of time or production. Hsieh (2001) postulated that permeability to oil phase consistently decreases as a function of time due to pore compaction, increase in GOR, and water influx from WOC. Thus, the decline rate itself is a function of time. He proposed a time-dependent Darcy equation to model the change in reservoir properties. **Table 6** shows the equations proposed by Hsieh (2001). The instantaneous decline rate, D is calculated by using the equation D = -1/q (dq/dt). n is the decline exponent and m is the hysteresis exponent in **Table 6**. He also showed using Arbuckle lime production data that his equation gave a better fit then earlier proposed methods.

Table 6: Decline Curve Equations Proposed by Hsieh (2001).

Hsieh Time-Dependent Darcy Equation	Decline Rate, D
$q = q_i t^{-(n+mt)}$	$D = m(1 + lnt) + n/t$

Blasingame and Rushing (2005) proposed a “quadratic” rate-cumulative correlation which was based on a rigorous coupling of the material balance equation for dry gas reservoir and the

stabilized flow equation for a reservoir producing at a constant BHP. The said correlation considered the change in gas properties as a function of pressure. Thus, the advantage of Blasingame's equation over Hsieh's equation was that it had a theoretical basis. **Table 7** shows the equations proposed by Blasingame and Rushing (2005) where G_p is the cumulative produced gas, G is the gas in place, p and z are pressure and gas deviation factors, respectively. Subscript wf refers to bottom hole flowing conditions while i refer to initial reservoir condition. During initial production period, when $G_p << G$, the third term in the equation is negligible and the Blasingame equation reduces to exponential decline.

Table 7: Decline Curve equations proposed by Blasingame and Rushing (2005)

Blasingame and Rushing (2005) Equation	Initial Decline Rate, Di
$q = q_i - D_i G_p + \frac{1}{2}\frac{D_i}{G} G_p^2$	$D_i = \frac{2q_i}{[1 - [\frac{p_{wf}/z_{wf}}{p_i/z_i}]^2]G}$

With increasing interest in shale reservoirs, the Arps, Fetkovich and Blasingame equations were also applied to the shale wells. Many operators found that hyperbolic equation with b=2 fitted very well to the production data from hydraulically fractured shale wells. Okouma et al. (2012) showed that the flow regimes experienced by a fractured horizontal shale well during early time is either linear flow, bilinear flow or multi-fracture flow. All of these are power-law flow regimes where flow rate is a function of time raised to some exponent. The hyperbolic equation itself can be reduced to a power-law form under certain conditions ($bD_{it}>>1$). Under these circumstances, with values of b = 2, 3 and 4, hyperbolic equation can model linear flow, multi-fracture flow and bilinear flow, respectively. Thus, this explains the widespread application of hyperbolic equation to predict shale well production performance. However, fitting the early time data with b >= 2 and extrapolating the same curve at late times, almost always leads to overestimation of reserves (Rushing et al. 2007 and Lee and Sidle 2010). The industry practice is

to fit the hyperbolic decline at early time and then at the end of linear flow, apply exponential decline (called composite decline curve model, Childers and Callard 2015). This assumes that the well enters the SRV dominated boundary flow. Another major assumption in this method is that reservoir properties do not change throughout the well life. This is not true as we will see later and thus, the application of composite decline curve model may induce some errors in the EUR estimation.

Many other researchers came up with specialized correlations for predicting shale well production performance. Ilk et al. (2008) proposed the Power-Law loss ratio model. **Table 8** shows the equation proposed by them. D_1 in the equation refers to decline rate after one-time unit and D_∞ refers to the decline rate at large time when the well has entered SRV dominated flow. At large time, the decline rate becomes constant and the power-law exponential (PLE) equation reduces to the exponential decline equation. The authors proposed that their model is flexible enough to model transient, transition and boundary dominated flow. This model like the composite decline model follows the assumption that the well enters the SRV dominated boundary flow at late times and the reservoir properties are constant. In the PLE model, there is no easy way to calculate the constants like D_∞, D_1 and n using the production data. If the early data is noisy, D_1 calculation might have considerable error. D_∞ and n can only be estimated through trial and error.

Table 8: Decline Curve equations proposed by Ilk et al. (2008)

Ilk et al. (2008) Power-Law Loss Ratio	Decline Rate or Loss ratio, D
$q = q_i \exp\left[-D_\infty t - \frac{D_1}{n} t^n\right]$	$D = D_\infty + D_1 t^{-(1-n)}$

Valko and Lee (2009) came up with another model called the Stretched Exponential Production decline (SEPD) which is based on the concept that production decline is made up of a large

number of contributing volumes, each of which is in exponential decline. The authors proposed that this model takes the heterogeneity of the reservoir into account. **Table 9** shows the equations proposed by Valko and Lee (2009). τ in the equation refers to the characteristic time parameter for the SEPD model.

Table 9: Decline Curve equations proposed by Valko and Lee (2009)

Valko and Lee (2009) SEPD	Decline Rate, D
$q = q_i \exp\left[-\left(\frac{t}{\tau}\right)^n\right]$	$D = \left(\frac{1}{\tau}\right)^n n t^{n-1}$

The equation for D not given in the original paper was simply calculated by using the formula D = -1/q (dq/dt). Taking log on both sides, the parameters τ and n can be calculated by plotting Log D (calculated from production data) versus Log t. The key advantage of the model is that for positive values of n, τ and q_i, the equation gives finite EUR even if no cutoff in rate or time is applied.

Duong (2010) proposed an empirical model developed from the observation that a log-log plot of rate over cumulative production versus time is fits a straight line. The assumption behind the model is that well production is dominated by linear or bilinear fracture flow and that wells rarely reach boundary dominated flow. **Table 10** shows the equation developed by Duong (2010). c in the equation refers to intercept constant. The equation for D not given in the original paper was simply calculated by using the formula D = -1/q (dq/dt). The equation proposes that at large times, if m <1 and a is positive, then q tends to q_i which does not seem logical. The author did observe m values > 1 for all the shale wells but he also observed values of m <1 for tight conventional reservoirs. The author suggested that the pseudo steady state flow in conventional reservoirs caused m values to be less than 1. Additionally, the initial decline rate in certain cases was found to be negative suggesting that the well flow rate increases with time. This

phenomenon observed in the shale reservoirs is due to well cleanup and fracture efficiency and not related to reservoir properties and fracture flow regimes.

Table 10: Decline Curve equations proposed by Duong (2010)

Duong (2010)	Decline Rate, D
$q = q_i t^{-m} e^{\frac{c}{1-m}(t^{1-m}-1)}$	$D = \frac{m}{t} - \frac{c}{t^m}$

Another important method developed for time-rate performance analysis of liquid-rich shales is the 'Transient Hyperbolic' relation developed by Fulford and Blasingame (2013). The method uses a hyperbolic function (with b_{max}) to represent early time linear flow and another hyperbolic function (with b_{min}) to model terminal production behavior of non-interfering fractures. Like Duong, transient hyperbolic decline method assumes that the well has not reached boundary dominated flow. The equation for rate and decline rate are given in **Table 11**. The key parameters in the equation like time to end of linear flow (t_{elf}), time to start of boundary flow (t_{bdf}), b_{max}, b_{min}, c_f which governs the transition between initial and final hyperbolic declines. make the method robust to model a variety of production scenarios. However, at the same time, estimating values for these constants for reservoirs where little is known about them can become difficult and hinder the application of this method.

Table 11: Decline Curve equations proposed by Fulford and Blasingame (2013)

Fulford and Blasingame (2013)
$q = q_i exp\left[-\int_0^t \frac{dt}{\frac{1}{D_i} + b_{max}t + \frac{b_{max}-b_{min}}{c_f}\left[Ei\left[-exp\left[-c_f(t-t_{elf}) + exp[\gamma]\right]\right] - Ei\left[-exp\left[-c_f t_{elf} + exp[\gamma]\right]\right]\right]}\right]$
$D(t) = \frac{1}{\frac{1}{D_i} + b_{max}t + \frac{b_{max}-b_{min}}{c_f}\left[Ei\left[-exp\left[-c_f(t-t_{elf}) + exp[\gamma]\right]\right] - Ei\left[-exp\left[-c_f t_{elf} + exp[\gamma]\right]\right]\right]}$

2.2 Need for a New Method

The accurate prediction of the impact of frac hits requires accurate production modeling and forecasting. The unconventional shale production is mainly dominated by fractures (Ilk et al. 2008; Valko and Lee 2009; Duong 2010). Thus, the production in shale reservoirs has a strong dependence on the fracture permeability/conductivity. Therefore, if the fracture permeability changes with time, it will change the production accordingly. Many researchers (Zhang et al. 2014 and Mittal et al. 2017) have shown that the fracture permeability decreases as a power-law function with time. Thus, a very important assumption in the various DCA models that reservoir and completion properties do not change with time does not hold true. As long as the fracture permeability is changing in the well, the decline rate will be changing and thus, will not be constant. Therefore, the well cannot experience exponential decline. Researchers argue that the production continually changes the stress-field around the well. Thus, it may be impacting the fracture permeability as long as the well is producing. Therefore, a fractured shale well may never see an exponential decline during its production life. In practice, after prolonged production, the rate of change of fracture permeability is very small essentially acting like a constant. It is to be noted that this effect has nothing to do with flow regime around the well because changes in flow-regime are additional independent components which must be looked separately.

Fractured shale wells experience a large variety of flow regimes depending on well type, number of fracture stages, well and fracture stage spacing and matrix permeability. Shale wells generally experience linear, bilinear flow, multi-fracture flow during early time, and SRV dominated boundary flow, compound linear flow, post-linear flow during late times (Okouma et al. 2012 and Bone et al. 2017). Generally, any kind of linear flow can be modelled by a power-law

equation as shown by Okouma et al. 2012. Similarly, any kind of boundary dominated flow can be approximated by constant decline rate or exponential decline model.

Thus, in an actual shale well, the resultant decline rate or production performance is governed by the coupled effects of change in reservoir, completion properties, and flow regimes. For instance, the decline rate during early time may be a coupled effect of infinite conductivity linear fracture flow and the declining fracture permeability. Thus, the decline rate seen in the production data is a sum of power-law decline due to linear flow and another power-law decline due to fracture closure. During late time, the flow regime may change to SRV dominated boundary flow which can be represented by a constant decline while fracture conductivity may still be declining following a power-law function. Basic algebra suggests that sum of /difference of/multiplication of two power-law functions give a power-law function. Similarly, adding, subtracting, multiplying, or dividing a power-law function by a constant also gives a power-law function. This is revealing because it suggests that as long as fracture conductivity/reservoir properties are changing with time (due to production), no matter what the flow regime is, well production will experience a power-law decline. To show the behavior of the actual field decline rate, production data for 2755 wells were taken from Haynesville shale. The 6-months, 12-months, 24-months, and 60-months cumulative production was extracted for each well and cross-plotted with each other to calculate the decline percentage as shown in **Figure 13**. For instance, the top-right plot shows that 12-months production is roughly 1.55 times the 6-months production. Thus, from 6-12 months, the production declines by 45%. The monthly decline during this period is 45/6 = 7.5 %. Similarly, the monthly declines were calculated for the other two plots. The plot at bottom left shows that the monthly decline plotted for the three periods and it suggests that decline rate in Haynesville can be modelled using a power-law function. Therefore, based on this revelation,

a new decline curve equation was created by replacing the constant decline rate in Arps exponential equation with a power-law decline rate. The power-law function can account for both changes in fracture permeabilities and different flow regimes, thus giving a better fit and forecast for the production data in shales.

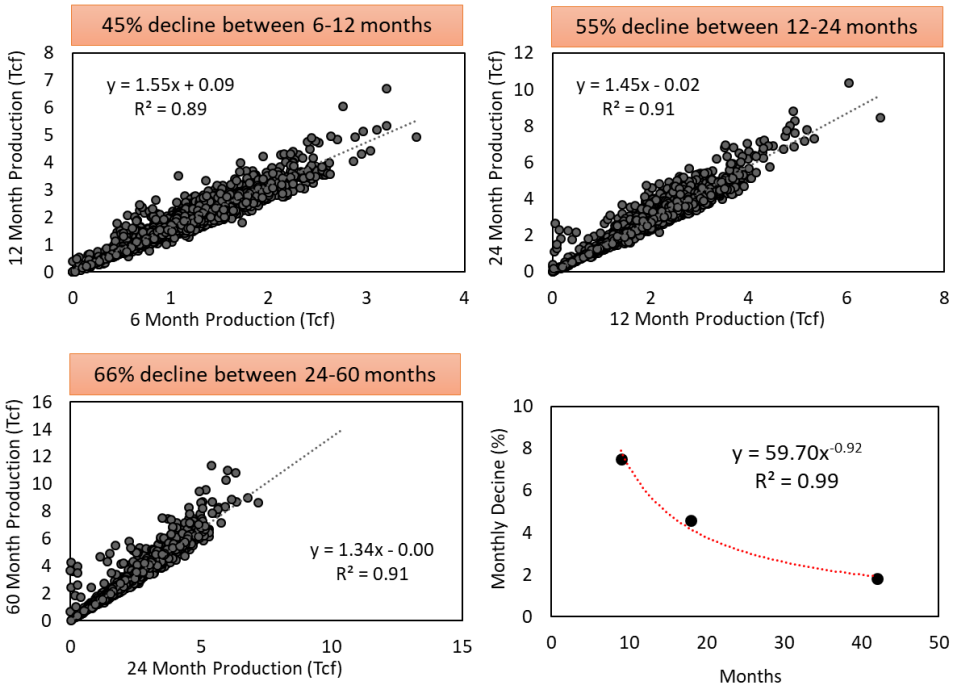

Figure 13: Data from 2755 wells in Haynesville. The 6-months, 12-months, 24-months, and 60-months cumulative production are cross-plotted with each other to calculate the decline percentage. For instance, the top-right plot shows that the 12-months production is roughly 1.55 times the 6-months production. Thus, from 6-12 months, the production declines by 45%. The monthly decline during this period is 45/6 = 7.5 %. Similarly, the monthly declines were calculated for the other two plots. The plot at bottom left shows that the monthly decline plotted for the three periods and it suggests that the decline rate in Haynesville can be modelled using a power-law function.

2.3 Derivation of Variable Decline Modified Arps (VDMA)

The petrophysical measurements and the field data both corroborate that decline rate in unconventional shales follows a power-law function. This relation can be generalized using

Equation 7. In the equation, constant 'a' governs the rate of change of initial decline rate D_i. This power-law function decline rate (D_{PL}) can account for both the different linear flow regimes and changes in fracture conductivity.

$$D_{PL} = D_i t^{-a} \quad \text{.....(7)}$$

The exponential decline equation (**Equation 8**) is limited by the fact that decline rate is assumed constant. However, this equation can be generalized by replacing the constant Decline Rate (D_i) with variable decline rate D_{PL} from **Equation 7**. The resultant equation is shown as **Equation 9** and **Equation 10** represents the final simplified form (Variable Decline Modified Arps, VDMA model).

$$q = q_i e^{-D_i t} \quad \text{.....(8)}$$

$$q = q_i e^{-D_i t^{-a} t} \quad \text{.....(9)}$$

$$q = q_i e^{-D_i t^{(1-a)}} \quad \text{.....(10)}$$

Next, there was a need to identify if parameters D_i and a can be obtained from the production data, instead of using trial and error. By definition, D = -1/q (dq/dt). Thus, differentiating **Equation 10** with respect to t, we get **Equation 11**.

$$\frac{dq}{dt} = -q_i D_i (1-a) t^{-a} e^{-D_i t^{(1-a)}} \quad \text{.....(11)}$$

Now multiplying both sides with -1/q, LHS becomes D. Also, using the value of q from **Equation 10** on RHS, it simplifies to **Equation 12**.

$$D = D_i (1-a) t^{-a} \quad \text{.....(12)}$$

Now, taking log on both sides, **Equation 12** can be represented as

$$\text{Log } D = Log\big(D_i(1-a)\big) - aLog(t) \quad \text{.....(13)}$$

Equation 13 shows that calculating D from the field production data using D = -1/q (dq/dt) and then cross-plotting it with Log t, the slope gives the value of 'a' and the intercept can give value

of D_i. Here, D_i represents the initial decline rate and 'a' is the decline rate exponent. 'a' determines the rate of change of decline rate. They are both functions of completion parameters and reservoir properties. Best wells are characterized by low initial decline rate due to larger SRV and stronger matrix support (due to higher matrix permeability and porosity) and the decline rate changes little with time, therefore, a smaller value of decline exponent 'a'. On the other hand, poor wells are characterized by higher initial decline due to smaller SRV and inadequate matrix support.

It is noteworthy to highlight that Variable Decline Modified Arps (VDMA) model reduces to exponential decline for the limiting case when 'a'=0. Also, as time approaches infinity, D and q both approach 0. This represents the hypothetical case where fracture is completely closed. This also shows that the model is self-constrained and would not lead to over-estimation of reserves.

2.4 Application of VDMA to Haynesville and Eagle Ford

Twenty wells were taken each from Haynesville shale (dry gas) and Eagle Ford shale (liquids-rich) for applying the VDMA model to predict the production performance (**Figure 14 and Figure 15**). Ideally, the production data can be used to calculate both D_i and 'a'. But, the production data was taken from a public database and it represents the back allocated data based on random field well tests. Typically, the production is measured at a battery or collection tank connected to several wells. Production well tests done randomly on individual wells is used to allocate the continuous battery production back to individual wells. Thus, the data is noisy and as can be seen in the graphs on the left-hand side, the actual decline rate calculated from the production data is noisy too. Thus, the workflow followed was to use trial and error to estimate D_i and 'a' to best fit the 12-month data and then extrapolate the fit and compare it with the actual production data. The graphs on the right-hand side show the actual production data and predicted

profiles from VDMA equation. The arrow marks the 12-month production till which, the production data was used for the fit. Finally, a QC step was to use the estimated D_i and 'a' values and calculate a value of Decline rate (D, from **Equation 12**) and plot it on the left-hand side graphs to compare with the actual D values. If the fit was widely off, then new values of D_i and 'a' were estimated. The noise in the decline rates is higher for liquid-rich Eagle Ford shale wells compared to dry-gas Haynesville wells. This is expected because in Eagle Ford wells, gas production along with oil production affected the decline-mechanism of primary oil phase and caused greater noise.

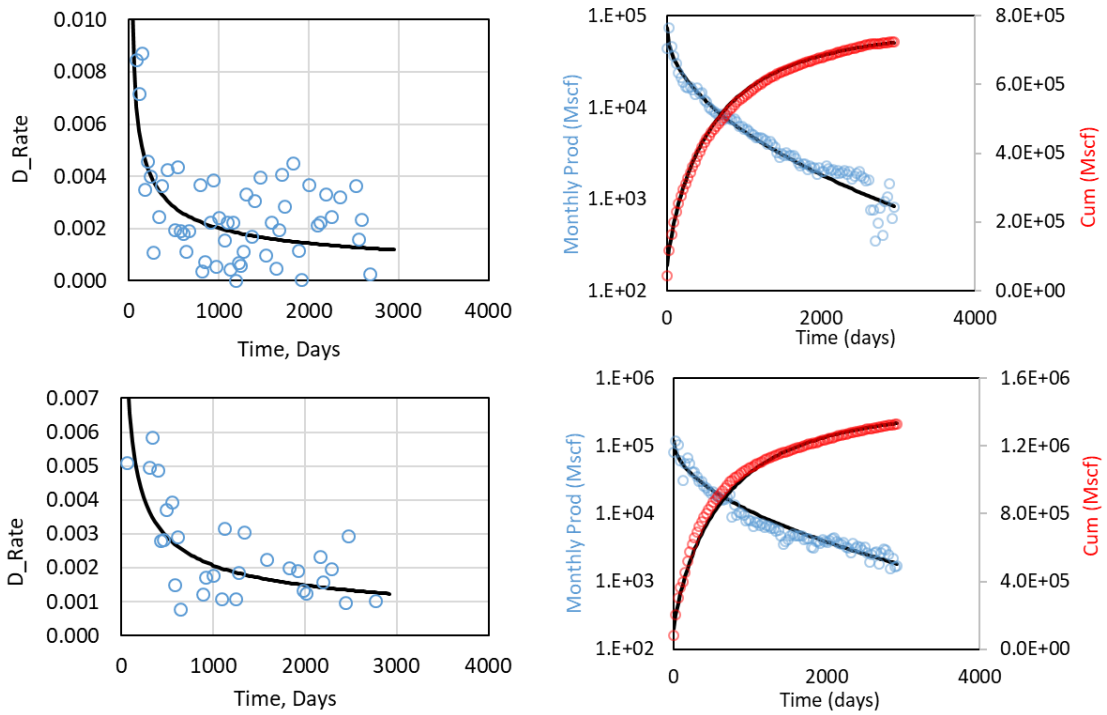

Figure 14: Variable Decline Modified Arps (VDMA) equation applied to actual field wells from Haynesville. Two wells are shown out of the 20 wells in which the same exercise was carried out. The graphs on the right-hand side show the actual production data (red and blue bubbles) and predicted profiles (black curves) from VDMA equation. The arrow marks the 12-month production, which was used for the fit. The LHS plots show the predicted decline rate (black curve) along with the calculated decline rate (bubbles) from the observed production data.

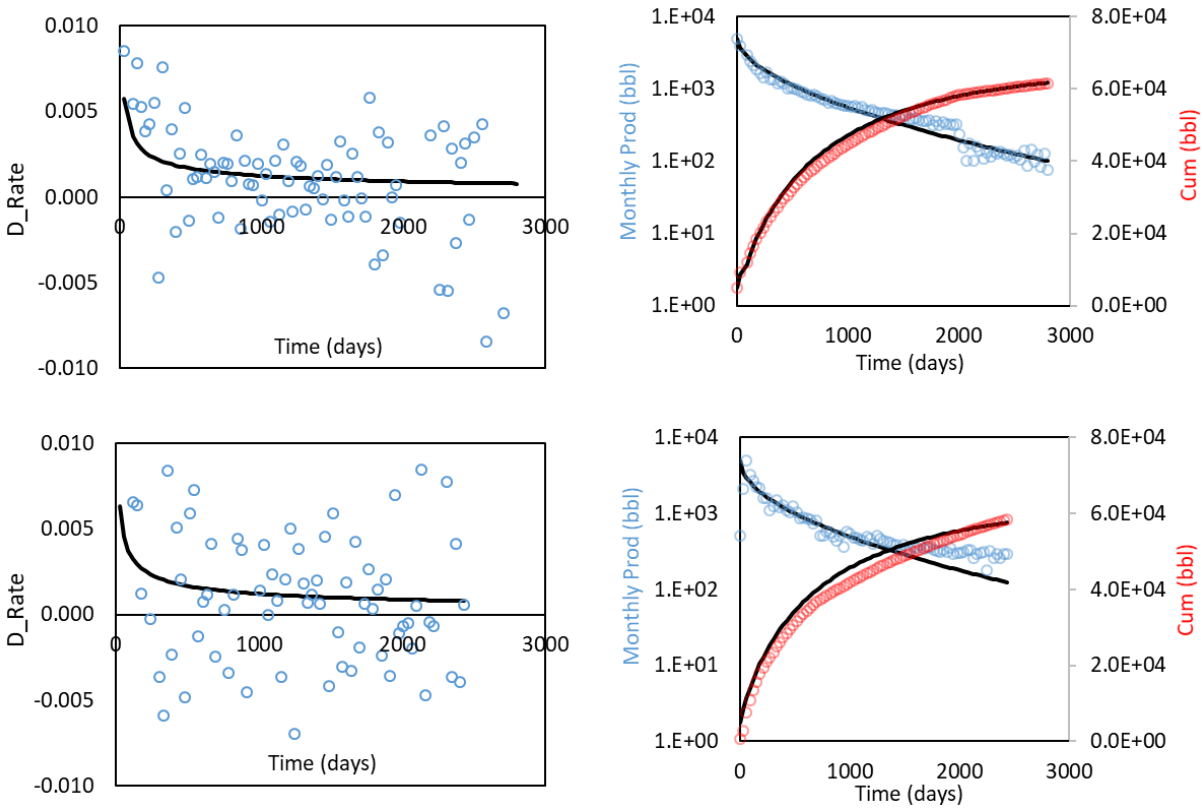

Figure 15: Variable Decline Modified Arps (VDMA) equation applied to actual field wells from Eagle Ford. Two wells are shown out of the 20 wells, all of which were primarily oil producers. The graphs on the right-hand side show the actual production data (red and blue bubbles) and predicted profiles (black curves) from VDMA equation. The arrow marks the 12-month production, which was used for the fit. The LHS plots show the predicted decline rate (black curve) along with the calculated decline rate (bubbles) from the observed production data.

Figure 16 shows the range of values for the initial decline rate, D_i, decline exponent, 'a' and the error in prediction of the cumulative volume for the 20 wells (in Eagle Ford) and 20 wells (in Haynesville) where VDMA model was applied. The average error for the 20 wells was only 3% in Haynesville and 2% in Eagle Ford which suggests that the VDMA model gives a very accurate representation of the production performance in the both dry gas and liquids-rich shale wells.

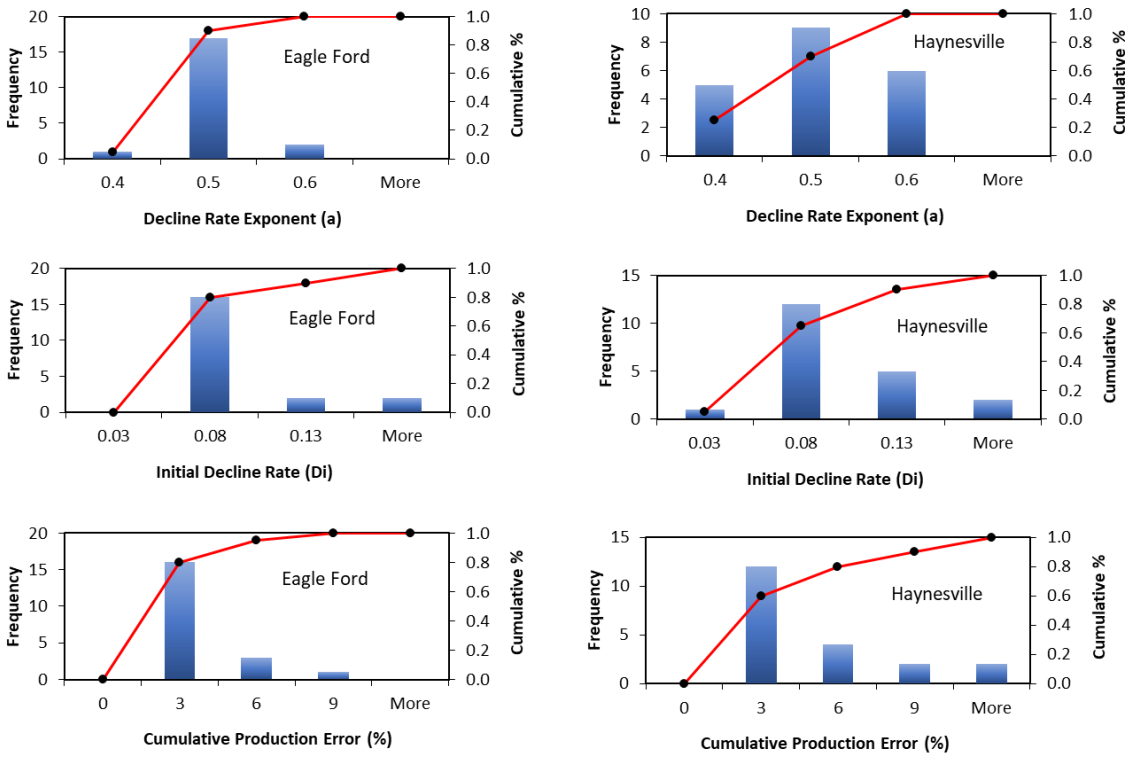

Figure 16: The figure shows the range of values for the initial decline rate, D_i, decline exponent, 'a' and the error in prediction of the cumulative volume for 20 wells (in Haynesville) and 20 wells (in Eagle Ford) where VDMA model was applied.

Different industry wide used DCA methods were compared with the VDMA model developed in this study. The six-decline curve analysis (DCA) methods that were used for comparison are Arp's harmonic, Fetkovich, Duong, Hsieh, Power-Law Exponential, Stretched-Exponential. The comparison was made for six wells in dry-gas Haynesville formation and other six wells in liquids-rich Eagle Ford formation; the comparison is shown in **Figure 17**. Only first 12-months production data was used for the fit. The general conclusion obtained by comparing different methods is that Arps harmonic, Fetkovich and Duong methods tend to give stabilized rates towards the end, causing the cumulative production estimates to exceed the actual production. On the other hand, Hsieh method generally tends to give steep declining rates towards the end, causing cumulative production estimates to be less than the actual. The power-law exponential

Stretched -exponential and Variable Decline Modified Arps (VDMA) tends to fit the production data the best and give least error estimates. The average error in cumulative production for both Haynesville and Eagle Ford wells are shown in **Figure 18**. The values of different parameters obtained by trial and error to match the production performance in different wells in Haynesville and Eagle Ford wells, are summarized in **Table 12** and **Table 13**, respectively.

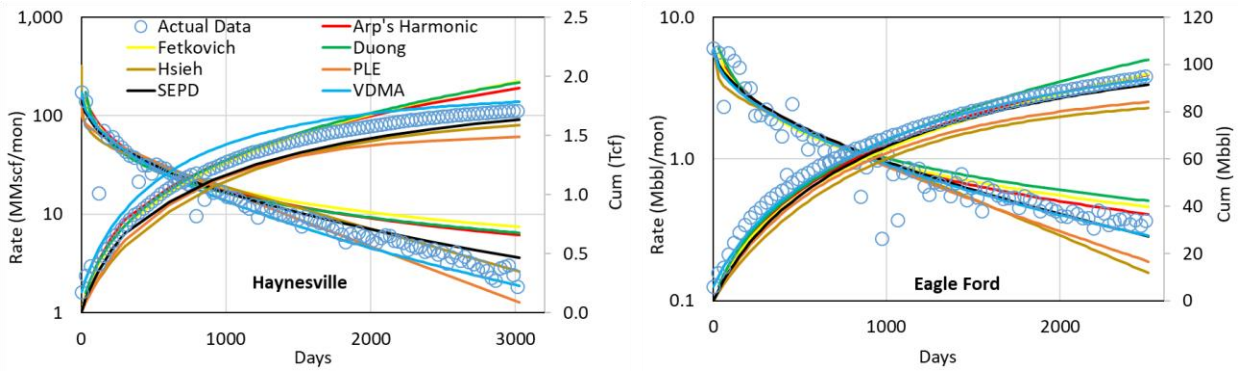

Figure 17: Comparison of the six most commonly used decline curve analysis (DCA) methods namely Arp's harmonic, Fetkovich, Duong, Hsieh, Power-Law Exponential, Stretched-Exponential with the model developed in this study i.e. Variable Decline Modified Arps (VDMA). The comparison was made for six wells in dry-gas Haynesville and liquid-rich Eagle Ford formations. The comparison is shown for one well for Haynesville and one well for Eagle Ford. The general conclusion by comparing different methods is that Arps harmonic, Fetkovich and Duong methods tend to give stabilized rates towards the end, causing the cumulative production estimates to exceed the actual production. On the other hand, Hsieh method generally tends to give steep declining rates towards the end, causing cumulative production estimates to be less than the actual. The Power-Law exponential, Stretched-Exponential and Variable Decline Modified Arps (VDMA) tends to fit the production data the best, and give least errors.

Finally, a small test was considered to evaluate the performance of the VDMA model in different flow regimes. The fit of the VDMA model was checked against the radial flow, linear flow, and pseudo-steady state flow. Published analytical solutions were used to generate production profiles for the test (Bourdet 2002 and Kushtanova 2015). The equations used are given below (**Equation 14** – **Equation 16**) and the values used for reservoir and completion properties are given in **Table 14**.

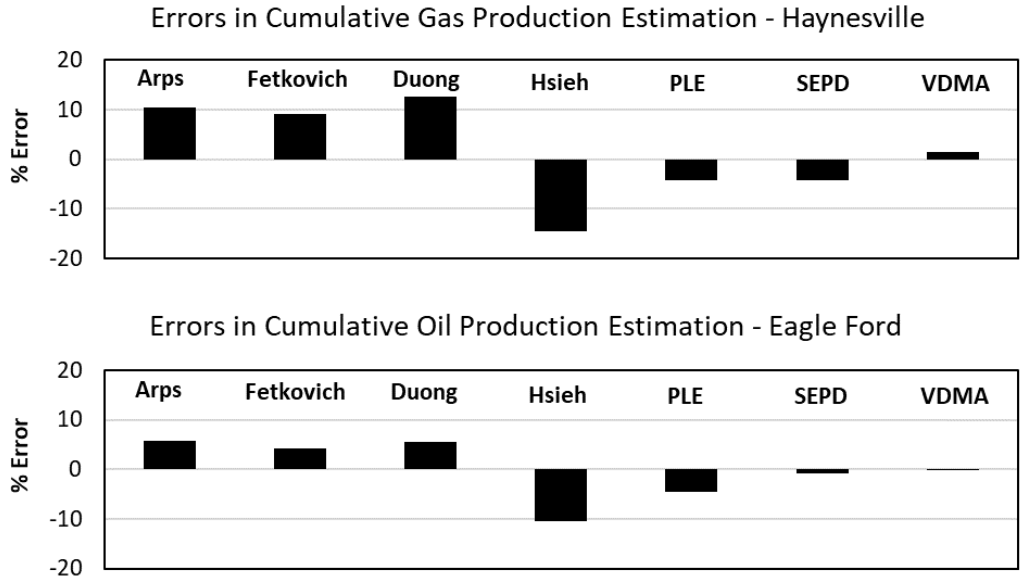

Figure 18: The above figures give the average error in cumulative production estimates for the different methods. The average is calculated from the six wells each in Haynesville and Eagle Ford, respectively. The average error reiterates the prior conclusion that Arps, Fetkovich and Duong methods tend to slightly overestimate production performance, while Hsieh tends to underestimate. The power-law exponential, Stretched-exponential and Variable Decline Modified Arps (VDMA) tend to give the least errors. The robustness of the VDMA model is evident since it gives least error among all the methods.

$$q = kh\Delta p * \frac{1}{162.6B\mu} * [log\Delta t + log\frac{k}{\emptyset\mu c_t r_w^2} - 3.23 + 0.87s]^{-1} \text{ (radial flow) } \ldots\ldots\ldots\ldots..(14)$$

$$q = hx_f\Delta p * \frac{1}{0.623B} * \sqrt{\frac{\emptyset k c_t}{\mu}} * \frac{1}{\sqrt{\Delta t}} \text{ (linear flow) } \ldots\ldots\ldots\ldots\ldots\ldots\ldots..(15)$$

$$q = \Delta p * [\frac{0.234B\Delta t}{\emptyset c_t hA} + 162.6\frac{B\mu}{kh}\left(log\frac{A}{r_w^2} - \log(C_A) + 0.351 + 0.87s\right)]^{-1} \text{(Pseudo-Steady State Flow) } \ldots\ldots(16)$$

In the above equations, q represents the flow rate in bbl/d, k represents the formation permeability in md, h represents the formation thickness in ft, Δp represents the pressure drop in psi, μ represents the viscosity in cp, Δt represents the production time in days, Φ represents the porosity in fraction, c_t represents the total formation compressibility in 1/psi, r_w represents the wellbore radius in ft, s represents the dimensionless skin, x_f is the fracture half-length in ft, B is the formation volume factor, A represents the cross sectional area to flow in ft_2, C_A is the shape factor and assumes constant values for different reservoir geometries (Craft and Hawkins 1959).

Table 12: The values of different parameters obtained by trial and error to match the production performance in six wells in Haynesville formation.

	Arps	Fetkovich	Duong	Hsieh	PLE	SEPD	VDMA
W1	b=1, D_i=0.009	n=2.8, G=2E6	m=1.2, a=1.59	n=0.22, m=0.0001	n=0.13, D_i=0.45, D_{inf}=0.0012	n=0.45, Tau=150	D_i=0.07, a=0.48
W3	b=1, D_i=0.008	n=2.8, G=1.5E6	m=1.2, a=1.62	n=0.16, m=0.0002	n=0.40, D_i=0.10, D_{inf}=0.0007	n=0.50, Tau=180	D_i=0.066, a=0.48
W9	b=1, D_i=0.0055	n=2.5, G=1.3E6	m=1.18, a=1.59	n=0.12, m=0.0002	n=0.59, D_i=0.03, D_{inf}=0.0001	n=0.50, Tau=280	D_i=0.055, a=0.486
W10	b=1, D_i=0.011	n=3.0, G=1.1E6	m=1.2, a=1.59	n=0.175, m=0.0002	n=0.59, D_i=0.05, D_{inf}=0.00004	n=0.50, Tau=140	D_i=0.103, a=0.528
W13	b=1, D_i=0.009	n=3.2, G=1.3E6	m=1.19, a=1.55	n=0.12, m=0.00026	n=0.35, D_i=0.13, D_{inf}=0.0009	n=0.48, Tau=180	D_i=0.073, a=0.493
W16	b=1, D_i=0.015	n=3.3, G=1.3E6	m=1.19, a=1.43	n=0.27, m=0.00015	n=0.35, D_i=0.20, D_{inf}=0.0006	n=0.48, Tau=105	D_i=0.164, a=0.576

Table 13: The values of different parameters obtained by trial and error to match the production performance in six wells in Eagle Ford formation.

	Arps	Fetkovich	Duong	Hsieh	PLE	SEPD	VDMA
W2	b=1, D_i=0.007	n=3, G=75000	m=1.19, a=1.59	n=0.2, m=0.0001	n=0.25, D_i=0.20, D_{inf}=0.001	n=0.43, Tau=180	D_i=0.048, a=0.44
W4	b=1, D_i=0.0055	n=3, G=1.3E5	m=1.18, a=1.61	n=0.14, m=0.00013	n=0.40, D_i=0.08, D_{inf}=0.0007	n=0.55, Tau=330	D_i=0.052, a=0.48
W7	b=1, D_i=0.007	n=3, G=2.5E5	m=1.19, a=1.61	n=0.1, m=0.00023	n=0.40, D_i=0.08, D_{inf}=0.0009	n=0.70, Tau=330	D_i=0.054, a=0.45
W10	b=1, D_i=0.007	n=2.7, G=2E5	m=1.19, a=1.59	n=0.1, m=0.00025	n=0.40, D_i=0.1, D_{inf}=0.0005	n=0.65, Tau=300	D_i=0.048, a=0.44
W11	b=1, D_i=0.0025	n=2.5, G=1.2E5	m=1.16, a=1.59	n=0.05, m=0.00013	n=0.28, D_i=0.10, D_{inf}=0.0005	n=0.6, Tau=700	D_i=0.038, a=0.49
W12	b=1, D_i=0.014	n=3.2, G=1.1E5	m=1.19, a=1.45	n=0.25, m=0.00013	n=0.34, D_i=0.20, D_{inf}=0.0005	n=0.5, Tau=130	D_i=0.14, a=0.565

Table 14: Reservoir and Completion Parameters used to generate production profiles for different flow regimes

Reservoir Property	Assumed Value	Reservoir Property	Assumed Value
Permeability, k (md)	100	FVF, B	1.0
Porosity, Φ (fraction)	0.1	Viscosity, μ (cp)	1.0
Skin, s	0.0	ΔP (psi)	100
Well Radius, r_w (feet)	0.5	r_e (feet)	500
Total Compressibility, c_t (psi-1)	1E-5	x_f (feet)	100
Thickness, h (ft)	1.0	Shape Factor, C_A	31.62
Drainage Area, A (ft^2)	785,000		

Figure 19 shows the match between production profiles generated using analytical solutions and VDMA model. The initial decline rate, D_i and decline exponent 'a' were changed to best match the analytical production profiles. It is evident that VDMA model gives an excellent fit to linear and radial flow regimes and gives a reasonable fit to pseudo-steady state flow regimes. The final values of D_i and 'a', used to get the match in **Figure 19**, are given in **Table 15**.

Table 15: Final match parameters for different flow regimes

Flow Regime	Initial Decline Rate, D_i	Decline Exponent, a
Radial Flow	0.38	0.90
Linear Flow	2.50	0.87
Pseudo-Steady State Flow	0.20	0.55

VDMA method not only gives superior performance as compared to industry wide used DCA methods like Arps Harmonic, Fetkovich, Duong, Hsieh, power-law exponential and Stretched-exponential but also demonstrates excellent ability to model different flow regimes. Thus, it perfectly aligns with the objective of generating accurate fits and forecasts for production wells in shales to be analyzed in later chapters for frac hit impact. The accuracy of DCA method is instrumental in correctly determining the impact of frac hits on both parent and child wells in different shale reservoirs.

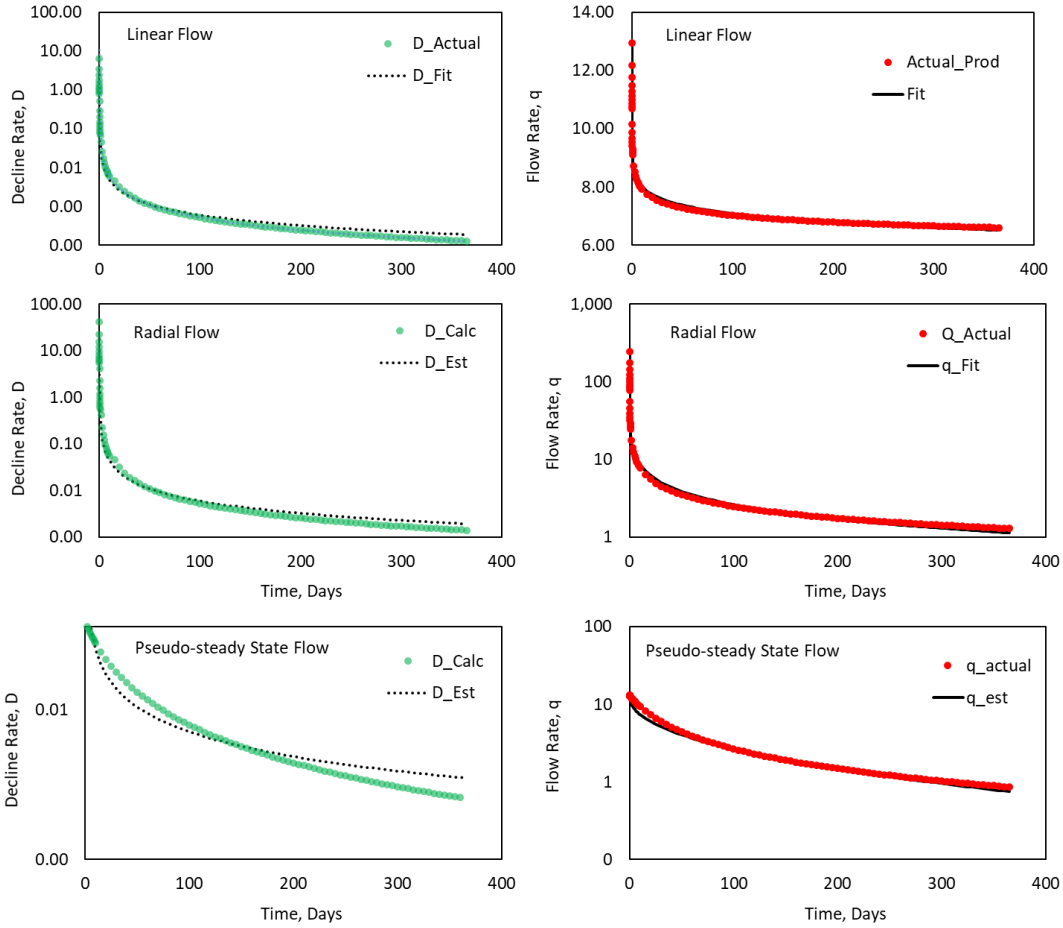

Figure 19: The figure shows the match between production profiles generated using analytical solutions and VDMA model. The initial decline rate D_i, and decline exponent a, were changed to best match the analytical production profiles. It is evident that VDMA model gives an excellent fit to linear and radial flow regimes and gives a reasonable fit to pseudo-steady state flow regimes.

Chapter 3: Big Data Analysis to analyze impact of Frac Hits

This chapter discusses the machine learning framework which was created to systematically analyze field production and completions data to understand the impact of frac-hits on the parent and child wells. The machine learning analyses generates regression models to predict the impact of frac hits. These regression models are coupled with economic analysis to determine optimum spacing for any given completion design or optimum completion design for any given spacing.

3.1 Workflow and Methodology

In this chapter, data from three formations namely Meramec, Woodford and Wolfcamp were analyzed. The chapter focusses on the analysis of large production and completion datasets to understand the impact of frac hits individually on parent and child wells and total impact on parent and child wells together. The production and completion data available are listed in **Table 16** and was taken from a public database. The methodology adopted (**Figure 20**) includes managing the data in an SQL database, followed by analysis using visual basic (VBA) in Excel. First, the production data was used to identify wells that have experienced frac hits, then once the frac hits and the corresponding parent wells are identified, the probable child wells that are responsible for those frac hits can be identified using a search algorithm. Once, the parent and child wells are identified, their production can be modeled using decline curve analysis (DCA) and the resulting curves can be used to quantify short and long-term impact of frac hits. Finally, the results can be transferred to a machine learning platform along with other data including completions to understand which factors control the frac hits and if these factors or variables can be used to create a frac hit systematics. This systematics is combined with economic modeling to give optimum spacing/completion recommendations.

Table 16: Production and completion data available for Meramec, Woodford and Wolfcamp

Formation	Production	Completion
Meramec	550 wells, Daily data	Lateral length, Total Fluid and Proppant
Woodford	1160 wells, Monthly data	
Wolfcamp	4400 wells, Monthly data	

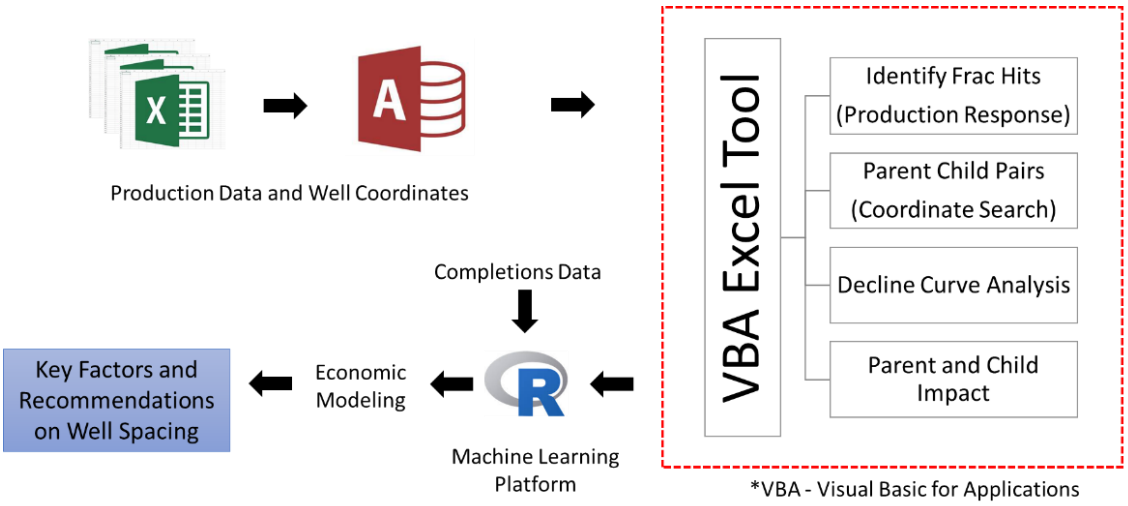

Figure 20: Methodology adopted to study impact of frac hits on parent and child wells in different formations. The data was managed in Excel and processed using several pieces of VBA code to identify frac hits, corresponding parent and child wells, and fits decline curve analysis to quantify impact on the parent and child wells. Finally, data was transferred to R to understand the key factors driving the frac hits. The regression models developed in R can be combined with economic models to run sensitivity, find optimum spacing or completion size.

Since, the production data was taken from public database, there was no information on frac hits, parent or child wells. Thus, frac hits were determined using production data as frac hits have a characteristic production response (McDowell et al. 2019). When an operator fracs a child well, they generally shut in the nearby parent wells to avoid producing excess water. So, the production data typically shows a shut-in before the frac hit (**Figure 21**). After the shut-in, because of increased water saturation around the parent well, the affected well starts at a lower oil rate and very high water cut. The GOR also decreases due to increased pressure around the

parent well. Slowly, the parent well cleans up, increasing the oil and exhibits a ramp production. In this study, this characteristic response was used to identify frac hits. First, hard cut-offs like water rate changes by 100% or more, GOR and oil rate changes by 30% or more, were used to define a frac hit. Manual QC was done to quality check the frac hits picked up by the code and to identify some frac hits which the code could not pick up.

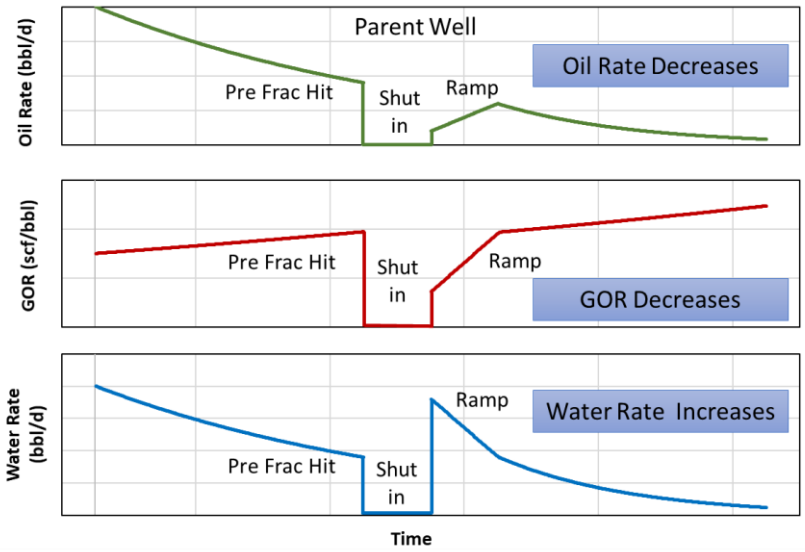

Figure 21: Typical response of a parent well production to a frac hit. The parent well is usually shut-in prior to fracturing the child well to avoid producing excess water. The oil rate and GOR generally decrease while water rate increases when the well is opened after the frac hit.

Once frac hits were identified, the wells receiving the frac hits were termed as parent wells. The downhole locations of all the parent wells were used to identify the associated child wells using a search algorithm. The child wells were searched within a 2000-ft Euclidean radius of the parent well. Typically, wells completed around the parent well at the time of frac hits were classified as child wells. The other constraint used was that the child and the parent well must be drilled at least 6 months apart because otherwise it becomes difficult to identify the production decline trend in the parent well before frac hit. Based on these set of rules, the number of parent and child wells identified for each formation are shown below in **Table 17**.

Table 17: Number of parent and child wells identified in different formations

Formation	No. of Parent Wells	No. of Child Wells
Meramec	109	247
Woodford	107	234
Wolfcamp	272	656

Decline curve equations were fitted on both child and parent wells to quantify both short- and long-term impact of frac hits. Gupta et al. (2018) have shown that power-law function is key to define production decline in low permeability reservoirs. This is because different flow regimes typically seen in horizontal wells show that production declines as a power-law function of time. Lab experiments (Gupta et al. 2019) also suggest that sharp decline in production in hydraulically fractured wells, can be attributed to decline in fracture conductivity which again shows a strong power-law dependence. Thus, as detailed in chapter 2, VDMA method was used to fit the production data in both parent and child wells.

However, before the parent and child well productions can be compared, they need to be normalized for the different lateral lengths and completion sizes. Generally, the longer the well, the greater the fluid and proppant used to fracture the well, i.e. completion size is proportional to lateral length. Thus, lateral length alone was used to normalize production in both parent and child wells. It is important to point out that child and parent wells may be in different reservoir quality areas having different rock properties. For this work, it is assumed that petrophysical and geomechanical properties do not change between the parent and child wells. Hence, lateral length normalization is all that is needed to be accounted for before comparing the parent and the child wells.

The next step was to calculate the impact of frac hits on both parent and child wells. For the parent well (**Figure 22 left**) the initial production before the frac hit and then the production after the frac hit were fitted using the VDMA DCA method. This gives ‘no frac hit’ curve and a ‘frac

hit' curve. Then, using the both curves the difference in production can be calculated for the parent well as a function of time. This difference in production represents the impact of the frac hit on the parent wells. Similarly, for child wells, the VDMA DCA was used to fit the production data on the child wells. The child wells should behave like the parent well (no frac hit curve) if there was no impact from frac hit. The difference in their performance calculated as delta production (**Figure 22 right**) for each child well is the impact of frac hits on the child wells.

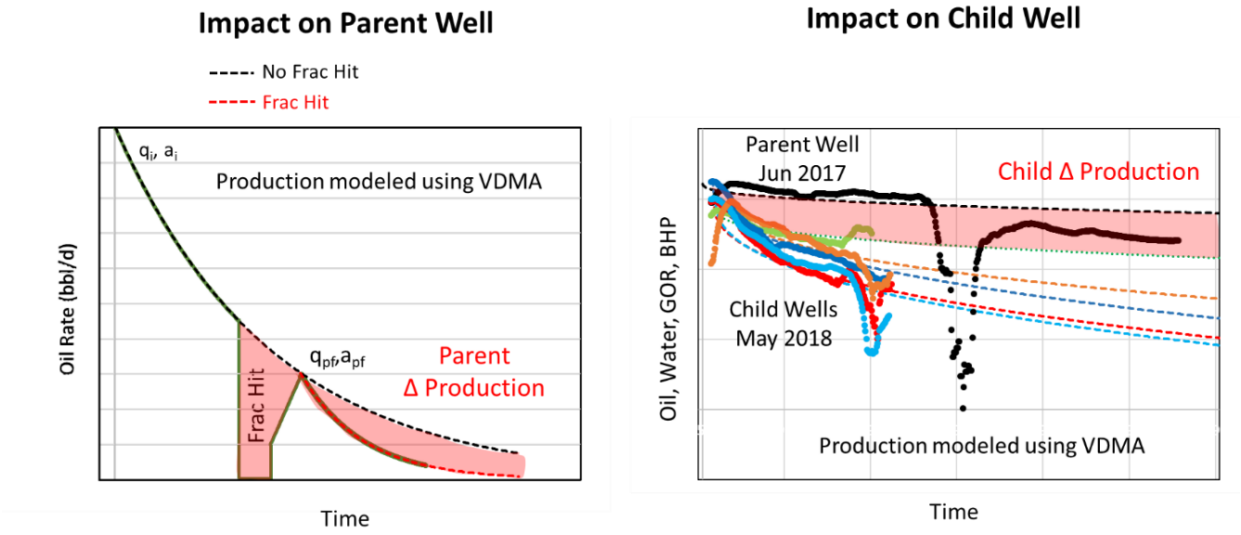

Figure 22: Methodology to calculate the impact of frac hit on the parent well (left). The DCA curves fitted to the data before and after the frac hit can be used to identify the "delta" production impact of frac hit. Methodology to calculate the impact of frac hit on the child well (right). The DCA curve on the parent well before the frac hit and the DCA curve of the child well are used to identify delta production impact on the child well.

3.2 Impact of Frac Hits

The distribution of the impact of frac hits on the parent and child wells is shown in **Figure 23**. The x-axis shows the percent impact on EUR and y-axis shows the number of wells. Negative means frac hits cause loss of production, positive means frac hits cause a gain in production. The number of parent wells negatively impacted in Meramec, Wolfcamp and Woodford are 62%, 60% and 67%, respectively. The number of parent wells positively impacted are 38%, 40% and

33%, respectively. The number of child wells negatively impacted in Meramec, Wolfcamp and Woodford are 85%, 84% and 71%, respectively. The small fraction of child wells that are positively impacted are likely drilled in better reservoir quality regions.

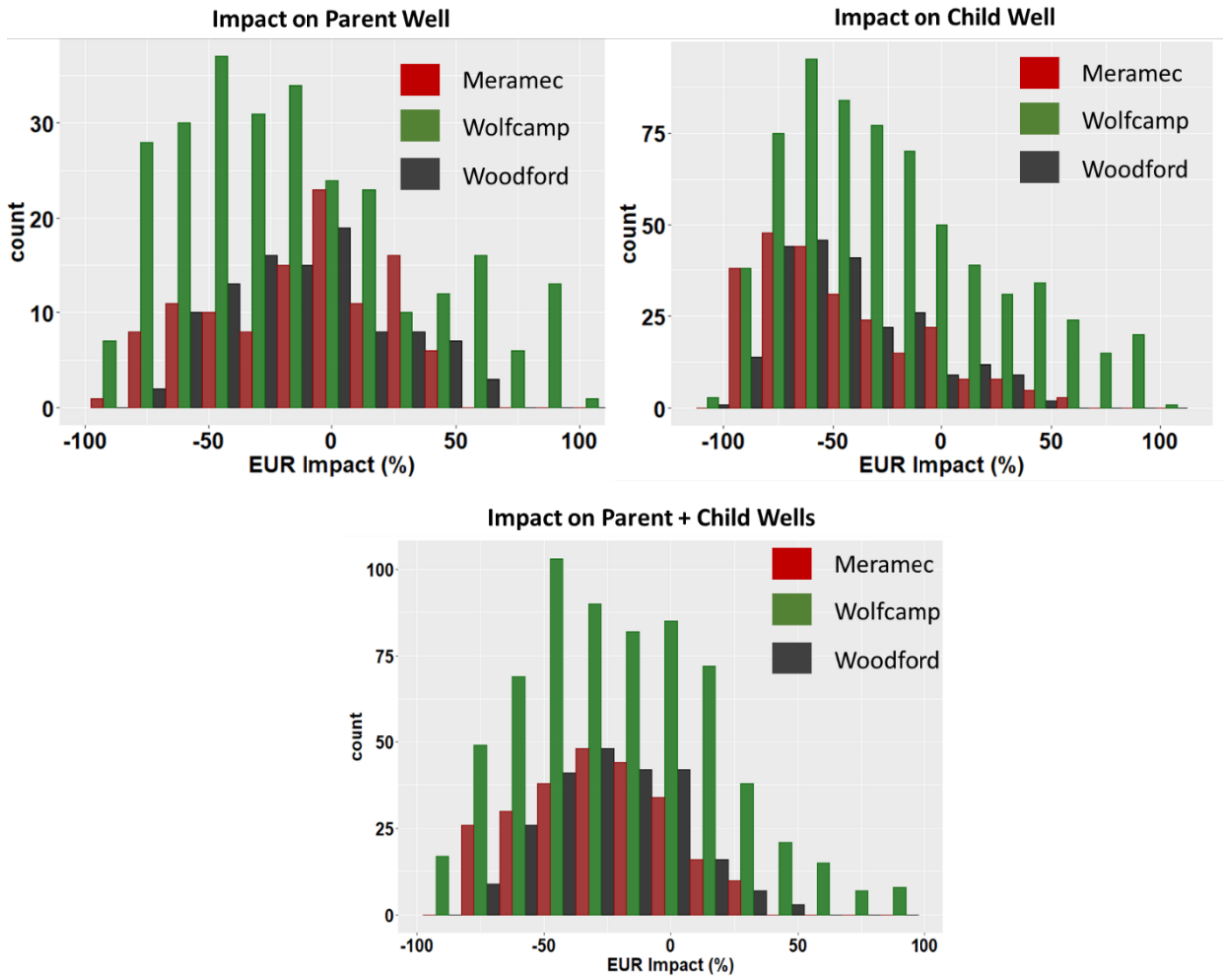

Figure 23: Impact of frac hits on parent wells (top left), impact of frac hits on child wells (top right), and total impact of frac hits on parent and child wells together (bottom). The number of parent wells negatively impacted in Meramec, Wolfcamp and Woodford are 62%, 60% and 67%, respectively. The number of child wells negatively impacted in Meramec, Wolfcamp and Woodford are 85%, 84% and 71%, respectively. Looking at the total impact, the parent-child pairs that were negatively impacted are 82%, 69% and 80% in Meramec, Wolfcamp and Woodford, respectively.

Lindsay et al. (2018) also analyzed the impact on child wells in several shale formations. Based on their investigation of several shale formations they reported 49 to 78% of the infill child wells

had a lower productivity compared to the parent wells and 22 to 51% of the child wells have a higher productivity than the parent wells. Their results compare well with the present study. **Figure 23** also shows the distribution of total impact on parent and child wells together. Looking at the total impact, the parent-child pairs that were negatively impacted are 82%, 69% and 80% in Meramec, Wolfcamp and Woodford, respectively.

Table 18 presents statistics on the total impact of frac hits for 1 to 5 years on cumulative oil production of parent wells, child wells, and total impact on parent and child wells together. As per the table, average percent impact on parent well production is negative in all the three formations. Parent wells loose between 10 to 20 percent of their oil volumes in 1-5 years. In terms of actual oil barrels, the loss varies between 2 to 15 million barrels in different formations.

Table 18: Average percent loss of cumulative oil volumes because of frac hits.

	Meramec			Woodford			Wolfcamp		
	Parent	Child	Total	Parent	Child	Total	Parent	Child	Total
1 Yr (%)	-12.0	-35.0	-23.3	-12.0	-34.0	-22.8	-10.2	-18.7	-15.4
2 Yr (%)	-14.0	-36.0	-25.9	-15.0	-35.0	-24.6	-14.5	-19.6	-17.9
5 Yr (%)	-16.0	-39.0	-29.1	-19.0	-37.0	-27.0	-20.1	-21.9	-21.7
1 Yr (MMbbl)	-2.6	-22.0	-29.9	-2.0	-23.0	-27.0	-4.6	-42.8	-52.4
2 Yr (MMbbl)	-3.7	-27.0	-38.4	-2.8	-25.0	-31.1	-7.9	-51.8	-68.0
5 Yr (MMbbl)	-5.9	-37.0	-55.7	-4.4	-30.0	-39.2	-14.8	-52.4	-82.4

Figure 24 shows a more accurate representation of loss in barrels of oil for different formations. The figure normalizes the total volumes by the number of wells to give loss per well. It shows the loss in oil volumes in five-year period. It is evident that parent wells lose 40,000 to 50,000 bbls in different formations in five years. Similarly, **Table 18** shows that child wells have a bigger impact on being drilled near existing parent wells. They lose 18 to 40% of their oil volumes in 1-5 years. **Figure 24** shows that child wells lose 80,000 to 150,000 oil barrels per well in five years. The biggest impact on child wells is seen in Meramec and the least impact is

seen in Wolfcamp. Overall, combining the impact on parent and child wells, a parent-child pair on average loses 15 to 30 percent of their oil volumes in 1-5 years (**Table 18**). A parent-child pair together loses somewhere between 125,000 to 225,000 bbls in 5 years with Meramec suffering the largest impact and Wolfcamp the least impact (**Figure 24**). The difference between Mearmec and Wolfcamp is likely due to combination of various factors as listed in **Figure 3**. The petrophysical and geomechanical properties were not available for the wells analyzed and thus, it is difficult to determine the reservoir factors that might be causing this difference. But, looking the at the completion data, it was observed that average completion size (frac fluid per ft, proppant per ft) in a parent-child pair in Meramec was on average 40% higher than in Wolfcamp. Larger completion size may result in larger fracture overlaps and cause stronger frac hits.

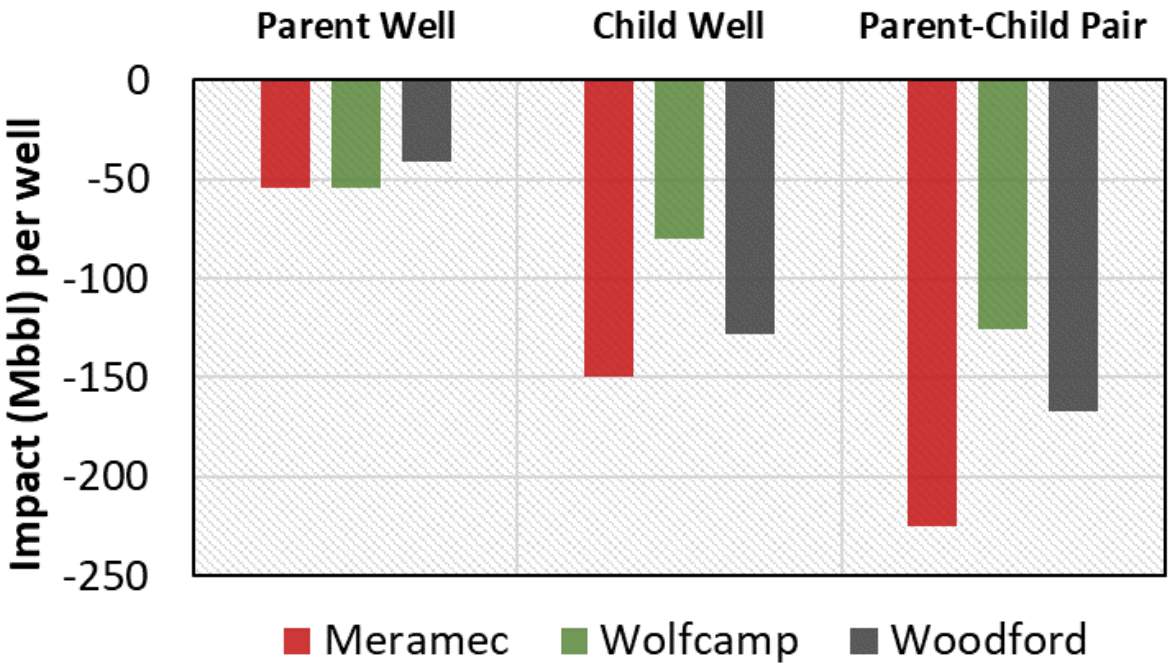

Figure 24: Impact of frac hits on parent well, child well and total impact on both parent and child wells together in five years. The parent-child pair represents the impact on two wells, parent and child. The total impact of frac hits is greatest in Meramec formation, and least in Wolfcamp.

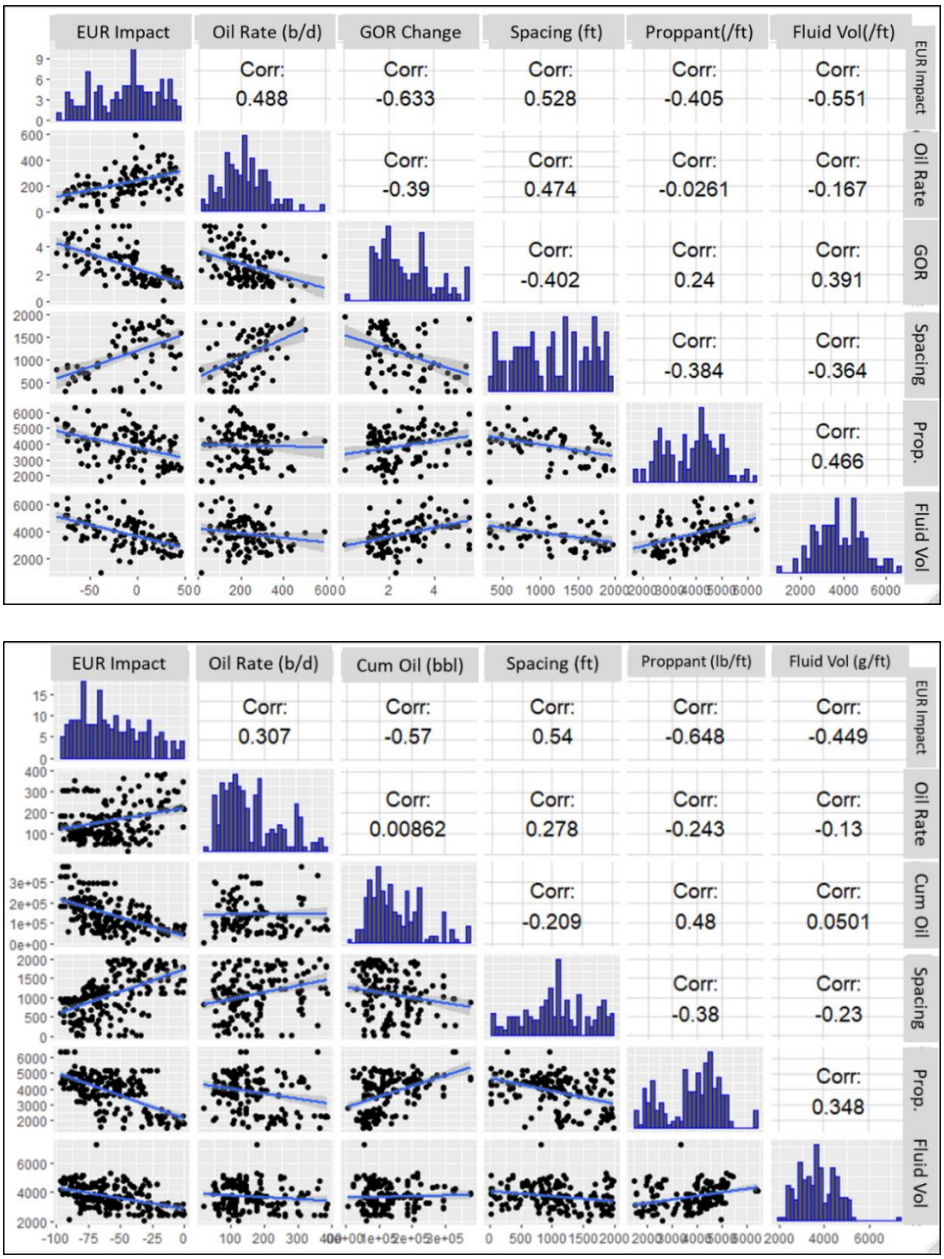

Figure 25: Matrix cross plot showing correlations between impact on EUR and various other completion and production factors. The fluid and proppant in the figure represent the sum of fluid and proppant in both parent and child wells. The top plot is for EUR impact of parent wells and bottom plot is for EUR impact of child wells. The first column (both plots) shows the correlation between EUR and the other factors. The corresponding correlation coefficient values are listed in the first row. It is evident that the impact on EUR in both parent and child wells is directly proportional to completion size, and inversely proportional to spacing and oil rate of parent well. The parent well EUR impact is also a function of change in GOR (compared to initial), with larger changes correlated with stronger negative impacts. The child well EUR impact is a strong function of parent well depletion, with larger depletion causing stronger negative impact on child wells.

3.3 Key Production and Completion Parameters Controlling Frac Hits

Once the impact of frac hits was quantified on the parent and the child wells, the data was loaded in a machine learning platform like R to understand which factors control the frac hits. **Figure 25** shows the matrix cross plot for Meramec formation showing correlations between impact on EUR and various other production and completion factors. It is evident that the impact on EUR in both parent and child wells is directly proportional to the completion size, and inversely proportional to spacing and oil rate of the parent well. The parent well EUR impact is also a function of change in GOR (compared to initial), with larger changes correlated with stronger negative impacts. This suggests that presence of free gas results in larger negative impact on parent well production. The child well EUR impact is a strong function of parent well depletion, with larger depletion causing stronger negative impact on child wells. The matrix cross plots were also created for the Wolfcamp and Woodford formations, and they show similar dependencies.

Spacing between the parent and child wells is a dominant parameter. **Figure 26** shows the impact of spacing on EUR of parent and child wells in different formations. On the x-axis there are two groups, one with shorter average spacing of 550 to 700 ft and the other with longer average spacing of 1350 to 1600 ft. It is evident that shorter spacing leads to higher negative impact on the EURs of both parent and child wells.

Completion size (fluid and proppant both) was found to be another important variable. **Figure 27** shows the impact of frac fluid on EUR of parent and child wells. On the x-axis there are two groups, one with smaller average frac fluid quantity of 20 to 70 bbl/ft and the other with larger average frac fluid quantity of 50 to 110 bbl/ft. This represents the sum of frac fluid in both parent and child wells. The plot shows that larger completion size has a stronger negative impact on

EUR in both parent and child wells. The other thing to note is like spacing, the impact of frac hits on child wells is worse than parent wells. The trend here is shown for frac fluid but a similar trend was also seen for proppant quantity. The impact of frac hits on parent well EUR was found to be a strong function of free gas around the parent well. This has been explained in the literature (Jacobs 2017a) as gas trapping by water phase which hinders the oil production. The free gas around the parent well was estimated using the increase in GOR prior to a frac hit compared to the initial GOR. GOR increase factor shown in **Figure 28** represents the ratio of GOR prior to frac hit and initial GOR. Higher value means greater increase in GOR and likely represent higher free gas saturation around the parent well. **Figure 28** shows that higher GOR increase leads to greater negative impact on parent well EUR.

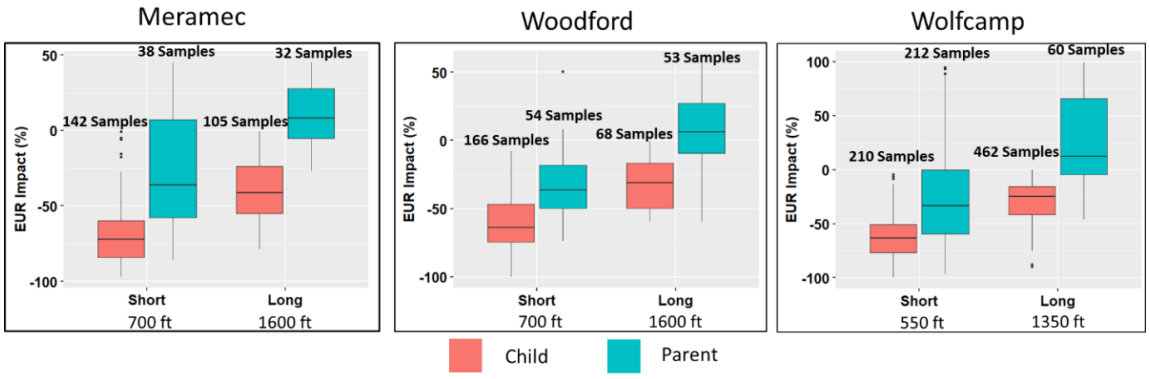

Figure 26: Impact of well spacing on EUR of parent and child wells in different formations. On the x-axis there are two groups, one with shorter average spacing of 550 to 700 ft and the other with longer average spacing of 1350 to 1600 ft. It is evident that shorter spacing leads to higher negative impact on the EURs of both parent and child wells.

Similarly, for the child well, impact of depletion on the EUR was studied using cumulative production in a parent well prior to a frac hit as a proxy for depletion (**Figure 29**). Again, several studies (Lindsay et al. 2018; Xu et al. 2019; Rafiee et al. 2012) show that depleted parent wells cause asymmetric fracture growth in child wells causing preferential growth in the zones depleted by the parents causing a negative impact on EUR of the child wells. **Figure 29** shows

that higher cumulative production by parent well (~ higher depletion) leads to greater negative impact on child EUR.

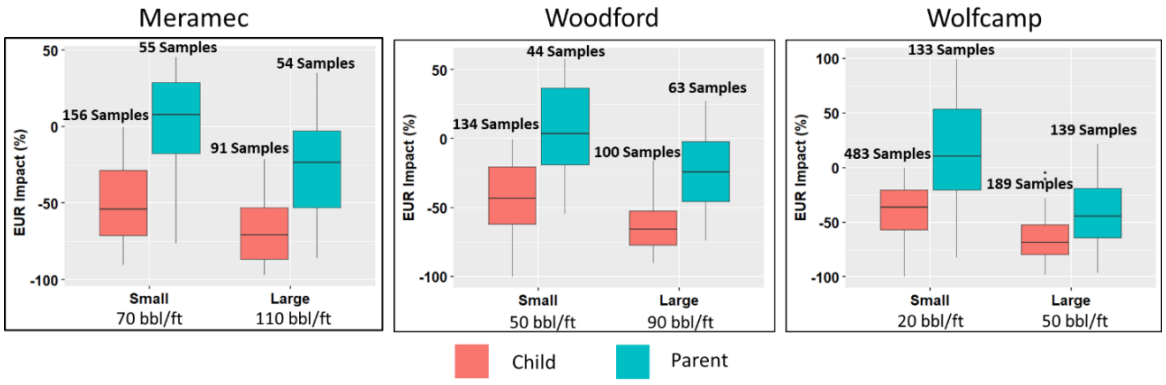

Figure 27: Impact of frac fluid on EUR of parent and child wells in different formations. On the x-axis there are two groups, one with smaller average frac fluid quantity of 20 to 70 bbl/ft and the other with larger average frac fluid quantity of 50 to 110 bbl/ft. This represents the sum of frac fluid in both parent and child wells. The plot shows that larger completion size has a stronger negative impact on EUR in both parent and child wells.

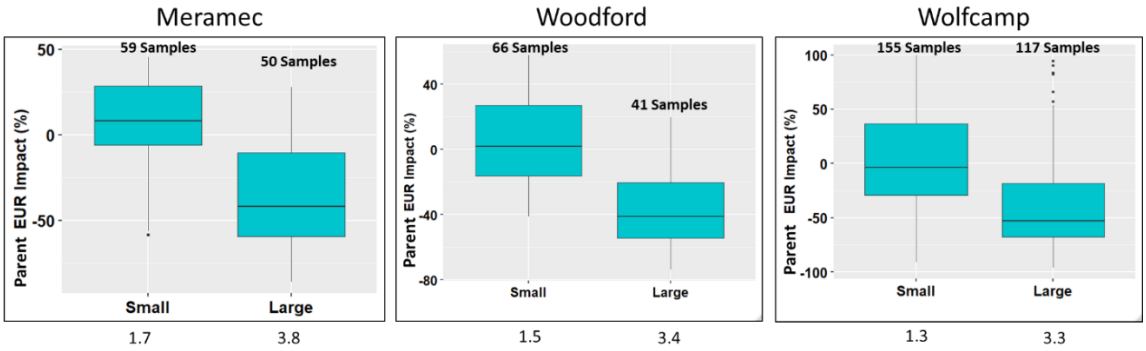

Figure 28: The groups on the x-axis represents GOR changes which is the ratio of GOR prior to frac hit and initial GOR. Higher value (or large group) means higher increase in GOR likely representing higher free gas saturation around the parent well. Higher GOR increase leads to greater negative impact on parent well EUR in all the three formations.

3.4 Regression Modeling to Predict Frac Hit Impact

The important factors that govern frac hits like spacing, completion size, oil rate and cumulative oil production of the parent well before frac hit can be combined using multi-linear regression to

create predictive models. Linear regression models were developed separately for all the three formations and give reasonable accuracy in prediction as shown in **Figure 30**. The multi-linear predictive models for the parent and child wells can also be combined to give the models for total impact (average percent gain or loss in EUR in a parent-child pair). The total impact is a function of production characteristics of parent wells (GOR change, cumulative oil production before frac hit), completion design of parent and child wells, and spacing between them. **Equation 17, 18** and **19** represent the equations for total EUR impact in Meramec, Wolfcamp and Woodford, respectively.

$$EUR_{Impact}(\%) = 4.3 * Rate - 6.5 * Proppant - 7.3 * GOR - 9.4 * Fluid + 5.0 * Dist - 5.0 * CumOil - 34.9 \quad \text{.....17}$$

$$EUR_{Impact}(\%) = 8.1 * Rate - 11.6 * Proppant - 3.4 * GOR - 8.2 * Fluid + 9.0 * Dist - 3.0 * CumOil - 30.8 \quad \text{.....18}$$

$$EUR_{Impact}(\%) = 6.5 * Rate - 6.5 * Proppant - 4.2 * GOR - 2.6 * Fluid + 9.9 * Dist - 3.0 * CumOil - 32.1 \quad \text{.....19}$$

Figure 29: Impact of depletion on the EUR of child wells was studied using cumulative production by a parent well prior to frac hit as a proxy for depletion. The groups on the x-axis represent the parent well production before child well was drilled. The low group represents the average cumulative production of 50,000 to 80,000 bbl by parent well before child well is drilled. The high group represents the average cumulative oil production of 180,000 to 220,000 bbl. The figure shows that higher cumulative production by parent well (~ higher depletion) leads to higher negative impact on child EUR.

In the above equations, total impact represents the average percent impact on any parent-child pair, rate represents the oil rate of the parent wells before frac hit, Proppant represents the sum of proppant amount per ft of lateral length in both parent and child wells, Fluid represents the sum

of frac fluid per ft of lateral length in both parent and child wells, Dist. represents the parent-child spacing, CumOil represents the cumulative oil produced by parent well before the frac hit, GOR represents the change, i.e. ratio of current GOR of parent well before frac hit divided by its initial GOR. All the variables are normalized using the **Equation 20** which normalizes each value by subtracting mean of the distribution and dividing the result by standard deviation of the distribution.

$$Norm_{Variable} = \frac{Variable - mean\ (variable)}{standard\_Deviation(variable)} \quad \text{.....20}$$

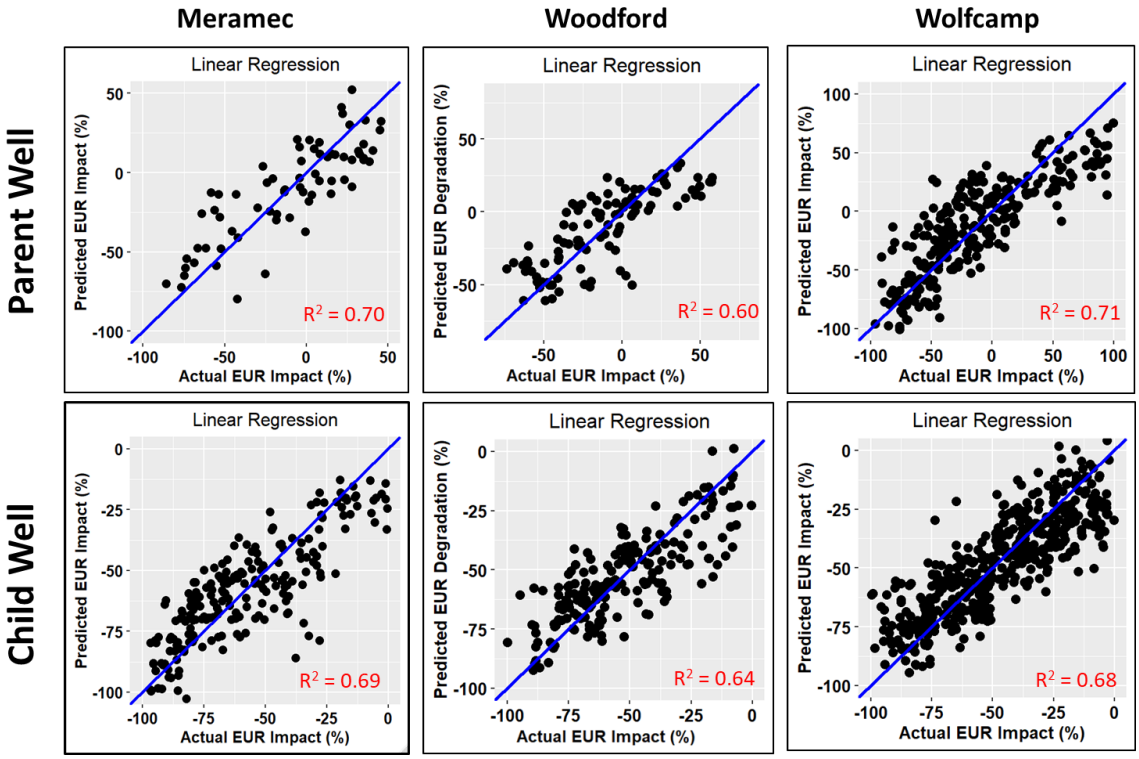

Figure 30: Results of machine learning to predict impact of frac hits on EUR of parent and child wells in Meramec, Woodford and Wolfcamp. The resulting models can be used in sensitivity studies and can be incorporated in any operator's budgeting and planning workflows to account for frac hits.

For instance, to calculate normalized proppant amount, the amount of proppant used in a parent-child pair is normalized using the mean proppant and standard deviation of the proppant amount

for different parent-child pairs in the study area. This is required for two purposes: first, normalized variables generally vary within a narrow range (~-3 to +3), thus any bias because of the magnitudes of different variables is removed. For example, proppant whose value ranges in thousands is treated the same as GOR change whose value ranges in single digits (~<10). Second, using normalized variables the equations can be easily compared between different formations. The data in **Equations 17, 18** and **19** show Wolfcamp is most sensitive to proppant amount while Meramec is most sensitive to GOR change.

3.5 Application of Regression Models

The predictive models once developed have numerous applications. They can be simply incorporated in budgeting, planning and reserves calculation algorithms of operators to account for frac hits. More importantly, they can be used to optimize spacing. An example of a spacing recommendation plot is shown in **Figure 31**. The spacing recommendation plot was generated using the predictive model for total average EUR impact (**Equation 17**) in Meramec formation. To create the plot, oil rate and GOR change factor were kept constant at 280 bbl/d and 2.7, respectively. Different lines represent different completion designs and the plot shows the recommended spacing as a function of cumulative oil production in the parent well. This plot was created for no impact on EUR. The arrows show an example for the completion design 70 bbl/ft and 3200 lbs/ft, and for cumulative oil produced by the parent well equal to 0.2 MMbbl, the recommended spacing would be 1000 ft. Such plots can be created for different constraints and can be used by operators to get spacing estimates. These estimates can be combined with other studies like numerical simulation, microseismic analysis, downhole pressure interference tests to get more definitive spacing recommendations.

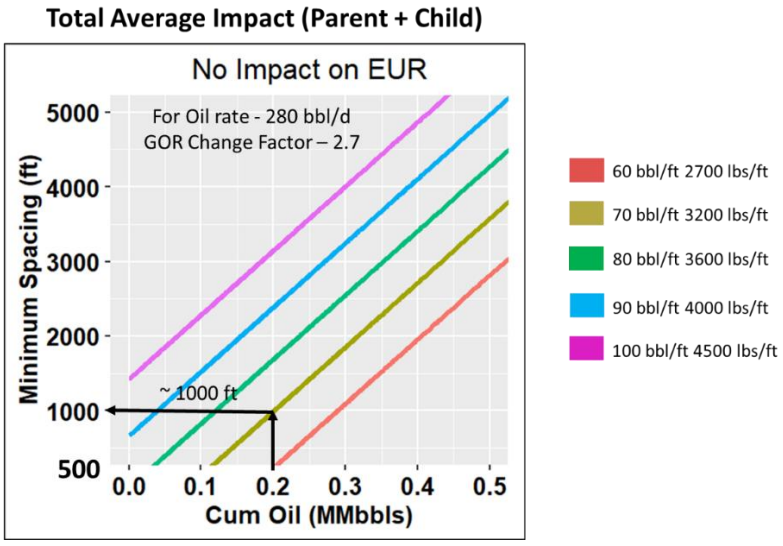

Figure 31: The spacing recommendation plot generated using the predictive model for total EUR impact (Equation 17) in Meramec formation. To create the plot, oil rate and GOR change factor were kept constant at 280 bbl/d and 2.7, respectively. Different lines represent different completion designs and the plot shows the recommended spacing as a function of cumulative oil production in the parent well. This plot was created for no impact on EUR. The arrows show an example for the completion design 70 bbl/ft and 3200 lbs/ft, and for cumulative oil produced by parent well equal to 0.2 MMbbl, the recommended spacing would be 1000 ft.

Figure 31 shows that for the constraints used in the example, spacing recommendations vary between 500 to 5000 ft which appear to be very optimistic. This is because placing the wells at such large spacing may result in avoiding frac hits but that means putting a smaller number of wells in a section which may not be the most economic exploitation of the section. Thus, to determine the most economic spacing, the predictive models can be combined with a simple economic model as shown below to calculate the optimum spacing. The different constants used for the simple economic model are given in **Table 19**. Three different scenarios were created i.e. P10, P50 and P90. In the different scenarios (P10, P50 and P90), the oil rate of the parent well was kept at high, medium and low values. These values were obtained from the actual P10, P50 and P90 distribution of the initial oil rates in the Meramec formation.

Table 19: Key parameters used for economic modeling. The economic modeling was run for the Meramec formation. Three different scenarios were created i.e. P10, P50 and P90. In the different scenarios, the oil rate of the parent well was kept at high, medium and low values. These values were obtained from the actual P10, P50 and P90 distribution of the initial oil rates in the Meramec formation. The average decline parameters to predict rates were taken from Meramec formation.

Parameters for Economic Modeling					
Oil Price ($/bbl)	55	CAPEX ($MM)	6	P50 Oil Rate (bbl/d)	1100
D, D and A ($/bbl)	8	Discount Rate (%)	10	P90 Oil Rate (bbl/d)	350
OPEX ($/bbl)	10	P10 Oil Rate (bbl/d)	1570	VDMA, a factor	0.55
VDMA, Di factor	0.1				

The idea is to sequentially increase number of wells in a section from 1 to 15. A section is 5280 ft by 5280 ft. Each well is assumed to be 1 mile (or 5280 ft) in length. For the first case, when there is one well (only parent well in the lease), there is no frac hit. Then, when an additional child well is added, the spacing of the child well from the parent well is 2640 ft (5280/2). In the third case, when there are two child wells, one child well would be at 1760 ft from the parent well and the other child well would be at 3520 ft from the parent well. Similarly, spacing for all the wells can be calculated up to 15 wells scenario (one parent + 14 child wells). Now, predictive models for parent and child (**Figure 30**) can be used to determine the impact on EUR using the spacing values for the parent and different child wells in various scenarios. Other variables like GOR change factor, oil rate of parent well before the frac hit, and completion size were kept constant. To study the impact of depletion, the cumulative oil produced by parent well before child well inception was varied between 0 (no depletion case) and 100,000 (depletion case). Jacobs (2019) recommends a 100,000 bbl limit under which there is minimal impact of parent well depletion on child well production. The results of economic modeling are shown in **Figure 32**. Two economic parameters are plotted, i.e. Net Present Value (NPV) and ROI (Return on Investment). Looking at the P10 results, the case when there is no depletion, drilling 15 wells in

the section at 352 ft. spacing gives the highest NPV though the ROI is lowest 52%. But considering the effects of depletion, there is an inflection point in NPV graph at 8 wells per section at 660 ft spacing. This shows that impact of depletion on frac hits can cause significant changes in optimum spacing. The above is considering the best-case scenario, i.e. wells are drilled in the best reservoir. For the P50 case, i.e. when the wells are drilled in the average reservoir (green); the number of optimum wells is 5 and 4 for no depletion and depletion cases, respectively. The pessimistic case (P90) when wells are drilled in poor reservoir are not economic for any number of wells in the section. This suggests that optimum spacing is complex function of operator-controlled parameters like reservoir quality (porosity, permeability, etc.), parent-child spacing, completion size, and well scheduling (parent well depletion).

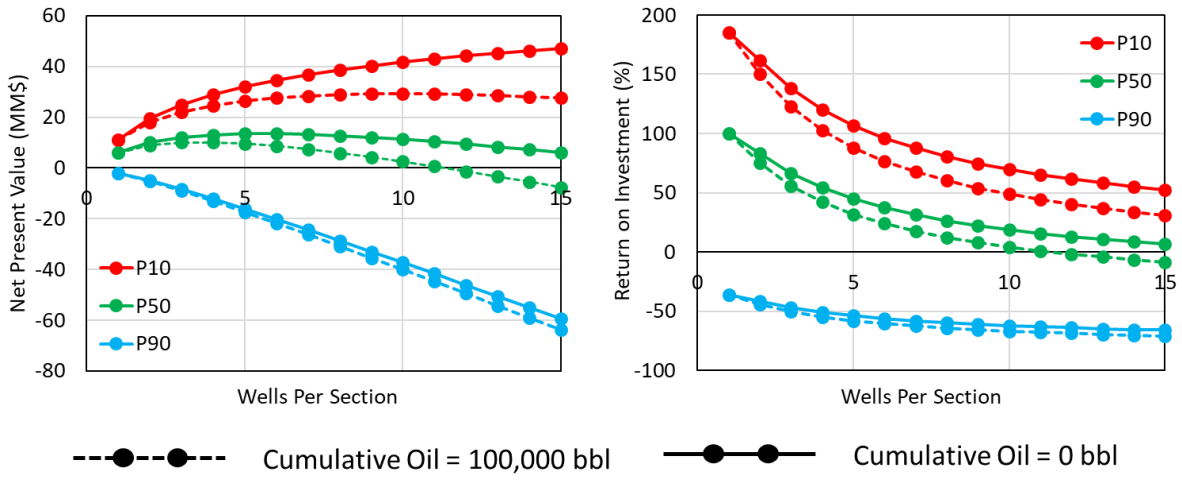

Figure 32: NPV and ROI plots generated using economic modeling to identify optimum spacing for different reservoir quality regions (P10, P50 and P90). Predictive models (Figure 30) were used to determine the impact on EUR using the spacing values for all wells in different scenarios. Other variables like GOR change factor, oil rate of parent well before the frac hit, and completion size were kept constant. To study the impact of depletion, the cumulative oil produced by parent well before child well inception was varied between 0 (no depletion) and 100,000 bbl. The results suggest that for P10 case, 15 wells per section at tight spacing of 352 ft give the highest NPV. This is for no depletion scenario. However, when parent well has produced 100,000 bbl, the frac hits have more severe impacts which reduces the optimum number of wells per section to 8. For the P50 case, the number of optimum wells is 5 and 4 for no depletion and depletion cases, respectively. In P90 case, none of the scenarios result in a positive NPV.

Such plots (**Figure 32**) can also be created for different completion designs, parent well production characteristics and reservoir quality to determine optimum spacing for the new child wells. Jacobs (2019) recommended that child wells drilled before or at 100,000 bbl production by parent well, do not suffer from negative consequences of frac hits. However, results in **Figure 32** show this limit is clearly not valid for Meramec where impact of depletion is felt at 100,000 bbl production by parent wells and frac hits cause significant negative impact. Thus, cut-offs of cumulative production that control positive or negative impact of frac hits are variable and must be determined on case-by-case (reservoir/study area) basis.

3.6 Summary

This chapter presented the analysis of more than 6000 wells in Meramec, Woodford and Wolfcamp to identify around 500 frac hits, corresponding parent wells and over 1100 child wells associated with the frac hits. The average impact of frac hits is negative on both parent and child wells in all the three formations. Parent wells lose 40,000 to 50,000 bbls in different formations in five years. Child wells have a greater impact when drilled near the existing parent wells. They lose 18 to 40% of their oil volumes in 1-5 years or between 80,000 to 150,000 oil barrels per well in five years. The greatest impact on child wells is seen in Meramec and the least impact in Wolfcamp. Overall, combining the impact on parent and child wells, a parent-child pair on average loses 15 to 30 percent of their oil volumes in 1-5 years or between 125,000 to 225,000 bbls in 5 years with Meramec having the largest impact and Wolfcamp having the least impact. The negative impact on EUR in both parent and child wells is directly proportional to the completion size, and inversely proportional to parent-child spacing and oil rate of the parent well. The parent well EUR impact is also a function of change in GOR (compared to initial), with larger changes correlated with stronger negative impacts. The child well EUR impact is also

a strong function of the parent well depletion, with larger depletion causing stronger negative impact on child wells. The empirical correlations presented in this chapter can be simply incorporated in budgeting, planning and reserves calculation algorithms of operators to account for frac hits. The correlations can also be coupled with economic models to give optimum spacing for given completion design and parent well production scenario. Even though the approach used in this chapter can be beneficial, this simple approach must be supplemented by an understanding of reservoir petrophysical and geomechanical properties and in situ stresses. It requires petrophysical logs, core measurements, microseismic data, high frequency downhole pressure gauges, chemical tracers and radioactive proppant data. Integrating the empirical correlations with other valuable petrophysical, geomechanical and field measurements will increase their accuracy and improve their predictability. Next few chapters focus on smaller areas where such extensive data is present. These chapters help evaluate the impact of petrophysical and geomechanical properties of the reservoir on frac hits. This understanding will play a critical role when creating mitigation strategies for frac hits as will be evident in Chapter 7.

Chapter 4: Reservoir Control on Fracture Dimensions in Meramec

The data for this study was taken from a section in Meramec where extensive data was available to analyze the impact of petrophysical and geomechanical reservoir properties on frac hits. The logs were used to calculate pore pressure, closure stress profiles, mechanical properties like Young's modulus and Poisson's ratio. Fracture modeling and microseismic data helped understand fracture growth, i.e. fracture dimensions, complex versus planar fracture networks, stage interactions and stress shadow effects. This additional information provided critical insights into frac hits. While it is desired to have logs and cores in every well drilled, engineering acumen lies in doing more with less. Thus, this chapter also shows how surface drilling data can be used as proxy for predicting mechanical rock properties along the borehole. In the field these correlations should only be attempted if enough cores and log data are available for calibration.

4.1 Production and Completion Data Analysis

In this study, seven wells in the section A are analyzed. Well 1 represents the parent well and the other six wells as shown in **Figure 33** represent the child wells drilled 600 days after Well 1. The objectives of this infill study were to primarily understand the parent-child interactions, impact of frac hits, optimum wells per section, number of stages, stage spacing, understand fracture propagation patterns (planar vs. complex), and the existence of fracture barriers. The completion summary of the section A wells is given below in **Table 20** and **Table 21**. Overall, the designs are similar, but there are some variations. Generally, the lateral lengths, number of stages and clusters are very similar between the wells. Well 4 and Well 6 have the highest breakdown pressure. Wells 5, 6 and 7 have reduced amount of slick water and increased amount of X-link gel in the fluid design. It will be interesting to see if and how these variations affect the fracture propagation.

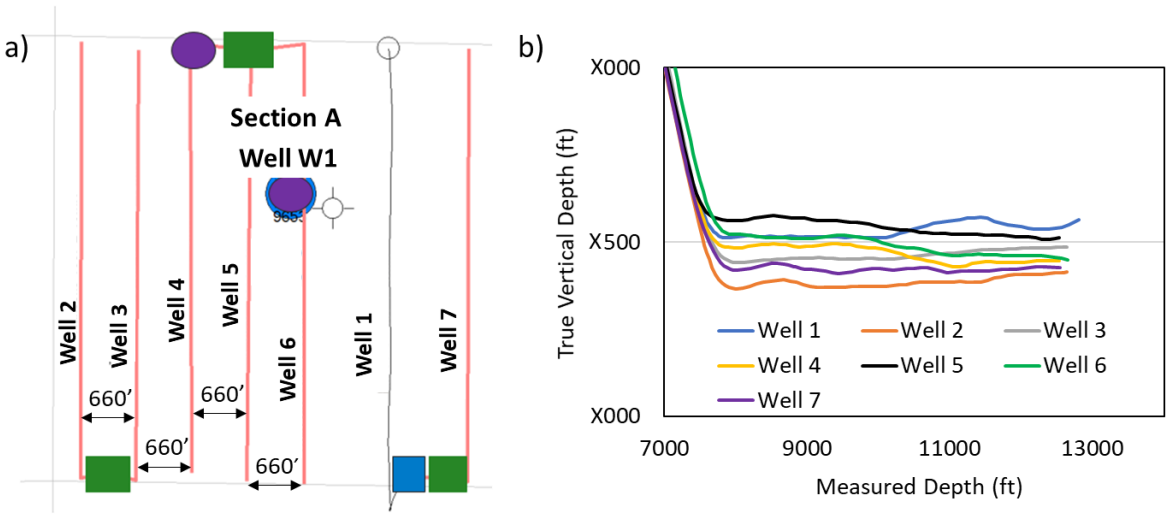

Figure 33: (a) Areal well locations of section A wells. (b) Vertical well locations of section A wells. Well W1 is a pre-existing vertical well used as a seismic observation well.

Table 20: Summary of the fracturing operations in section A. CPS stands for clusters per stage and PPS stands for perforations per stage. The complete dataset for Well 1 was not available. Generally, the lateral lengths, number of stages and clusters are very similar between the wells. Well 4 and Well 6 have the highest breakdown pressure.

Well	Frac Dates	CPS	Total Stages	PPS	Lateral Length (ft)	Avg Pump Rate (BPM)	Avg ISIP (psi)	Avg Frac Grad (psi/ft)	Avg Breakdown Press (psi)
Well 1	06/01/15				4880				
Well 2	04/18/17 to 05/03/17	5	34	30	4668	79	2003	0.70	4850
Well 3	04/18/17 to 05/03/17	5	34	30	4672	79	1662	0.66	4208
Well 4	05/05/17 to 05/18/17	5	33	30	4527	73	1924	0.59	5980
Well 5	05/20/17 to 05/26/17	5	34	30	4727	78	2526	0.64	4485
Well 6	05/05/17 to 05/17/17	5	33	30	4479	72	1745	0.56	5743
Well 7	04/10/17 to 04/16/17	5	33	30	4473	68	2062	0.70	5120

The tables (**Table 20** and **Table 21**) can be used to compare the different wells. However, there are large variations in petrophysical and mechanical properties along the wellbore length which is evident by the varying initial shut-in pressures and breakdown pressures between different

stages in **Figure 34**. This is indicative of the heterogeneous nature of the Meramec formation. This heterogeneity might also arise due to the depth differences both within and between the different wells (**Figure 33b**). **Figure 35** shows the variation of proppant and fluid amount between various stages in different wells. Completion design is similar but varying rock properties will cause disproportionate and non-uniform fracture growth between different stages which might increase the risk of frac hits. There is one interesting trend observed; that initial shut-in pressure (ISIP) increases with increasing stage number for all the wells. This suggests adjacent stages are interacting with each other and can be indicative of stress shadow effects. Stress shadow can further facilitate disproportionate fracture growth and increase the risk of frac hits (Zheng et al. 2019).

Table 21: Details of proppant and fluid used in the fracturing treatments for the section A wells. Wells 5, 6, and 7 have reduced amount of slick water and increased amount of X-link gel in the fluid design. Well 7 also has lower total fluid compared to the other wells.

Well	30/50 Prop (lbs) Per Stage	100 Mesh Prop (lbs) Per Stage	Total Prop (lbs)	Slick Water (bbl)	Linear Gel (bbl) per Stage	X-link Gel (bbl) per Stage	Total Fluid (bbl)
Well 1			8758849				172893
Well 2	233693	120542	12043970	4421	1203	1174	231112
Well 3	237061	116751	12029600	4282	1192	1165	225702
Well 4	245006	116899	11637080	4198	866	1318	207952
Well 5	238449	122211	12262430	2463	689	2475	191288
Well 6	238645	118812	11633363	2629	710	2454	191161
Well 7	237399	117797	11366260	1838	1089	1625	145700

Next, the production data was compared for the different wells. **Figure 36** shows the production data for Well 1 (parent well) and the different child wells (Well 2 to Well 7). The figure shows that frac hits from the child wells negatively impact the performance of the parent well. The depletion by the parent well also impacts the child wells and all the child wells perform poorly compared to the parent well.

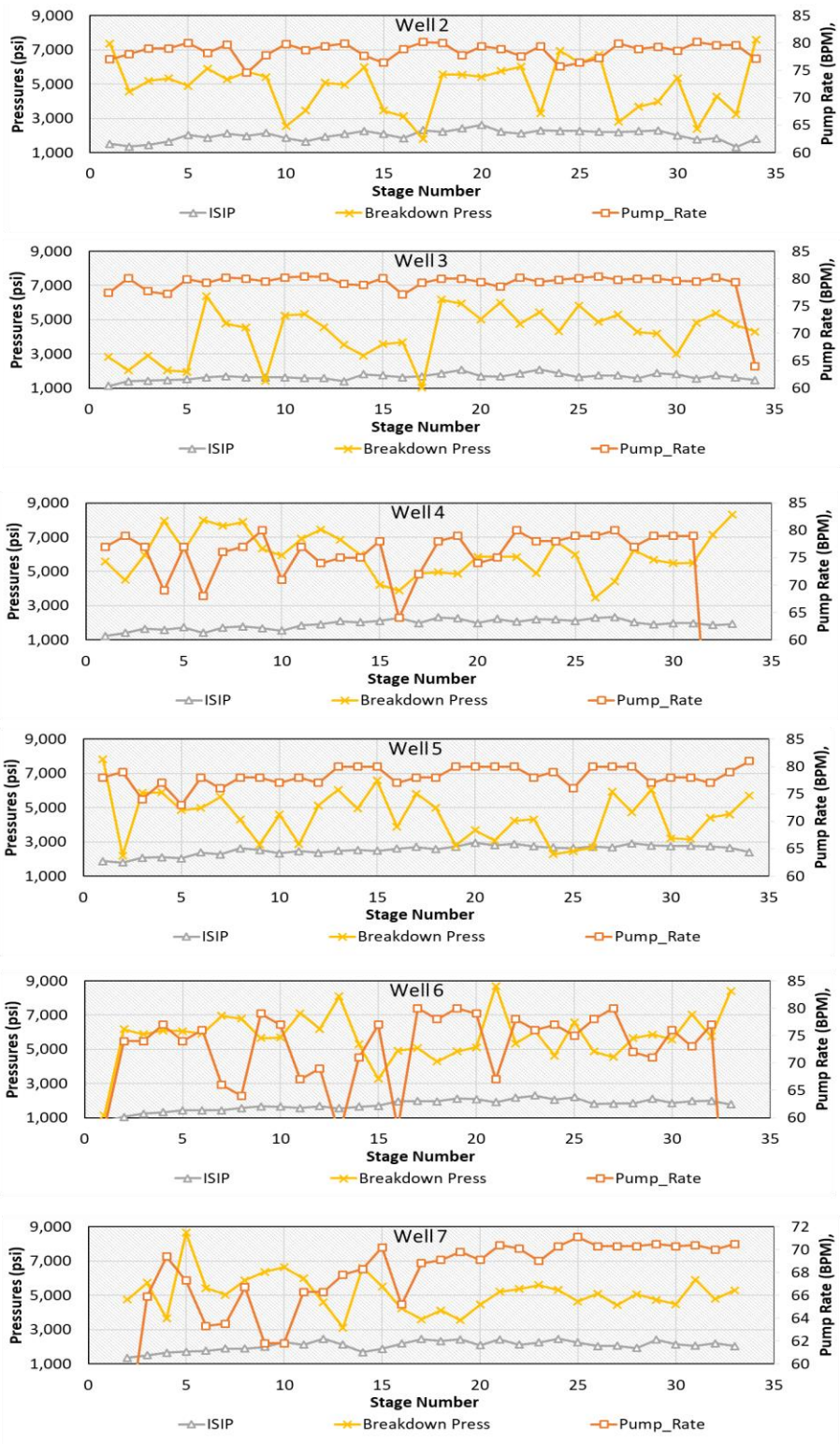

Figure 34: Variation of initial shut-in pressure (ISIP), breakdown pressure and pump injection rate for different stages in wells in Section A. The ISIP shows an increasing trend with ISIP values in later stages being ~30 % higher than the ISIP values in the earlier stages.

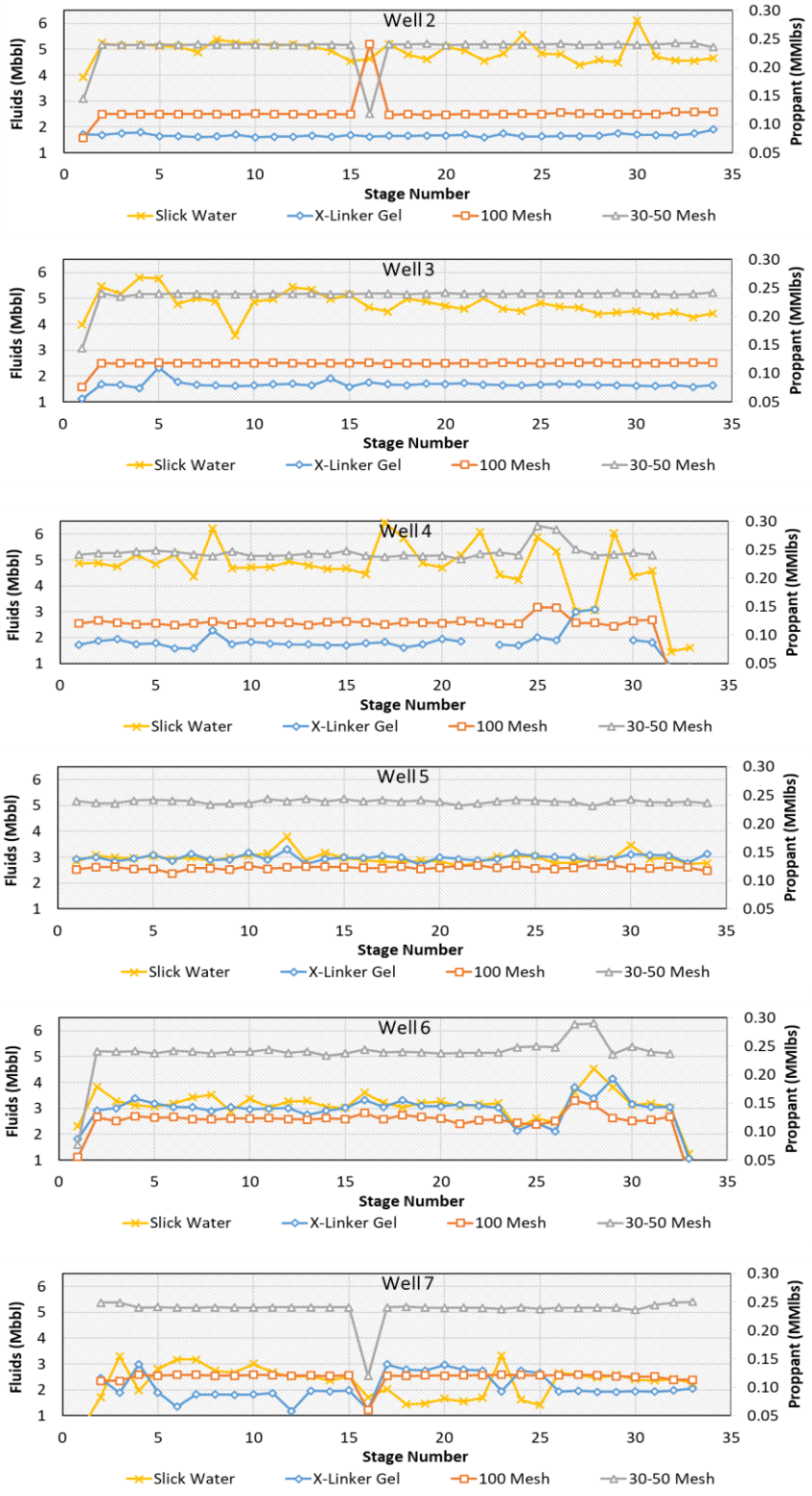

Figure 35: Variation of proppant and fluids for different stages in wells in section A. Wells 2, 3 and 4 used larger amount of slick water per stage compared to Wells 5, 6 and 7.

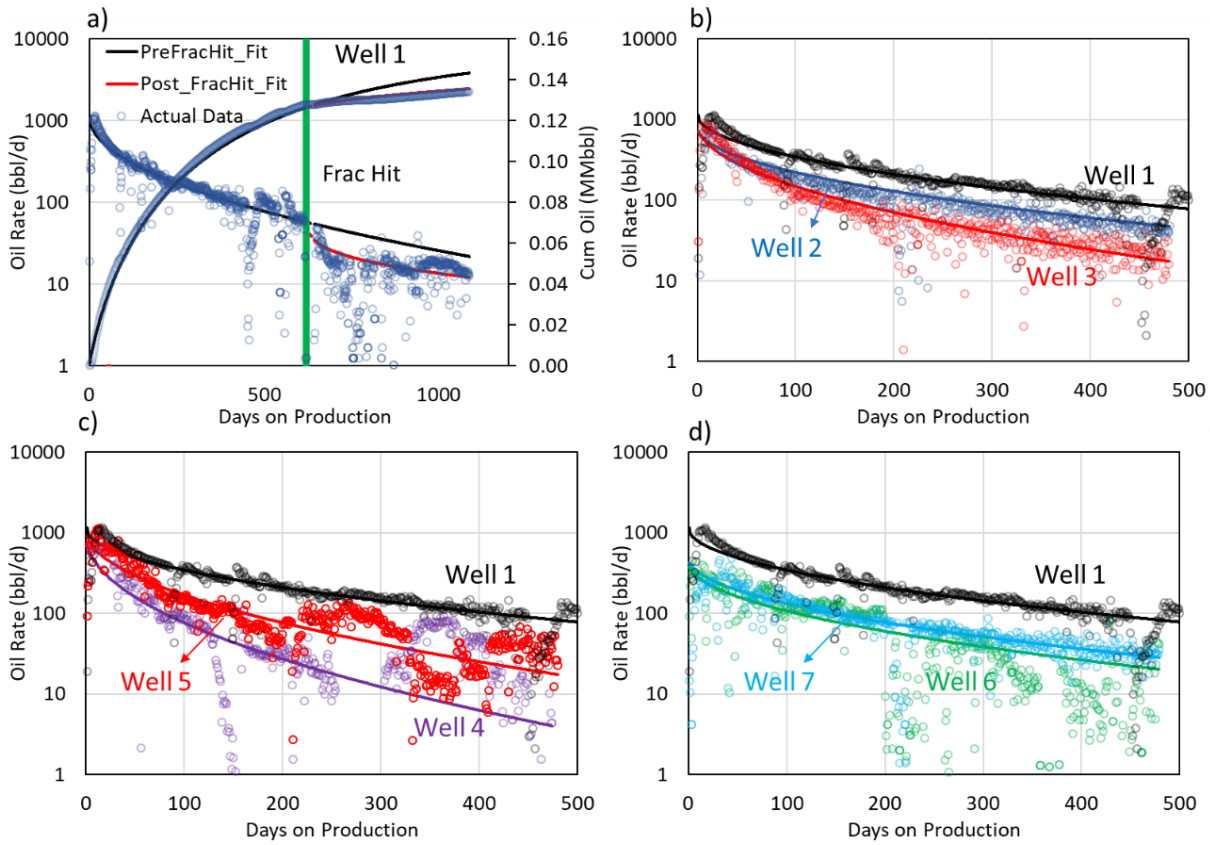

Figure 36: a) Production data for Well 1, i.e. the parent well. The production data is fitted before and after the frac hit using VDMA method. The production data shows negative impact of the frac hits on the parent well. b) Production data for child wells 2 and 3. The symbols represent the actual data and the solid lines represent the VDMA fits. The x-axis is normalized so that the parent and child wells could be compared. The child wells do not perform as well as the parent well. c) Production data for child wells 4 and 5. They also have a poor performance compared to the parent well. d) Production data for child wells 6 and 7. Again, the child wells perform poorly compared to the parent well.

The production data was analyzed to calculate the impact of frac hits and loss of production in both parent and child wells. **Table 22** shows the percent loss of production in child wells for a 5-year period. Different wells have similar lateral length but different completion designs (proppant and fluid). Thus, cumulative oil was normalized by lateral length, total proppant and fluid used to compare the parent well performance with child well performance. The table also shows the normalized cumulative production of the different child wells. Looking at the well locations in **Figure 33**, it is evident that Well 2 is farthest away from the parent well. Thus, it

should have the least impact of parent well depletion. **Table 22** shows that well 2 performs better compared to the other child wells. Wells 6 and 7 are closest to the parent well. However, Well 7 production is relatively good because it is not surrounded by any well on one side and is also far away from rest of the child wells which might explain its relatively better production performance. Well 6 is the second least productive child well. It is strongly impacted by parent depletion as well by interference from other child wells. However, the worst production performance is for well 4. It is interesting to note that **Table 20** shows that wells 4 and 6 also have high breakdown pressure. Higher breakdown pressures may suggest higher rock strength and as a result smaller fracture dimensions which might explain poor performance considering other things constant. Thus, to test the theory, the normalized cumulative production for 5-year period for all the child wells were plotted as a function of breakdown pressure (**Figure 37**). The figure clearly shows that there is an inverse relationship between production performance and breakdown pressure. Breakdown pressure is function of petrophysical and mechanical properties of the rock. Thus, these properties cannot be ignored and must be characterized and integrated with other factors like interference to understand production performance.

Table 22: Cumulative oil production for the different wells for 5-year period. Different wells have similar lateral length but widely different completion design (proppant and fluid). Thus, cumulative oil was normalized by lateral length, total proppant and fluid used for the well. The fourth column shows the percent loss in production for all the child wells.

Well	5-Yr Cum Oil (bbl.)	Norm 5-Yr Cum Oil (bbl.)	% Loss Actual
Well 1	152564.0	169568.0	
Well 2	94029.4	80586.2	52.5
Well 3	55738.5	48326.3	71.5
Well 4	30385.6	28799.0	83.0
Well 5	62687.1	57794.2	65.9
Well 6	43787.7	43756.5	74.2
Well 7	56424.5	65426.5	61.4

Table 23 shows the impact of the frac hits on the parent wells. **Table 24** summarizes the cumulative oil volume loss and average percent loss in oil production for the parent well, the six child wells and parent + child wells. All the child wells started producing together and after 600 days from the start of production in the parent well. The child wells not only interact with the parent well but also with each other. Thus, the figures in the **Table 22** do not truly represent just the impact of the parent well. It shows the cumulative effect of interference between the parent and child wells and all the child wells with each other. The results (**Table 24**) clearly show that wells in section A lose on average 58% of their oil production due to interference effects. Thus, the spacing of 660ft is too optimistic and it needs to be increased to reduce interference effects.

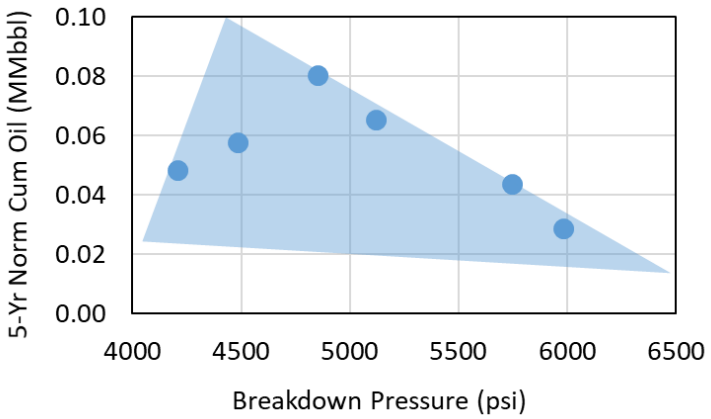

Figure 37: The plot showing an inverse relationship between breakdown pressure and production performance. The correlation is not expected to be perfect considering there are other factors like interference strongly impacting the production performance.

Table 23: Impact of frac hits from child wells on the production of the parent well. The second column shows the cumulative production before frac hit. The third column shows the cumulative oil production in five-year period after the frac hit considering pre-frac hit decline rate i.e. black curve in Figure 36 (a). The fourth column shows the cumulative oil production in five-year period after the frac hit considering the new decline after the frac hit i.e. red curve in Figure 36 (a). The fourth column shows the loss in production in percent due to frac hits.

Parent Well	Pre Frac-Hit Cum Oil (bbl)	Pre-Frac Decline 5-Yr Cum Oil (bbl)	Post-Frac Decline 5-Yr Cum Oil (bbl)	% Loss
Well 1	125284.5	30075.7	20157.0	32.9

Table 24: The impact of frac hits on the parent well, the child wells and all the wells together. Each child well should behave like parent well if there were no interference. The child well loss was calculated by calculating the difference between parent well production and child well production for each child well. The total loss in all the wells together was calculated by summation of the losses in the parent and child wells.

Total Oil loss in child wells (bbl)	Avg Percent Oil loss in child wells (%)	Total Oil loss in Parent well (bbl)	Avg Percent Oil loss in Parent well (%)	Total Oil loss in all wells (bbl)	Avg Percent Oil loss in all wells (%)
692719	68.1	9919	32.9	702638	58.4

Again, to get a rough estimate of the optimum number of wells in the section A, the economic model (**Figure 32**) and the multi-linear regression models (**Figure 30**) developed for Meramec formation in Chapter 3 were used to determine optimum number of wells per section. The economic parameters (CAPEX, expenses and oil price) considered in modeling were same as shown in **Table 19**. The cum oil, GOR change factor, producing oil rate before frac hit and VDMA decline parameters were obtained from Well 1 and were used to predict the NPV and ROI for different scenarios where different number of child wells are drilled. The results in **Figure 38** show section A well performance (under the current economic model) does not give a positive NPV and adding additional child wells only increase the losses. This model as shown earlier does not account for strong inter-well communication among the child wells and actual losses from the section would likely be larger. It simply appears that cost of drilling and completing a well is too high compared to the revenue generated at the current oil price. That is why even a parent well by itself in the section is not often economic. The measures that could be taken are to reduce the completion size to reduce CAPEX, increase recovery from current wells, find better reservoir quality regions or leave this section till oil price is high enough to make this section's development economic. Even though under given conditions, section A wells may not be economic, the data acquired is vital and must be analyzed to make economic development decisions in other nearby sections.

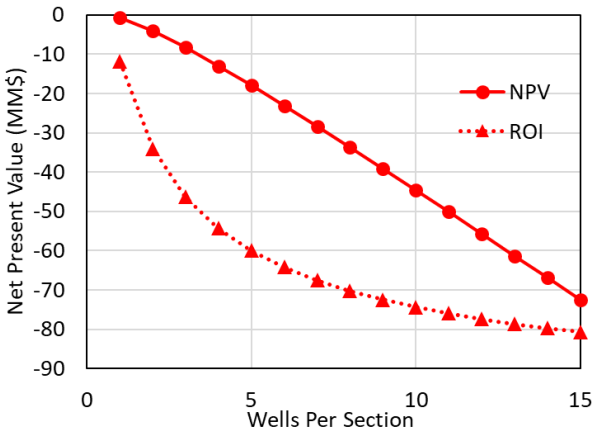

Figure 38: Economic modeling for section A using the economic model for Meramec formation developed in Chapter 3. It is clear that section A well performance (under the current economic model) does not give a positive NPV and adding additional child wells only increase the losses. This model, as shown earlier, does not account for strong inter-well communication among the child wells and actual losses from the section A would be likely greater.

4.2 Well Log Analysis

To further understand the impact of different petrophysical and mechanical properties on fracture propagation, well logs were analyzed. Several logs namely gamma ray, resistivity, density, photoelectric effect (PE), neutron porosity, dipole sonic and nuclear magnetic resonance (NMR) were acquired in the vertical pilot hole of well 4. There was no core data available in section A. **Figure 39** shows a snapshot of the different logs in the vertical section of well 4. **Table 25** shows the average log values for different Meramec zones. GR is a strong indicator of mineralogy. Within different Meramec zones, Meramec B, C and F seem to be more shaly compared to the other zones. Considering shales are ductile, these zones may inhibit fracture growth. PE value for sandstone is 1.8, for limestone 5.08 and for shale typically around 3.4. Considering that different Meramec zones are predominantly a mix of above three lithologies, an increasing value of PE may indicate increasing carbonate content supported by other logs like lower values of GR, high density, high resistivity and low sonic travel times. Based on this,

Meramec A and Osage seem to be carbonate rich and may act as frac barriers because of their ductility at high temperatures and high breakdown pressure. Meramec D appears to be the best target in well 4 due to its low carbonate and clay content (low GR) and comparatively higher NMR porosity.

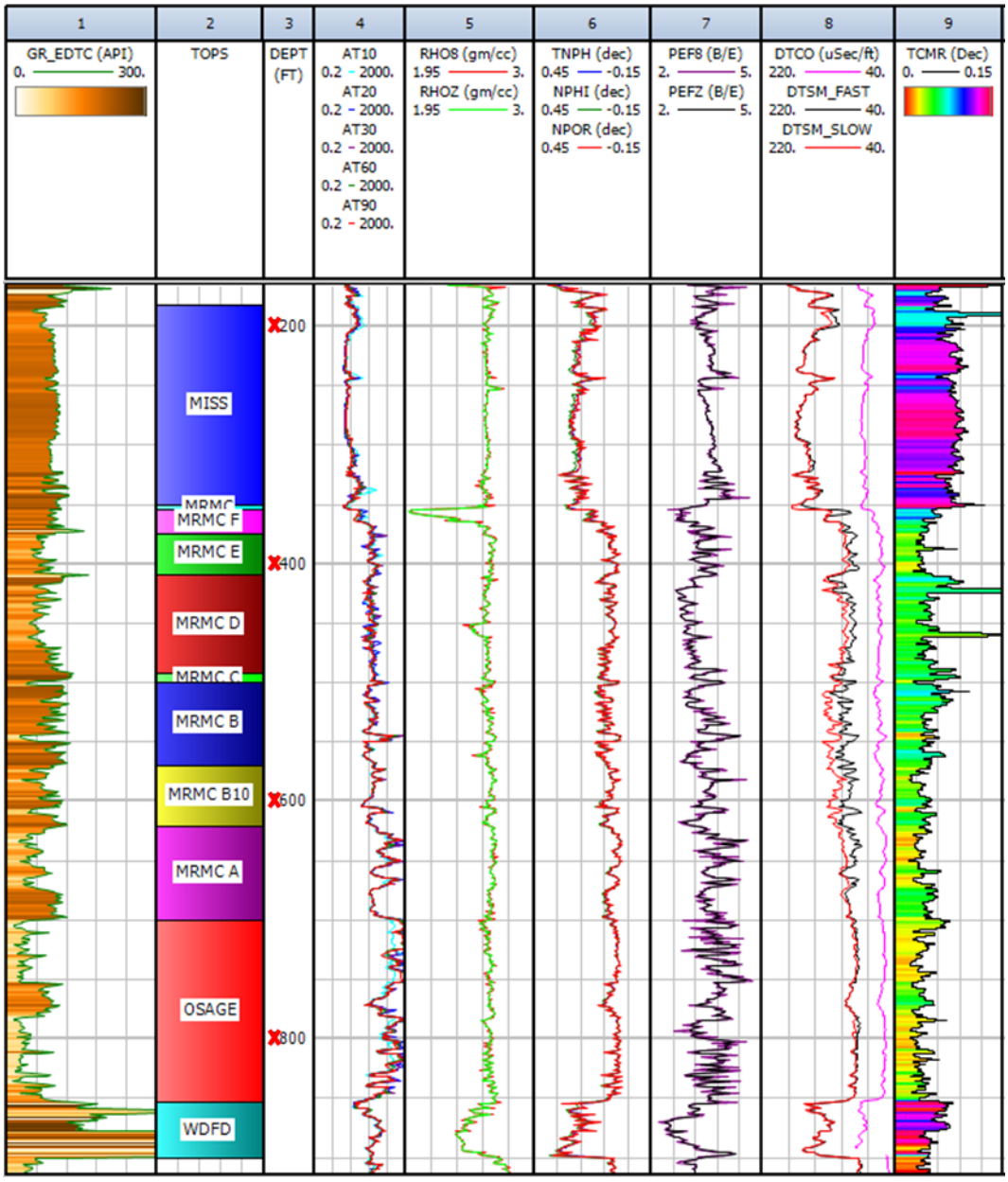

Figure 39: Snapshot of the different logs available in the Well 4 vertical pilot hole. The different tracks from left to right show gamma ray (GR), well tops, MD, resistivity, density, neutron porosity, PE, sonic travel times and NMR porosity.

Table 25: Average values of different logs (petrophysical properties) for different zones in Meramec formation in Well 4.

Zone	Thickness (ft)	GR (API)	Density (gm/cc)	Resistivity (ohm-m)	DTC (µs)	DTS (µs)	PE (B/E)	NMR Porosity (fraction)
MISS	168.5	93.6	2.61	7.87	80.3	156.2	3.59	0.085
MRMC F	20.5	99.1	2.37	35.5	66.9	125.6	3.03	0.050
MRMC E	34.5	73.9	2.65	72.6	58.3	106.2	3.45	0.039
MRMC D	83.0	79.0	2.60	59.4	62.1	104.8	3.07	0.060
MRMC C	7.5	110.9	2.61	82.3	62.2	114.4	3.41	0.062
MRMC B	70.5	92.0	2.62	78.4	62.5	113.8	3.37	0.053
MRMC B10	51.5	82.1	2.64	81.8	59.5	113.7	3.48	0.039
MRMC A	78.5	69.7	2.65	272.8	57.1	101.8	3.68	0.040
OSAGE	153.0	48.2	2.63	668.7	55.9	94.3	3.72	0.039

The logs were processed to get mechanical properties of the rocks namely Poisson's ratio, Young's modulus, shear modulus, bulk modulus, overburden gradient, pore pressure, and closure stress. Meramec formation in this area seem to be weakly anisotropic, less than 10% (Jing Fu Personal Communication). Thus, equations of mechanical properties for isotropic medium, proposed by Birch (1966) were used to calculate the mechanical properties (**Equations 21, 22, 23 and 24**).

$$Poisson's\ Ratio, PR = 0.5 * \frac{((V_p/Vs)^2 - 2)}{(V_p/Vs)^2 - 1)} \quad \text{.....21}$$

$$Bulk\ Modulus, K = \rho * \left(V_p^2 - 4/3\, V_s^2\right) \quad \text{.....22}$$

$$Shear\ Modulus, G = \rho * (V_s^2) \quad \text{.....23}$$

$$Young's\ Modulus, E = 2 * G(1 + PR) \quad \text{.....24}$$

The overburden gradient (OB_{Grad}) was calculated by integrating the density log. The pore pressure was calculated using the Eaton's Pore Pressure Method (Mouchet and Mitchell 1989). The method is applicable to shales or shaly sands where the pores are sufficiently small so that the pore fluids cannot escape and can develop over-pressure. The theory behind the method is

that with increasing depth, the overburden increases which increases the effective stress on the rock. This causes a reduction in the pore space and since, the fluids cannot escape, they develop over pressure. Decrease in porosity and increase in consolidation of the rock, is generally evident in logs like sonic and resistivity. Sonic travel times (compressional wave) in shales generally decrease with increasing depth due to reduction in porosity and increase in consolidation. This deviation from the normal hydrostatic trend is used by Eaton's method to calculate pore pressure. The method identifies a depth interval (generally at shallow depths) where the pore pressure is hydrostatic, and the sediments are normally compacted i.e. show a hydrostatic trend. This trend line is picked, and it is called Normal Compaction Trend Line (NCTL). Then the values predicted using the NCTL and the actual sonic log are used to calculate the pore pressure using **Equation 25:**

$$PP_{Grad} = OB_{Grad} - [OB_{Grad} - 0.465]\left(\frac{\Delta t_n}{\Delta t_o}\right)^3 \quad \text{.....25}$$

Where PP_{Grad} is the pore pressure gradient, OB_{Grad} is the overburden gradient, Δt_n is the sonic travel time in μs/ft along the NCTL and Δt_o is the measured sonic travel time at the same depth. Knowing the overburden gradient and pore pressure gradient, the closure stress can be calculated using the standard uniaxial strain equation (Mullen 2007).

$$P_c = \frac{v}{1-v}(OB_{Grad} - \alpha PP_{Grad}) + PP_{Grad} + \sigma_t \quad \text{.....26}$$

Where, v is the Poisson's ratio, α is the Biot coefficient, and σ_t is the regional horizontal tectonic stress. The above equation is applicable for an isotropic or nearly isotropic rock. Friedrich and Monson (2013) suggested that since closure stress is equivalent to minimum horizontal in-situ stress, to calculate closure pressure, σ_t can be neglected. Thus, to use the above equation Biot coefficient is needed. Biot coefficient can be calculated using the **Equation 27**.

$$\alpha = 1 - \frac{K_{dry}}{K_{grain}} \quad \text{.....27}$$

Laboratory velocity (Vp, Vs) data for vertical cores in dry state was available for nearby well outside section A (Personal Communication Jing Fu). The data was used to calculate the value of K_{grain} by extrapolating the fit between K_{dry} versus NMR saturated porosity to y-axis (**Figure 40a**). Next, the value of K_{grain} was used to calculate Biot coefficient using **Equation 27** and the coefficient was plotted as a function porosity (**Figure 40b**). There is a decent correlation and this correlation was then applied to calculate Biot coefficient in well 4 well using the NMR porosity log. Finally, closure pressure was calculated using **Equation 26**.

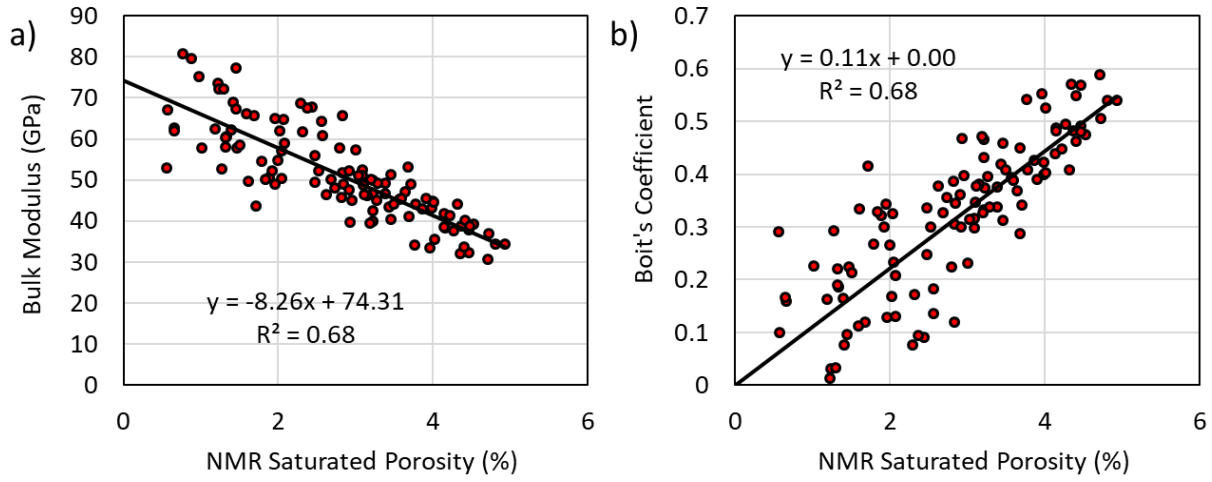

Figure 40: (a) Plot of dry bulk modulus versus porosity in nearby well. At zero porosity, the fit line should theoretically give the value of K_{grain}. (b) Plot of Biot coefficient versus porosity.

Table 26 reports the summary of the mechanical properties for different Meramec zones and **Figure 41** shows the calculated mechanical properties. The calculated pore pressure log was checked against a single DFIT pore pressure measurement and it appeared to lie on the trend giving confidence in the pore pressure log. Looking at the table, Meramec B, B10 and C seem to have high Poisson's ratio suggesting they are likely ductile. This implies that these three zones

may not be ideal landing zones. At the top of Meramec, Mississippian has very high closure stress. Thus, it may be hard to break because of higher minimum in-situ pressure (closure pressure is generally considered equal to minimum in-situ pressure). Similarly, looking at Meramec A and Osage, both these formations have high Young's moduli and high closure stress. Considering, Young's modulus is proportional to tensile strength of the rock (Sun et al. 2018), these two zones will likely have very high breakdown pressures. Thus, as concluded based on the raw logs, these two zones are likely fracture barriers. The fracture barriers play an important role in controlling the fracture height and thus control vertical well spacing and well placement strategies. In this scenario, since there are no strong fracture barriers inside the Meramec formation, it is likely that single well can drain the entire Meramec height and the efforts should then focus on optimizing the lateral spacing between the wells.

Table 26: Summary of mechanical properties for different zones in Meramec in well 4.

Zone	Thickness (ft)	GR (API)	PR	K (GPa)	G (GPa)	E (GPa)	OB_{Grad} (psi/ft)	PP_{Grad} (psi/ft)	Closure Stress Grad (psi/ft)
MISS	168.5	93.6	0.31	24.3	10.3	27.1	0.96	0.71	0.85
MRMC F	20.5	99.1	0.26	28.4	16.2	40.6	0.96	0.56	0.78
MRMC E	34.5	73.9	0.26	41.6	23.3	58.7	0.95	0.37	0.65
MRMC D	83.0	79.0	0.25	35.1	20.7	51.6	0.95	0.48	0.70
MRMC C	7.5	110.9	0.30	39.0	18.0	46.8	0.95	0.49	0.74
MRMC B	70.5	92.0	0.30	39.1	17.9	46.6	0.95	0.50	0.78
MRMC B10	51.5	82.1	0.30	43.6	19.6	51.1	0.94	0.60	0.88
MRMC A	78.5	69.7	0.28	45.7	23.0	58.9	0.94	0.56	0.83
OSAGE	153.0	48.2	0.24	43.2	27.3	67.6	0.93	0.54	0.76

4.3 Hydraulic Fracture Modeling and Recovery Factor Calculations

To further analyze the cause of strong interference between wells, fracture modeling was done using GOPHER^{TM} software. The data for fracture modeling was taken from well 4 in section A in Meramec. The petrophysical and geomechanical properties (closure stress, pore pressure,

Young's modulus and Poisson's ratio) used in the numerical modeling are shown in **Figure 39** and **Figure 41**. The completion design used for the base case is summarized in **Table 20** and **Table 21**. The results of fracture modeling are shown in Error! Reference source not found..

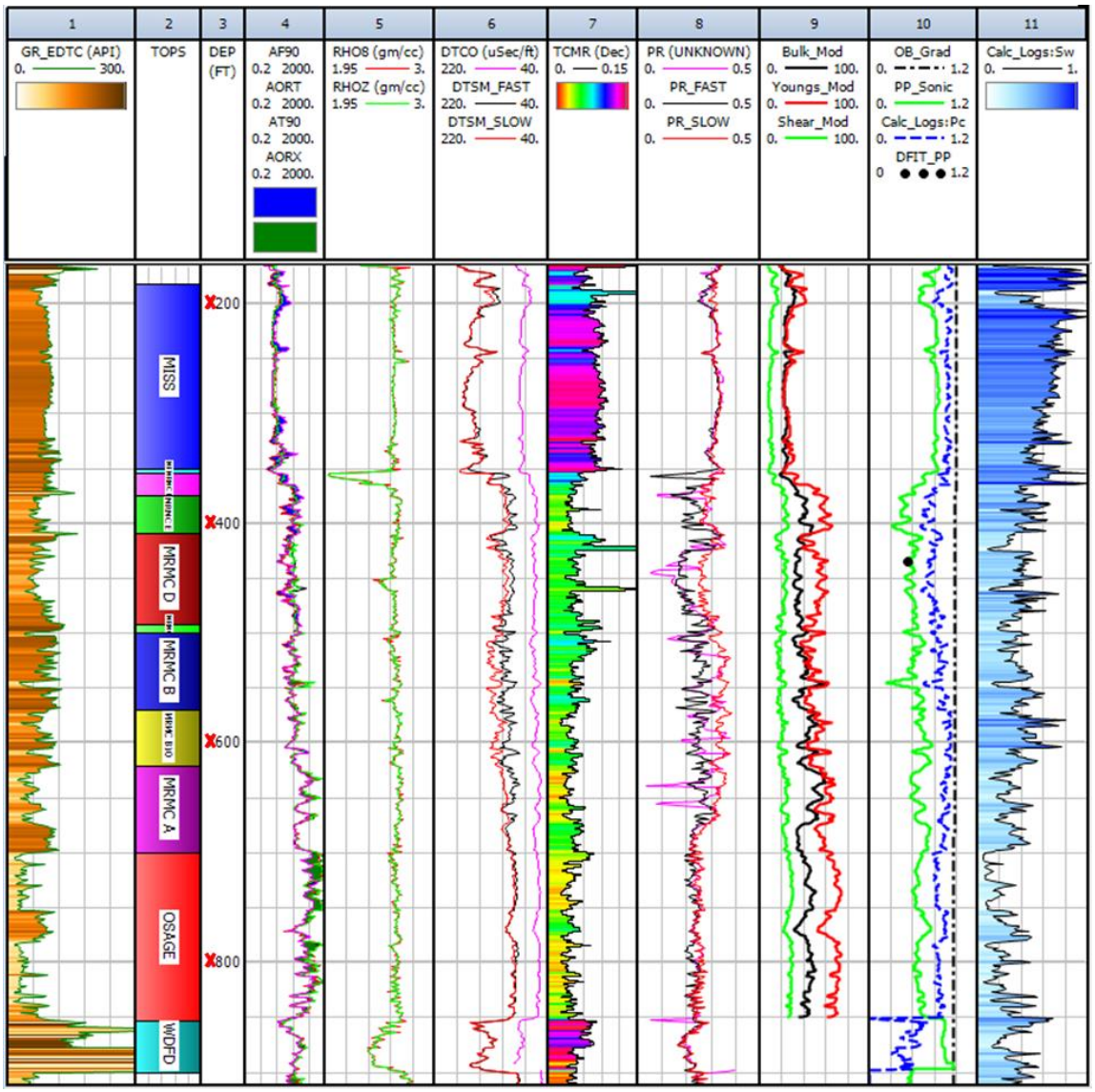

Figure 41: Raw logs and the calculated mechanical properties for the Meramec formation in well 4. Track 1 has GR, track 2 has well tops, track 4 has deep resistivity logs from several runs, track 5 has density logs, track 6 has compressional wave as wells as fast and slow shear waves, track 7 has NMR porosity, track 8 has Poisson's ratio calculated from fast and slow shear waves, track 9 has calculated logs like bulk modulus, Young's modulus and shear modulus, track 10 has calculated over burden gradient, sonic pore pressure log (green), closure stress profile (blue) and single DFIT derived pore pressure point (black dot) and finally track 11 has calculated water saturation using Archie's equation (a=0.8, m=2, n=2, Rw = 0.01 ohm-m, density porosity).

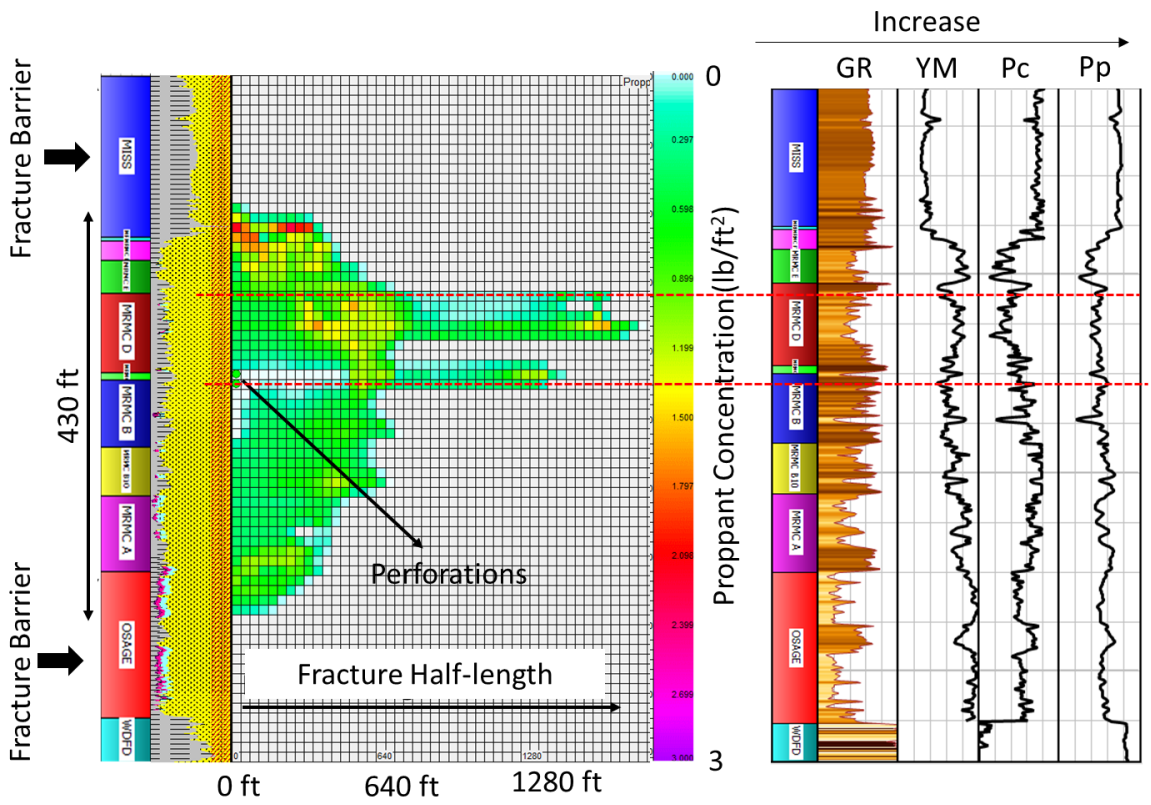

Figure 42: Output of fracture modeling from GOPHER™. The plot shows the proppant concentration across fracture length and height. It appears that fracture can propagate all the way through Meramec up until the Mississippian. The fracture growth seems to be restricted by Mississippian at the top and Meramec A and Osage at the bottom. Higher sand content (higher brittleness) and lower pore pressure (depletion in the parent well) causes extensive lateral fracture growth in Meramec D.

It appears that fractures can propagate all the way through Meramec up until the Mississippian. The fracture growth seems to be restricted by Mississippian at the top likely due to the high closure stress. At the bottom, the fracture growth is restricted by Meramec A and Osage likely due to their high closure stresses and Young's moduli. The fracture growth in Meramec is ellipsoidal except in Meramec D where it shows extensive lateral growth. The perforations are at the bottom of MRMC D, and MRMC D is bounded by local barriers shown as GR peaks on the log plot (Error! Reference source not found.). These local barriers can act to confine fractures and coupled with lower pore pressure, lower closure stress, this causes long extended fractures in

MRMC D. This shows how minor variations in lithology and rock properties can control fracture growth and why it is important to study them.

The microseismic data from the same well is shown in

Figure 43. The top and side view of microseismic events corroborate numerical modeling as fracture half-length and height predicted by numerical modeling lies in the range delineated in the microseismic maps. A further calibration was done by doing analytical production modeling using GOPHER^{TM} and comparing it to the actual well production.

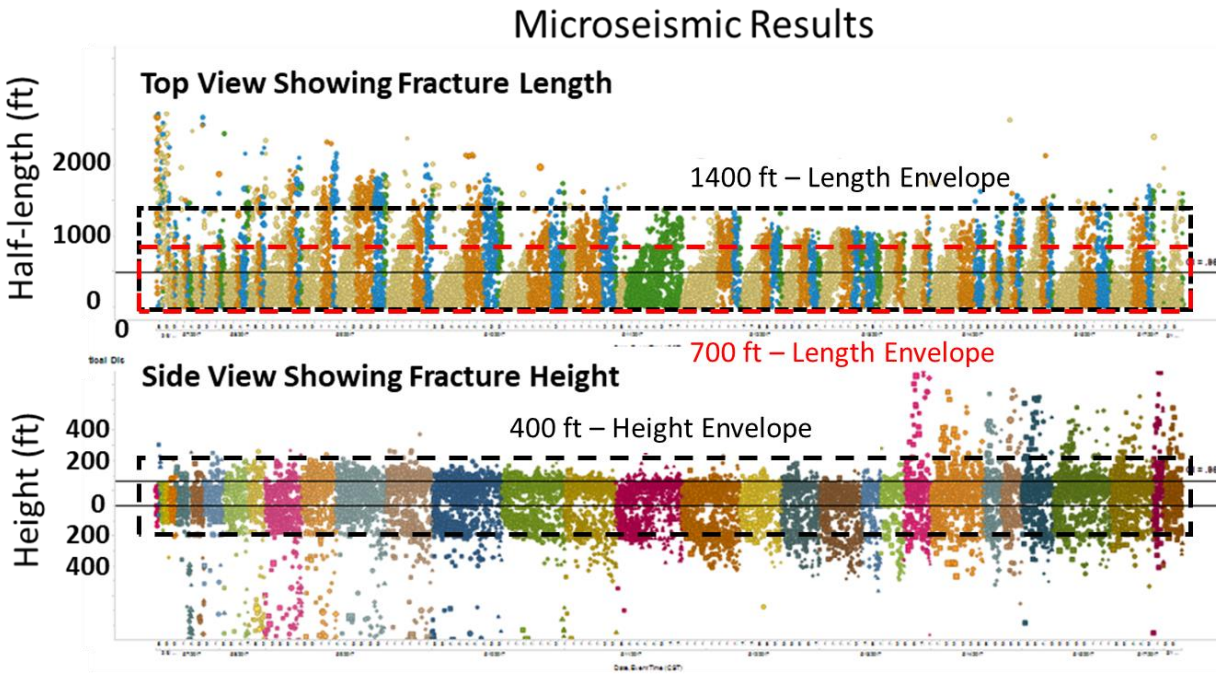

Figure 43: Microseismic event maps showing the lateral and vertical extent of fractures in different stages in Well 4 in section A. The zero in both the graphs represent the level of the well. Thus, in fracture half-length plot, positive values mean fracture growth on the right side of the well, and negative values mean fracture growth on the left side. In fracture height plot, positive values represent upward fracture growth and negative values represent downward fracture growth. In the top plot for fracture half-length, points are colored by proppant type. In the bottom plot for fracture height, the data points are colored by frac stage. The numerical modeling results are further validated by microseismic data which show fracture half lengths varying between 700 to 1400 ft. and fracture heights averaging around 400 ft. There appear to be significant outliers both in the early stages and later stages shown as points outside the envelope. These microseismic events were measured in the 2 surrounding faults and fracture networks of neighboring wells.

Figure 44 shows the comparison between the production predicted by GOPHER based on the modelled frac dimensions compared to the actual production data for the well. The predicted curve matches very well with the actual production during the early history of the well but deviates around the time child wells were drilled. Thus, the deviation is likely due to frac hits received by the parent well. The frac hits were not included in the numerical modeling. Only the parent well production was considered for matching as child well production is affected by well interference which was not accounted for in GOPHER.

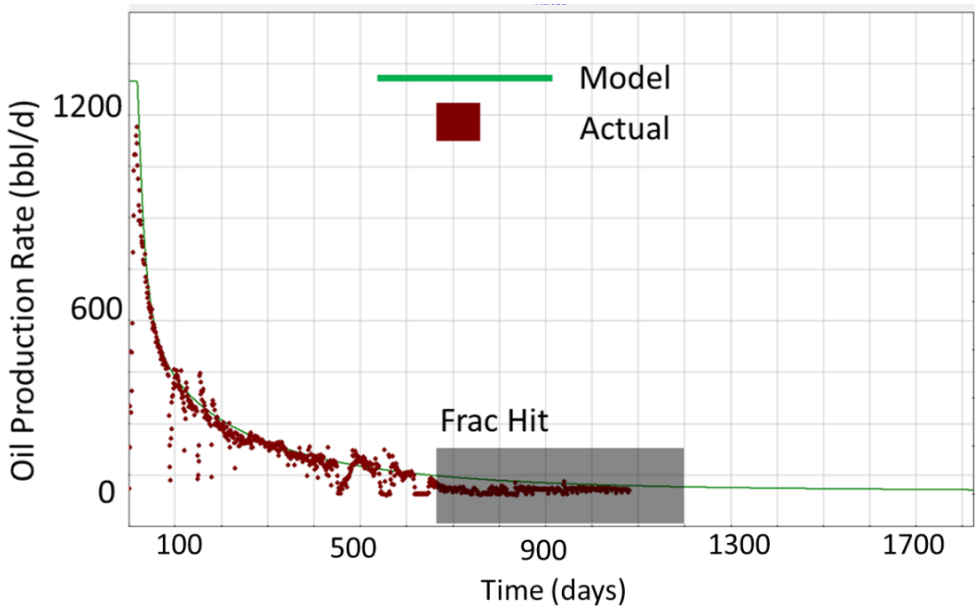

Figure 44: A comparison between the production predicted by GOPHER based on the modelled frac dimensions compared to the actual production data for the well. The predicted curve matches very well with the actual production during the early history of the well, but deviates around the time child wells are drilled. Thus, the deviation is likely due to frac hits received by the parent well. The frac hits were not included or in the numerical modeling.

Based on the calibrated fracture model, the propped fracture half-length is about 1400 ft. but the fracture narrows considerably beyond 700 ft with low proppant concentration. It is likely that effective fracture length during production will be around 700 ft. The well spacing in this area is 660 ft which restricts the fracture half-length to 330 ft for no interaction with adjacent wells.

Based on effective propped frac half-length of 700 ft, fractures in adjacent wells will likely overlap which explains the strong interference seen in the production data. Clearly, well spacing of 660ft is too optimistic.

A quick side-calculation was also done to get the recovery factors for the different wells. The saturation log was calculated using Archie's equation (Archie 1952) and is shown in **Figure 41**. The values of constants a, m, n were assumed to be 0.8, 2, 2 (Personal communication Ali Tinni) based on the analysis of core data in nearby wells. The product of NMR porosity and hydrocarbon saturation (1 – Sw) was multiplied with log depth interval (0.5 ft) and summed across the Meramec zone. The number came out to be 8.1. Oil formation volume factor was assumed to be 1. This number can be multiplied by the product of well lateral length and well spacing (or fracture half-length * 2) to get hydrocarbon in place (HCIIP) for each well. The fracture half-length for each well would vary based on completion size, rock properties; but, enough data is not available to calculate fracture dimensions for each stage in each well. Propped fracture-length is about 700 ft (350'*2) which is generally more than the well spacing (~660ft). Thus, 660ft was taken as width of the drainage area and multiplied by lateral length to calculate the drainage area. The drainage area was then used to calculate in-place estimate. The recovery factor calculations are shown below in **Table 27**. The EUR period was taken to be 50 years though there was a negligible cumulative contribution after 10 years. The recovery factors are very low. The recovery factors for children are much lower than the parent well. Thus, another way to improve section A economics could be to increase recovery per well. The answer to increase recovery is not just increasing completion size (proppant and fluid amount) as they will only increase the inter-well communication. Other possible methods to increase recovery that could be investigated are increasing fracture complexity, lazy-Z fracturing (Mann et al. 1983),

miscible gas EOR (Dang et al. 2019) or surfactant application (Gupta et al. 2020, sent for review).

Table 27: Calculations for recovery factor in different section A wells. The product of lateral length and well spacing (660ft) was taken as the areal extent of the reservoir for each well. It was multiplied by the log calculated value of 8.1 which was the product of porosity and oil saturation summed over Meramec zone. The EUR was calculated from DCA using a time frame of 50 years. Calculated recovery factors are very small suggesting there is scope to increase them and improve economics of the section A wells.

Well	Lateral Length (ft)	Width for HCIIP Calculations (ft)	HCIIP (Mbbl)	EUR (Mbbl)	Recovery Factor (RF, %)
Well 1	4880	660′	9.33	0.158	3.40
Well 2	4668	660′	8.93	0.096	2.16
Well 3	4672	660′	8.94	0.056	1.26
Well 4	4527	660′	8.66	0.030	0.70
Well 5	4727	660′	9.04	0.062	1.38
Well 6	4479	660′	8.57	0.046	1.08
Well 7	4473	660′	8.56	0.058	1.36

4.4 Surface Drilling Data Analysis

The log-based mechanical property calculations and fracture modeling examples show that exhaustive data collection (core, log, pressures) is key to understand fracture propagation and explain occurrence of frac hits. However, it is not economic to collect the exhaustive data in all the wells. Generally, the data that is collected in all the wells is GR and surface drilling data. Next, an exercise was done to see if this basic data can be used to say something about the petrophysical and mechanical properties of the rock. The surface drilling data (Weight on Bit (WOB), RPM, Rate of Penetration (ROP), Torque, bit size) can be combined to calculate Mechanical Specific Energy (MSE) using **Equation 28** (Davarpanah et al. 2016).

$$MSE = \frac{480 * torque * RPM}{d_{bit}^2 * ROP} + \frac{4 * WOB}{\pi d_{bit}^2} \quad \text{.....28}$$

where d_{bit} is the diameter of the bit. GR is an indicator of lithology while MSE represents the amount of energy required to break a unit volume of the rock. MSE depends upon lithology

(Moronkeji et al. 2017), pore pressure (Kalinec et al. 2019), minimum in-situ stress and other mechanical properties. Thus, four groups were created on the GR and MSE cross plot as shown in **Figure 45 (a)**. The box plots in **Figure 45 (b)** and **Figure 45 (c)** show that different groups have characteristically different Poisson's ratios and Young's moduli. Generally, shales have higher MSE compared to sandstone (Moronkeji et al. 2017) and high GR indicates shaly lithology. Thus, high GR and high MSE group (HMHG) likely represents clay-rich lithology and that explains its higher Poisson's ratio. The other extreme low MSE and low GR (LMLG) likely represents quartz rich lithology considering sandstones have lower MSE than shales (Hamrick 2011, Moronkeji et al. 2017) and sandstones also have low GR. This also explains the lowest Poisson's ratio of this group. **Figure 45 (c)** shows that Young's modulus is increasing from left to right which can be explained by the increasing quartz-content. The closure stress was looked at based on MSE alone (**Figure 45 (d)**). It is evident that when stresses are low, it is easier to break the rock. Thus, low MSE roughly correlates with lower closure stress. This shows that when reasonable and representative core and log data are available, it can be used to derive relations between GR and surface drilling data and different petrophysical and mechanical rock properties, which can then be used across the play to characterize the rock. This is crucial for understanding the fracture propagation, understanding the occurrence of frac hits and optimally design completions.

Even though logs were available in only well 4, surface drilling data is available in 4 wells namely 4, 5, 6 and 7. MSE was calculated for all the four wells using surface drilling parameters. The data was then extracted for completed lateral section and plotted on GR and MSE cross plot shown below in **Figure 46**. The plot shows that all the four wells have data distributed in all the four groups suggesting widely varying petrophysical and mechanical properties between

different stages. Thus, all stages cannot be expected to perform equal. Moreover, wells 4 and 6 has large portion of the data that primarily lies in the HMHG (High MSE, High GR) group. This is the clay-rich formation group and is expected to have smaller fracture dimensions due to high clay content, high MSE and high closure stresses. This can also be a contributing factor to its high breakdown pressure observed in **Table 20** and corresponding poor production performance in **Table 22**.

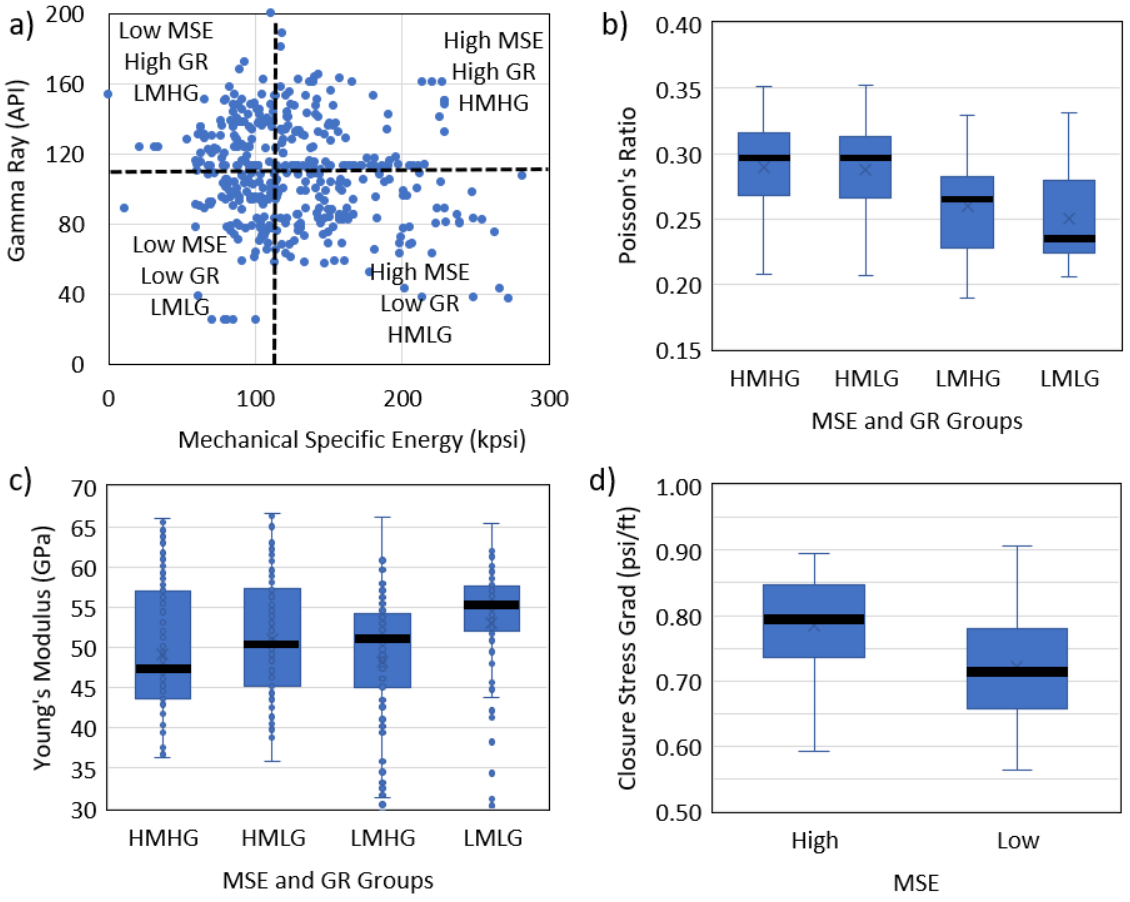

Figure 45: (a) Cross plot of GR and MSE where four different groups were identified. (b) Different groups identified on GR-MSE cross plot have characteristically different Poisson's ratios and (c) Young's moduli. HMHG represents the group with high MSE, high GR, high Poisson's ratio and low Young's modulus. These characteristics typically befits clay-rich formations. Similarly, LMLG groups represents low MSE, low GR, low Poisson's ratio and high Young's modulus. These characteristics befit quartz-rich formations. (d) MSE alone is also an indicator of closure stress (or minimum horizontal stress) with both exhibiting a proportional relationship.

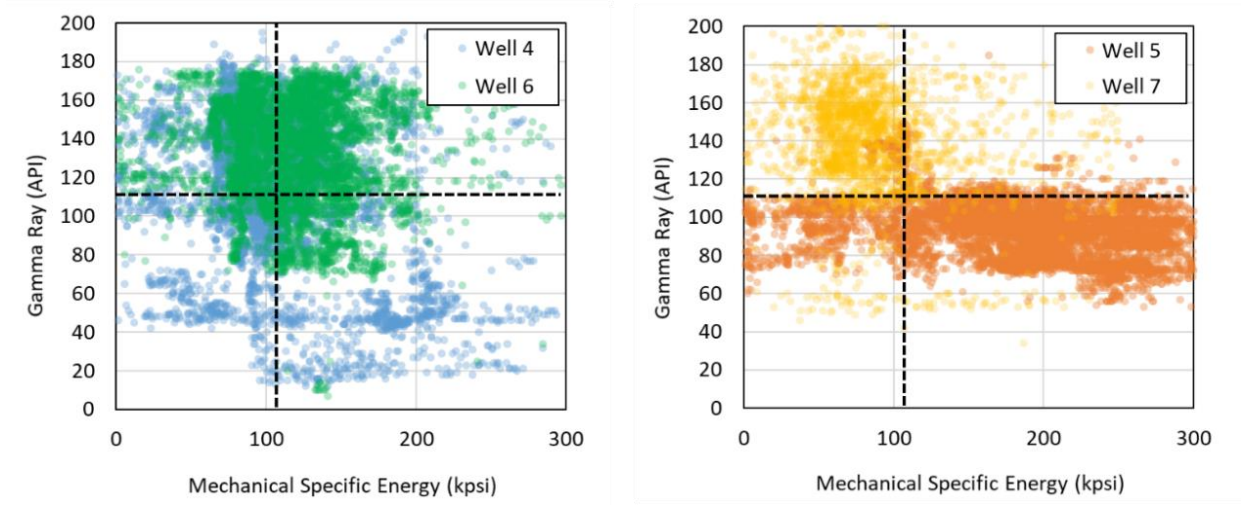

Figure 46: Data pertaining to the lateral section of four wells plotted on GR and MSE cross plot. The plot shows that all the four wells have data distributed in all the four groups suggesting widely varying petrophysical and mechanical properties between different stages.

4.5 Microseismic Data Analysis

Microseismic data was available in 4 wells namely 2, 3, 4 and 6. The data was analyzed to gain insights on hydraulic fracture propagation and occurrence of frac hits. Microseismic data also gives an opportunity to study stage by stage performance. However, production logging, high resolution logs along lateral section or fiber-optics data are required to support the conclusions based on microseismic interpretations. Since, these data are not available, microseismic data cannot be exploited to its full potential. **Figure 47** shows the top view of microseismic cloud for the four wells. The microseismic data in Wels 5 and 6 was recorded using two wells namely well W1 and Well 4 in **Figure 33**. Microseismic tool string was lowered to the deepest part possible in the heel of the Well 4 and about roughly 8000 ft. in the W1 wellbore to straddle the Meramec. For wells, 2 and 4, only well W1 was used for monitoring. Well 2 shows westward bias especially towards later stages (>25). This is likely due to fault reactivation shown by high density of those microseismic events along the picked fault (**Error! Reference source not found.**).

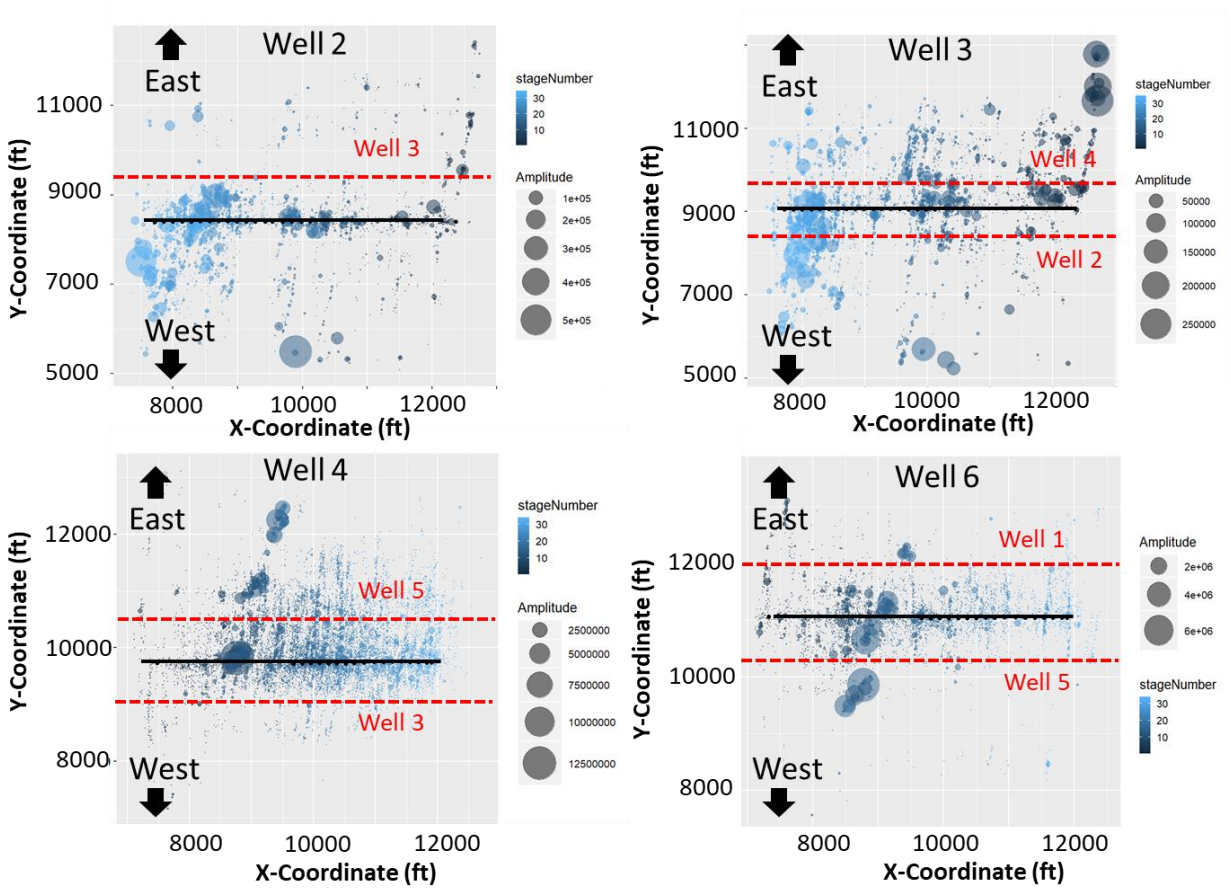

Figure 47: Top view of microseismic cloud for the four wells. Well 2 shows westward bias especially towards later stages. Well 3 shows a strong east ward bias towards Well 1 in earlier stages and westward bias in later stages probably due to the same reason as well 2. Well 4 also shows a strong eastward bias in earlier stages towards well 1. Well 6 which is closest to well 1 shows more symmetric growth. This is likely due to big change in its completion design in which amount of slick water was reduced to half and x-linker gel was doubled. Compared to other wells, well 6 shows much smaller fracture dimensions possibly due to clay-rich facies.

Well 3 shows a strong eastward bias towards Well 1 (parent well) in earlier stages and westward bias in later stages probably due to the same reason as well 2. Well 4 also shows a strong eastward bias in earlier stages towards well 1. Well 6 which is closest to well 1 shows more symmetric growth. This is likely due to big change in its completion design in which amount of slick water was reduced to half and x-linked gel was doubled. Compared to other wells, well 6 also shows much smaller fracture dimensions possibility due to clay-rich facies (**Figure 46**).

Overall, the overlap of microseismic cloud between adjacent wells (shown by microseismic cloud exceeding the red lines which represents neighboring wells) suggest strong inter-well interactions.

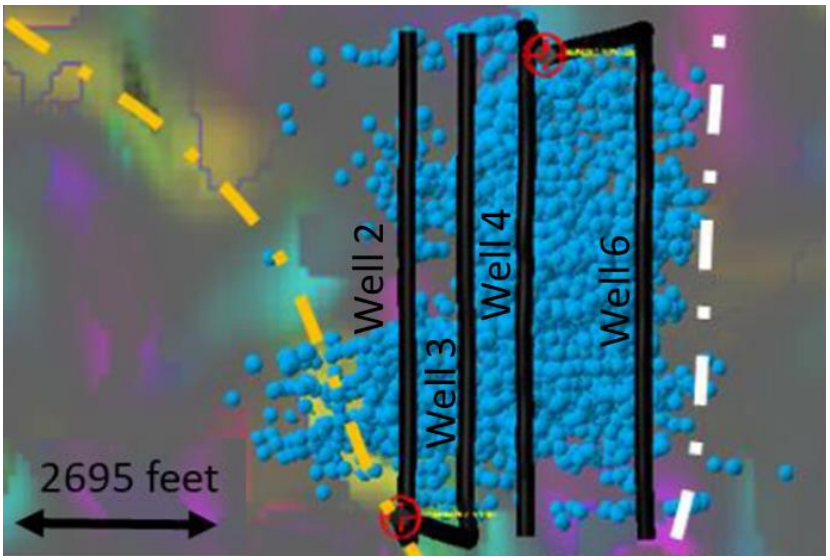

Figure 48: Picked faults (dashed yellow and white lines) in the section A (Personal Communication Swetal Patel). The large microseismic events in the later stages of wells 2 and 3 are likely due to fault (yellow) shown in the figure. Lot of microseismic events were generated as the fault was activated. Majority of the events generated below Meramec zone were also along the faults.

Stage-wise analysis was performed using fracture complexity plot proposed by Warpinski (2009). Because of uncertainty in the microseism location, it is difficult to say with accuracy if there is one fracture or multiple fractures, or what is the exact path of fracture propagation, but the data can be used to suggest if the fracture network is complex or planar. For each stage, the seismic data was processed to calculate the length and width of the microseismic cloud. The width in this plot represents the width of the microseismic cloud and not individual fractures. The ratio of the total width to total length is called Fracture Complexity Index (FCI). Planar fractures generally have microseismic data distributed close to the main fracture and hence show lower values of FCI. On the contrary, complex fractures have microseisms distributed far away

from the main fracture, thus, they show large values for FCI. **Figure 49 (a)** shows the original FCI plot published by Warpinski (2009) with the data plotted for several sandstone and shale formations. Sandstones in the plot generally condense in the lower region and they appear to have high FCI but only because lengths are short. The figure shows Barnett shale's high FCI values and it represents a good example of complex fracturing in shale formations. **Figure 49 (b)** shows the FCI plot generated for wells in section A. The different points represent different stages. It clearly shows that hydraulic fracturing in Meramec is more like shales than sandstones. The average FCI values for the wells are also plotted back on Warpinski (2009) plot (**Figure 49a**) for comparison., It appears that well 3 has the lowest FCI and well 6 has the highest FCI. Thus, fractures are expected to be more planar in well 3 while they are more complex in well 6. Fracture network is more complex in well 6, but the total length and width of the fractures are less compared to well 3. Smaller fracture dimensions of wells 4 and 6 are partially attributed to complex fracture development and partially to higher breakdown pressure as shown in **Table 20**.

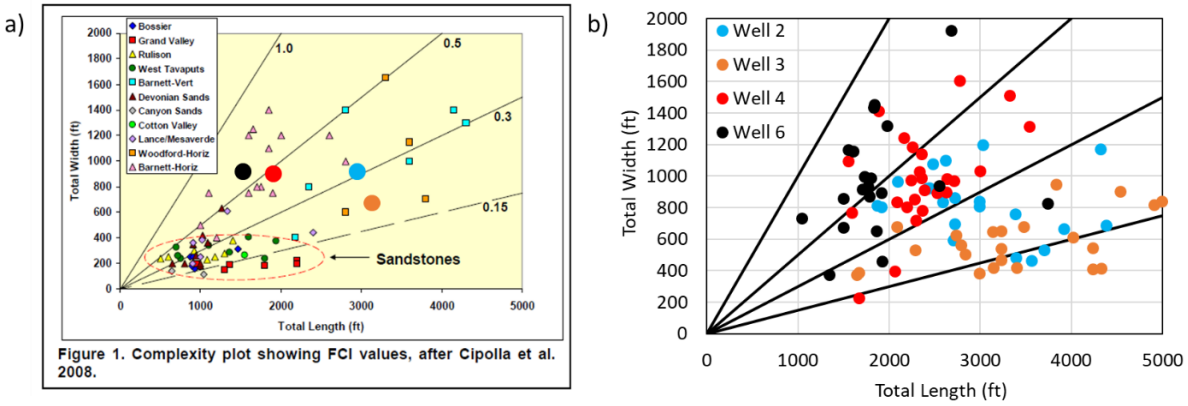

Figure 49: (a) Original FCI plot published by Warpinski (2009) with the data plotted for several sandstone and shale formations. Sandstones in the plot generally condense in the lower region and they appear to have high FCI but only because lengths are short. (b) FCI plot generated for different section A wells. The different points represent different stages. The average value for the well is superposed on the Warpinski (2009) plot for comparison. Looking at the average values, it appears that well 3 has the lowest FCI and well 6 has the highest FCI. Thus, fractures are expected to be more planar in well 3 while they should be more complex in well 6.

Further, Warpinski (2009) presented a network development plot where he showed that planar fracture propagation showed a square root of time dependence while complex fracture propagation does not show square root of time dependence. The mechanics of hydraulic fracture generation in planar versus complex fractures is quite different. In planar fractures, the fracture front propagates into the reservoir, the high fluid leak-off from the main fracture destabilizes and shears the nearby formation creating secondary network and releasing energy in the process which is measured by geophones. Shapiro et al. (2002) reported that microseismic events occur due to pore pressure relaxation in media with anisotropic hydraulic diffusivity. The propagation of microseismic triggering front is controlled by permeability tensor. In complex fracture development, the fluid diffuses to the natural fractures and other formation discontinuities. The natural fractures get activated and the network width for each cluster in the stage is developed almost immediately. Microcracks gradually connect with each other across the entire fracture zone creating a complex fracture network and generating microseisms in the process. Thus, generally for complex fractures, a square-root time-dependence is not seen. Shapiro (2015) reported that fractured shales may in some cases show parabolic time$^{1/3}$ dependence. **Figure 50** shows the original Warpinski (2009) plot where he shows this difference between planar and complex fracture development.

The data for the four section A wells was analyzed for the square root of time dependence. The data shown in **Figure 51** show that while some stages clearly show the square root of time dependence (LHS plots), i.e. planar fracture development, the other stages (RHS plots) do not show a square-root time dependence, i.e. show more complex development. Well 6 particularly shows predominantly complex fractures in 67 percent of its stages. On the contrary, well 3 shows planar fractures in 74% of its stages. Another noticeable point is that in all the wells, generally

early stages show more complex fracture development while later stages show more planar fracture development. This could be due to increased stress shadow effect as the hydraulic fracturing is progressing from stage to stage. The increased stresses due to stress shadows inhibit complex fracturing and rather facilitate planar fractures (Wu et al. 2012). This is also consistent with increasing ISIP trend seen in **Figure 34** which is another likely effect of stress shadow.

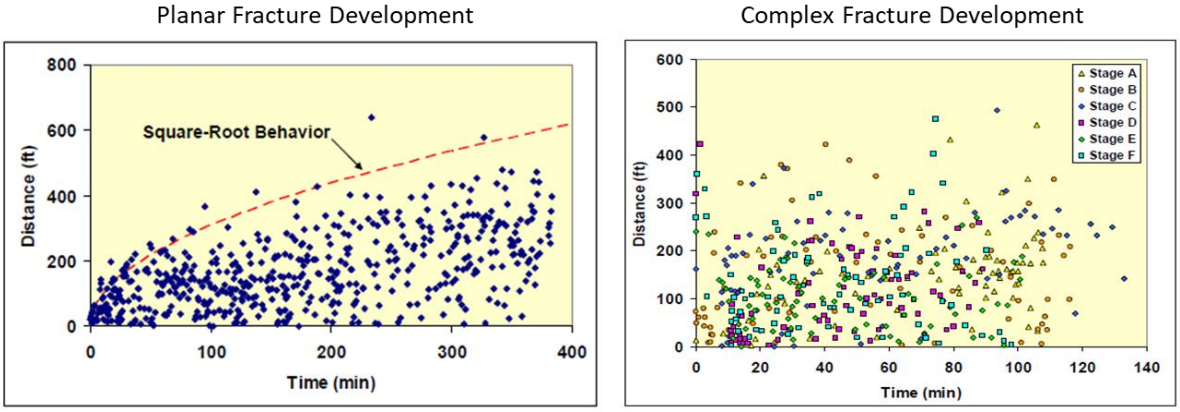

Figure 50: Original plot from Warpinksi (2009). (a) Planar fracture propagation shows square root of time dependence. (b) Complex fracture development does not show the square root of time dependence.

Lastly, the cumulative moment derived from the microseismic data was plotted as a function of time (**Figure 52**). The premise is that hydraulic fractures in shales generally occur when the low viscosity fluid activates, dilates and shear-offsets the natural fractures.. The cumulative moment is a function of shear displacement and shear modulus. It is a stable number that does not change too much with noise and other operational issues and it is mainly dominated by the large microseismic events. The LHS in **Figure 52** shows the cumulative moment versus time plots for different section A wells. There is a general trend that seismic moment increases with increasing stage numbers. This is attributed to the impact from the previous stages. This suggests that adjacent stages strongly interact with each other. Thus, the stage spacing may be too optimistic and it can be further optimized.

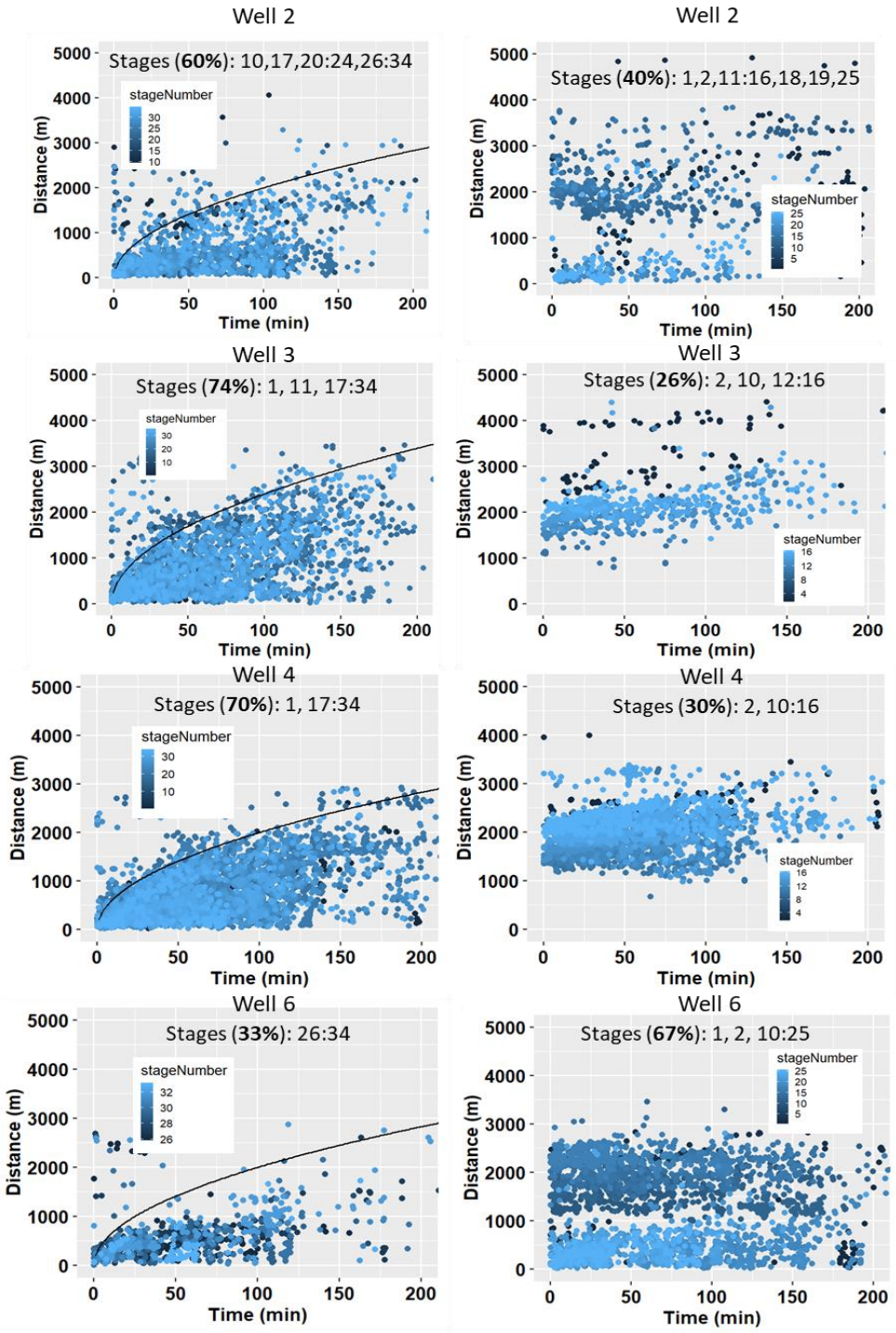

Figure 51: Network development plot for section A wells. Each plot lists the stages from which the data was taken. Generally, data from stages 3 to 9 were removed from all the wells as there appeared to be an issue with acquisition and hence the reliability of the data. Some stages (LHS) clearly show the square root of time dependence and predict more planar fracture development. Other stages (RHS) do not show square root of time dependence i.e. have possibly more complex fracture development.

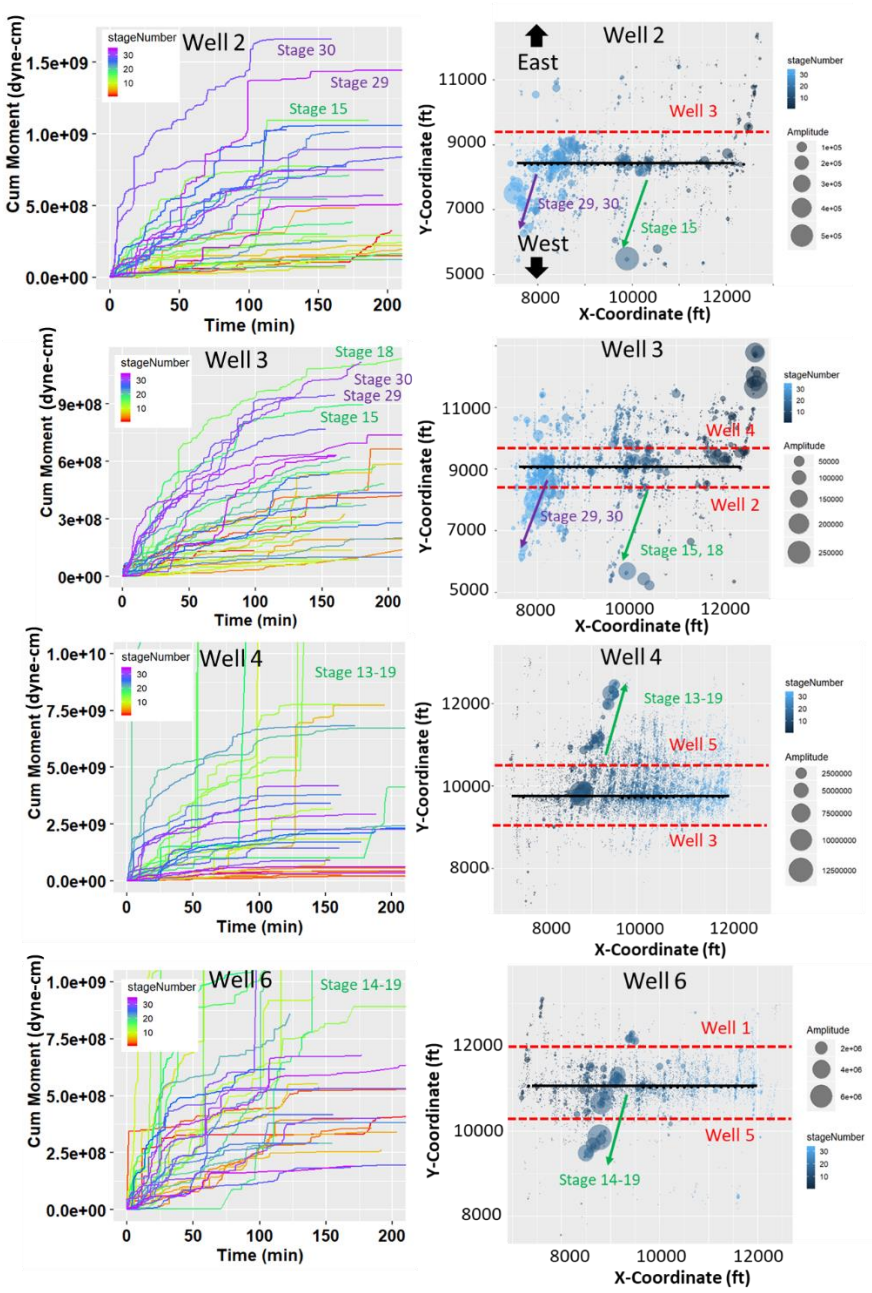

Figure 52: (LHS) Cumulative moment derived from the microseismic data plotted as a function of time. For each stage, the time zero roughly corresponds to start of frac fluid injection/pumping for the stage. There is a general trend that seismic moment increases with increasing stage numbers. This is attributed to stress shadow effect. Some stages show abnormally high cumulative moment. This can happen when the fluid injection during that stage starts interacting with faults, a fracture network of parent wells or other formation discontinuities like natural fractures or high permeability streaks. These likely interactions with faults or depleted parent well is also shown in microseisms x-y location plots on the RHS.

Lastly, in all the plots, there appears to be some stages which have significantly high cumulative moment compared to the other stages. For instance, in well 2, stages 15, 29 and 30 have abnormally high cumulative moment. This can happen when the fluid injection during that stage starts interacting with fault, fracture network of parent wells or other formation discontinuities like natural fractures, and high permeability streaks. Fracturing into faults and high natural fracture density areas can cause very large magnitude microseisms which can skew the cumulative moment plot. These likely interactions with faults or depleted parent well are also shown in microseisms x-y location plot on the RHS. The same is done for other wells as well. The presence of faults is already confirmed in the region by the working geophysicists (Error! Reference source not found.) which along with depleted parent well fracture network is likely causing the high magnitude microseisms.

4.6 Summary

The objective of this infill study was to primarily understand the parent-child interactions, impact of frac hits, optimum wells per section, number of stages, stage spacing, understand fracture propagation patterns (planar vs. complex), and existence of fracture barriers.. Based on the analysis, section A child wells strongly interact with the parent wells and each other (**Table 22**, **Figure 36**). The fracture modeling (Error! Reference source not found.) and microseismic (**Figure 47**) data analysis clearly show overlap of fracture stages in the different wells. It suggests that well spacing of 660ft is quite optimistic. The stage ISIP (**Figure 34**) and microseismic analysis (**Figure 52**) showed that stages are strongly interacting with each other causing stress shadow effects. This clearly manifests itself in fracture geometry where earlier stages likely have complex fractures and later stages likely develop more planar fractures. The planar versus complex fractures in different stages were indirectly interpreted using seismic

(**Figure 51**). This gives an opportunity to optimize the stage spacing. The fracture modeling (Error! Reference source not found.) and log interpretation (**Table 26**) show that Mississippian, Meramec A and Osage are potential frac barriers. Lastly, GR and MSE cross plot (**Figure 45** and **Figure 46**) shown in several wells can help identify mechanical property variation across the wellbore in real-time and can be used to optimize completion design by avoiding the high GR and high MSE (HMHG) clay-rich regions for completion.

Chapter 5: Sensitivity on Completion Design in Meramec

Acquiring field data for all possible permutations and combinations is not only expensive but unnecessary given the current scientific understanding and numerical modeling capabilities. Numerical modeling is frequently used to run sensitivity analysis which can both fill data gaps and help interpret field data. This chapter shows results of the numerical modeling to define response surfaces for key completion design parameters to reduce uncertainty and improve decision making. The results also provide useful insights on possible designs that can minimize the risk of frac hits.

Fundamentally, from a technical standpoint, everything seems to center around the cluster as it is the contact point between the laterals and the reservoir. A cluster being the entry point of fluid and proppant to the formation, controls individual fractures. Thus, the sensitivity study in this chapter looks at four critical completion design parameters namely fluid per cluster, proppant per cluster, cluster spacing and number of clusters per stage. The fluid and proppant per cluster values were calculated by dividing the total proppant and frac fluid used per well by the product of number of stages and number of clusters per stage. Similarly, cluster spacing was determined by dividing the completed lateral length by the product of number of stages and number of clusters per stage. The data required for building numerical models is taken from well 4 in section A in Meramec. The fracture model and its calibration results are shown in Error! Reference source not found.**,**

Figure 43 and **Figure 44.**

5.1 Completion Trends for Meramec and Permian

To carry out sensitivity study, it is important to look at the trends over the years of different completion design parameters which can be used to define range of values over which the

sensitivity must be carried out. **Figure 53** shows the fluid per cluster trend with time for both Meramec and Permian. The range for sensitivity in fluid per cluster was taken to be 500 to 3000 bbl. In general, the plots suggest that Meramec formation typically uses more fluid per cluster compared to Permian. Additionally, in both Meramec and Permian, the average values of fluid per cluster has decreased with time. This is contradictory to what is expected as **Figure 2** shows that the fluid used per well generally show an increasing trend over time. It appears that the large increase in number of clusters per stage over the same time period caused the decreasing trend of fluid per cluster. Similarly, **Figure 54** shows the trend for proppant per cluster with time. The range for sensitivity was taken as 25000 to 100000 lbs. With respect to proppant per cluster, both formations show opposite trends with an increasing trend in Meramec and a decreasing trend in Permian. Meramec trend has plateaued around 2016.

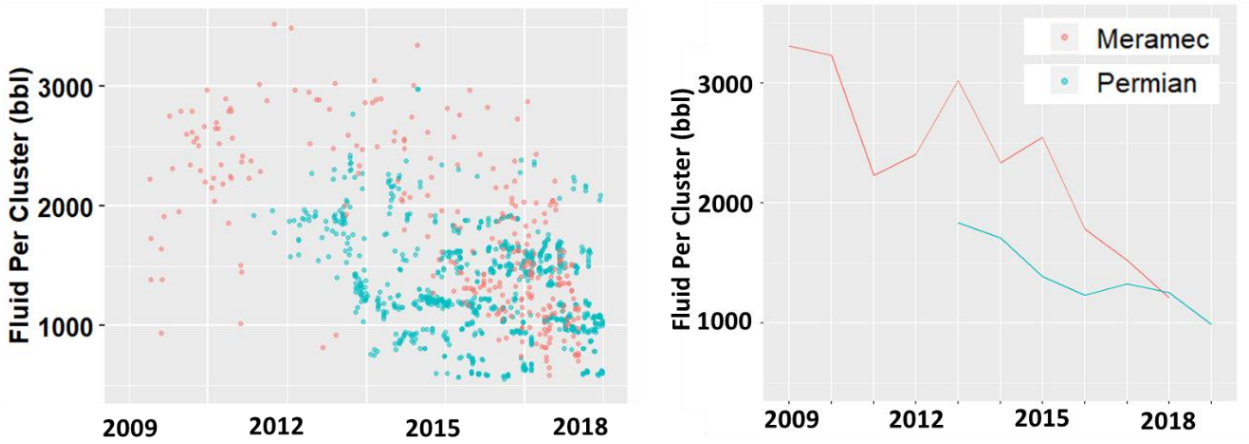

Figure 53 (Left) Fluid per cluster in different wells in Meramec and Permian. (Right) Average value of fluid per cluster averaged over a year. First, Meramec seems to use greater fluid per cluster compared to Permian. Second, in both formations, fluid per cluster decreases with time.

Figure 55 shows the values of cluster spacing in Meramec and Permian; the range for sensitivity was taken as 10 to 75 ft. The data also show a strong decreasing trend in cluster spacing in both Meramec and Permian. Average cluster spacing in the Meramec is slightly higher than the

Permian which is expected considering higher matrix permeability of the Meramec. **Figure 566** shows that number of clusters per stage show an increasing trend in both Meramec and Permian. The range for sensitivity was taken as 3 to 10.

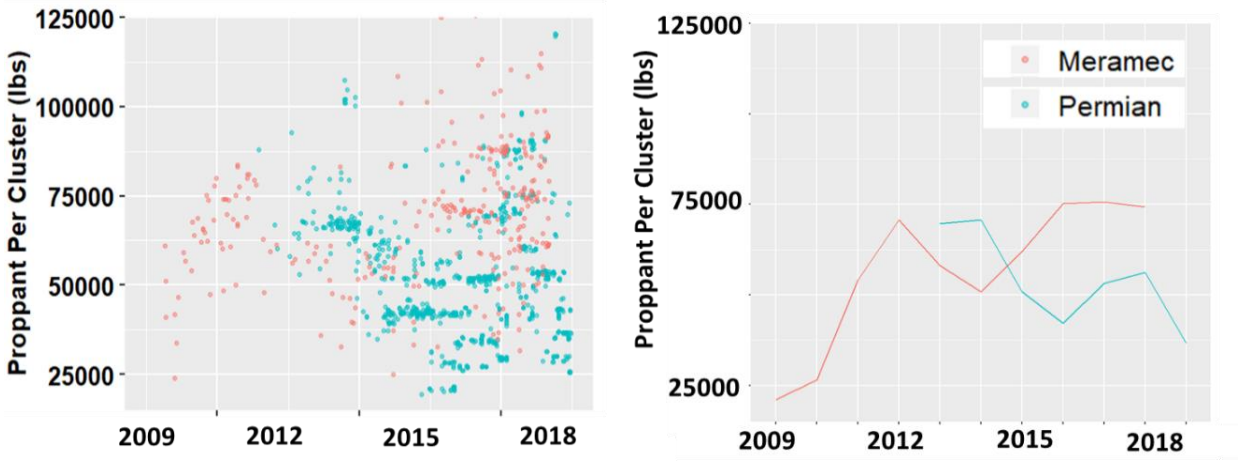

Figure 54: (Left) Proppant per cluster in different wells in Meramec and Permian. (Right) Average value of proppant per cluster averaged over a year. The data shows an increasing trend with time in Meramec and a decreasing trend in Permian. Meramec appears to reach a plateau around 2016. The range of values appear to be in the same range.

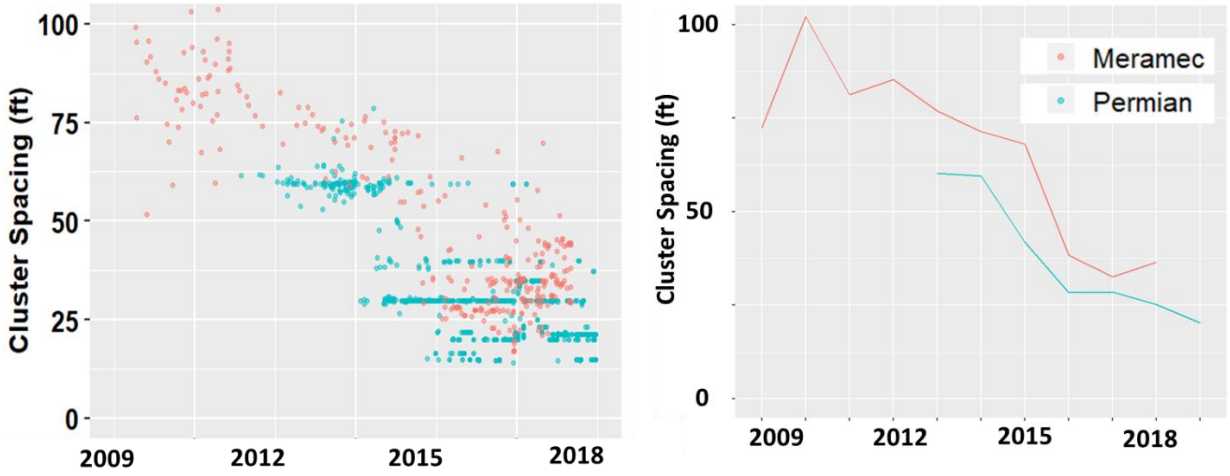

Figure 55: (Left) Cluster spacing in different wells in Meramec and Permian. (Right) Average value of cluster spacing averaged over a year. Both Meramec and Permian show a reduction in cluster spacing with time.

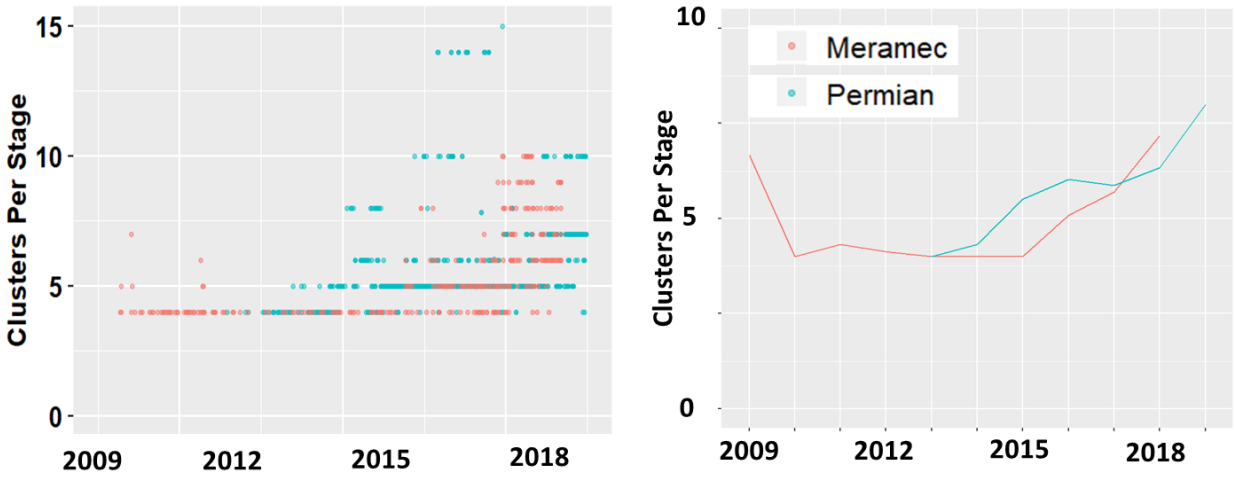

Figure 56 (Left) Number of clusters per stage with time in Meramec and Permian. (Right) The average value of clusters per stage increases in both Meramec and Permian.

5.2 Results of Sensitivity Analysis

5.2.1 Impact of Fluid Per Cluster

The fluid per cluster was varied between 500 to 3000 bbl per cluster while other parameters were held constant (proppant per cluster = 50,000 lbs., cluster spacing = 33 ft. and clusters per stage = 5). **Figure 57** shows the results of sensitivity on fluid per cluster. It is evident that both length and height are directly proportional to the amount of fluid per cluster. Effective length and height are obtained by applying a minimum cut-off of 0.5 lb/ft^2 proppant concentration. Effective length is much shorter than total length while effective height is slightly less than total height. This suggests that fracture has a higher tendency to close in the lateral direction compared to the vertical direction.

Fluid per cluster because of its strong correlation with fracture dimensions is one of the important optimization parameters to control well productivity and risk of frac hits. Such correlations (**Figure 57**) prepared using numerical models and calibrated using field data (microseismic, tracer surveys) are recommended to optimize completion design. **Figure 11**

showed that staggered (or offset) well placement is an effective strategy to minimize frac hits. **Figure 58** provides evidence that corroborates this statement. In **Figure 58**, two cases of well placement are shown. In case 1, the two wells are placed directly above each other. In case 2, the two wells are offset laterally. In general for this area, numerical modeling in **Figure 57** shows that effective and total height are similar while effective length is much shorter than total length. This suggests that in case 1, since fractures remain open in vertical direction, there is high likelihood that well 1 and well 2 would be in communication during the production phase. In case 2, fractures would likely close in lateral direction, well 1 and well 2 may not be in communication during the production phase.

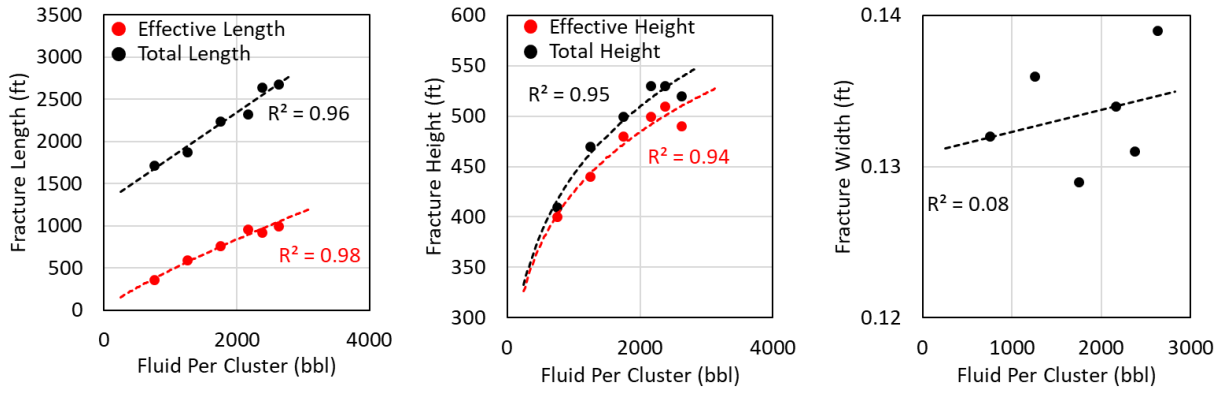

Figure 57: Results of sensitivity on fluid per cluster. It is evident that both length and height are directly proportional to the amount of fluid per cluster. Effective length and height are obtained by applying a minimum cut-off of 0.5 lb/ft^2 proppant concentration. Effective length is much shorter than total length while effective height is slightly less than total height. This suggests that fracture has a higher tendency to close in the lateral direction compared to the vertical direction. No correlation was seen between the fluid per cluster and fracture width.

Production prediction and net present value (NPV) calculation were also carried out for all the sensitivity cases. The economic parameters for NPV calculation are shown in **Table 19**. The results of production modeling and NPV for different fluid per cluster values are shown in **Figure 59**. Since, well productivity is directly proportional to fracture dimensions, there is strong

positive correlation between fluid per cluster and well 60-day IP (initial production). However, completion costs are prohibitive as increasing the completion size results in lower NPV. Two crude oil price points show at the current oil price ($55) this well is uneconomic, but it becomes economic at high oil price of $100.

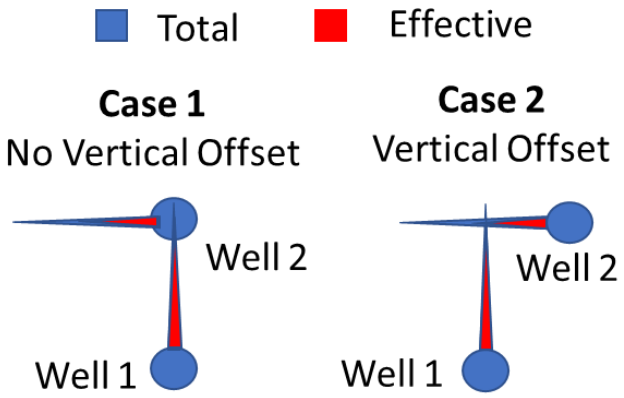

Figure 58: Two cases of well placement. In case 1, the two wells are placed directly above each other. In case 2, the two wells are offset laterally. In case 1, since effective (propped) height is similar to the total height, there is high likelihood that well 1 and well 2 would be in communication during the production phase. In case 2, since effective (propped) length is much shorter than total length, well 1 and well 2 may not be in communication during the production phase.

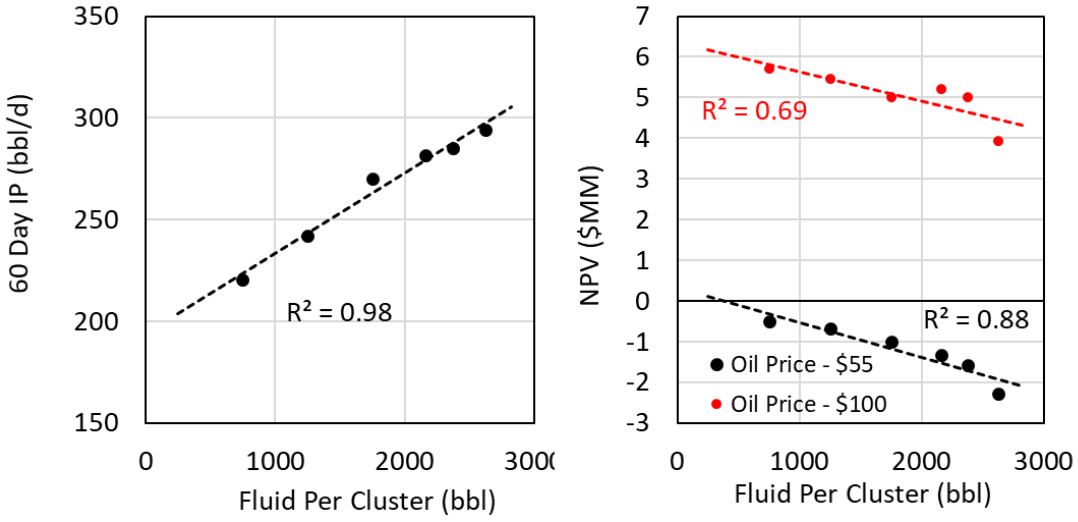

Figure 59: Production modeling and NPV results for different fluid per cluster values. Since, well productivity is directly proportional to fracture dimensions, there is strong positive correlation between fluid per cluster and well 60-day IP. However, completion costs are prohibitive as increasing the completion size results in lower NPV.

5.2.2 Impact of Proppant Per Cluster

The proppant per cluster was varied between 25,000 to 100,000 lbs while other parameters were held constant (fluid per cluster = 2150 bbl, cluster spacing = 33 ft and clusters per stage = 5). **Figure 60** shows the results of sensitivity on proppant per cluster. There is a small dynamic range of fracture height and length for a wide range of proppant per cluster. This suggests that proppant per cluster does not exert a strong control on fracture length and height. The inverse relation of length with proppant amount is likely because higher proppant concentration restricts fluid movement hence reducing the fracture length. Fracture width shows positive correlation with proppant amount which is expected as proppant goes in between the fracture surfaces to prevent it from closing and hence, determines the fracture width. With respect to well productivity, higher proppant concentration, i.e. larger fracture width is favorable as it directly controls the fracture conductivity. But, with respect to frac hits, larger proppant amount may lead to stronger frac hits and prolonged interaction between parent and child wells.

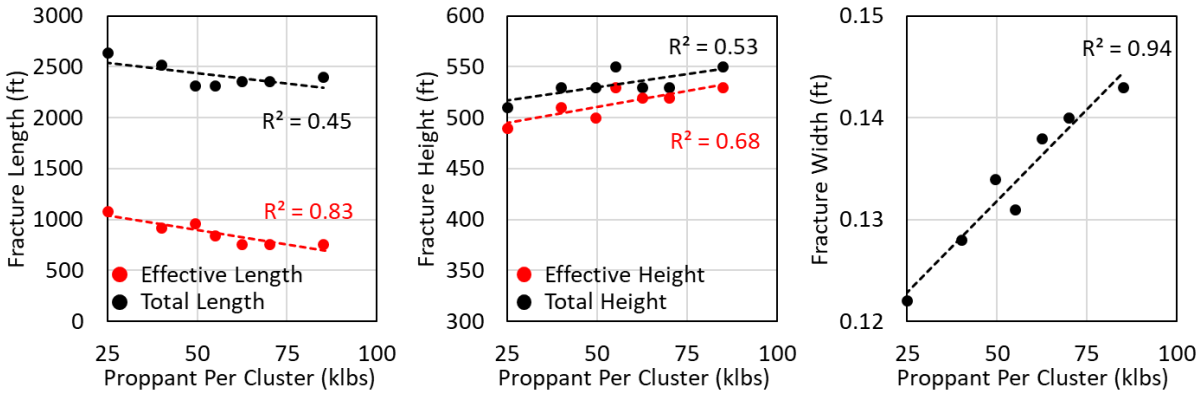

Figure 60: Results of sensitivity on proppant per cluster. There is a small dynamic range of fracture height and length for a wide range of proppant per cluster. This suggests that proppant per cluster does not have a strong control on fracture length and height. On the other hand, proppant per cluster strongly controls the fracture width.

The results of production modeling and NPV results for different proppant per cluster values are shown in **Figure 61**. Proppant per cluster shows a positive correlation with well productivity

considering it directly correlates to fracture width. However, since length and height control SRA which is the key predictor of well productivity, the proppant per cluster sensitivity plot shows a narrow range of productivity. Like fluid, proppant costs are prohibitive as increasing the proppant amount results in lower NPV. Again, at current oil price ($55) the well is uneconomic but becomes economic at a higher oil price of $100.

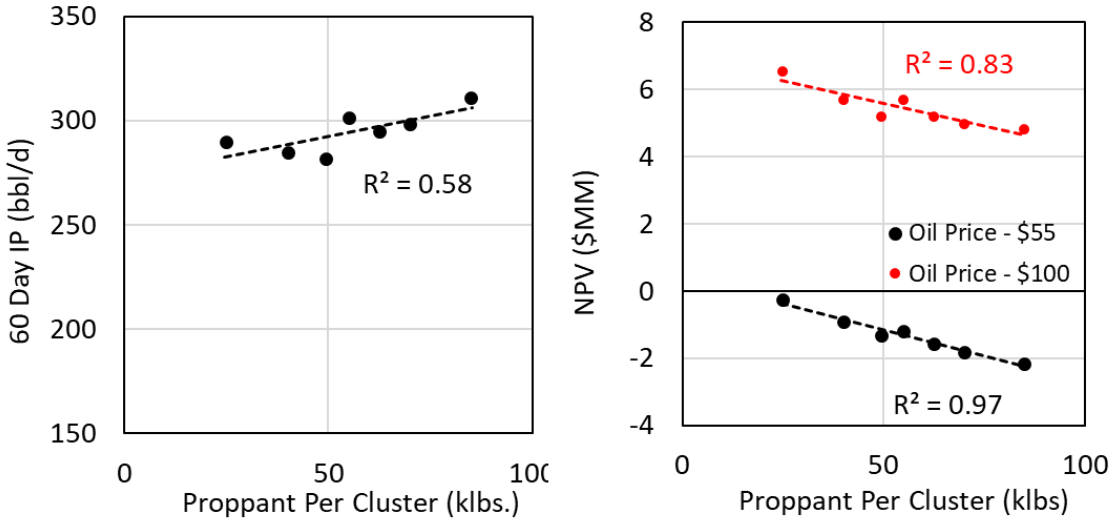

Figure 61: Proppant per cluster shows a positive correlation with well productivity considering it directly correlates to fracture width. However, since length and height control SRA which is the key predictor of well productivity, the proppant per cluster has a narrow range of productivity. Like fluid, proppant costs are prohibitive as increasing the proppant amount results in lower NPV.

5.2.3 Impact of Cluster Spacing

Figure 62 shows the results of sensitivity on cluster spacing. The cluster spacing was varied between 16 to 75 ft while other parameters were held constant (fluid per cluster = 2150 bbl, proppant per cluster = 50,000 lbs and clusters per stage = 5). There appears to be no correlation between fracture height/length/width and cluster spacing. This is likely because stress shadow was assumed to be zero for this analysis. Thus, since the fluid and proppant per stage (or cluster) did not change, fracture dimensions are not affected.

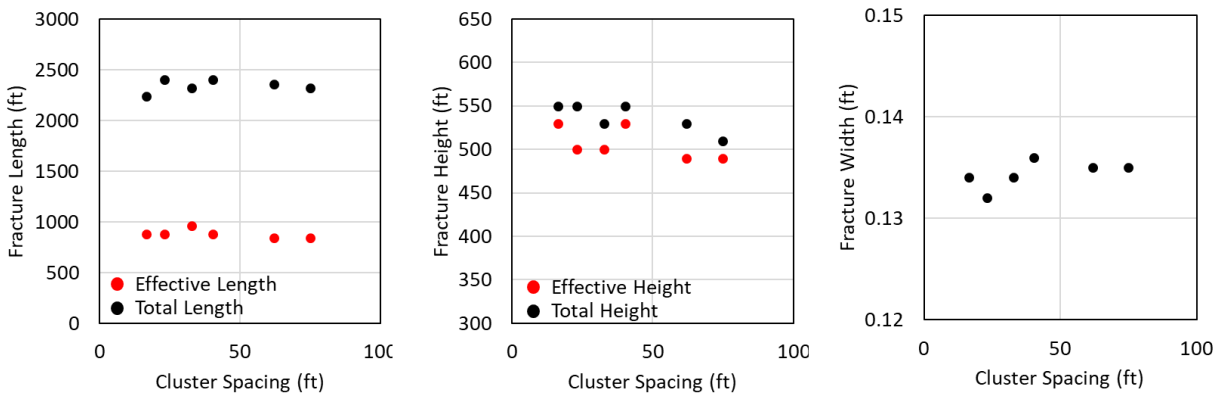

Figure 62: Results of sensitivity on cluster spacing. There appears to be no correlation between fracture height/length/width and cluster spacing.

5.2.4 Impact of Number of Clusters per Stage

The results of sensitivity on clusters per stage are shown in **Figure 63**. The number of clusters were varied between 3 and 9 while other parameters were held constant (fluid per cluster = 2150 bbl, proppant per cluster = 50,000 lbs and cluster spacing = 33 ft). No stress shadow was assumed in the calculations. All fracture dimensions length/height/width are positively correlated to the number of clusters. This is unexpected as proppant and fluid per cluster were kept constant. As we increase the number of clusters per stage, the total fluid and proppant per stage increases. If each cluster was taking in the same fluid and proppant, then it would not matter. However, due to varying mechanical properties along the wellbore, some clusters are easier to breakdown, and they can take the bulk of the fluid and proppant (**Figure 64**). Thus, this disproportionate fluid intake by clusters cause large fracture geometries. This finding has strong impact on frac hits as traditionally it was believed that increasing the number of clusters would cause smaller fractures which would minimize the risk of frac hits. Clearly, the assumption that all clusters are equal is not true. Larger number of clusters can actually increase the risk of frac hits especially in high heterogeneity reservoirs.

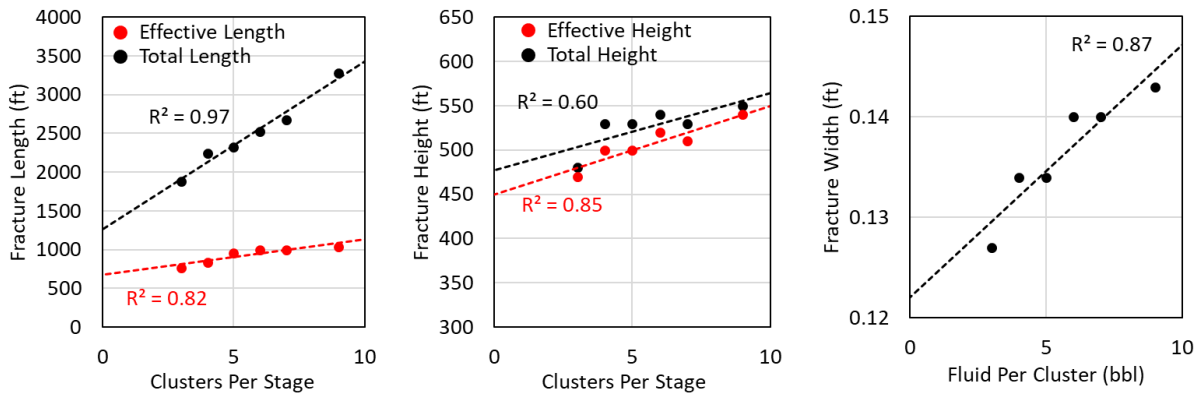

Figure 63: Results of sensitivity on clusters per stage. No stress shadow was assumed in the calculations. All fracture dimensions length/height/width are positively correlated with the number of clusters. This is unexpected as proppant and fluid per cluster were kept constant for all the sensitivity cases. As we increase the number of clusters per stage, the total fluid and proppant per stage increases. If each cluster took in the same fluid and proppant, then it would not matter. However, due to varying mechanical properties along the wellbore, some clusters are easier to breakdown and take the bulk of the fluid and proppant. Thus, this disproportionate fluid intake by clusters can cause large fracture geometries.

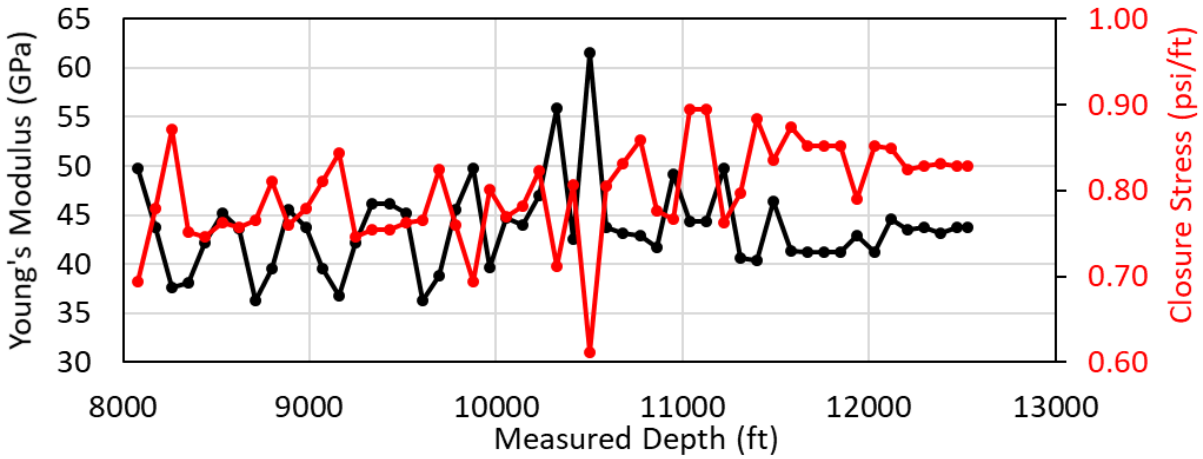

Figure 64: Lateral variation of mechanical properties like Young's modulus and closure stress across the lateral length of Well 4. This large variation in mechanical properties may promote disproportionate fluid intake by different clusters. Lower Young's modulus implies lower rock strength. Thus, the rock will break more easily at clusters having lower Young's modulus. Since, fluid and proppant follow the path of least resistance, these clusters could take the majority of the proppant and fluid, causing much larger fracture dimensions compared to the other clusters.

5.3 Stress Shadow Analysis

Stress shadow refers to accumulation of stresses in nearby stages or wells due to hydraulic fracturing of a stage or a well, respectively (**Figure 65**). GOPHER™ can model stress shadow. In GOPHER, two equations (**Equations 29 and 30**) are used to model the stress shadow (Barree 2019). The equations are numerically solved for each grid block in the model. Since, the net pressure or fracture width changes along the fracture, the fracture is divided into several grids each having a specific net pressure or fracture width. The stress shadow is then determined perpendicular to the fracture face using **Equations 29 and 30**. Each grid has its own Young's modulus.

$$\sigma = \frac{3*144*P}{2\pi Z^t} \quad \text{.....29}$$

$$\sigma = \frac{wE}{12Z^t} \quad \text{.....30}$$

In the equations, σ is the stress buildup due to stress shadow in psi, P is the net pressure from hydraulic fracture treatment in psi, Z is the distance from fracture face in ft, t is a constant called transverse exponent, w is the fracture width in inches and E is Young's modulus in psi. During the pumping there is a direct relationship between the net pressure, modulus and width as defined by deformation solution (Perkins and Kern 1961). Using this relationship, the two methods yield identical results while pumping. The value of t for homogenous, permeable and linear-elastic rocks is 2. The value for laminated, low-permeability unconventional rocks vary between 1 to 1.5 and most commonly used value is 1.2. The exponent controls the variation of stress with distance. Lower values indicate slow dissipation leading to stronger interference. **Equation 29** and **Equation 30** are used to model the stress shadow in GOPHER™.

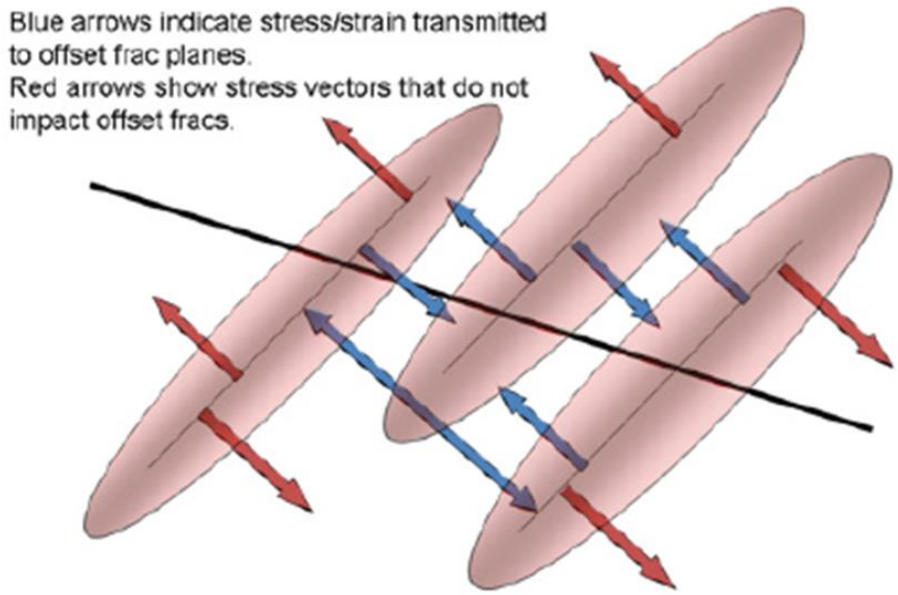

Figure 65: A hypothetical model showing stress shadow in nearby stages due to hydraulic fracturing. Stress shadow propagates perpendicular to the fracture face (Barree 2019).

To model the stress shadow, an additional stage (stage 2) was modelled in all the sensitivity cases where the stress shadow option in GOPHER was turned on. The way it is set up is that stage 2 experienced stress shadow due to stage 1 using **Equations 29 and 30**. The impact of stress shadow on fracture dimensions, well productivity and economics were evaluated. Key variables impacting the extent of stress shadow were also analyzed. **Figure 66** shows the impact of stress shadow on fracture length, height and width. It is evident that stress shadow on average reduces fracture length by 50%, fracture height by 25% and fracture width by 20%. **Figure 67** shows the impact of stress shadow on well productivity and NPV. Again, stress shadow has a strong impact on well productivity as it reduces well productivity by 25%. It also causes NPV to decrease on average by $1.15MM. The key factors impacting the stress shadow are cluster spacing and proppant per cluster as shown in **Figure 68**. The cluster spacing directly impacts Z i.e. distance from fracture face and proppant per cluster impacts fracture width both of which directly controls the stress shadow (**Equations 29 and 30**). Larger cluster spacing increases Z

and decreases the stress shadow. More proppant per cluster increases fracture width w and increases the stress shadow.

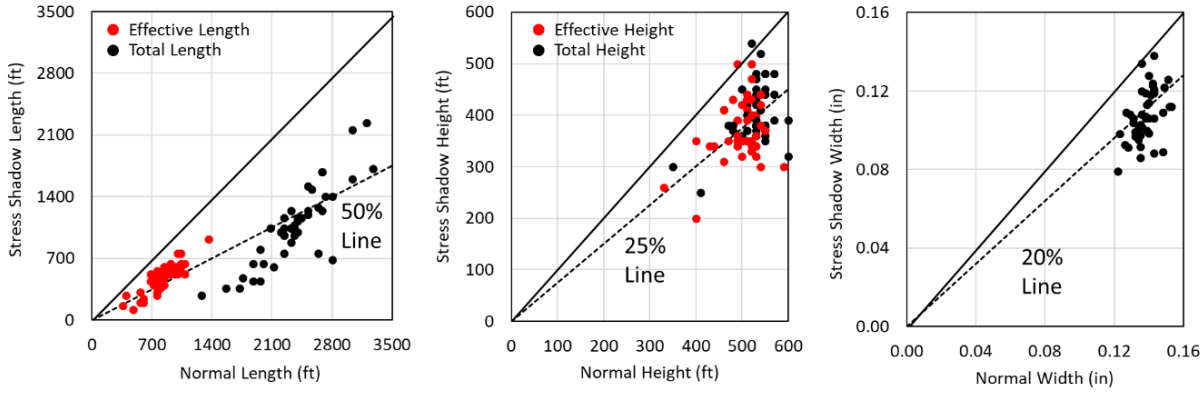

Figure 66: Impact of stress shadow on fracture length, height and width. On the x-axis, the actual length, height and width from stage 1 is plotted. Stage 1 does not experience stress shadowing. On the y-axis, the fracture length, height and width are plotted from stage 2 where stage 2 experiences stress shadow due to stage 1. It is evident that stress shadow on average reduces fracture length by 50%, fracture height by 25% and fracture width by 20%.

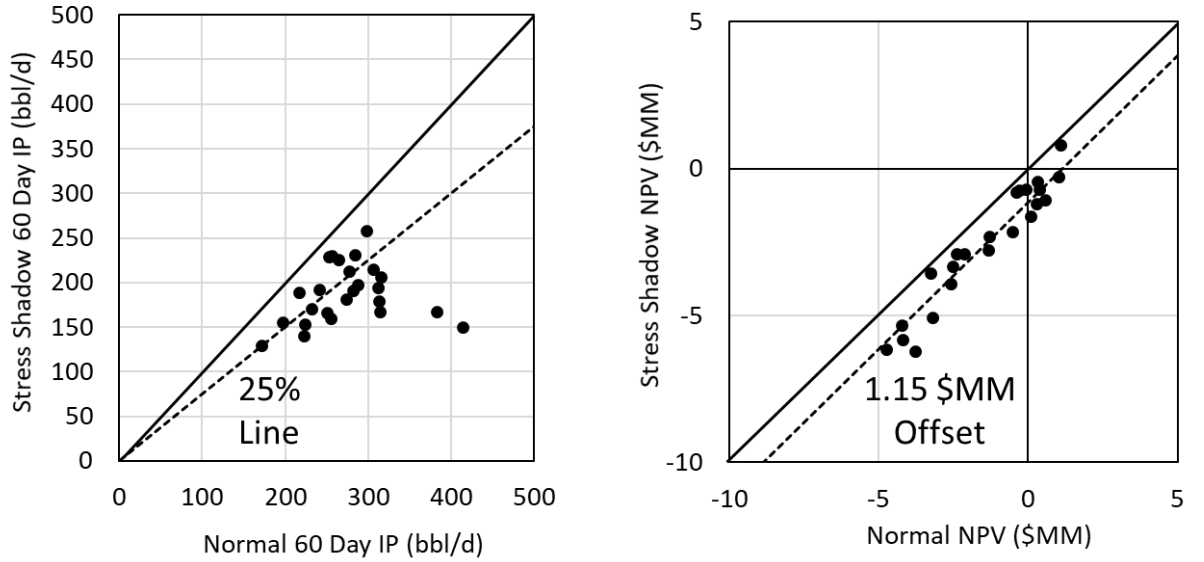

Figure 67: Impact of stress shadow on well productivity and NPV generated from the well. Again, on x-axis values are reported from stage 1 without any stress shadow impact and y-axis reports values from stage 2 with stress shadow impact from stage 1. Stress shadow on average reduces 60 Day IP by 25% and NPV by $1.15MM.

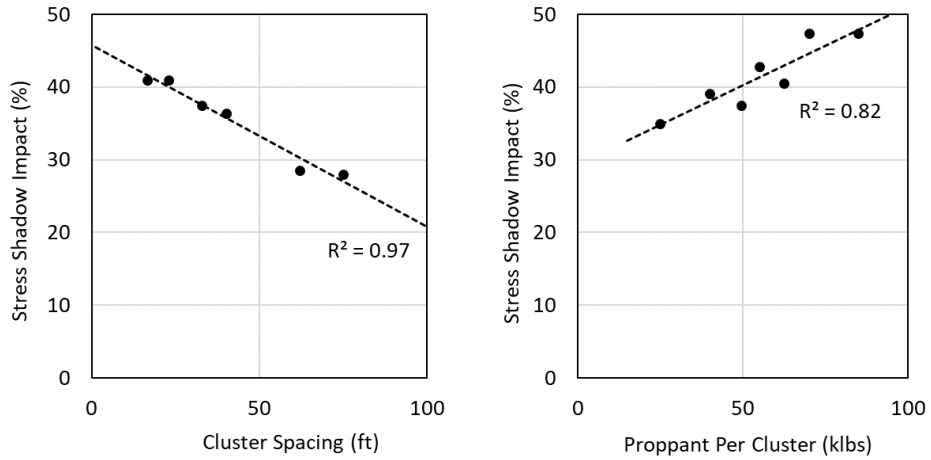

Figure 68: The impact of stress shadow here refers to percentage reduction in length due to stress shadow. The two key factors responsible for stress shadows are cluster spacing and proppant per cluster. Larger cluster spacing reduced the stress shadow impact. This is likely because larger cluster spacing increase the distance from fracture face (Z). Greater proppant per cluster on the other hand increased the stress shadow impact. This is likely because greater proppant increases the fracture width (w) which increases the stress shadow impact.

The sensitivity study shows that stress shadow significantly reduces fracture dimensions and smaller cluster spacing leading to stronger stress shadow. In the field, operators often increase the number of clusters in a stage (i.e. reduce the cluster spacing) as a remedy to reduce fracture dimensions and frac hits. Reducing the fluid and proppant per cluster can reduce fracture dimensions and are an efficient tools to mitigate frac hits. But, a smaller cluster spacing can increase stress shadow effects causing inefficient clusters; further, unwanted reduction in fracture dimensions due to stress shadow, loss in well productivity and economic realization. Thus, stress shadow considerations must be taken into account while doing any completion optimization.

5.4 Response Surfaces

Another key objective of the sensitivity analysis was to define response surfaces for important completion design parameters to reduce uncertainty and improve decision making. Large number of simulations are required to generate response surfaces with four variables. For instance,

considering 5 sampling points from each variable, the total number of simulations required are 5^4 i.e. 625 simulations. Due to limited time and resources, a statistical sampling technique called Latin Hypercube Sampling (LHS) was used to reduce the number of simulations (McKay et al. 1979). LHS divides the sampling space into M equal probable intervals, where M is the number of simulations specified by the user and then randomly takes a sampling point out of each of the M probable intervals. To generate the response surfaces, a total of 25 simulations were chosen. **Figure 69** shows the results for LHS. LHS technique is very effective and using 25 simulations as the figure shows, it can effectively cover the entire variable space.

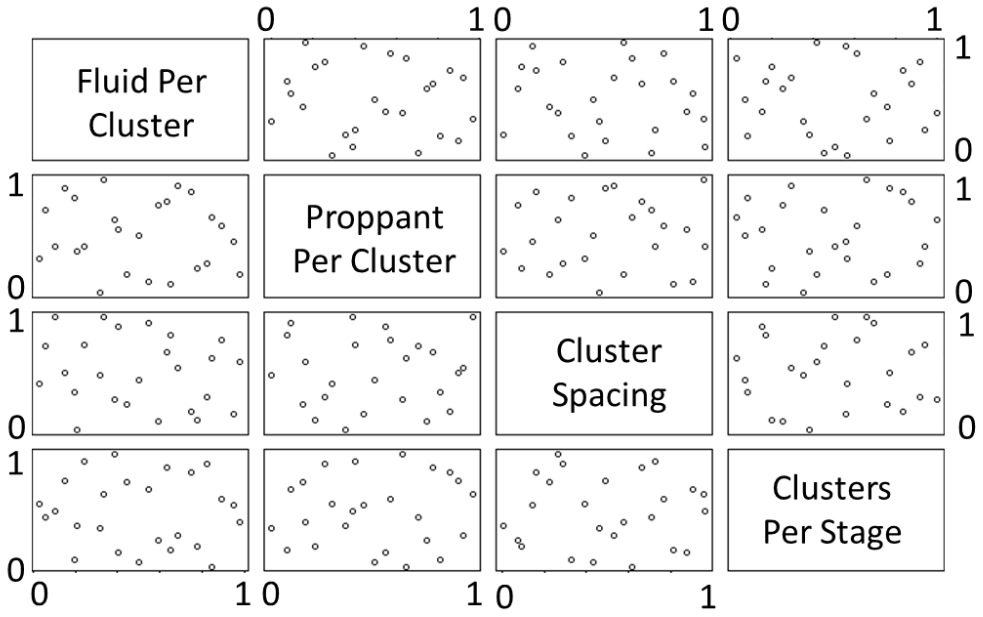

Figure 69: Latin Hypercube Sampling Matrix Plot for 25 simulations. The plot shows the distribution of the 25 simulations on the different cross plots among the four variables of interest. LHS technique is very effective and using 25 simulations it can effectively cover the entire variable space.

The response surfaces for the fracture length and fracture height are shown in **Figure 70**. The response surfaces were created with fluid per cluster and clusters per stage variables as these variables were most sensitive to the fracture dimensions. The figure shows that larger fracture

lengths and heights are promoted by greater fluid per cluster. Additionally, larger number of clusters can cause disproportionate fluid intake and can also lead to larger fracture lengths and heights. The response surfaces for fracture length and height can help select optimum completion design to increase productivity and/or minimize frac hits. However, the response surfaces need extensive calibration using the field data acquired through various fracture diagnostic techniques discussed in **Chapter 1**.

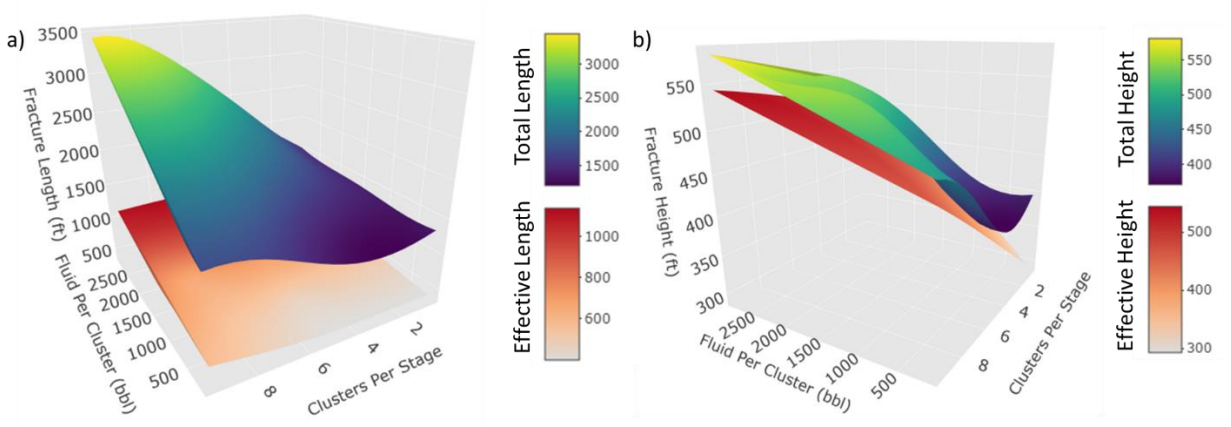

Figure 70: (a) Response surfaces for fracture length and (b) fracture height. Larger fracture lengths and heights are promoted by greater fluid per cluster values. Larger number of clusters can cause disproportionate fluid intake and can also lead to larger fracture dimensions.

5.5 Summary

To summarize this chapter, sensitivity analysis showed that fluid per cluster is probably the most important factor controlling fracture length and height (**Figure 57**) while proppant per cluster controls the fracture width (**Figure 60**). The fracture lengths are also more susceptible to closure compared to fracture heights based on which vertical offset (or staggering) is recommended to minimize frac hits (**Figure 58**). Another interesting find was that larger number of clusters does not necessarily lead to smaller fractures as the assumption that all clusters within a stage are equal does not apply to heterogenous shale reservoirs. A greater number of fractures can cause

disproportionate fracturing and may increase the risk of frac hits **(Figure 63** and **Figure 64**). Stress shadows can significantly reduce fracture dimensions (**Figure 66**). Traditionally, it is believed that larger number of clusters can prevent frac hits by generating smaller fractures. This, however, is not the economic solution as it comes at a huge completion cost. Simple economic solution would be to reduce amount of frac fluid/proppant without changing the cluster spacing. Finally, the response surfaces (**Figure 70**) can help evaluate multiple completion variables at the same time and can significantly improve the decision making process with regards to choosing the right completion size.

Chapter 6: Reservoir Control on Fracture Dimensions in Marcellus

The data for this chapter comes from the Marcellus Shale Energy and Environment Laboratory (MSEEL) test-site in the Marcellus shale in West Virginia. The dataset contains drilling measurements, geomechanical and petrophysical logs, borehole image logs, microseismic and fiber optic data (temperature and acoustic measurements). This chapter analyzes the relationship between pre-existing natural fracture network and its impact on hydraulic fracture geometry and resulting production from the well. The chapter also analyzes the correlation between natural fractures and other geomechanical properties such as Young's modulus and Poisson's ratio. In practice however, this information is rarely available in real-time and requires tedious and time-consuming processing of logs (including image logs), core, microseismic data and fiber optic sensor data. Post-completion analyses is generally too late for corrective action leading to wells with a low probability of success and increasing risk of frac hits. Thus, this chapter also shows a machine learning workflow using surface drilling data to infer various mechanical properties of the rock. The methodology described here can easily be applied to real-time processing of surface drilling data for optimal landing of laterals, placing of fracture stages, optimizing production and minimizing frac hits.

6.1 Study Area and Data Description

The data used in this study was acquired from public database from Marcellus Shale Sustainable and Environmental Research (MSEEL, West Virginia). The data can be accessed from http://mseel.org/. **Figure 71** shows the well locations for the different wells on MSEEL test site. There are four horizontal wells MIP3H, MIP4H, MIP5H and MIP6H. There is an additional vertical observation well named MIPSW. MIP4H and MIP6H wells already existed at the time MSEEL test site was established. Therefore, majority of the advanced data (open hole and image

logs, core, microseismic and fiber optics) were available in either MIP3H or MIP5H. In this study, only MIP3H and MIP5H are used for analysis.

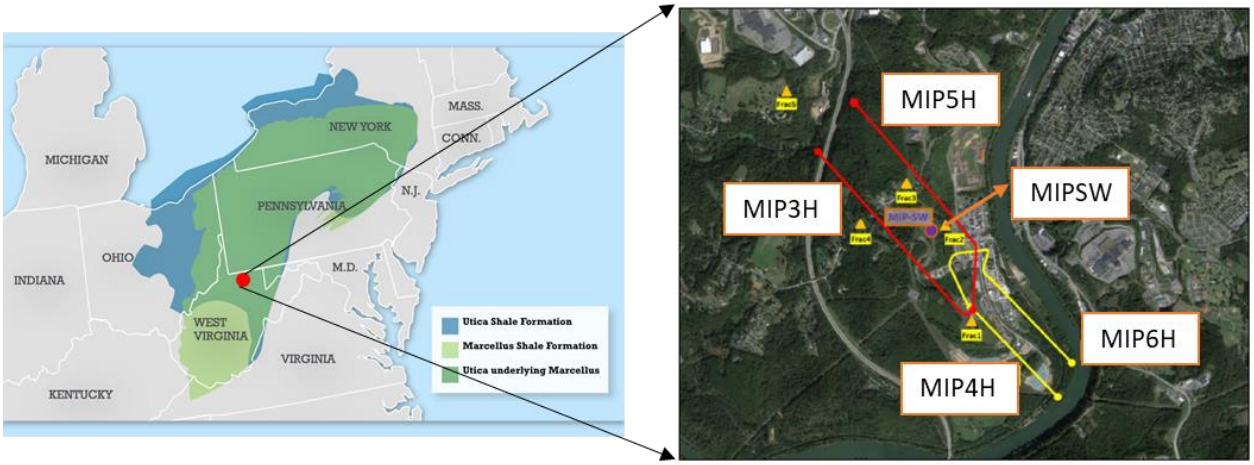

Figure 71: Well Locations in MSEEL test site (Pankaj et al. 2018). There are four horizontal wells MIP3H, MIP4H, MIP5H and MIP6H. There is an additional vertical observation well named MIPSW.

The fiber optics data was available in MIP3H and can be used to calculate the stage contribution to production rate. The gas production per stage was calculated using distributed temperature sensing (DTS) and distributed acoustic sensing (DAS) and was provided as a part of the public dataset. Readers interested in knowing more about how fiber optics data can be used for production profiling are referred to Abukhamsin (2017**). Figure 72** shows the gas production per stage. In the figure, it is evident that the production varies widely for different stages which is likely controlled by the varying petrophysical (porosity, permeability, saturation) and geomechanical properties (brittleness, fracability) of the rock encountered in different stages.

The petrophysical logs in MIP3H were acquired in both vertical and lateral sections of the well. The image log was used to summarize the natural fracture count per stage (**Figure 73**). Openhole logs in MIP3H contain a large suite of logs like triple combo and sonic logs. These logs were also used to generate mechanical rock properties like Young's modulus and Poisson's ratio using

Equations 24 and **21**, respectively (Birch 1966). The core data when available was used to quality check the available and derived logs. The various available and derived logs in MIP3H are shown in **Figure 74.**

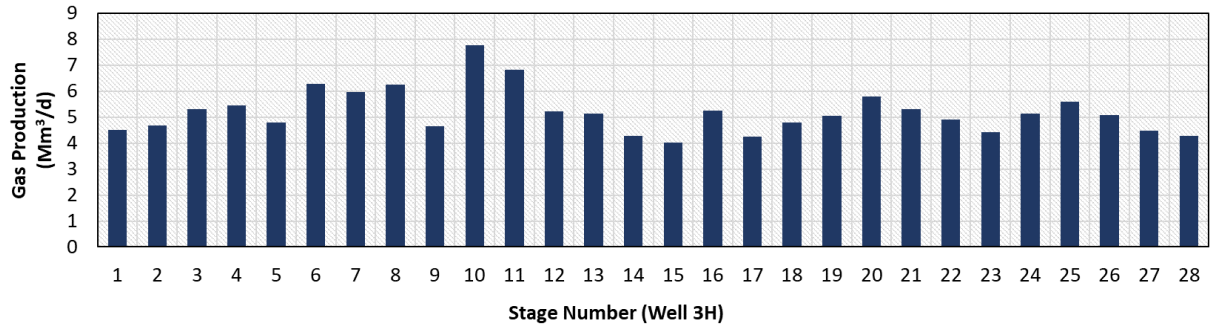

Figure 72: Gas Production per stage in well MIP3H.

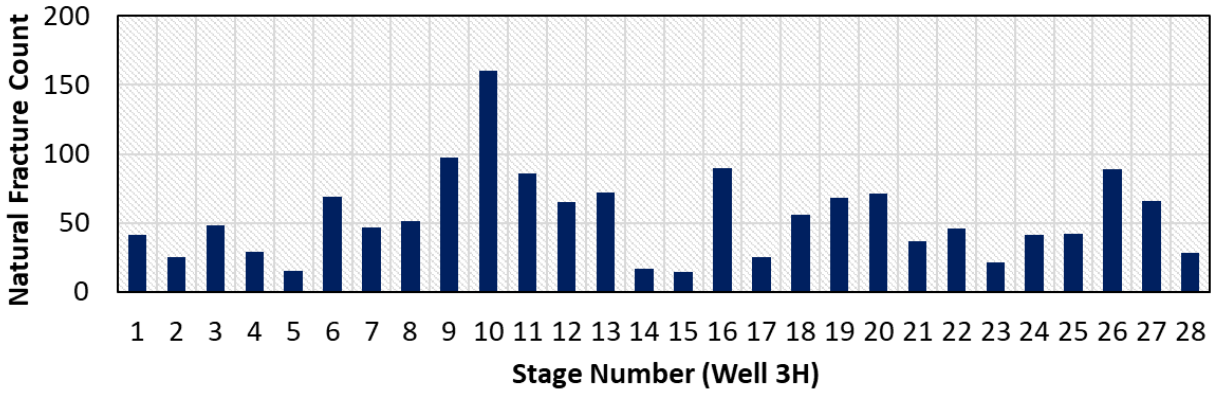

Figure 73: Natural Fracture Count per Stage in well MIP3H

The surface drilling data was available in both MIP3H and MIP5H. The various drilling parameters available are rate of penetration, hook load, standpipe pressure, pump strokes, rotary RPM (revolutions per minute), rotary torque, weight on bit, total mud volume, total pump output, inclination, azimuth, downhole pressure, bit RPM, instantaneous ROP, total mud gain/loss, differential pressure, mechanical specific energy (MSE), motor RPM, gamma at bit and relative MSE. The histograms of some key drilling variables are shown in **Figure 75**. The study shows that drilling data can be used to predict mechanical properties in Marcellus and also characterize

the natural fracture density. Since drilling data was available in both MIP3H and MIP5H, both these wells were included in the machine learning workflow.

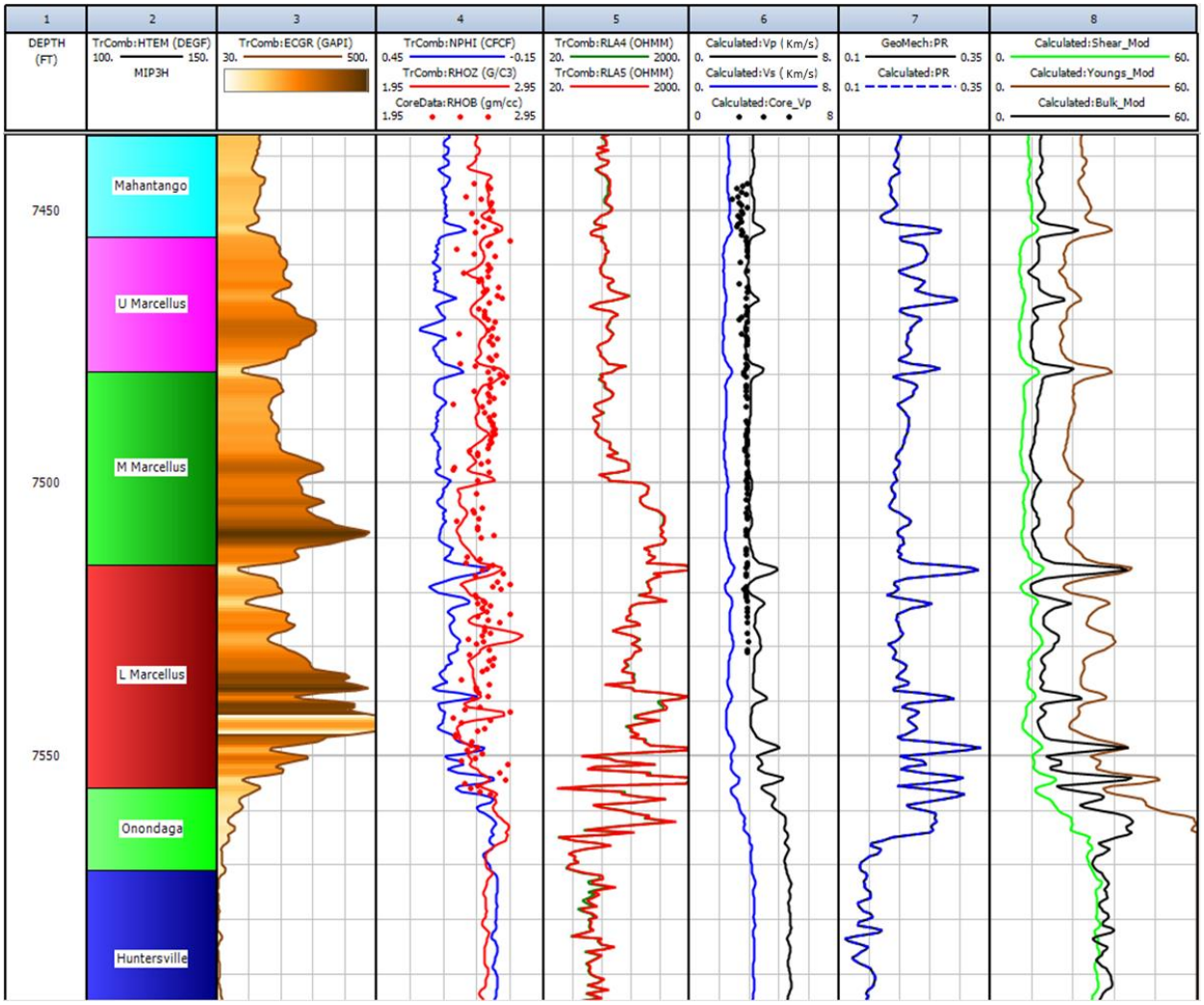

Figure 74: Snapshot of petrophysical logs available in the MIP3H well. The first track shows the measured depth. The second track shows the various Marcellus zones. The third track shows the gamma ray. The fourth track shows the core bulk density measurements, neutron porosity and bulk density logs. The fifth track shows the resistivity. The sixth track shows the sonic logs and core V_p measurements. Tracks seven and eight show the various calculated mechanical property logs.

Lastly, microseismic data was also available in both MIP3H and MIP5H as shown in **Figure 76**. The microseismic data can be used to calculate stage fracture length and height and assess complex versus planar fractures.

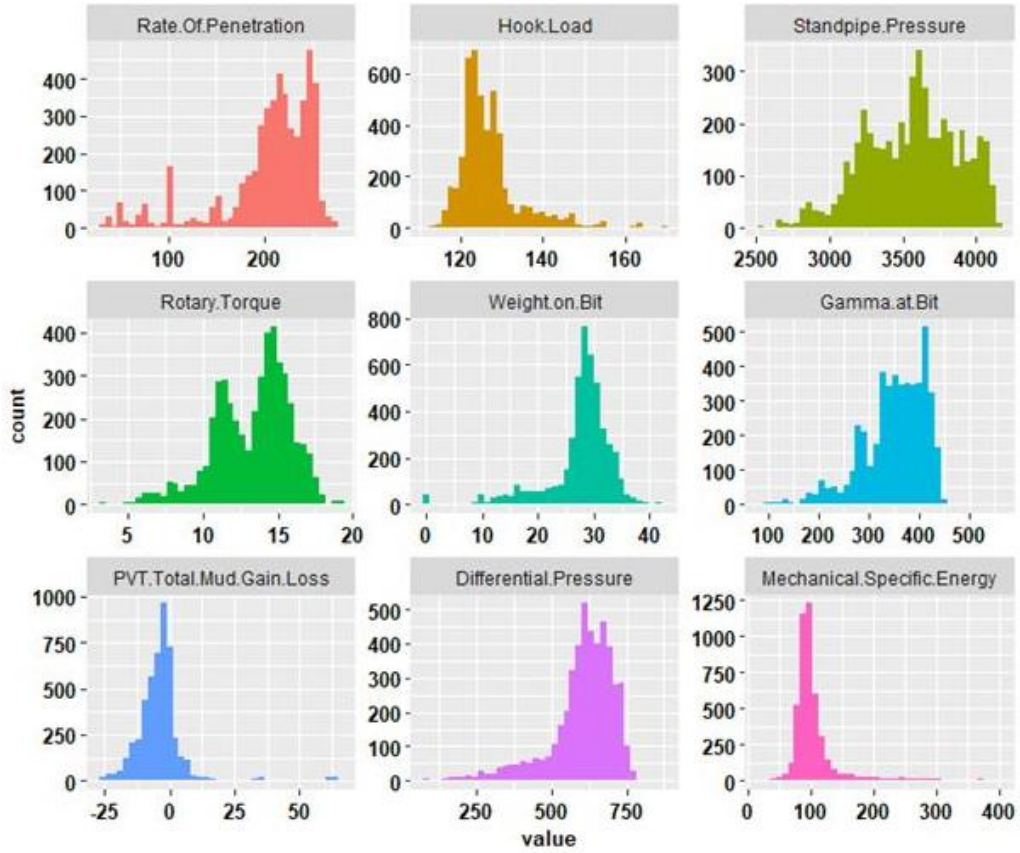

Figure 75: Histograms of drilling parameters. Different parameters show either right or left skewness and appear to have several outliers.

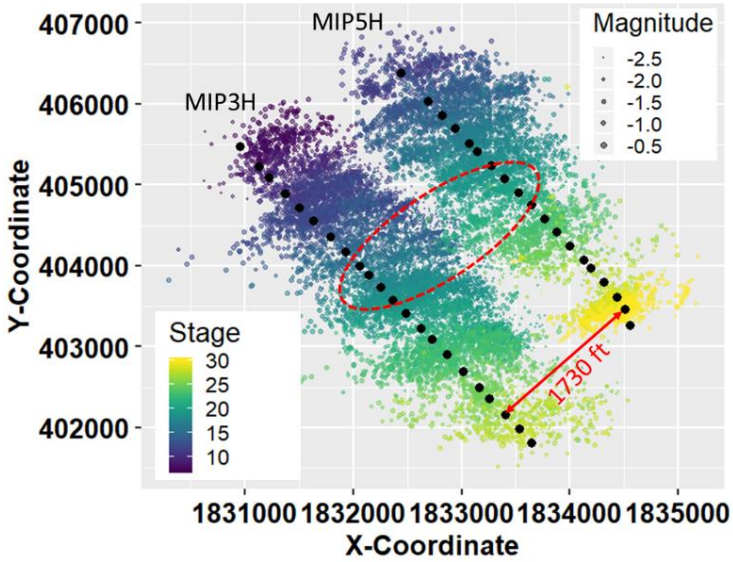

Figure 76: Microseismic data in MIP3H and MIP5H. The red circle shows some minor interaction between the stages of MIP3H and MIP5H.

6.2 Understanding Cause of Frac Hits in Marcellus

In Chapter 3, analysis mainly focused on oil wells in the most prolific liquid-rich shale plays in US. However, impact of frac hits on gas plays like Marcellus can be equally detrimental. Lawal et al. (2014) and Lindsay et al. (2018) have also shown strong negative impact of frac hits on both parent and child wells in Marcellus. **Figure 77** shows an example where wells near the MSEEL test site were evaluated for frac hit impact. Among the wells analyzed, there was one parent well and two child wells. Both parent and child wells had strong impact on production from the frac hits. Parent well lost 19% of the gas volume (47 Bcf) in 5-year period. The child wells lost 22% (56 Bcf) and 40% (100 Bcf) gas volumes during the same period. The loss is proportional to the distance between the parent and child wells with child well closer to the parent well losing more production due to the frac hit.

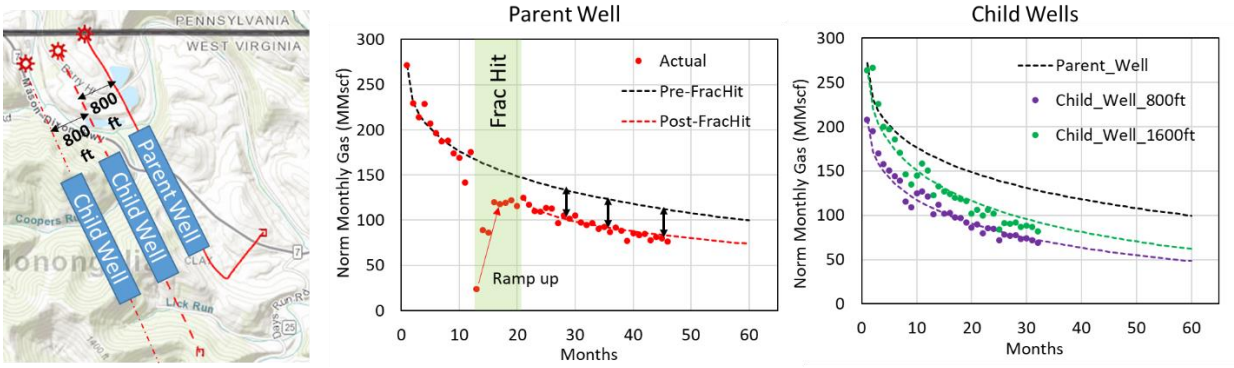

Figure 77: Production analysis of a well pad near the Marcellus test site with one parent well and two child wells. The parent well plot shows the fitted VDMA DCA curves on pre- and post-frac hit production. Similarly, in the child well plot, black curve shows the pre-frac hit parent well production fit. The green and purple curves are fitted on the child well production data. Both parent and child wells show strong impacts on production from the frac hits. The parent well lost 19% of the gas volume (47 Bcf) in 5-year period. The child wells lose 22% (56 Bcf) and 40% (100 Bcf) gas volumes during the same period. The loss is proportional to the distance between the parent and child wells.

The frac hits are generally caused by a few culprit stages that extend into neighboring wells (Kurtoglu and Salman 2015). **Figure 76** shows that a few middle stages in the MIP3H and

MIP5H are possibly interacting with each other. It is important to identify reservoir property control on fracture dimensions and hence, frac hits. Warpinski and Teufel (1987), King (2014), and Kurtoglu and Salman (2015) have stressed the importance of reservoir properties like presence of natural fractures, faults, and bedding planes in determining the fracture geometry and hence, the extent of frac hits. This can help explain why certain stages behave differently from each other in spite of having similar completion design parameters. The borehole image data (**Figure 73**) shows that Marcellus is naturally fractured. Presence of natural fractures promote more complex fracture networks with shorter fracture half-lengths and heights. The microseismic data in MIP3H (**Figure 76**) was used to calculate fracture length and height for all stages. The product of fracture height and length, i.e. fracture area was cross-plotted against natural fracture count obtained from image logs as shown in **Figure 78**. The weak negative correlation confirms that higher natural fracture density leads to shorter fractures. The correlation is weak possibly because many other factors impact fracture geometry like varying completion design across stages, different reservoir properties and increasing stress shadow effect.

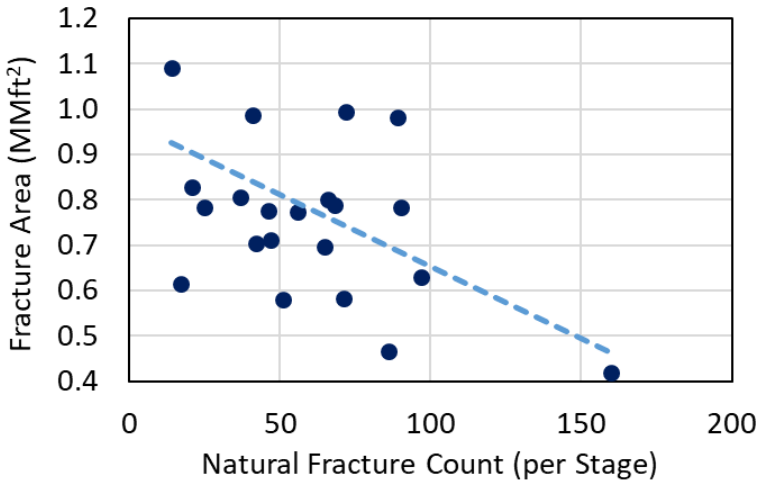

Figure 78: Weak correlation between natural fracture count per stage and primary (main) fracture area. Secondary fracture network was not included in fracture area calculations. Negative correlation suggests higher natural fracture density causes complex but smaller fractures.

While natural fractures lead to smaller hydraulic fractures as suggested by **Figure 78**, microseismic data was used to evaluate if natural fractures also lead to more complex fracture networks, i.e. higher proportion of secondary fracture network. Warpinksi (2009) method of looking at the time-distance plots was used to evaluate different stages in well MIP3H. **Figure 79** shows the time-distance plots for two stages, i.e. stage 10 and stage 15. These stages were chosen due to stark contrast in their natural fracture count from image logs. In stage 10, the distance versus time plot suggests that fracture development is complex as it does not follow square root of time dependence. In Stage 15, the distance versus time plot follows square root dependence on time suggesting that the fracture development is planar.

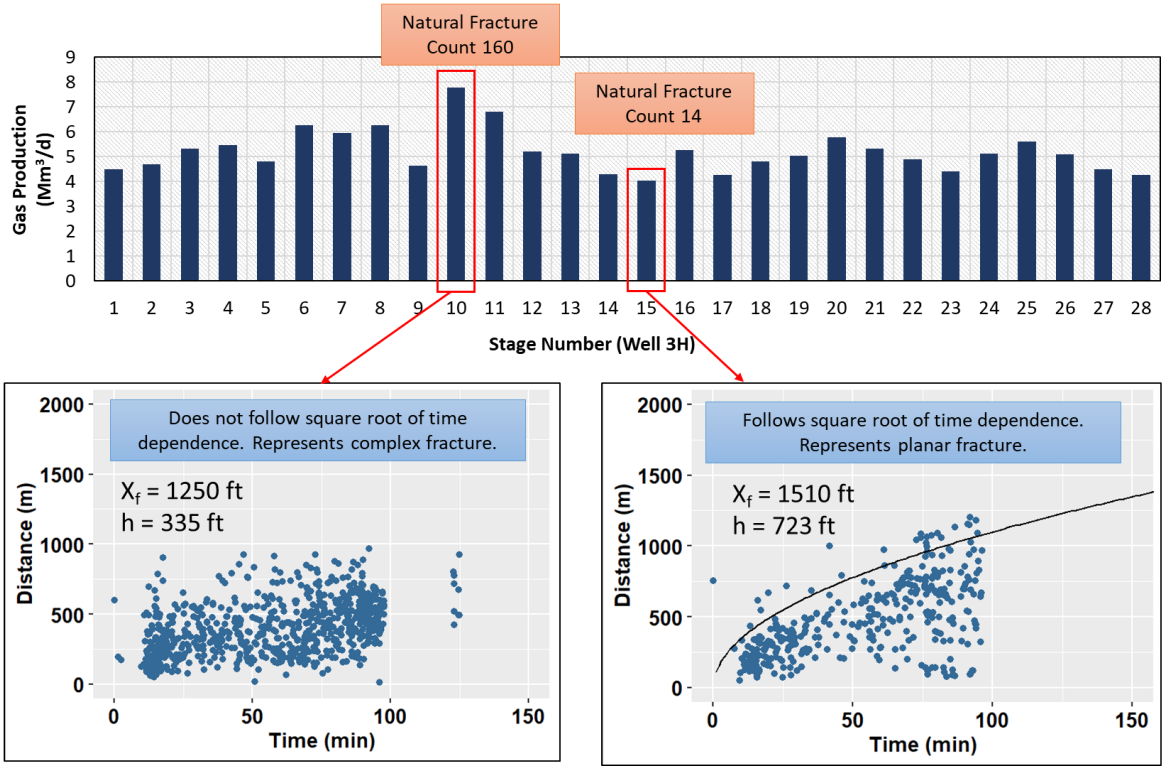

Figure 79: Time-Distance plots for two stages, i.e. stage 10 and stage 15. These stages were chosen due to stark contrast in their natural fracture count from image logs. In stage 10, the distance versus time plot suggests that fracture development is complex as it does not follow square root of time dependence. In stage 15, the distance versus time plot follows square root dependence on time suggesting that the fracture development is planar. The black curve in the plot shows the general trend for square root of time dependence.

The microseismic and image log interpretation in MIP3H clearly suggests that natural fractures correlate to shorter and more complex fractures. This is important as it suggests that by understanding natural fracture distribution in this area, one can predict fracture geometry which can prove useful in avoiding or minimizing the frac hits. However, image logs are difficult and expensive to acquire. It is important to evaluate if natural fractures correlate to other mechanical properties.. **Figure 80** shows the correlation between natural fracture count and mechanical properties specifically, Young's modulus and Poisson's ratio. Higher fracture content correlates with lower values of Young's modulus and Poisson's ratio.. It is likely because rocks with lower Young's modulus are easier to break and rocks with lower Poisson's ratio are more brittle. Thus, rocks which break easily and are more brittle tend to develop more natural fractures.

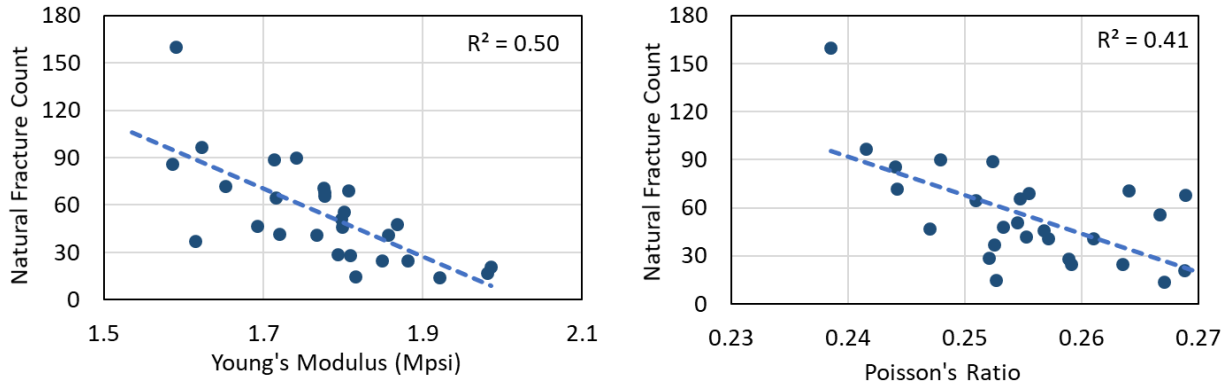

Figure 80: The correlation between natural fracture count and mechanical properties specifically, Young's modulus and Poisson's ratio. Lower values of Young's modulus and Poisson's ratio leads to higher natural fracture count. This is reasonable because rocks with lower Young's modulus are easier to break and rocks with lower Poisson's ratio are more brittle. Thus, rocks which break easily and are more brittle tend to develop more natural fractures.

6.3 Fracture Complexity and Gas Production

The natural fractures promote complex fracture networks and they typically increase the reservoir contact area or stimulated reservoir area (SRA). In low permeability reservoirs, matrix

flow is highly restricted which implies that the well productivity is directly proportional to the reservoir contact area created by hydraulic fractures. Thus, in shales and tight reservoirs, natural fracture density should be inherently tied to production. **Figure 81** shows the gas production per stage cross-plotted with natural fracture count per stage. The weak positive correlation suggests that larger natural fracture count leads to higher production from a stage.

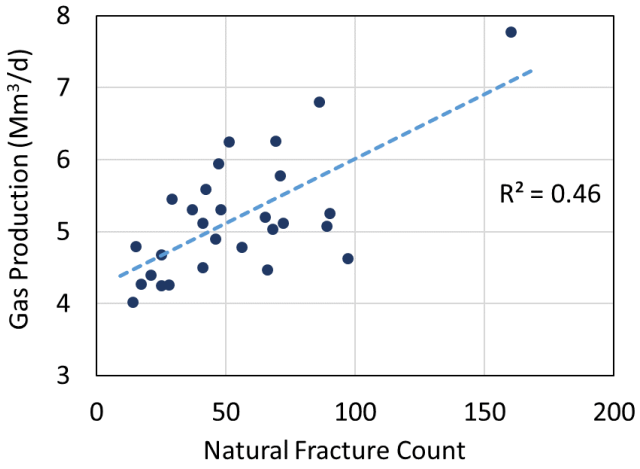

Figure 81: The gas production per stage is plotted as a function of natural fracture count per stage. The weak positive correlation suggests that larger density of natural fractures leads to higher production from a stage which is likely because larger natural fracture density increases the complexity of the fracture.

For further proof of concept, wells MIP3H and MIP5H were compared to each other. Warpinski (2009) suggested that a simplest measure of fracture complexity is the ratio of width of the microseismic cloud for a stage to the length of the microseismic cloud of the same stage. The width here does not represent the primary (main) fracture width. It represents the lateral extent of the microseismic cloud. The microseismic cloud includes both the primary and secondary fracture networks. Warpinski named this metric as Fracture Complexity Index (FCI). Higher values of FCI represent more complex fracture networks. **Figure 82(a)** shows the FCI values for the different stages in MIP3H and MIP5H wells. Looking at the individual stage and average values for the wells, MIP3H seems to develop more complex fractures compared to MIP5H

Figure 82(b) shows that that MIP3H produced 17% more gas than MIP5H likely due to more complex fracture networks. This simple plot shows the significance of developing complex fracture networks and its impact on production.

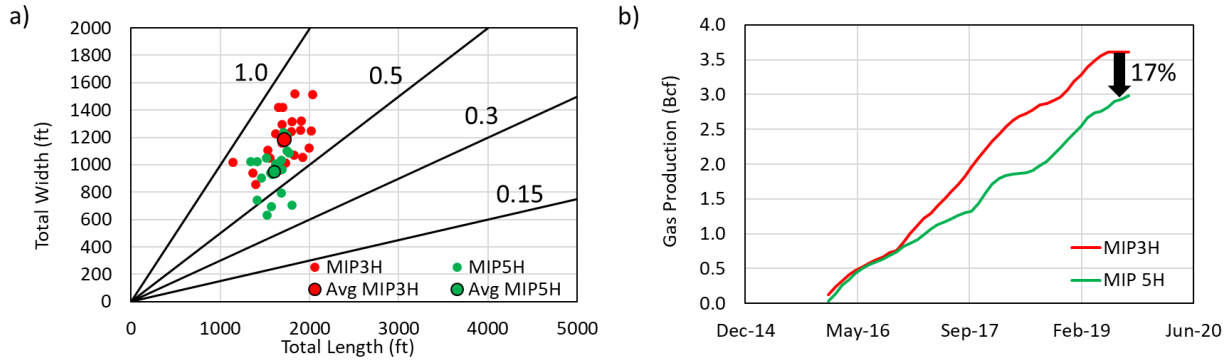

Figure 82: (a) FCI plot showing the FCI values for the different stages in MIP3H and MIP5H wells. The smaller point size represents the individual stages while bigger point size represents the average value for all the stages, i.e. represent the entire well. The black lines show the FCI lines for values 1, 0.5, 0.3 and 0.15. Looking at the individual stage and average values, MIP3H seems to develop more complex fractures compared to MIP5H (b) Cumulative gas production plot for MIP3H and MIP5H. It is evident that MIP3H produced 17% more gas than MIP5H likely due to more complex fracture networks.

The natural fractures in Marcellus increase reservoir contact area leading to higher production. They also lead to shorter fractures (length and height) which minimizes the risk of frac hits. Thus, optimum completion zones in Marcellus are those with higher natural fracture density. Even though image logs and open hole logs (sonic and density) can identify zones with high natural fracture density, these logs are only acquired in a small percentage of total number of wells. Next, the possibility of using surface drilling data to characterize mechanical properties of the formation and its natural fracture density were evaluated.

6.4 Use of Surface Drilling Data to Characterize Mechanical Properties

The biggest advantage with surface drilling data is that it is free and available in all the wells. The workflow utilized to get mechanical properties from the surface drilling data is shown in

Figure 83. The first step is data preparation. Under data preparation, log and drilling data is analyzed to remove outliers and handle missing values. Finally, the cleaned data is prepped for analysis by scaling it and creating some additional derived variables (also called feature engineering) that may boost the predictive efficiency. Next, since it is easier to predict some finite number of facies where each facies has characteristic mechanical properties (Poisson's ratio, Young's modulus, natural fracture count) rather than predicting actual values of different mechanical properties, clustering is done as an intermediate step. The unsupervised learning technique creates clusters having geomechanical significance. K-Means method is applied on the derived variables Young's modulus and Poisson's ratio, for classification. The numbers of clusters are optimized by silhouette width and within sum of squares. The classification identifies the clusters of varying brittleness/fracability. Finally, using supervised learning techniques, models are built to predict geomechanical clusters using the drilling data. The data is randomly split into training and test sets with 75% for training and 25% for testing. The various supervised techniques used include K-nearest neighbors, gradient boosting, random forests and neural networks.

6.4.1 Data Preparation

The first step is to analyze the data for outliers, handle missing variables and create new variables or features. Few additional variables like Young's modulus, Poisson's ratio and MSE were calculated from the available log and drilling variables. This is called feature engineering in machine learning and it means using domain knowledge of the data to create features or new variables that improve the efficiency of machine learning algorithms. For instance, **Figure 80** clearly shows that Poisson's ratio and Young's modulus are strongly correlated to the natural fracture count. Thus, it is better to use these new variables rather than sonic and density logs

themselves. **Figure 84** shows the histogram of the Young's modulus (Mpsi) and Poisson's ratio calculated from the sonic and density logs. The histograms show a normal distribution and few outliers.

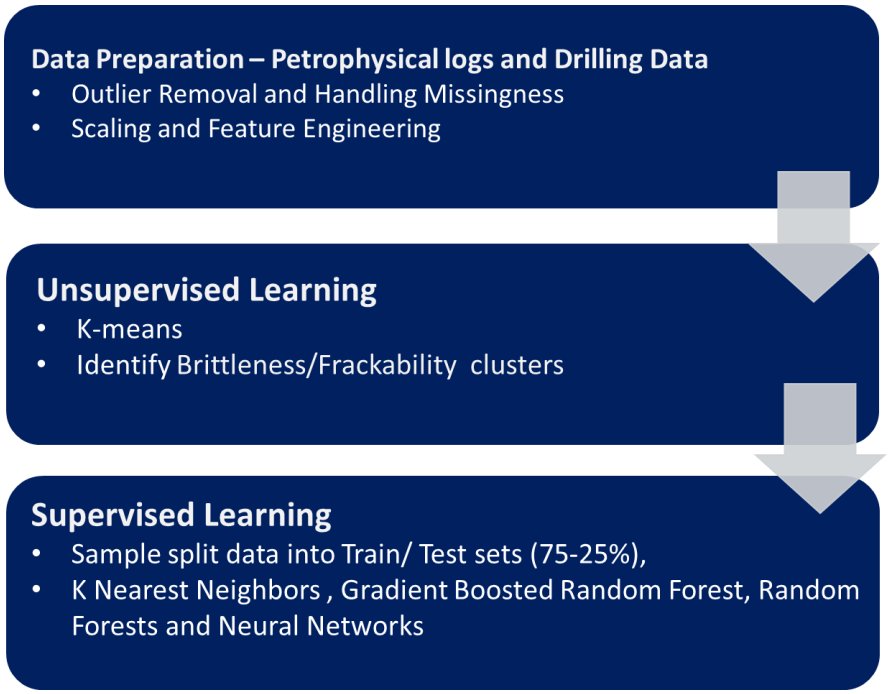

Figure 83: Modeling workflow. First step is data preparation which basically prepares the data for unsupervised and supervised learning. It includes outlier removal, scaling and feature engineering. Unsupervised learning helps creates geomechanical clusters and supervised learning helps train models to predict those clusters using the drilling data.

The histograms in **Figure 75** display the distributions of the important drilling parameters. Different parameters show either right or left skewness and appear to have several outliers. Next, the important variables used in supervised and unsupervised clustering were checked for "missingness". "Missingness" represents the percentage of total number of entries for any variable that is missing. For this dataset, it means the percentage (or fraction) of total depth, for which any variable is missing. For any variable having a missingness more than 70%, it should be removed from the study due to high uncertainty. **Figure 85** shows the results of missingness for the key drilling and log variables used in unsupervised and supervised learning. It reveals that

the variables have no more than 2% missingness. The missing variables can either be imputed i.e. predicted using the other variables which are not missing. The advantage with this method is that it prevents loss of information and data, which may be crucial when the dataset is limited. The other option is removing all the rows of data having missing variables which is acceptable when a dataset is large and missingness is below 5%. Since the missingness in this study is quite low (<2%) removing all missing values would not significantly affect the analysis. Thus, rows having the missing values were removed.

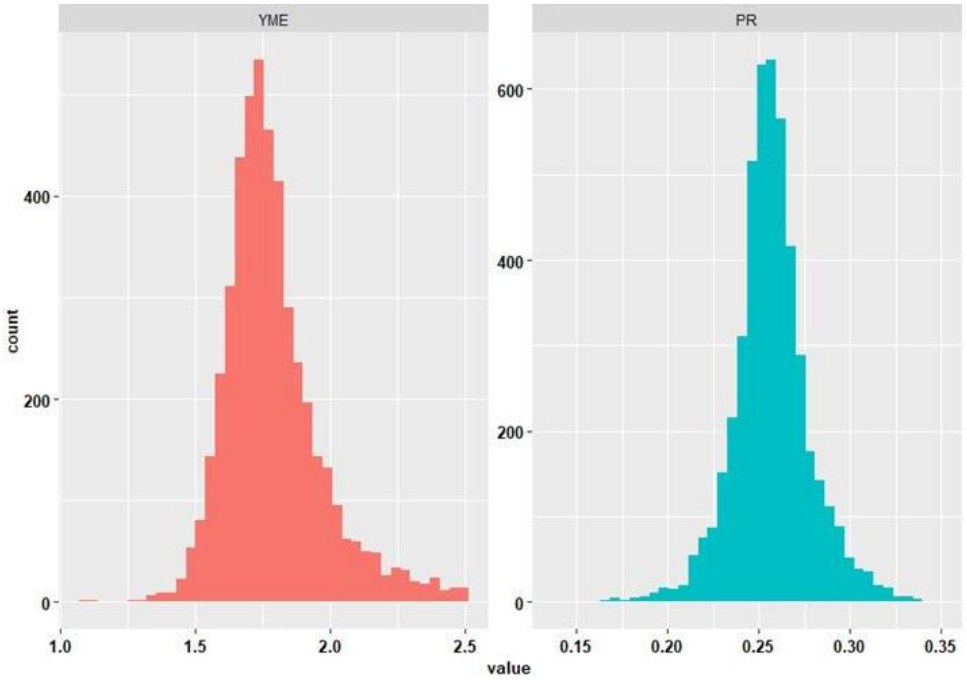

Figure 84: Histogram of the (left) Young's modulus (Mpsi) and (right) Poisson's ratio calculated from the sonic and density logs. The histograms show normal distributions with few outliers.

The outliers were removed before data were used for clustering. EnvStats package (Barnett and Lewis 1995) in the R language was used to detect the outliers. The Rosner test function (Barnett and Lewis 1995) was used. The function performs the Rosner generalized extreme studentized deviate test to identify the potential outliers in a data set, assuming the data without any outliers come from a normal (Gaussian) distribution. Finally, the data was normalized to remove bias.

There are several techniques to scale or normalize the data. In this study, a particular variable was scaled by subtracting the mean value of all the observations and then divide by the standard deviation of all the observations (equation 30).

$$Var_{Ai} = \frac{Var_{Ai} - mean(Var_A)}{StdDev(Var_A)} \quad \text{.....30}$$

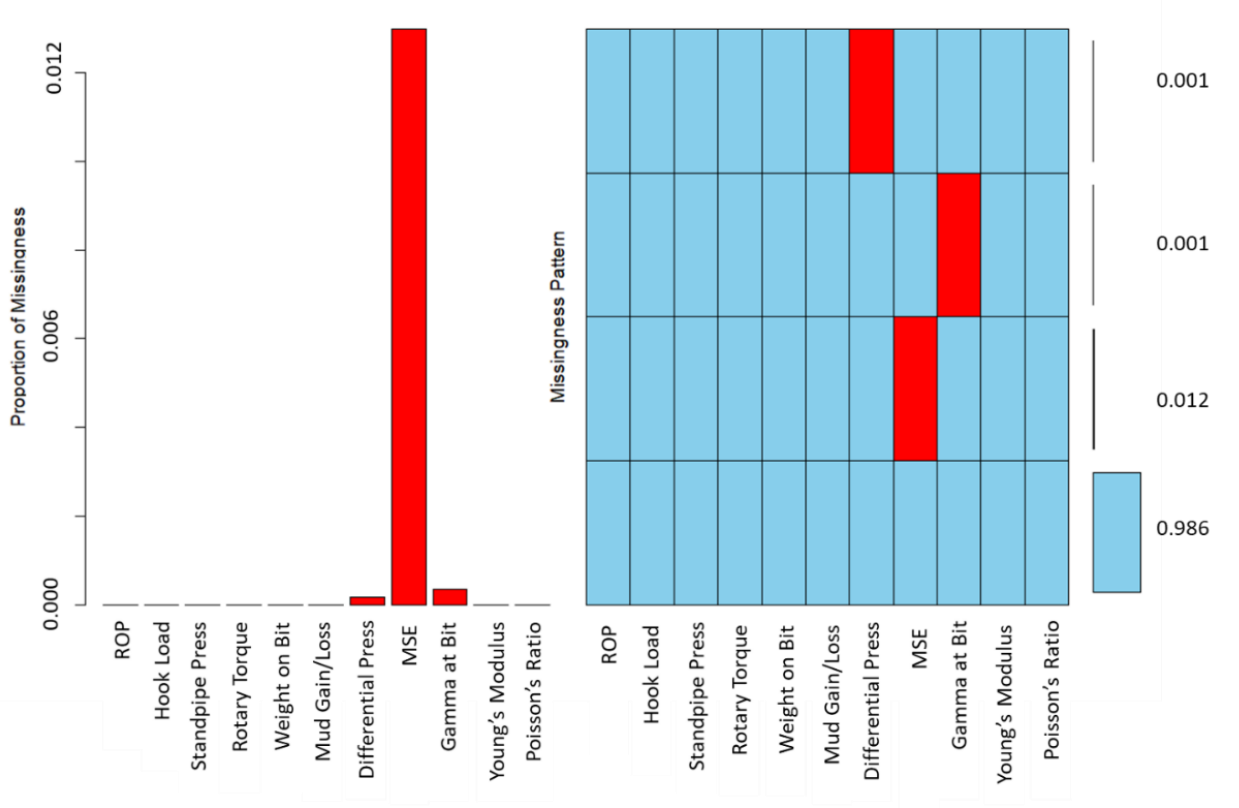

Figure 85: (Left) Missingness in different drilling and log variables to be used for unsupervised and supervised learning. The units of missingness reported on the y-axis is given as a fraction. It is evident that missingness in general is very low (<2%). MSE has the largest proportion of missing variables. (Right) Missingness pattern helps evaluate if there is any pattern or structure in the missing observations. The plot suggests that over 98.6% of the data does not have any missing values. About 1.2% data has MSE as missing variable. The missing pattern in some cases could also suggest variables which could be potentially used for imputing missing values.

6.4.2 Unsupervised Learning

Before K-means is applied, the optimal numbers of clusters are determined based on sensitivity done with number of clusters. Ideal clusters should have data that are very similar to each other

within a cluster and very different from the data in the other clusters. **Figure 86 (Left)** shows the cross plot of average variance within the clusters and number of clusters. As the number of clusters increase, data within a cluster decrease leading to a decrease in sum of variance within a cluster i.e. data within a cluster become more alike. It appears that increasing the clusters beyond 3-4 does not decrease the variance within the clusters appreciably. **Figure 86 (Right)** shows silhouette plot (Maechler et al. 2019) which is another method to determine optimum number of clusters. Silhouette width is calculated as

$$s(i) = \frac{b(i)-a(i)}{max(a(i),b(i))} \quad \text{.....31}$$

s(i) represents the silhouette width, a(i) is average dissimilarity between any data point i and all other data points in the same cluster, b(i) is the dissimilarity between data point i and its 'neighbor' cluster i.e. nearest one to which it does not belong. Higher average silhouette width indicates good clustering. Both plots in **Figure 86** together suggest that optimum number of clusters is 3.

K-means was used to cluster the Young's modulus and Poisson's ratio variables into three clusters. These two variables are strong indicators of natural fracture count as shown in **Figure 80**, and the objective of clustering is to identify clusters of geomechanical significance. Readers interested in inner working of K-means clustering technique are referred to Gupta (2017). **Figure 87** shows the results of K-means clustering. The three clusters identified are shown on the Poisson's ratio-Young's modulus cross plot. The characteristics of the three clusters are summarized in **Table 28**. **Figure 87 (d)** also shows the actual dynamic brittleness calculated using equation proposed by Altamar and Marfurt (2014) as shown below (**Equation 32**) which uses normalized values of Young's modulus and Poisson's ratio. The brittleness increases from cluster 1 to 3.

$$Brittleness = \frac{Young's\_Mod_{norm} + Poisson's\_Rat_{norm}}{2} \quad \ldots\ldots\ldots\ldots\ldots\ldots\ldots\ldots 32$$

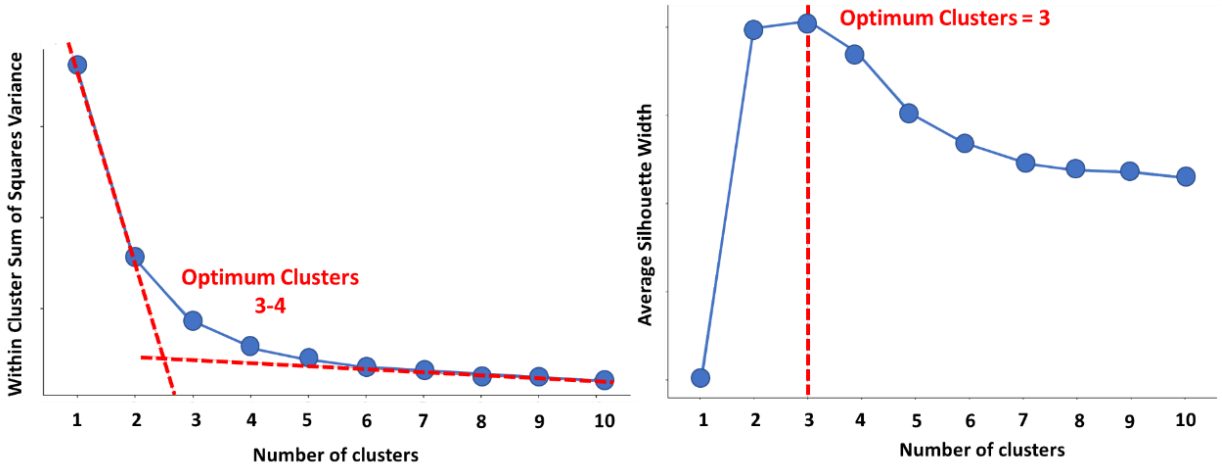

Figure 86: (left) Cross plot of variance within the clusters and number of clusters. As the number of clusters increase, data points within a cluster decrease leading to a decrease in sum of variance within a cluster. It appears that increasing the clusters beyond 3-4 does not decrease the variance within the clusters appreciably. (Right) Silhouette plot is another approach to measure quality of clustering. A high average silhouette width indicates good clustering. The plot suggests that 3 is the optimum number of clusters.

Table 28: K-means clusters characteristics

Clusters	Characteristics
1	Low Brittleness, Low Fracability
2	Moderate Brittleness, Moderate Fracability
3	High Brittleness, High Fracability

6.4.3 Supervised Learning

The different clusters identified using K-means have characteristically different mechanical properties in terms of brittleness and fracability. Since, Poisson's ratio and Young's modulus are correlated to the natural fracture count (**Figure 80**) which is itself correlated to fracture complexity (**Figure 79**) and production performance (**Figure 81**), the three clusters are also believed to be strongly correlated to the production performance. In this section, an attempt is made to train regression models using the drilling variables and four supervised techniques,

namely K-nearest neighbors (KNN), gradient boosted random forest (GBM), random forest and multi-layer perceptron (MLP) neural networks to predict the different clusters.

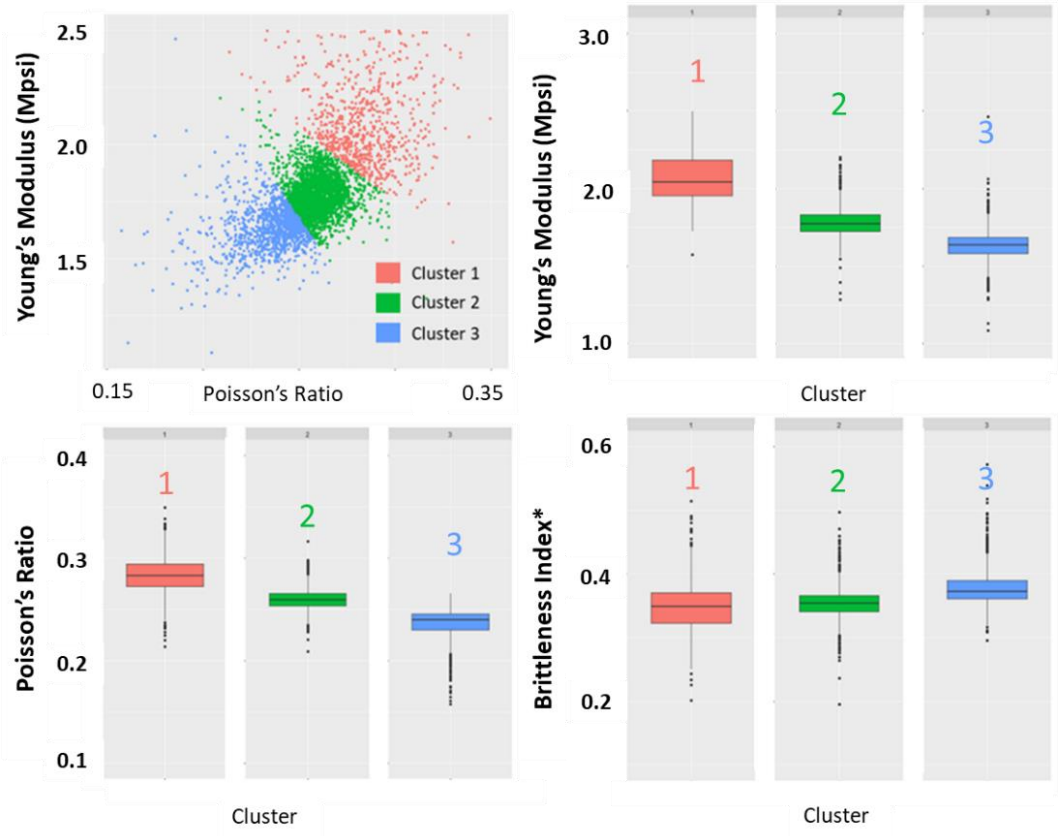

Figure 87(a) The three clusters identified using K-means shown on Young's modulus and Poisson's ratio cross-plot. (b) The Young's modulus decreases from cluster 1 to 3. Generally, smaller Young's modulus implies that the rock is easy to break. Therefore, fracability, i.e. ease of breaking the rock increases from cluster 1 to 3. (c) The Poisson's ratio also decreases from cluster 1 to 3. Typically, lower Poisson's ratio implies increased brittleness. Therefore, brittleness increases from cluster 1 to 3. (d) Calculated brittleness index increases from cluster 1 to 3.

K-nearest neighbors is a non-parametric technique that is used for statistical estimation and pattern recognition. Simply stated, it uses predefined number of nearest neighbors to determine the value of an unknown observation. The nearest neighbors are calculated based on distance. Several different measures of distance can be used like Euclidean, Manhatten and Minkowski. For a detailed discussion on the KNN technique, readers are referred to Altman (1992) and

James et al. (2013). The tuning hyperparameter for the KNN technique is “number of neighbors K” which can be determined by running a sensitivity with different K’s and choosing the one that gives minimum error on the training data. Both random forests and gradient boosted random forests belong to the group of tree-based classification techniques. A decision tree is a flowchart like structure in which each internal node represents a “test” on an attribute (i.e. in this case drilling variables), with two branches coming out of the node depending on the outcome of the test (True or False). A decision tree can be very complex (100’s of nodes) and the end nodes (also called leaf nodes) represent the class labels (i.e. in this case geomechanical clusters). Random forests (Breiman 2001) create multiple decision trees. In each tree, only ***m*** out of total p attributes (drilling variables) are used for splitting the tree. This collection of ***m*** attributes changes across the different trees inducing degree of randomness. Finally, trees that give minimum error are averaged to give the final model. Gradient boosting (Breiman 1997) also uses multiple decision trees but trees are created in a succession where each set of trees is sensitive to the residuals of the previous set. Gradient boosted random forests combines the advantage of the two popular tree-based methods. The hyperparameters that can be optimized in tree-based techniques are number of trees, minimum number of data points in the leaf nodes, interaction depth which specifies the maximum depth of each tree and number of variables (or predictors) available for splitting at each node. For a complete list of hyperparameters readers are referred to caret package in R (Kuhn 2008). Lastly, multi-layer perceptron (MLP) neural networks are fully connected feedforward networks. Neural networks (Lecun et al. 1998, Nielson 2015) generally have multiple layers and each layer has several neurons. Each neuron receives one or multiple inputs, multiplies it with a weight and generates an output signal. Typically, neurons in one layer are connected to all the neurons of the adjoining layers. The neural network can be trained for

instance with the drilling variables as inputs and geomechanical clusters as output. The weights are optimized to minimize the error. The hyperparameters for neural networks would be number of layers and number of neurons (or nodes) in each layer.

The drilling parameters selected for predicting the geomechanical clusters were ROP, rotary torque, weight on bit, mud gain/loss, differential pressure, MSE and gamma at bit. These variables are a direct result or are heavily influenced by the interactions between the bit and the formation. The mechanical and petrophysical properties of the rock surrounding the bit have a strong influence on these measurements and therefore, these measurements are best suited to predict geomechanical clusters. The dataset in MIP3H well consisting of the seven drilling variables, was split into training and validation datasets in the ratio 75:25. Hyperparameter tuning was done on the training dataset. **Figure 88** shows the results for hyperparameter tuning and **Table 29** summarizes the optimal values of hyperparameters for different supervised learning techniques. Caret package (Kuhn 2008) was used for modeling different supervised classification techniques.

The trained models were tested on the validation dataset to determine the best technique for predicting geomechanical clusters from the drilling data. **Table 30** summarizes the different accuracy metrics on the validation dataset for different techniques. AUC represents area under the ROC (Receiver Operating Characteristic) curve and is a useful metric to evaluate any classification model's performance (Fawcett 2006). Simply stated, it represents the ability of a model to distinguish the different classes. Kappa is another metric to evaluate model's accuracy and it is more robust compared to simple percent (or fraction) agreement as it takes into account the possibility of the agreement occurring by chance. For more details on the Kappa metric, readers are referred to McHugh (2012). The accuracy metric simply represents fraction

agreement, i.e. fraction of the test dataset predicted correctly. The accuracy for individual clusters are also shown in **Table 30** and all the three classes have very similar accuracy suggesting that the training models are robust enough to differentiate between the different geomechanical clusters.

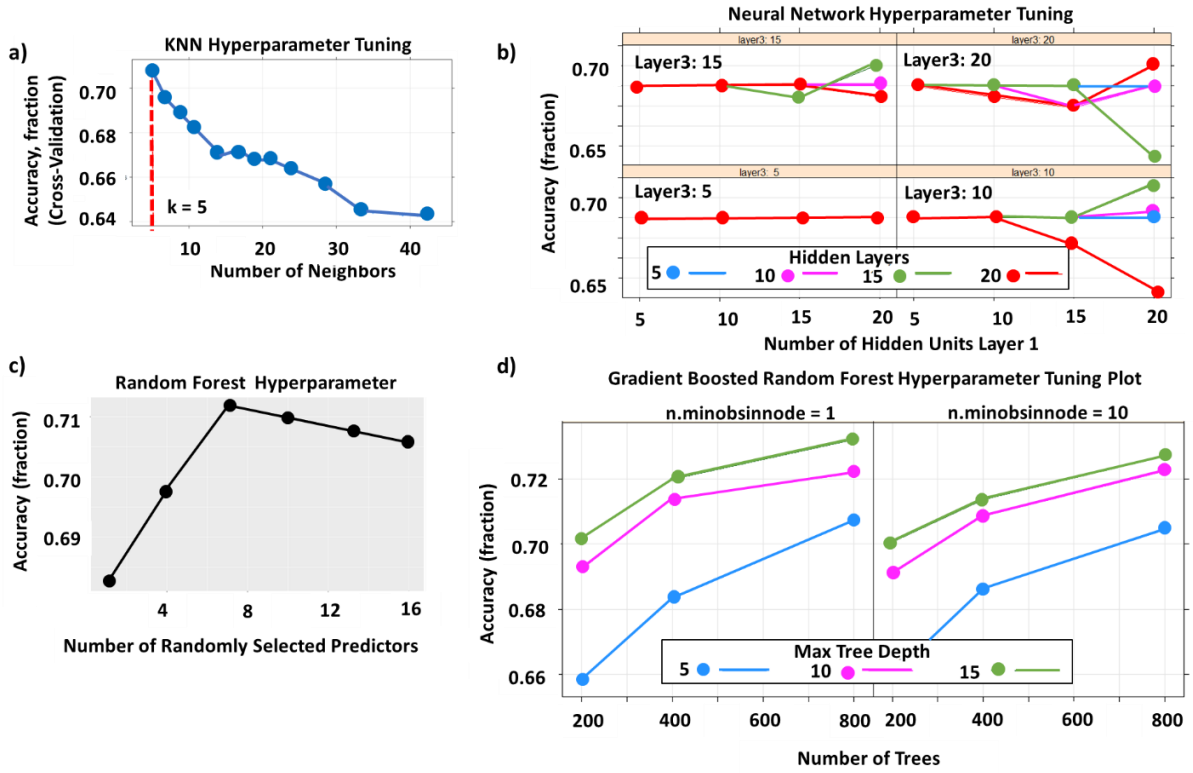

Figure 88: (a) Hyperparameter optimization for K-nearest neighbor (KNN) method. As the numbers of neighbors increases, the accuracy for the model decreases. The optimal number of neighbors is 5. (b) Hyperparameters for neural networks include number of nodes (units) in each layer. The number of layers were kept constant at 3. The optimal hyperparameters are layer 1: units = 20, layer 2: units = 15 and layer 3: units = 15 (c) Hyperparameter tuning for random forest method. The plot shows that optimum number of parameters to be available for split at any tree node should be 7. (d) Hyperparameter optimization for gradient boosted random forest method (GBM). Larger number of trees having larger tree depths lead to higher accuracy. Similarly, lower limit for minimum number of observations (n.minobsinnode) in the leaf nodes lead to higher accuracy. The optimal hyperparameters are number of trees = 800, max tree depth = 15 and n.minobsinnode = 1.

Comparing the different techniques, gradient boosted random forests shows the highest overall accuracy, Kappa and AUC values, suggesting it gives the best prediction among the four

techniques. The highest accuracy on validation dataset was found to be 74%. The reason for lower accuracy is that training dataset is limited due to availability of a single well MIP3H. However, higher accuracy is expected when this workflow is expanded to a larger dataset with multiple wells.

Table 29: Summary of optimal hyperparameters for different supervised classification techniques. Caret package in R was used for modeling the different supervised classification techniques.

Method	Optimal Hyperparameter Values
KNN	Number of Neighbors = 5
MLP Neural Networks	Layer 1: units = 20, Layer 2: units = 15 and Layer 3: units = 15
Random Forests	mtry = 7
Gradient Boosted RF	Number of trees = 800, max tree depth = 15, n.minobsinnode = 1

Table 30: Different accuracy metrics on the validation dataset for different supervised classification techniques. Gradient boosted random forests shows the highest overall accuracy, Kappa and AUC values, suggesting it gives the best prediction among the four techniques. Accuracy here is shown in fraction which represents the fraction of the test dataset predicted correctly.

Methods	AUC	Kappa	Overall Accuracy	Accuracy Cluster 1	Accuracy Cluster 2	Accuracy Cluster 3
K-Nearest Neighbors	0.80	0.47	0.71	0.73	0.71	0.78
Gradient Boosted RF	0.84	0.52	0.74	0.73	0.73	0.80
Random Forest	0.80	0.45	0.71	0.72	0.70	0.70
MLP Neural Network	0.76	0.43	0.70	0.70	0.69	0.76

Figure 89 also shows the visual comparison of the actual geomechanical clusters identified using K-means and those predicted using the different supervised learning techniques. The visual observations show that MLP neural networks do not perform as well as the other techniques.

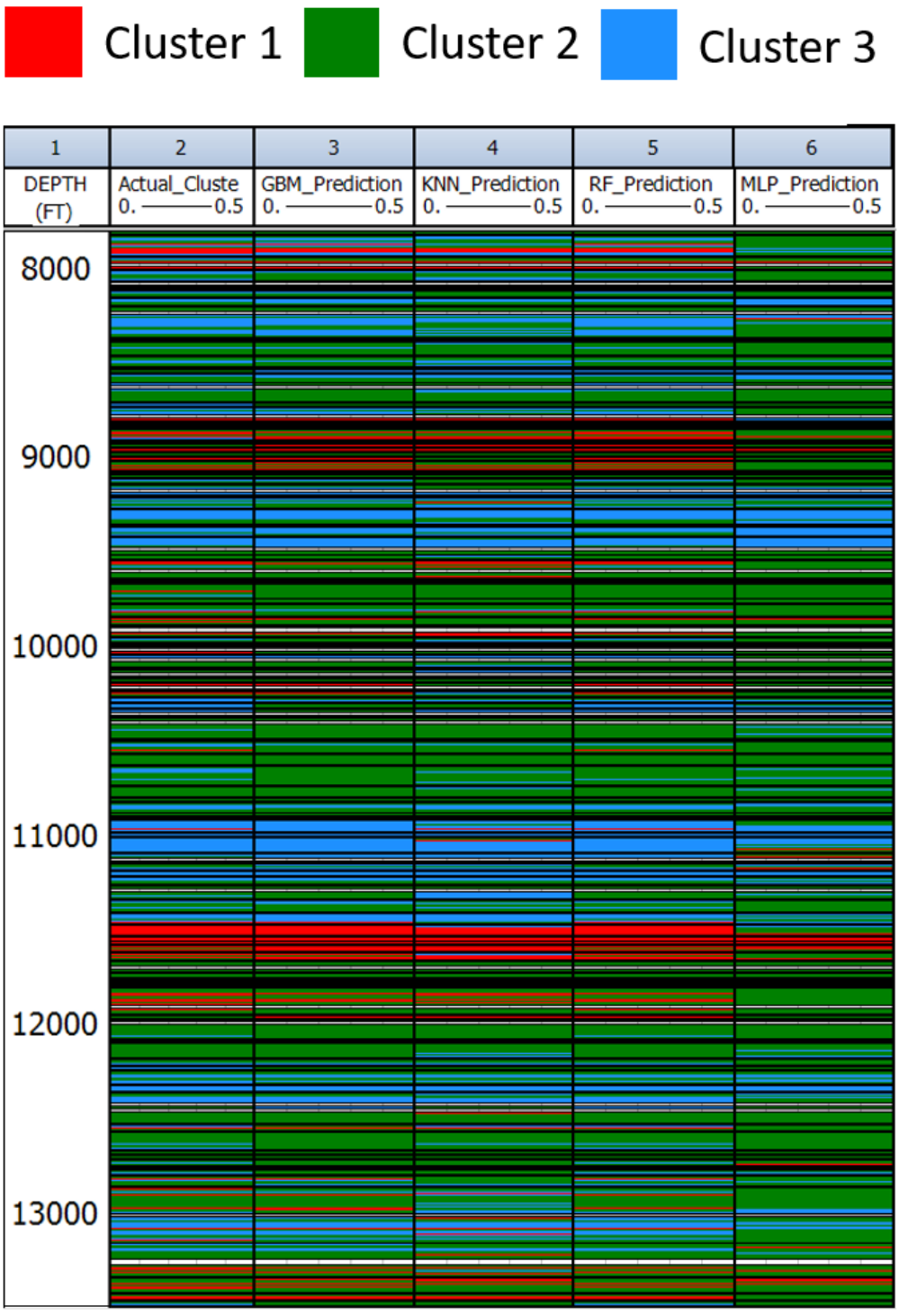

Figure 89: Visual comparison of the actual geomechanical clusters (Track 2) identified using K-means and those predicted using the different supervised learning techniques (Track 3 to Track 6). The visual observations show that MLP neural networks (Track 6) do not perform as well as the other techniques (Track 3 to Track 5).

The last step of supervised learning is to analyze the predictive models to understand which predictors (drilling variables) are important. This step helps in decoding the 'black box predictions', i.e. explain the output of the predictive models and generate confidence in the models. We use Shapley values which are calculated for each predictor (drilling variables) and each cluster (geomechanical facies) combination. Mathematically, they represent the average of the marginal contributions across all permutations (Lundberg and Lee 2016). In simple terms, a higher value of Shapley for a predictor-cluster combination suggests that the predictor is important to identify the cluster. The Shapley values were calculated using Shapley Additive Explanations (SHAP) package in python. The input to the SHAP is any machine learning model like gradient boosted random forest and corresponding predictors (drilling variables) and output clusters used to build the machine learning model. The first plot (**Figure 90a**) generated using SHAP shows a variable importance plot which lists the most significant variables in descending order. The plot shows that gamma.At.bit, Mechanical.Specific.Energy (MSE) and mud_gain _loss are the three most important variables to define the geomechanical clusters.

However, looking at individual Shapley values for the different clusters helps in understanding the variable importance, i.e. important predictors to identify that a particular cluster. In this study, cluster 3 was found to be the cluster of interest, i.e. most brittle and productive. Thus, it is important to understand which drilling variables are important to identify cluster 3 and what is the relationship of these variables to cluster 3. **Figure 90b** shows the Shapley values for cluster 3 and different drilling variables. Taking any variable in the plot for instance, Gamma.at.bit, the different points represent the different observations, i.e. depths in the dataset. First, the different variables are ranked in order of importance, i.e. Gamma.at.bit and mud_gain_loss are the two most important variables to identify cluster 3. Second, the color represents whether the drilling

variable is high or low value for that observation. The x-axis shows the Shapley values and a higher value means greater impact on cluster prediction. The majority of high SHAP values comprise of low gamma values. This suggests that low gamma is a key characteristic of cluster 3.

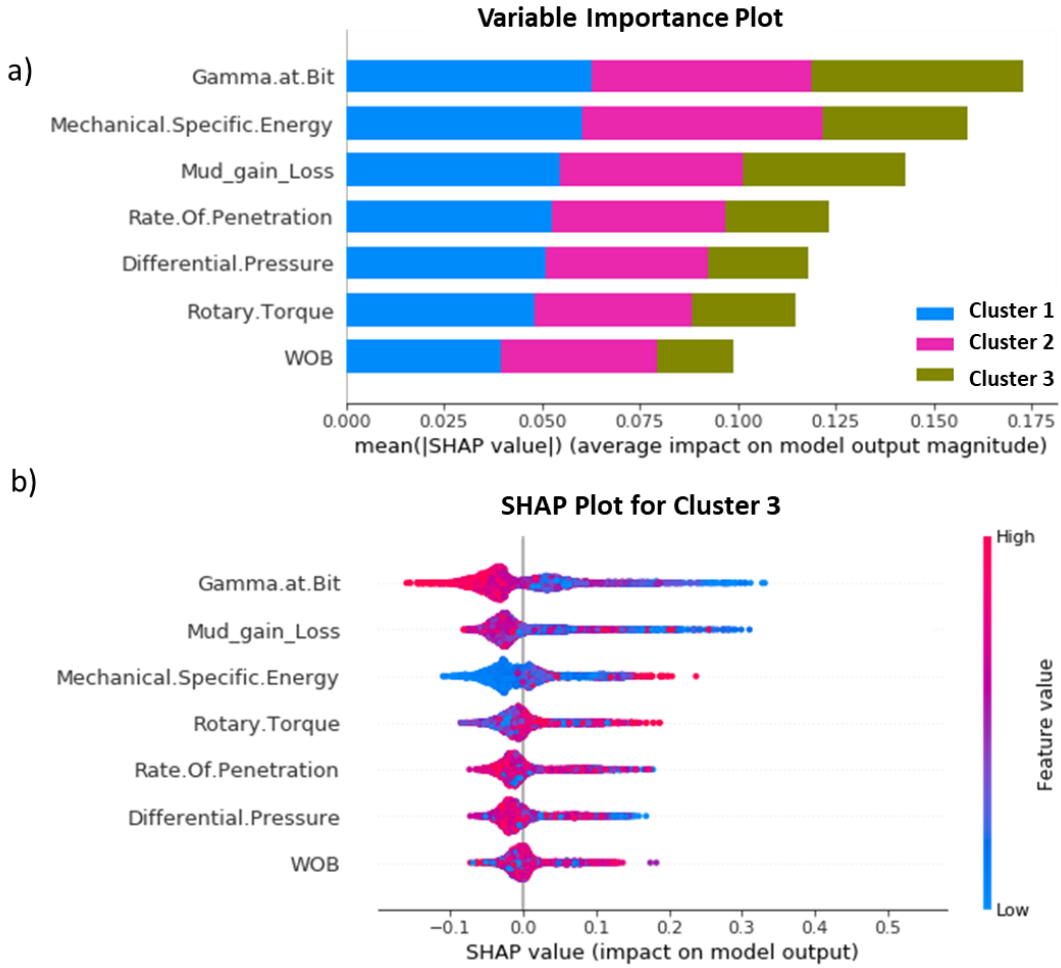

Figure 90: (a) Variable importance plot which lists the most significant variables in descending order. This plot averages the Shapley values for all the observations (depths) over the three clusters for the different predictors. The plot shows that gamma.at.bit, Mechanical.Specific.Energy (MSE) and mud_gain_loss are the three most important variables to define the geomechanical clusters. (b) Shapley values for cluster 3 and different drilling variables. Taking any variable in the plot for instance, gamma.at.bit, the different points represent the different observations, i.e. depths in the dataset. The plot shows that gamma.At.bit and mud_gain_loss are the two most important variables to identify cluster 3. The color in the plot represents whether the drilling variable is high or low value for that observation. The x-axis shows the Shapley values and a higher value means high impact on cluster prediction. Cluster 3 is characterized by low values of gamma.at.bit mud_gain_loss.

The majority of high SHAP values are comprised of low mud_gain_loss values suggesting cluster 3 is again characterized by low values of mud_gain_loss variable. Now, cluster 3 has high natural fracture count, is brittle, and has low Young's modulus and Poisson's ratio. These are all characteristics of quartz-rich lithology which has low gamma ray. Similarly, mud_gain_loss represents the mud flow rate at return line minus the mud flow rate at inlet. It has both positive and negative values. Negative values occur when mud flow rate at return line is lower, i.e. mud is lost to the formation. Again, cluster 3 has high natural fracture count which can lead to the high mud losses. This explains the low values of mud_gain_loss variable for cluster 3. Analyzing the SHAP plots for cluster 3 in this study provided further confidence that the predictive models developed in this study have some underlying physical basis and can be applied to neighboring wells.

6.4.4 Validation on MIP5H

The geomechanical and petrophysical logs were only available in MIP3H, thus MIP5H could not be included in the training dataset. However, MIP5H had drilling data and it could be used as a test well where the trained models can be used to predict the geomechanical clusters. The predicted clusters were grouped by stage to get the percentage of each cluster in each stage. From **Table 28** cluster 3 has the highest brittleness and fracability, and lowest Young's modulus and Poisson's ratio. Based on **Figure 80**, cluster 3 likely has the highest natural fracture density and therefore, expected to develop complex fractures. Microseismic data in MIP5H was used to generate distance-time plots for few stages and the fracture development (planar vs. complex) was classified. The results are shown in **Figure 91**. In the figure, gradient boosted random forest model was used to predict the clusters as it was the best predictive model in MIP3H analysis. The bar chart at the top shows the percent of cluster 3 in different stages in MIP5H well. The

microseismic data was available for only a few stages and completion design also varied across the lateral length. The data was analyzed to find consequent stages which had the same completion design and had a large contrast between cluster 3 percentage. Thus, stages 14 to 17 were selected for analysis.

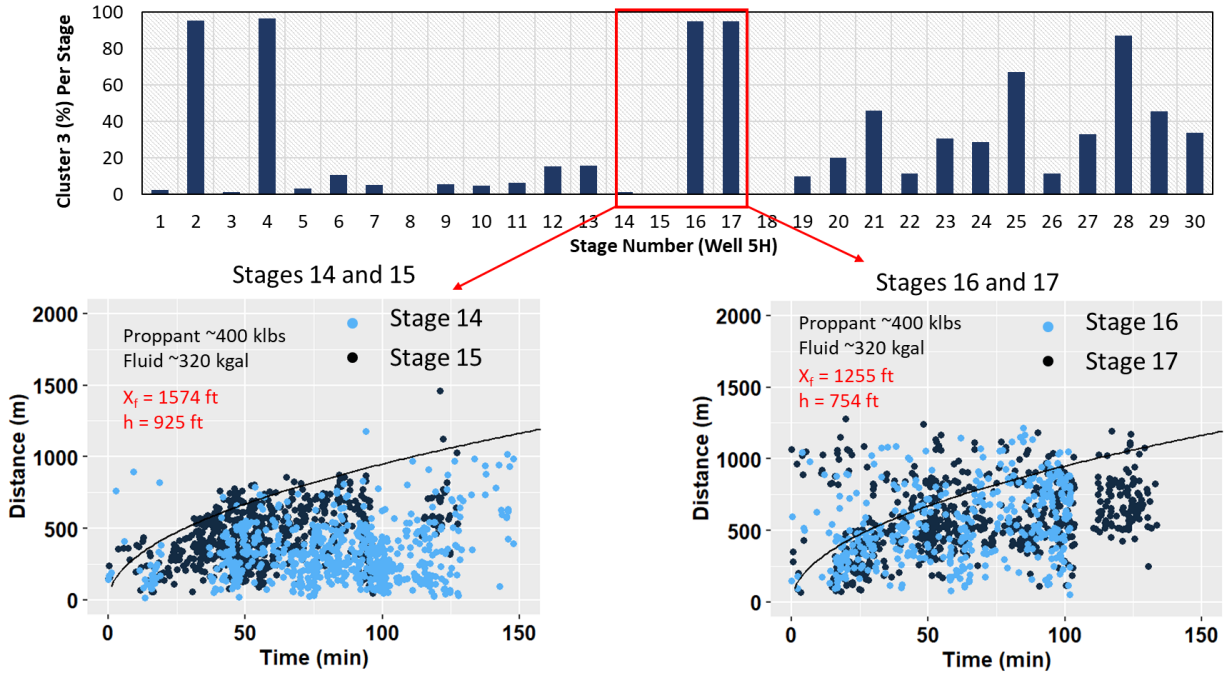

Figure 91: The bar chart (top) shows the percent of cluster 3 in different stages in MIP5H well. Cluster 3 is the most fracable and has the highest brittleness. Thus, it will likely develop more complex fractures. The bottom cross plots show the distance-time plots for stages 14 to 17. The different colors in the plots represent the different stages. The black curve shows the trend for square root of time dependence. It is evident that stages 14 and 15 which has a negligible fraction of cluster 3 and follow square root of time dependence indicating development of planar fracture network. On the other hand, stages 16 and 17 had a high fraction of cluster 3 and they do not follow square root of time dependence, suggesting more complex fracture development.

Looking at the microseismic distance-time plots, it is evident that stages 14 and 15 which have almost negligible fraction of cluster 3 follow square root of time dependence indicating development of planar fracture network. On the other hand, stages 16 and 17 had a very high fraction of cluster 3 and do not follow square root of time dependence, suggesting more complex fracture development. Stages 14 and 15 also had larger fracture dimensions compared to stages

16 and 17 and is attributed to planar fracture development. This shows that drilling data in MIP5H can successfully predict geomechanical clusters based on a trained model in near-by well MIP3H.

6.5 Summary

To summarize this chapter, integrating the extensive data collected in MSEEL like microseismic, image and sonic logs, and fiber optics, it was evident that fracture geometry is strongly controlled by the rock properties (Young's modulus and Poisson's ratio) and the natural fracture density. Completing brittle and fracable zones with high natural fracture density also lead to higher production. Another key finding is that the drilling data can be used to estimate rock properties and differentiate between brittle and ductile, easy-to-frac and hard-to-frac rock real-time while drilling. This gives an opportunity to geosteering engineers who use mainly gamma ray to steer the well. The idea is not to just stay within shale but chose the best spot to place the well within the shale. Lastly, the study shows the potential of drilling data to minimize frac hits by avoiding fracturing in ductile zones which generates longer planar fractures that can intersect neighboring parent wells and cause frac hits. Fortunately, in this area in Marcellus, the solution is simple – generate complex fractures to maximize production and reduce frac hits.

Chapter 7: Recommended Frac Hit Mitigation Approach

The recommended workflow is given in **Figure 92**. Step 1 of this approach involves characterizing the reservoir, i.e. calculating reservoir properties that control fracture geometry and propagation. Next, correlations are attempted between surface drilling data and these key reservoir properties. This is done to ensure that some basic reservoir characterization can be done in majority of the wells. Frac hit diagnostics involve calculating actual fracture geometry and level of interaction between adjacent wells. These data along with reservoir properties are critical for generating and calibrating empirical and numerical models. Models provide a predictive tool for decision making. In Step 2, key decisions are made regarding well placement, well scheduling and completion design based on knowledge acquired in Step 1. The literature review in **Table 3** suggests that total impact of frac hits on parent and child wells is on average negative. The parent wells can sometimes be positively impacted if their pore pressure is high and they were under stimulated. Thus, the approach in this section aims to minimize the total negative impact of frac hits on the parent and child wells. The recommendations are given on timing of the child wells to facilitate the positive impact on the parent wells. Finally, in Step 3, the results of the decisions implemented in the field are evaluated and feedback is provided for further improvement.

7.1 Reservoir Characterization

The key petrophysical and geomechanical properties of interest as shown in **Figure 93(a)**. These properties govern fracture geometry and are key inputs for modeling. Overburden stress can be calculated by integrating the density log, Young's modulus and Poisson's ratio can be calculated using dipole sonic, pore pressure, porosity and mineralogy can be calculated using triple combo logs (Mouchet and Mitchell 1989), minimum horizontal stress can be calculated using uniaxial

strain equation (Mullen 2007), matrix permeability can be calculated using NMR logs (Chang et al. 1997). Calibrating the calculated logs is critical and can be done by acquiring cores and running lab measurements (Young's modulus, Poisson's ratio, permeability, Biot coefficient, elastic anisotropy), acquiring field DFIT data (closure stress, pore pressure, permeability) and doing RTA analysis (permeability.). Different methods of measurements have advantages and disadvantages. For instance, drilling data is noisy and affected by bit wear and mud performance but it is cheap, and available real-time for majority of the wells. Seismic data has low resolution, but it is a continuous data available across the study area even before drilling a well. Logs and cores are most accurate, have the highest resolution but are also expensive and generally acquired in less than 10% of the total wells.

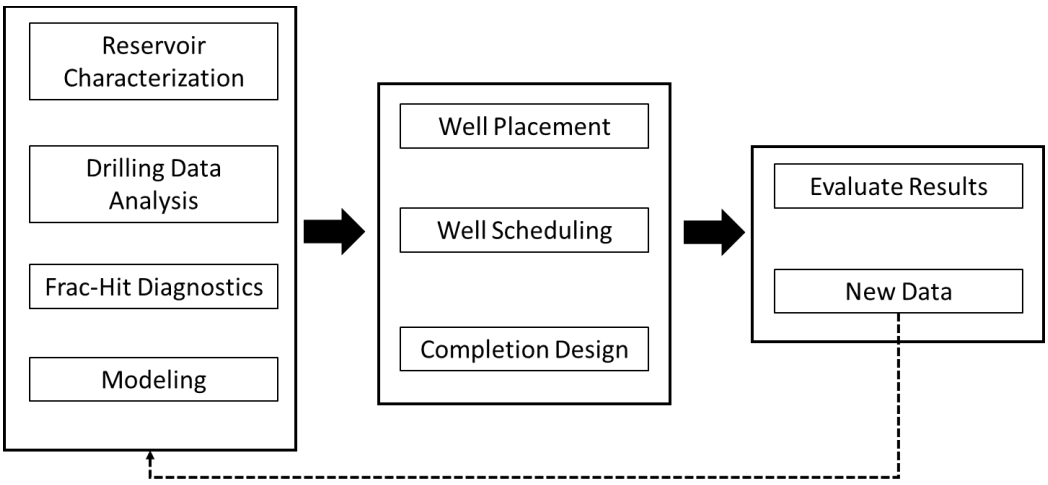

Figure 92: Proposed workflow to minimize negative impact of frac hits. The first step involves understanding petrophysical and geomechanical properties of the reservoir and using the modeling techniques and field-based empirical correlations to understand fracture growth and impact of frac hits. In Step 2, this understanding is used to make key decisions about infill wells like spacing, timing with respect to existing wells, and completion design. In Step 3, frac hit impact, fracture geometry, etc. are studied on the new infill wells and the data is further evaluated to improve the infill well spacing, infill-well timing and completion design.

It is also important to identify fracture barriers as strong fracture barriers may dictate staggered development (Jacobs 2018a). Generally, thick carbonate and shale layers with high closure stress

act as fracture barriers. Shales may have low Poisson's ratio which makes them brittle, however, they have greater anisotropy which leads to much higher horizontal stresses and thus, effective fracture barriers. Mineralogy estimated from logs and cores and closure stress profiles can help identify fracture barriers.

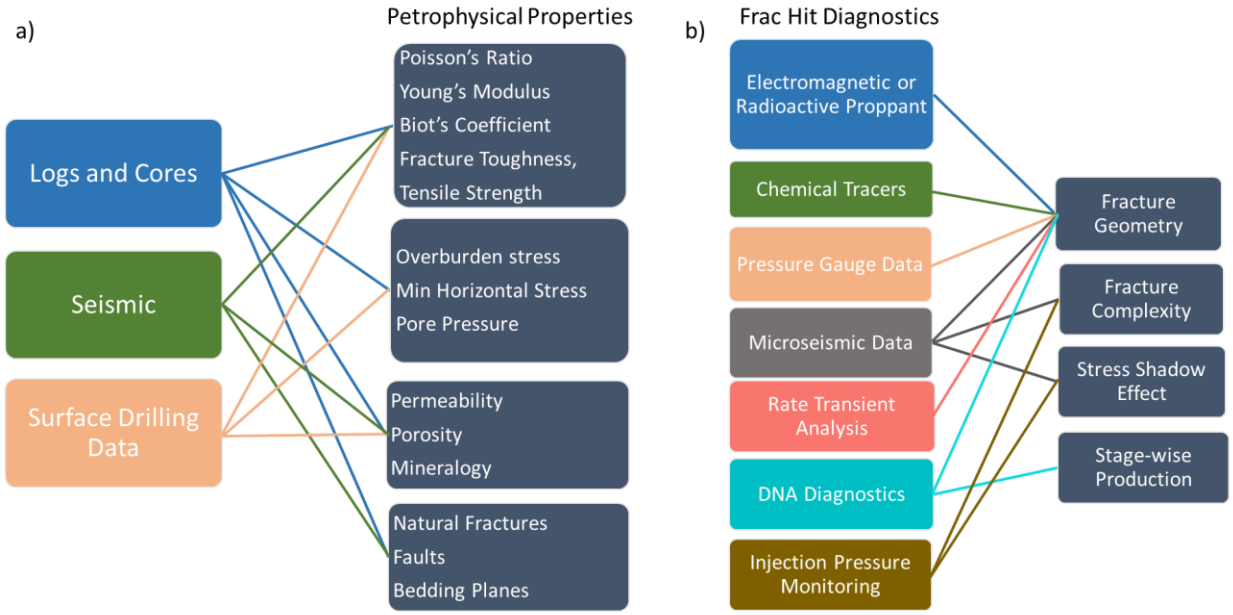

Figure 93: a) The important petrophysical, geomechanical and geological properties that control fracture propagation and fracture geometry and sources of obtaining these different properties. b) The different frac hit diagnostic tests that can help calculate fracture geometry, complexity, stress shadow effect and even stage-wise production.

Presence of reservoir discontinuities like natural fractures, faults, and high-perm streaks are important as they can cause disproportionate fracture growth and increase the risk of negative frac hits. Faults can be identified by seismic interpretation, natural fractures can be identified using a combination of image logs and seismic (Pollock et al. 2018), high perm streaks can be identified using permeability logs or inferred using gas tracking during drilling (Schaeffer et al. 2017). Natural fractures are desired in majority of the cases as they facilitate complex fracturing and hence, increase connected stimulated reservoir area (SRA). However, presence of thief zones

with very high density of natural fractures which may form a strong connection with adjacent wells must be avoided. Layering and bedding cause stunted fracture height (Warpinski 2009; Ng et al. 2019) and prevent frac hits in vertically offset wells. Bedding plane alterations can be quantified using lithofacies, electrofacies or rock type logs generated using core, log and geological data.

Fluid properties like GOR, bubble point pressure, fluid type (gas/oil), compressibility are important to determine poroelastic affects and hence determine the extent of stress shadow region. Laboratory PVT tests can be used to quantify fluid properties.

7.2 Drilling Data Analysis

Surface drilling data is the only data available in all the horizontal wells. It is also the data that is available real-time when drilling the wells. One of the best strategies to mitigate frac hits is to be able to modify the completions in real time while drilling the well (Paryani et al. 2017, Rainbolt and Esco 2018, Jacobs 2019). This includes stage spacing, cluster spacing, proppant and fluid type and amount. One simple example could be to modify stage spacing to avoid high permeability streaks. Thus, any information that could be obtained using drilling data is a big step towards adjustable completions. Schaeffer et al. (2017) suggested to track the gas emissions during drilling as high gas emissions could indicate higher matrix permeability. Kalinec et al. (2019) presented a workflow to calculate pore pressure using the drilling data. Jacobs (2018b) reported that FractureID can use accelerometer data to identify depleted zones. In Chapter 4 (**Figure 45** and **Figure 46**) and Chapter 6 (section 6.4), drilling data was used to assess the mechanical properties of the rock using simple cross-plots and advanced machine learning models, respectively. Gupta et al. (2020) have also shown the use of drilling data to characterize lithology using different machine learning techniques. Any effort to characterize reservoir

properties using drilling data needs exhaustive calibration data (core, DFIT, logs) due to inherent noise in the drilling data.

7.3 Frac Hit Diagnostics

Frac hit diagnostics (**Figure 93b**) are critical to understand fracture growth and impact of frac hits. Surface and downhole pressure data, chemical fluid tracer data, or microseismic can be used to study the fracture dimensions and occurrence and impact of frac hits in neighboring wells as a function of time (Sullivan et al. 2019 and Rainbolt and Esco 2018). Several studies (Rassenfoss 2016 and Ng et al. 2019) have reported application of electromagnetic proppants to track propped height and length of the hydraulic fractures. The long-term connectivity is indicated by propped fracture dimensions. Together with pressure and chemical fluid tracer tests, such proppant studies generate critical data for well spacing optimization. Sullivan et al. (2019) also recommended use of downhole pressure data to calculate stage-wise fracture complexity and hence, stage efficiency. The microseismic data can further give insights about the fracture propagation, complex versus planar fractures, stage-wise performance, oversized frac fluid design, stage interaction and stress shadow effects (**Figure 49**, **Figure 51**, **Figure 52**, **Figure 79** and **Figure 91**). DFITs are recommended throughout the development area to estimate pore pressures, initial shut-in pressures (ISIP), breakdown pressure, closure stress, matrix permeability, and pressure dependent leak-off. DNA diagnostics (Lascelles et al. 2017) can be used to identify fracture height growth and stage-wise production performance. RTA can be used to derive reservoir permeability, and connected fracture area before and after the frac hit, which can help predict impact of frac hits on parent wells. The frac hit diagnostics must be chosen strategically to avoid unnecessary costs.

7.4 Numerical and Empirical Modeling

The next step in the workflow is to integrate all the available data, i.e. production and completions, reservoir properties, and frac hit diagnostics and use it to make key decisions regarding well placement, well completion and well scheduling. It can be done in multiple ways. The easiest one is to make some rules of thumb like if loss of EUR is seen below 1000 ft. spacing, fix the parent-child spacing as 1000 ft. The slightly more complex method is using the data to generate empirical models where production and completion parameters can be used to estimate the impact on EUR. This analysis was done for Meramec, Woodford and Wolfcamp formations as discussed in Chapter 3. First, it can help quantify the impact of frac hits on the parent wells, child wells and total impact on parent + child wells (**Figure 23**, **Figure 24** and **Table 18**). Second, it can help identify important factors like spacing, completion size, depletion and change in GOR in the parent well. which control the impact of frac hits (see **Figure 25** to **Figure 29**). Empirical models combined with economic modeling can give an estimate of the optimum spacing (see **Figure 30** to **Figure 32**) which can be further refined/constrained using the reservoir characterization and frac hit diagnostic results. Finally, the most complex method is doing full scale numerical modeling. As the model gets complex, more accurate results and higher predictability are expected. In general, an advantage of modeling is its cheaper than acquiring actual data and can be used for sensitivity analysis. The shortcomings of complex models are that they are data intensive and due to uncertainty in inputs,yield non-unique answers. Several studies have used modeling for parent-child spacing optimization (Bharali et al. 2014; Wallace et al. 2016; Belyadi et al. 2016 and Gakhar et al. 2016), cluster-spacing optimization (Fowler et al. 2019), parent-child interactions and predict frac hits (Krishnamurthy et al. 2019; Gakhar et al. 2016; Khodabakhshnejad et al. 2017; Anusarn et al. 2019 and Jin and

Zoback 2019), effectiveness of repressuring parent wells to avoid frac hits from child wells (Li et al. 2019 and Zheng et al. 2019), refrac timing (Pankaj et al. 2016), natural fracture modeling (Yu et al. 2017), understanding stress distributions around parent well fractures, stress reversals and stress shadow effects (Rafiee et al. 2012; Schaffer et al. 2017; Rezaei et al. 2017; Peterson et al. 2018; Guo et al. 2018 and Agrawal and Sharma 2018), and understand impact of layering/bedding planes (Rho et al. 2018). Chapter 5 discusses a case study where sensitivity analysis was used to generate response surfaces for various fracture designs and gain critical insights into fracture propagation. Such analysis can provide a useful tool to optimize completion design when actual field data is limited. However, to carry out numerical modeling, at least some field tests are necessary to calibrate the numerical models.

7.5 Well Placement

Well placement includes well spacing (both vertical and lateral), azimuth and orientation of the parent and the child wells. Simple changes in parent-child orientation (**Figure 94a**) and offsetting fracture stages in parent-child wells (**Figure 94b**) can also be effective in reducing the impact of frac hits. There are several techniques to estimate fracture geometry especially length and height, thus they can be used as tools to decide well spacing (**Figure 95**). Microseismic and fluid tracers generally give optimistic estimates as they include all kinds of fractures that developed due to hydraulic fracturing process. Some of these fractures which are called aligned fractures (i.e. neither propped nor have an offset) close during the production phase. Production monitoring and pressure gauge data give more conservative estimates and mainly consist of open and connected fractures. These fractures are kept open either by proppant or asperities of the fracture surface due to shear offset. Electromagnetic proppants give most conservative spacing estimates as it measures only the propped fractures. All the fractures suffer loss of conductivity

with time but rate of loss is highest for aligned fractures and lowest for propped fractures. Production and pressure data are cheapest to obtain in the majority of the wells and are recommended for exhaustive analysis. Chapter 3 shows how production and completion data from public databases can be utilized to ascertain optimum spacing through empirical modeling. The other data wherever available must be used as calibration or check points based on the trend in **Figure 95**. Any technique to decide well spacing must be coupled with economics to determine optimum spacing.

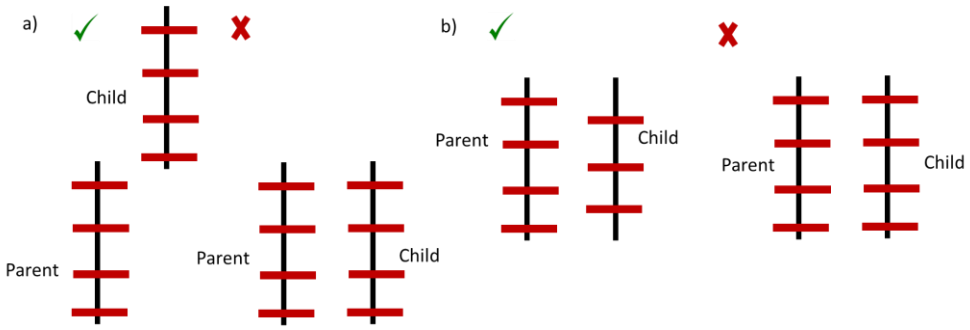

Figure 94: Simple effective strategies to reduce impact of frac hits. (a) Parent and child wells drilled toe to toe, rather than alongside each other. (b) The frac stages in parent and child wells offset with respect to each other. Between strategy (a) and (b), strategy (a) will lead to better mitigation of frac hits.

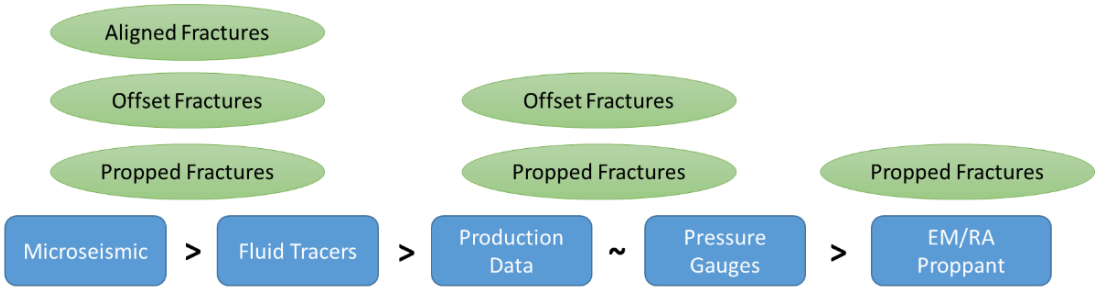

Figure 95: Different techniques to estimate fracture geometry especially length and height. Microseismic gives most optimistic estimate of fracture dimensions and EM/RA proppant gives the most conservative estimate. Propped fractures comprise both primary and secondary fractures, offset fractures are created by shear offset of natural fractures and faults which are kept open by fracture surface roughness and topography, aligned fractures are those fractures which are neither offset nor have proppant to keep them open. While propped fractures are most difficult to close, aligned fractures generally close shortly after production starts.

7.6 Well Scheduling

Based on literature survey (**Table 3**) and analysis in Chapter 3 (**Figure 23**) when child wells are drilled close to existing wells, they mostly suffer production loss as their fractures asymmetrically grow into the depleted zones of the parent wells. On the other hand, the impact of frac hits by child wells on parent wells can be very diverse, i.e. vary from negative to positive. The key reasons that are responsible for positive frac hits on the parent wells are – high pore pressure, smaller completion design, lower depletion in parent wells, and lower change in GOR compared to the initial GOR (Kurtoglu and Salman 2015 and Barree et al. 2017). Thus, well scheduling plays a key role to decide if the impact of frac hits on the parent wells would be positive or negative. Even though Jacobs (2019) reported 100,000 bbl production in parent well to be the cut-off which decides if the impact on the parent well will be positive or negative. Unfortunately, this number is variable and needs to be evaluated case by case. Empirical data analysis and modeling as shown in Chapter 3 is recommended to identify cut-off ranges of cum oil production in parent well, change in GOR in parent well.. With these cut-offs in hand, well scheduling can be done to make sure infill wells are drilled before this cut-off is exceeded in the parent wells. Frac hit diagnostic techniques (electromagnetic/radioactive proppant, downhole pressure gauges, microseismic analysis) can confirm the under stimulated parent wells. Preference should be given to these under stimulated parent wells while doing infill drilling as the percentage gains in these parent wells could be larger. Sometimes, it may not be possible to accommodate the cut-offs in certain parent wells due to logistics issue. Preventive measures like repressuring and refracturing with either water or gas (**Table 4**) of parent wells and far field divertors in child wells, must be taken to prevent negative impact of frac hits on both parent and child wells.

The above strategies are applied to sections which already has a parent well drilled. The best strategy to optimize recovery from a virgin section is co-development. This is because child wells in the majority of the cases have negative frac hits and the impact on child wells is generally larger than the magnitude of impact on parent wells. Doing preventive measures (repressuring, refracturing) in parent wells to minimize frac hit impact on child wells may be quite expensive and may not be justified by the small gain in parent well production. Two major techniques of co-development recommended in the literature, i.e. tank development (Thomson et al. 2018) and cube development (Jacobs 2018a) can be tried and tested to see which performs better for a certain area.

7.7 Completion Design

The key completion variables that must be optimized are amount of frac fluid and proppant per stage/cluster, type of frac fluid and proppant, injection rate of frac fluid, stage length, cluster spacing, and perforations per cluster. The empirical (Chapter 3) and numerical modeling (Chapter 5) can give a first estimate of amount of frac fluid and proppant for minimum impact on EUR for a given completion design and parent production characteristics. The empirical correlations for three major shale plays are shown in Chapter 3 (**Equations 17, 18, and 19**) which shows the utility of the public databases. This information can be further complemented by microseismic data especially the cumulative moment plot (**Figure 52**) which can identify injection time beyond which no additional shearing happens (Warpinski 2009). Field analysis of downhole pressure gauges and electromagnetic proppant identify propped fracture dimensions and whether completion size needs to be reduced or increased. Literature review (Rafiee and Grover 2017) suggests injecting at lower rates to maximize complex fracturing and increasing SRA. Lower viscosity slick-water also promotes complex fracturing but viscous fluid (HVFR, X-

linkers) may be required to provide adequate carrying capacity for the proppant. Similarly, bigger proppant size (20/40, 30/70) is important to prop open the primary fracture and provide higher conductivity, but 100-mesh proppant size is needed to prop open the secondary fracture network (Warpinski 1991) r. The 100-mesh proppant can also be useful to plug the high permeability pathways that increase the risk of frac hits. The ideal combination can be decided based on modeling and field tests (try different combinations and run fracture diagnostics to measure performance).

Majority of the studies (**Table 2**) that have analyzed frac hits have concluded that frac hits are caused because of disproportionate growth of fractures between various stages in the parent and child wells. A few fractures in child wells grow very long and intercept the parent wells or vice versa. When the formation shows large heterogeneity along the parent well, it is only appropriate to change the completion design for each stage based on the type of rock encountered (Paryani et al. 2017; Rainbolt and Esco 2018 and Jacobs 2019) also termed as 'on the fly' completions. Highly depleted and high permeability zones should be avoided as they can cause larger fractures which might connect with the adjacent wells. Literature review (Yi et al., 2019; Zheng et al., 2019 and Anderson et al., 2016) recommends reducing the number of perforations per cluster and reducing the number of clusters per stage to promote uniform fracture growth. The sensitivity study in chapter 5 also confirms that placing too many clusters per stage can cause disproportionate fluid intake leading to unnecessary long fractures in few clusters. Placing the clusters or stages too close also leads to stress shadow effects. While stress shadow generally reduces the fracture dimensions (length, height and width) as shown in chapter 5 (**Figure 66**), authors like Zheng et al. 2019 have also reported that stress shadow can promote longer planar fracture growth with reduced fracture width and subsequently increase the risk of frac hits. The

stage pumping data, numerical modeling studies and microseismic data can help understand if stress shadow effects are large, adjacent stages interacting or not and what effects they are causing on the fracture dimensions. This data can be used to optimize stage spacing, cluster spacing and number of perforations.

Chapter 8: Conclusions

The low perms in shales and the need to maximize reservoir contact has necessitated tighter well spacing and increased proppant and fracture fluid quantities which has led to a rise in frac hits. In this dissertation, Chapter 1 provides a critical review of the literature on the frac hits in unconventional reservoirs. Chapter 2 formulated a new decline curve analysis model VDMA more suited to unconventional reservoirs and Chapter 3 used this model to analyze more than 6000 wells in Meramec, Woodford and Wolfcamp to identify frac hits, corresponding parent and child wells and quantify the impact of frac hits. Chapter 4 analyzed the production, completions, petrophysical logs and microseismic data to gain further insights into fracture propagation in Meramec. Chapter 5 used the fracture modeling done in Chapter 4 to carry out sensitivity analysis with different completion design parameters. Chapter 6 integrated the extensive data collected in Marcellus formation at MSEEL test site like microseismic, image and sonic logs, and fiber optics to understand fracture growth. The key findings of the various chapters are:

1. Frac hit impact is dictated by a complex interplay of petrophysical properties (high-perm streaks, mineralogy, matrix permeability, natural fractures), geomechanical properties (near-field and far-field stresses, tensile strength, Young's modulus, Poisson's ratio), completion parameters (stage length, cluster spacing, pumping rate, fluid and proppant amount) and development decisions (well spacing and well scheduling).
2. The average impact of frac hits is negative on both parent and child wells in all the three formations. Parent wells lose 40,000 to 50,000 bbls in different formations in five years. Child wells have a bigger impact on being drilled near existing parent wells. They lose 18 to 40% of their oil volumes in 1 to 5 years or between 80,000 to 150,000 oil barrels per well in five years. The biggest impact on child wells is seen in Meramec and the least impact is seen

in Wolfcamp. Overall, combining the impact on parent and child wells, a parent-child pair on average loses 15 to 30 percent of their oil volumes in 1-5 years or between 125,000 to 225,000 bbls in 5 years with Meramec having the greatest impact and Wolfcamp having the least impact.

3. The negative impact on EUR in both parent and child wells is directly proportional to the completion size, and inversely proportional to parent-child spacing and oil rate of the parent well. The parent well EUR impact is also a function of change in GOR (compared to initial), with larger change correlated with stronger negative impacts. The child well EUR impact is also a strong function of the parent well depletion, with larger depletion causing stronger negative impact on child wells.
4. Linear regression models were developed using these key factors that control frac hit impact. These models can be used to predict frac hit impact and optimize completion size for a given spacing.
5. Child wells strongly were found to strongly interact with the parent wells and with each other in section A in Meramec. The fracture modeling and microseismic data analysis clearly shows overlap of fracture stages in the different wells. It suggests that well spacing of 660 ft in this section is quite optimistic. The economic analysis confirmed that under current economic model section A development is not economic.
6. The stage ISIP and microseismic analysis also showed that stages are strongly interacting with each other causing stress shadow effects. This clearly manifests itself in fracture geometry where earlier stages are predicted to be more complex fractures and later stages to develop more planar fractures. This gives an opportunity to optimize the stage spacing.

7. The fracture modeling based on isotropic uniaxial strain modeling shows that Meramec A and Osage are potential frac barriers.
8. GR and MSE cross plot shown in several section A wells can help identify mechanical property variation across the wellbore in real-time and can be used to optimize completion design.
9. The sensitivity analysis in Chapter 5 showed that fluid per cluster is probably the most important factor controlling fracture length and height while proppant per cluster controls the fracture width. The fracture lengths are also more susceptible to closure compared to fracture heights based on which vertical offset (or staggering) is recommended to minimize frac hits.
10. Another interesting find was that larger number of clusters does not necessarily lead to smaller fractures as the assumption that all clusters within a stage are equal does not apply to heterogenous shale reservoirs. Larger numbers of fractures can cause disproportionate fractures and may increase the risk of frac hits.
11. Stress shadow can significantly reduce fracture dimensions. Traditionally, it is believed that larger number of clusters can prevent frac hits by generating smaller fractures. This however is not the economic solution as it comes at a huge completion cost. Simple economical solution would be to reduce amount of frac fluid/proppant without changing the cluster spacing.
12. The response surfaces can help evaluate multiple completion variables at the same time and can significantly improve the decision-making process with regards to choosing the right completion size.
13. In Marcellus at MSEEL test site, it was evident that fracture geometry is strongly controlled by the rock properties (Young's modulus and Poisson's ratio) and the natural fracture

density. Completing brittle and fracable zones with high natural fracture density also lead to higher production.

14. Another key finding is that the drilling data can be used to estimate rock properties and differentiate between brittle and ductile, easy-to-frac and hard-to-frac rock in real-time while drilling. Ma and Zoback (2016) also showed that stages having high Sh_{min} (minimum horizontal stress) showed lower microseismic activity, took lesser proppant and lead to smaller fracture dimenions. This gives an opportunity to geosteering engineers who use mainly gamma ray to steer the well. The idea is not to just stay within shale but chose the best spot to place the well within the shale.
15. The study also shows the potential of drilling data to minimize frac hits by avoiding fracturing in ductile zones which generates longer planar fractures that can intersect neighboring parent wells and cause frac hits. Fortunately, in this area in Marcellus, the solution is simple – generate complex fractures to maximize production and reduce frac hits.

The recommended approach to manage frac hits starts with developing an understanding the type of rock and state of stresses which control the fracture growth. It is important to know Young's modulus, Poisson's ratio, fracture toughness and matrix permeability which can be calculated from the available logs, core and seismic data. This data when put into fracture modeling software can predict propped and unpropped fracture dimensions. This can help determine occurrence of frac hits as well as their temporary and permanent nature. Presence of natural fractures, high permeability streaks, faults and other formation discontinuities must be determined to understand inter-well fracture interaction. Proxy models must be developed using surface drilling data wherever possible because it is the only data that will be available in all the wells and if reservoir science is to become an essential part of decision-making process in every

well, surface drilling data has to be involved. Promising techniques have been published in the literature where surface drilling data is used to calculate a matrix-permeability indicator, pore-pressure, and mechanical property facies Each shale formation is unique and so is its response to frac hits. Frac hit diagnostics, i.e. specific field measurements directed towards fracture growth and extent like DFIT, RTA, microseismic, downhole pressure gauge data and electromagnetic proppant must be acquired and used to make decisions. It can also be used to calibrate numerical models which can further extend the knowledge base on formation response to fracturing. Numerical modeling can run several scenarios to optimize completion design to prevent stress shadow effects, facilitate uniform fracture growth and minimize occurrence of frac hits. Well placement and scheduling must be decided based on the reservoir. For instance, frac barriers may dictate separate wells with smaller completion rather than one well with large completion. Parent wells early in their life seem to benefit from frac hits possibly because they get access to new reservoir and they have enough energy to clean-up themselves after being inundated with completion fluid from child well. These cut-offs in terms of cumulative parent oil production and rate, change in GOR can be determined using existing wells. The industry is also slowly moving away from the parent-child concept to simultaneous lease development for the new leases. Simultaneous lease development using Tank and Cube methods give higher productivity than infill drilling.

References Cited

Abukhamsin, A.Y. 2017. Inflow Profiling and Production Optimization in Smart wells using distributed acoustic and Temperature Measurements. PhD Dissertation, Stanford University, Stanford, California, USA.

Ajani, A.A. and Kelkar, M.G. 2012. Interference study in shale plays. SPE-151045. Presented at SPE Hydraulic Fracturing Technology Conference held in the Woodlands, Texas, USA, 6-8 Feb.

Agrawal, S. and Sharma, M.M., 2018. Impact of Pore Pressure Depletion on Stress Reorientation and its Implications on the Growth of Child Well Fractures. Presented in Unconventional Resources Technology Conference, Houston, Texas, 23-25 July.

Ajisafe, F., Solovyeva, I., Morales, A., Ejofodomi, E. and Porcu, M.M. 2017. Understanding Impact of Well Spacing and Interference on Production Performance in Unconventional Reservoirs, Permian Basin. Presented in Unconventional Resources Technology Conference, Austin, Texas, 24-26 July.

Almasoodi, M.M. 2019. Numerical Modeling and Diagnostics of Inter- and Intra-Well Interference in Tight Oil Reservoirs: Towards Optimal Well Spacing Decisions. PhD Dissertation, University of Oklahoma, Norman, Oklahoma.

Altamar, R.P. and Marfurt, K. 2014. Mineralogy-based brittleness prediction from surface seismic data: Application to the Barnett Shale. Interpretation 2 (4): 255—271. http://dx.doi.org/10.1190/INT-2013-0161.1.

Altman, N. S. 1992. An introduction to kernel and nearest-neighbor nonparametric regression. The American Statistician. 46 (3): 175–185.

Anderson, D.M., Thompson, J.M., Cadwallader, S.D., Sebastian, H., Gil, I. and Lee, P., 2016. Maximizing Productive Stimulated Reservoir Volume in the Eagle Ford-An Infill Case Study. Presented in Unconventional Resources Technology Conference, San Antonio, Texas, 1-3 August.

Anusarn, S., Li, J., Wu, K., Wang, Y., Shi, X., Yin, C. and Li, Y., 2019. Fracture Hits Analysis for Parent-Child Well Development. Presented in 53rd US Rock Mechanics/Geomechanics Symposium held in New York, NY, 23-26 Jun.

Anschutz, D.A., Lowrey, T.A., Stribling, M. and Wildt, P.J., 2019. An In-Depth Study of Proppant Transport and Placement with Various Fracturing Fluids. Presented in SPE Annual Technical Conference and Exhibition. Society of Petroleum Engineers held in Calgary, Alberta, Canada, 30 Sep – 2 Oct.

Archie, G.E., 1952, Classification of carbonate reservoir rocks and petrophysical considerations: AAPG Bulletin, vol. 36, no. 2, p. 218–298.

Arps, J.J. 1944. Analysis of Decline Curves. Presented at A.I.M.E. Houston meeting, May 1944.

Awada, A., Santo, M., Lougheed, D., Xu, D. and Virues, C. 2015. Is that interference? A workflow for identifying and analyzing communication through hydraulic fractures in a multi-well pad. Presented in Unconventional Resources Technology Conference held at San Antonio, Texas, 20-22 July.

Ayers, K., Jacot, H. and Ayers, A., 2018. Statistical analysis of generational effect on Marcellus well completions using bottomhole gauge data. Presented in SPE/AAPG Eastern Regional Meeting held in Pittsburgh, Pennsylvania, USA, 7-11 Oct.

Barree, R.D., Miskimins, J.L. and Svatek, K.J., 2017. Reservoir and completion considerations for the refracturing of horizontal wells. SPE Production & Operations, 33(01), pp.1-11.

Barree, R.D. 2019. Stress Shadowing and Fracture Interference in GOPHER Software. https://www.halliburton.com/content/dam/ps/public/pinnacle/contents/Papers_and_Articles/web/gohfer-stress-shadowing-fracture-interference.pdf (accessed 20 Feb 2020).

Bazan, L.W., Larkin, S.D., Lattibeaudiere, M.G,. and Palisch, T.T. 2010. Improving Production in the Eagle Ford Shale with Fracture Modeling, Increased Fracture Conductivity, and Optimized Stage and Cluster Spacing along the Horizontal Wellbore. Presented in Tight Gas Completions Conference held in San Antonio, Texas, USA, 2-3 Nov.

Belyadi, H., Yuyi, J., Ahmad, M. and Wyatt, J., 2016. Deep Dry Utica Well Spacing Analysis with Case Study. Presented in SPE Eastern Regional Meeting held in Canton, Ohio, USA, 13-15 Sep.

Bharali, S.G., Sharma, A. and Sehra, S.S.M., 2014. Effect of Well Down Spacing on EUR for Shale Oil Formations. Presented in SPE Western North American and Rocky Mountain Joint Meeting held in Denver, Colorado, USA, 16-18 April.

Birch, F. 1966. Compressibility, Elastic Constants. Handbook of Physical Constants (Memoir 97), Geological Society of America, Boulder, Colorado, pp. 97-173.

Blasingame, T.A. and Rushing, J.A. 2005. A Production-based method for direct estimation of gas in place and reserves. Presented at 2005 SPE Eastern Regional Meeting held in Morgantown, W.V., 14-16 September 2005. SPE 98042.

Bommer, P., Bayne, M., Mayerhofer, M., Machovoe, M. and Staron, M., 2017. Re-Designing from scratch and defending offset wells: case study of a six-well Bakken zipper project, McKenzie County, ND. Presented in SPE Hydraulic Fracturing Technology Conference and Exhibition held in the Woodlands, Texas, USA, 24-26 Jan.

Bommer, P.A. and Bayne, M.A., 2018. Active Well Defense in the Bakken: Case study of a ten-well frac defense project, McKenzie County, ND. Presented in SPE Hydraulic Fracturing Technology Conference and Exhibition held in the Woodlands, Texas, USA, 23-25 Jan.

Bourdet, D. 2002. Well Test Analysis – The Use of Advanced Interpretation Models, Handbook of Petroleum Exploration and Production, 3. Elsevier. IBN 0-444-50968-2.

Breiman, L., 1997, Arcing the edge. Technical Report 486: Statistics Department, University of California, Berkeley.

Breiman, L., 2001, Random forests: Machine Learning, 45, 5–32, doi: 10.1023/A:1010933404324.

Chang, D., Vinegar, H., Morris, C. et al. 1997. Effective porosity, producible fluid and permeability in carbonates from nmr logging. The Log Analyst 38 (2): 60-72.

Cipolla, C.L., 1996. Hydraulic fracture technology in the Ozona Canyon and Penn Sands. Presented in Permian Basin Oil and Gas Recovery Conference held in Midland, Texas, 27-29 March.

Cipolla, C., Motiee, M. and Kechemir, A., 2018. Integrating microseismic, geomechanics, hydraulic fracture modeling, and reservoir simulation to characterize parent well depletion and infill well performance in the bakken. Presented in Unconventional Resources Technology Conference, Houston, Texas, 23-25 July.

Craft, B. C. and Hawkins, M. F. Jr. 1959. Applied Petroleum Reservoir Engineering, Prentice-Hall, Inc., Englewood Cliffs, N.J. 126, 206,224.

Dang, S.T., Sondergeld, C.H., and Rai, C.S. 2019. Interpretation of nuclear-magnetic-resonance response to hydrocarbons: Application to miscible enhanced-oil-recovery experiments in shales. SPE Reservoir Evaluation and Engineering. doi:10.2118/191144-PA.

Davarpanah, A., Zarel, M., and Nassabeh, M. 2016. Assessment of mechanical specific energy aimed at improving drilling inefficiencies and minimize wellbore instability, J Pet Environ Biotechnol, vol 7, issue 6, Doi: 10.4172/2157-7463.1000309.

Daneshy, A. and King, G., 2019. Horizontal well frac-driven interactions: types, consequences, and damage mitigation. Journal of Petroleum Technology, 71(06), pp.45-47.

Duong, A.N. 2010. An Unconventional rate decline approach for tight and fracture dominated gas wells. Presented at Canadian Unconventional Resources and International Petroleum Conference held in Calgary, Alberta, Canada, 19-21 Oct 2010. SPE 137748.

Eaton, B. A. 1975. The equation for geopressure prediction from well logs. In . Society of Petroleum Engineers. https://doi.org/10.2118/5544-MS.

Esquivel, R. and Blasingame, T.A., 2017. Optimizing the development of the Haynesville Shale—Lessons-Learned from well-to-well hydraulic fracture interference. Presented in Unconventional Resources Technology Conference, Austin, Texas, 24-26 July.

Fawcett, T. 2006. An introduction to roc analysis. Pattern Recognition Letters. 27 (8): 861–874. doi:10.1016/j.patrec.2005.10.010.

Fetkovich, M.J. 1973. Decline curve analysis using decline curves. Presented at SPE 48th Fall Meeting in Las Vegas, Sep 30 – Oct 3. SPE 4629.

Fisher, M.K., Heinze, J.R., Harris, C.D., Davidson, B.M., Wright, C.A. and Dunn, K.P., 2004. Optimizing horizontal completion techniques in the barnett shale using microseismic fracture mapping. Presented at the SPE Annual Technical Conference and Exhibition, Houston, Texas, 26–29 September.

Fowler, G., McClure, M. and Cipolla, C., 2019. A Utica Case Study: The impact of permeability estimates on history matching, fracture length, and well spacing. Presented in SPE Annual Technical Conference and Exhibition held in Calgary, Alberta, Canada, 30 Sep – 2 Oct.

Friedrich, M. and Monson, G., 2013. Two practical methods to determine pore pressure regimes in the Spraberry and Wolfcamp formations in the Midland basin. Presented in Unconventional Resources Technology Conference held in Denver, Colorado, USA, 12-14 Aug.

Fulford, D.S. and Blasingame, T.A. 2013. Evaluation of Time-Rate Performance of Shale Wells using the Transient Hyperbolic Relation. Presented at SPE Unconventional Resources Conference held in Calgary, Alberta, Canada, 5-7 Nov. SPE 167242.

Gakhar, K., Shan, D., Rodionov, Y., Malpani, R., Ejofodomi, E.A., Xu, J., Fisher, K., Fischer, K., Morales, A. and Pope, T.L., 2016. Engineered approach for multi-well pad development in Eagle Ford Shale. Presented in Unconventional Resources Technology Conference, San Antonio, Texas, 1-3 August.

Gakhar, K., Rodionov, Y., Defeu, C., Shan, D., Malpani, R., Ejofodomi, E., Fischer, K. and Hardy, B., 2017. Engineering an effective completion and stimulation strategy for in-fill wells. Presented in SPE Hydraulic Fracturing Technology Conference and Exhibition held in the Woodlands, Texas, USA, 24-26 Jan.

Gale, J.F.W. and Holder, J. 2010. Natural fractures in some US shales and their importance for gas production, Geological Society, London, Petroleum Geology Conference series, 7, 1131-1140, 1 January 2010, https://doi.org/10.1144/0071131.

Guo, X., Wu, K., Killough, J. and Tang, J. 2018. Understanding the mechanism of interwell fracturing interference based on reservoir-geomechanics-fracturing modeling in Eagle Ford Shale. Presented in Unconventional Resources Technology Conference, Houston, Texas, 23-25 July.

Gupta, I. 2017. Rock typing in organic shales: Eagle Ford, Woodford, Barnett and Wolfcamp formations, Masters Thesis, University of Oklahoma, Norman, OK, USA.

Gupta, I., Rai, C., Sondergeld, C. and Devegowda, D., 2018, Variable exponential decline-modified arps to characterize unconventional shale production performance. Presented in Unconventional Resources Technology Conference, Houston, Texas, 23-25 July.

Gupta, A., Rai, C., and Sondergeld, C. 2019. Experimental investigation of propped fracture conductivity and proppant diagenesis. Presented in Unconventional Resources Technology Conference held in Denver, Colorado, USA, 22-24 July.

Gupta, I., Tran, N., Devegowda, D., Jayaram, V., Rai, C., Sondergeld, C., and Karami, H. 2020. Looking ahead of the bit using surface drilling and petrophysical data: machine-learning-based real-time geosteering in Volve Field. SPE Journal. doi:10.2118/199882-PA

Hamrick, T., 2011. Optimization of operating parameters for minimum mechanical specific energy in drilling (No. TPR-3609). National Energy Technology Lab.(NETL), Pittsburgh, PA, and Morgantown, WV, USA.

Haustveit, K. and Greenwood, H., 2018. Delineating stacked pay with existing and emerging diagnostic tools. Presented in SPE Hydraulic Fracturing Technology Conference and Exhibition held in the Woodlands, Texas, USA, 23-25 Jan.

Hou, P., Gao, F., Gao, Y., Yang, Y. and Cai, C., 2017. Effect of pore pressure distribution on fracture behavior of sandstone in nitrogen fracturing. Energy Exploration & Exploitation, 35(5), pp.609-626.

Hsieh, F.S. 2001. Applying a time-dependent darcy equation for decline analysis for wells of varying reservoir type. Presented at SPE Rocky Mountain Petroleum Technology Conference held in Keystone, Colorado, 21-23 May 2001. SPE 71036.

Ilk, D., Rushing, J.A., Perego, A.D., and Blasingame, T.A. 2008. Exponential versus Hyperbolic decline in tight gas sands – Understanding the origins and implications for reserve estimates using Arps decline curves. Presented at 2008 SPE Annual Technical Conference and Exhibition held in Denver, Colorado, USA, 21-24 Sep 2008. SPE 116731.

Jacobs, T. 2017a. Oil and gas producers find frac hits in shale wells a major challenge. J Pet Technol 69(04), SPE-0417-0029-JPT. https://doi.org/10.2118/0417-0029-JPT.

Jacobs, T. 2017b. Frac hits reveal well spacing may be too tight, completion volumes too large. J Pet Technol, SPE-1117-0035-JPT. doi:10.2118/1117-0035-JPT.

Jacobs, T., 2018a. In the battle against frac hits, shale producers go to new extremes. Journal of Petroleum Technology, 70(08), pp.35-38, SPE-0818-0035-JPT.

Jacobs, T., 2018b. Three unconventional startups offer new clues on shale's biggest well spacing mysteries. Journal of Petroleum Technology, 70(09), pp.47-52.

Jacobs, T., 2019. To solve frac hits, unconventional engineering must revolve around. Journal of Petroleum Technology, 71(04), pp.27-31, SPE-0419-0027-JPT.

James, G., Witten, D., Hastie, T., and Tibshirani, R. 2013. An Introduction to Statistical Learning : with Applications in R. New York :Springer.

Jin, L. and Zoback, M., 2019. Depletion-Induced poroelastic stress changes in naturally fractured unconventional reservoirs and implications for hydraulic fracture propagation. Presented in SPE Annual Technical Conference and Exhibition held in Calgary, Alberta, Canada, 30 Sep – 2 Oct.

Kabir, C.H., Rasdi, F. and Igboalisi, B. 2011. Analyzing production data from tight oil wells. Journal of Canadian Petroleum Technology. The paper was also presented at Canadian Unconventional Resources and International Petroleum Conference held in Calgary, 19-21 Oct, 2010.

Kalinec, J., Paryani, M. and Ouenes, A., 2019. Estimation of 3d distribution of pore pressure from surface drilling data-application to optimal drilling and frac hit prevention in the Eagle Ford. Presented in Unconventional Resources Technology Conference held in Denver, Colorado, 22-24 July.

Khodabakhshnejad, A., Aimene, Y., Mistry, N., Bachir, A. and Ouenes, A., 2017. A fast method to forecast shale pressure depletion and well performance using geomechanical constraints-application to poro-elasticity modeling to predict mid and far field frac hits at an Eagle Ford and Wolfcamp well. Presented in SPE Eastern Regional Meeting held in Lexington, Kentucky, USA, 4-6 Oct.

King, G.E., Haile, L., Shuss, J.A. and Dobkins, T., 2008. Increasing fracture path complexity and controlling downward fracture growth in the Barnett shale. Presented in SPE Shale Gas Production Conference held in Fort Worth, Texas, USA, 16-18 Nov.

King, G.E. 2014. 60 Years of Multi-Fractured vertical, deviated and horizontal wells: What have we learned? SPE-170952. Presented in SPE Annual Technical Conference and Exhibition held in Amsterdam, Netherlands, 27-29 Oct.

King, G.E. and Valencia, R.L. 2016. Well integrity for fracturing and re-fracturing: What is needed and why?. SPE-179120. Presented at SPE Hydraulic Fracturing Technology Conference held in the Woodlands, Texas, USA, 9-11 Feb.

King, G.E., Rainbolt, M.F. and Swanson, C. 2017. Frac hit induced production losses: evaluating root causes, damage location, possible prevention methods and success of remedial treatments, SPE-187192, Presented at the SPE Annual Technical Conference and Exhibition held in San Antonio, Texas, USA, 9-11 Oct.

Krishnamurthy, J., Srinivasan, K., Layton, N. and Drouillard, M., 2019. Frac hits: Good or bad? A comprehensive study in the Bakken. Presented in SPE Annual Technical Conference and Exhibition held in Calgary, Alberta, Canada, 30 Sep – 2 Oct.

Kuhn, M. 2008. Building predictive models in R using the caret package. Journal of Statistical Software, 28(5), 1 - 26. doi:http://dx.doi.org/10.18637/jss.v028.i05.

Kumar, A., Seth, P., Shrivastava, K., Manchanda, R. and Sharma, M.M. 2018b. Well interference diagnosis through integrated analysis of tracer and pressure interference tests. Presented in Unconventional Resources Technology Conference, Houston, Texas, 23-25 July.

Kurtoglu, B. and Salman, A. 2015. How to utilize hydraulic fracture interference to improve unconventional development, SPE-177953, Presented in Abu Dhabi International Petroleum Exhibition and Conference held in Abu Dhabi, UAE, 9-12 Nov.

Kushtanova, G.G. 2015. Well Test Analysis. Kazan Federal University, Institute of Physics, Department of Radioelektronic.

Lalehrokh, F., and Bouma, J. 2014. Well spacing optimization in Eagle Ford. Presented in SPE/CSUR Unconventional Resources Conference held in Calgary, Alberta, Canada, 30 Sep – 2 Oct.

Lascelles, P., Wan, J., Robinson, L., Allmon, R., Evans, G., Ursell, L., Scott, N.M., Chase, J., Jablanovic, J., Karimi, M. and Rao, V., 2017. Applying subsurface DNA sequencing in Wolfcamp shales, Midland Basin. Presented in SPE Hydraulic Fracturing Technology Conference and Exhibition held in the Woodlands, Texas, USA, 24-26 Jan.

Lawal, H., Jackson, G., Abolo, N. and Flores, C. 2013. A novel approach to modeling and forecasting frac hits in shale gas wells, SPE-164898. Presented at EAGE Annual Conference and Exhibition, London, UK, 10-13 Jun.

Lawal, H., Abolo, N., Jackson, G., Sahai, V. and Flores, C.P. 2014. A quantitative approach to analyze fracture area loss in shale gas reservoirs. SPE-169406. Presented in SPE Latin America and Caribbean Petroleum Engineering Conference held in Maracaibo, Venezuela, 21-23 May.

Lecun, Y., Bottou, L., Bengio, Y., and Haffner, P. 1998. Gradient-Based learning applied to document recognition. Proceedings of the IEEE, vol: 86, Issue: 11, Pg. 2278 – 2324, DOI: 10.1109/5.726791.

Li, N., Wu, K. and Killough, J., 2019. Numerical investigation of key factors on successful subsequent parent well water injection to mitigate parent-infill well interference. Presented in Unconventional Resources Technology Conference, Denver, Colorado, 22-24 July.

Lindsay, G., Miller, G., Xu, T., Shan, D. and Baihly, J., 2018. Production performance of infill horizontal wells vs. pre-existing wells in the major US unconventional basins. Presented in SPE Hydraulic Fracturing Technology Conference and Exhibition held in the Woodlands, Texas, USA, 23-25 Jan.

Litchfield, T. and Lehman, J. 2014. Inter-Well Interference during stimulation, flowback and production history. SPE ATW Slide Presentation, SPE ATW on Flowback, San Antonio, TX, USA, 6-7 Nov.

Lougheed, D., Behmanesh, H. and Anderson, D., 2019, October. Does depletion matter? A child well workflow. Presented in Unconventional Resources Technology Conference, Denver, Colorado, 22-24 July.

Lundberg, S.M. and Lee, S.I. 2016. A unified approach to interpreting model predictions. Presented at the 31st Conference on Neural Information Processing Systems, Long Beach, CA, USA.

Ma, X. and Zoback, M.D. 2016. Geomechanical Study of Hydraulic Fracturing in Woodford Shale, Oklahoma. AAPG Search and Discovery Article #41909.

Mann P, Hempton MR, Bradley DC, et al. Development of pull-apart basins. J Geol. 1983;91(5):529–54. https://doi.org/10.1086/628803.

Maechler, M., Rousseeuw, P., Struyf, A., Hubert, M., Hornik, K.2019. cluster: Cluster Analysis Basics and Extensions. R package version 2.1.0.

Manchanda, R., Hwang, J., Bhardwaj, P., Sharma, M.M., Maguire, M. and Greenwald, J., 2018. Strategies for improving the performance of child wells in the Permian basin. Presented in Unconventional Resources Technology Conference, Houston, Texas, 23-25 July.

McDowell, B., Yoelin, A. and Pottebaum, B., 2019, October. Production effects from frac-driven interactions in the southeastern Midland basin, Reagan County, Texas. Presented in Unconventional Resources Technology Conference, Denver, Colorado, 22-24 July.

McHugh, M. L. 2012. Interrater reliability: The kappa statistic. Biochemia Medica. 22 (3): 276–282. doi:10.11613/bm.2012.031. PMC 3900052. PMID 23092060.

McKay, M.D., Beckman, R.J. and Conover, W.J. 1979. A comparison of three methods for selecting values of input variables in the analysis of output from a computer code. Technometrics. American Statistical Association. 21 (2): 239–245. doi:10.2307/1268522

Mittal, A., Rai, C.S., and Sondergeld, C.H. 2017. A study of propped-fracture conductivity: impairment mechanisms under laboratory conditions. Presented at SPWLA 58th Annual Logging Symposium held in Oklahoma City, Oklahoma, 17-21 Jun 2017

Mittal, A., Rai, C.S., and Sondergeld, C.H. 2018. Proppant-Conductivity testing under simulated reservoir conditions: impact of crushing, embedment, and diagenesis on long-term production in shales, SPE Journal, doi:10.2118/191124-PA.

Moronkeji, D., Villegas, R., Shouse, R. and Prasad, U., Rock strength prediction during coring operation. Presented in International Symposium of the Society of Core Analysts Held in Vienna, Austria (Vol. 27).

Mouchet, J.P. and Mitchell, A. 1989. Abnormal Pressures While Drilling: Origins, Predictions, Detection, Evaluation. Paris: Elf EP-Editions, Editions Technip, 255.

Mullen, M., Roundtree, R. and Turk, G.A. 2007. A composite determination of mechanical rock properties for stimulation design (What to do when you don't have a sonic log). Paper SPE 108139 presented at Rocky Mountain Oil & Gas Technology Symposium, April 16-18.

Ng, M., Umholtz*, N., Hammerquist, C., Wang, J., Aimene, Y. and Ouenes, A., 2019, October. Quantifying hydraulic fracture height reduction in the presence of laminations and weak interfaces—Validation with microseismic moment tensor inversion in the Montney Shale. Presented in Unconventional Resources Technology Conference, Denver, Colorado, 22-24 July.

Nielson, M.A. 2015. Neural Networks and Deep Learning. Determination Press. Weblink: https://skymind.ai/wiki/neural-network. Last accessed 27 April, 2019.

Okouma, V., Vitthal, S., Nair, N. and Miller, M.A. 2012. Play-wide well performance analysis in Montney siltstone. Presented in SPE Canadian Unconventional Resources Conference held in Calgary, Alberta, Canada, 30 Oct – 1 Nov.

Pankaj, P., Gakhar, K. and Lindsay, G. 2016, October. When to refrac? Combination of reservoir geomechanics with fracture modeling and reservoir simulation holds the answer. Presented in SPE Asia Pacific Oil & Gas Conference and Exhibition held in Perth, Australia, 25-27 Oct.

Pankaj, P., Shukla, P., Kavousi, P., and Carr, T. 2018. Hydraulic fracture and reservoir characterization for determining optimal well spacing in the Marcellus shale. Presented at the SPE Liquids-Rich Basins Conference-North America held in Midland, TX, USA, 5-6 Sep.

Paryani, M., Smaoui, R., Poludasu, S., Attia, B., Umholtz, N., Ahmed, I. and Ouenes, A., 2017. Adaptive fracturing to avoid frac hits and interference: A Wolfcamp shale case study. Presented in SPE Unconventional Resources Conference held in Calgary, Alberta, Canada, 15-16 Feb.

Patel, H., Cadwallader, S. and Wampler, J. 2016. Zipper fracturing: taking theory to reality in the Eagle Ford shale. Presented in Unconventional Resources Technology Conference, San Antonio, Texas, 1-3 August.

Patel, S., Sondergeld, C., and Rai, C. 2016. Laboratory studies of cyclic injection hydraulic fracturing. Presented at SEG International Exposition and 86th Annual Meeting. Paper 2016-13969713.

Perkins, T.K. and Kern, L.R. 1961. Widths of Hydraulic Fractures. SPE Journal. doi:10.2118/89-PA

Peterson, N., Ouenes, A., Ng, M., Hughes, R., Hlidek, B., Aimene, Y. Khodabakhshnejad, A. and Li, X., 2018. Case study of time-based stress shadow influences on new well fracture propagation patterns in the Montney. Presented in SPE Canada Unconventional Resources Conference held in Calgary, Alberta, Canada, 13-14 March.

Pollock, C., Seiler, C., Valcárcel, M. and Macaulay, E. 2018. A method of fracture prediction across multiple stratigraphic horizons in the Midland basin, Texas, USA. Presented in Unconventional Resources Technology Conference, Houston, Texas, 23-25 July.

Rafiee, M., Soliman, M.Y., Pirayesh, E. and Emami M.H. 2012. January. Geomechanical considerations in hydraulic fracturing designs. Presented in SPE Canadian Unconventional Resources Conference held in Calgary, Alberta, Canada, 30 Oct – 1 Nov.

Rafiee, M. and Grover, T. 2017. Well spacing optimization in Eagle Ford shale: An operator's experience. Presented in Unconventional Resources Technology Conference, Austin, Texas, 24-26 July.

Rainbolt, M.F. and Esco, J. 2018. Frac hit induced production losses: evaluating root causes, damage location, possible prevention methods and success of remediation treatments, Part II. Presented in SPE Hydraulic Fracturing Technology Conference and Exhibition held in the Woodlands, Texas, USA, 23-25 Jan.

Rassenfoss, S. 2016. Electromagnetic imaging offers first look at the propped rock. Journal of Petroleum Technology, 68(03), pp.32-40.

Rassenfoss, S. 2017. Rethinking fracturing: The problems with bigger fracs in tighter spaces. Journal of Petroleum Technology, 69(12), pp.28-34.

Rassenfoss, S. 2018. A look into what fractures really look like. Journal of Petroleum Technology, 70(11), pp.28-36.

Raterman, K. T., Farrell, H. E., Mora, O. S., Janssen, A. L., Gomez, G. A., Busetti, S., McEwen, J., Friehauf, K., Rutherford, J., Reid, R. Jin, G., Roy, B., and Warren, M. 2018. Sampling a Stimulated Rock Volume: An Eagle Ford Example. SPE Journal. doi:10.2118/191375-PA.

Rezaei, A., Rafiee, M., Siddiqui, F., Soliman, M. and Bornia, G. 2017. The role of pore pressure depletion in propagation of new hydraulic fractures during Refracturing of horizontal Wells. Presented in SPE Annual Technical Conference and Exhibition held in San Antonio, Texas, USA, 9-11 Oct.

Rho, S., Suarez-Rivera, R. and Noynaert, S. 2018. Consequences of rock layers and interfaces on hydraulic fracturing and well production of unconventional reservoirs. Geophysics, 83, 6, MR333-M344.

Rivera, R.S. 2018. What do hydraulic fractures may look like? Plenary presentation at SPE Hydraulic Fracturing Technology and Exhibition held at Woodlands, Texas, USA, 23-25 Jan.

Rucker, W.K., Bobich, J. and Wallace, K. 2016. Low cost field application of pressure transient communication for rapid determination of the upper limit of horizontal well spacing. Presented in Unconventional Resources Technology Conference, San Antonio, Texas, 1-3 August.

Sani, A.M., Podhoretz, S.B. and Chambers, B.D. 2015. The use of completion diagnostics in Haynesville shale horizontal wells to monitor fracture propagation, well communication, and production impact. Presented at the SPE/CSUR Unconventional Resources Conference held in Calgary, Alberta, Canada, 20-22 Oct.

Sardinha, C., Petr, C., Lehmann, J., Pyecroft, J. and Merkle, S. 2015 Determining interwell connectivity and reservoir complexity through fracturing pressure hits and production-interference analysis, Journal of Canadian Petroleum Technology, 54(2), pp. 88–91. doi: 10.2118/171628-MS.

Schaeffer, B., McGreaham, L. and Reshetnikov, A. 2017. Unconventional parent-child well completion evaluation via microseismic analysis: A Delaware Basin case study. Published in SEG Technical Program Expanded Abstracts 2017 (pp. 5312-5316). Society of Exploration Geophysicists.

Scherz, R.Y., Rainbolt, M.F., Pradhan, Y. and Tian, W. 2019. Evaluating the impact of frac communication between parent, child, and vertical wells in the Midland Basin Lower Spraberry and Wolfcamp reservoirs. Presented in SPE Hydraulic Fracturing Technology Conference and Exhibition held in the Woodlands, Texas, USA, 5-7 Feb.

Shapiro, S.A., Rothert, E., Rath, V. and Rindschwentner, J. 2002. Characterization of fluid transport properties of reservoirs using induced seismicity, Geophysics 67, 212-220.

Shapiro, S.A. 2015. Fluid Induced Seismicity. Cambridge University Press. ISBN 978-0-521-88457-0.

Sharma, A., Damani, A., Sondergeld, C. and Rai, C. 2013. Understanding the microscale physics of hydraulic fracturing: A laboratory approach. Presented in SEG Technical Program Expanded Abstracts 2013 (pp. 2916-2921) held in Houston, Texas, USA.

Shin, D. and Popovich, D. 2017. Optimizing vertical and lateral spacing of horizontal wells in Permian basin stacked bench developments. Presented in Unconventional Resources Technology Conference, Austin, Texas, 24-26 July 2017.

Shoemaker, M., Hawkins, J., Becher, J., Gonzales, V., Mukherjee, S., Garmeh, R. and Kuntz, D. 2019. Frac hit prevention and engineered treatment design in the Permian basin using in-situ stress from 3d seismic. Presented in Unconventional Resources Technology Conference held in Denver, Colorado, 22-24 July.

Somanchi, K., Brewer, J. and Reynolds, A. 2017. Extreme limited entry design improves distribution efficiency in plug-n-perf completions: Insights from fiber-optic diagnostics. Presented in SPE Hydraulic Fracturing Technology Conference and Exhibition held in the Woodlands, Texas, USA, 24-26 Jan.

Sullivan, M., Zanganeh, B., Springer, A. and Clarkson, C. 2019. Post-Fracture pressure decay: a novel (and free) stage-level assessment method. Presented in Unconventional Resources Technology Conference held in Denver, Colorado, 22-24 July.

Sun, W.J., Kothari, S. and Sun, C.C. 2018. The relationship among tensile strength, Young's modulus, and indentation hardness of pharmaceutical compacts. Powder Technology, 331, pp.1-6.

Swanson, C., Hill, W.A., Nilson, G., Griman, C., Hill, R., Sullivan, P., Aften, C., Jimenez, J.C., Pietrangeli, G., Shedd, D.C. and Pursley, J. 2018. Post-Frac-Hit mitigation and well remediation of Woodford horizontal wells with solvent/surfactant chemistry blend. Presented in Unconventional Resources Technology Conference, Houston, Texas, 23-25 July.

Thomson, J., Franciose, N., Schutt, M., Hartig, K. and McKenna, J. 2018. Tank development in the Midland Basin, Texas: a case study of super-charging a reservoir to optimize production and increase horizontal well densities. Presented in Unconventional Resources Technology Conference, Houston, Texas, 23-25 July.

Travers, P., Burke, B. and Dolan, M.P. 2019. Natural tracers differentiate flowback. special report: stimulation and completion technology, American Oil and Gas Reporter, Dec 2019, pg. 65-69.

Valko, P.P. and Lee, W.J. 2010. A better way to forecast production from unconventional gas wells. Presented at SPE Annual Technical Conference and Exhibition held in Florence, Italy, 19-22 September 2010. SPE 134231.

Vargas-Silva, S., Khodabakhshnejad, A., Paryani, M., Venepalli, K. and Ouenes, A. 2018. Pressure depletion's impact on induced strain during hydraulic fracturing in child wells: The key to mitigate fracture hits and pressure interference. Presented in SPE Canada Unconventional Resources Conference held in Calgary, Alberta, Canada, 13-14 Mar.

Vidma, K., Abivin, P., Fox, D., Reid, M., Ajisafe, F., Marquez, A., Yip, W. and Still, J. 2019. Fracture geometry control technology prevents well interference in the Bakken. Presented in SPE Hydraulic Fracturing Technology Conference and Exhibition held in the Woodlands, Texas, USA, 5-7 Feb.

Vincent, M. 2010. Refracs-Why do they work, and why do they fail in 100 published field studies? SPE 134330. Presented in SPE Annual Technical Conference and Exhibition held in Florence, Italy, 19-22 Sep.

Wallace, K.J., Aguirre, P.R., Jinks, E., Yotter, T.H., Malpani, R. and Silva, F. 2016, February. Understanding completion performance in Niobrara-Codell reservoirs through the use of innovative software-guided workflows and models. Presented in SPE Hydraulic Fracturing Technology Conference held in the Woodlands, Texas, USA, 9-11 Feb.

Walsh, J.B. 1981. Effect of pore pressure and confining pressure on fracture permeability. International Journal of Rock Mechanics and Mining Sciences, vol. 18, pp. 429-435, 1981.

Warpinski, N.R. and Teufel, L.W. 1987. Influence of geologic discontinuities on hydraulic fracture propagation (includes associated papers 17011 and 17074). Journal of Petroleum Technology, 39(02), pp.209-220.

Warpinski, N.R., Branagan, P.T., Sattler, A.R., Cipolla, C.L., Lorenz, J.C. and Thorne, B.J. 1990. Case study of a stimulation experiment in a fluvial, tight-sandstone gas. SPE Production Engineering, 5(04), pp.403-410.

Warpinski, N.R. 1991. Hydraulic fracturing in tight, fissured media. Journal of Petroleum Technology, 43(02), pp.146-209.

Warpinski, N.R., Lorenz, J.C., Branagan, P.T., Myal, F.R. and Gall, B.L. 1993. Examination of a cored hydraulic fracture in a deep gas well. SPE Production & Facilities, 8(03), pp.150-158.

Warpinski, N.R., Mayerhofer, M.J., Vincent, M.C., Cipolla, C.L. and Lolon, E.P. 2008. Stimulating unconventional reservoirs: Maximizing network growth while optimizing fracture conductivity. Presented in SPE Unconventional Resources Conference held in Keystone, Colorado, USA, 10-12 Feb.

Warpinski, N.R, 2009. Integrating microseismic monitoring with well completions, reservoir behavior, and rock mechanics. Presented in SPE Tight Gas Completions Conference held in San Antonio, Texas, USA, 15-17 June.

Whitfield, T., Watkins, M.H. and Dickinson, L.J. 2018. Pre-Loads: Successful mitigation of damaging frac hits in the Eagle Ford. Presented in SPE Annual Technical Conference and Exhibition held in Dallas, Texas, 24-26 Sep.

Wu, R., Kresse, O., Weng, X., Cohen, C.E. and Gu, H. 2012. Modeling of interaction of hydraulic fractures in complex fracture networks. Presented in SPE hydraulic fracturing technology conference held in the Woodlands, Texas, USA, 6-8 Feb.

Wutherich, K., Srinivasan, S., Downie, R. and Katon, B. 2019. Identifying depleted induced fractures from offset wells using common drilling data. Presented in SPE Annual Technical Conference and Exhibition. Society of Petroleum Engineers held in Calgary, Alberta, Canada, 30 Sep – 2 Oct.

Xu, T., Lindsay, G., Zheng, W., Yan, Q., Escobar Patron, K., Alimahomed, F., Panjaitan, M.L. and Malpani, R. 2018. Advanced modeling of production induced pressure depletion and well spacing impact on infill wells in Spraberry, Permian Basin. Presented in SPE Annual Technical Conference and Exhibition held in Dallas, Texas, USA, 24-26 Sep.

Xu, L., Ogle, J. and Collier, T. 2019. Fracture hit mitigation through surfactant-based treatment fluids in parent wells. Presented in SPE Liquids-Rich Basins Conference-North America held in Odessa, Texas, USA, 7-8 Nov.

Yadav, H. and Motealleh, S. 2017. Improving quantitative analysis of frac-hits and refracs in unconventional plays using RTA. Presented in SPE Hydraulic Fracturing Technology Conference and Exhibition held in the Woodlands, Texas, USA, 24-26 Jan.

Yi, S., Wu, C.H. and Sharma, M.M. 2019. Optimization of plug-and-perforate completions for balanced treatment distribution and improved reservoir contact. SPE Journal, doi:10.2118/194360-PA.

Yu, W., Wu, K., Zuo, L., Tan, X. and Weijermars, R. 2016. Physical models for inter-well interference in shale reservoirs: relative impacts of fracture hits and matrix permeability. Presented at Unconventional Resources Technology Conference, San Antonio, Texas, 1-3 August.

Yu, W., Xu, Y., Weijermars, R., Wu, K. and Sepehrnoori, K. 2017. Impact of well interference on shale oil production performance: a numerical model for analyzing pressure response of fracture hits with complex geometries, SPE-184825. Presented at SPE hydraulic fracturing technology conference and exhibition held in the Woodlands, Texas, USA, 24-26 Jan.

Zhang, J., Kamenov, A., Hill, A. D., and Zhu, D. 2014. Laboratory measurement of hydraulic-fracture conductivities in the Barnett Shale. SPE Journal. doi:10.2118/163839-PA.

Zheng, S., Manchanda, R., Gala, D. and Sharma, M. 2019. Pre-Loading depleted parent wells to avoid frac-hits: some important design considerations. Presented in SPE Annual Technical Conference and Exhibition held in Calgary, Alberta, Canada, 30 Sep – 2 Oct.

Zuckerman, G. 2013. Breakthrough: The accidental discovery that revolutionized american energy. business, Wall Street Journal. Weblink: https://www.theatlantic.com/business/archive/ 2013/11 (read 4 Nov 2019).